EVALUATION OF CFRP-CONCRETE BOND BEHAVIOUR IN FIELD CONDITIONS: A CHAMPLAIN BRIDGE CASE STUDY

By

ISSA FOWAI

Thesis submitted to the University of Ottawa
in partial Fulfillment of the requirements for the
Doctor of Philosophy in Civil Engineering

Department of Civil Engineering
Faculty of Engineering
University of Ottawa

Author's Declaration

I hereby declare that I am the sole author of this thesis. This is a true copy of the thesis, including any required final revisions, as accepted by my examiners.

I understand that my thesis may be made electronically available to the public.

Abstract

In 2019, the last Canadian infrastructure report card rated the state of the nation's infrastructure to be at risk. One such structure was the Champlain bridge in Montreal, which exhibited signs of significant damage to structural components including the girders, deck, diaphragms, and foundation elements. Before it was closed in 2019, the Champlain Bridge was one of Canada's busiest bridges. Following a series of extensive but ultimately unsuccessful rehabilitative measures, the historic Champlain Bridge was eventually replaced at a cost to taxpayers of over $4 billion. Carbon fibre-reinforced polymer (CFRP) materials were extensively used to strengthen deteriorated components of the Champlain Bridge. Even though CFRP are commonly used to strengthen bridges globally, comprehensive studies on their long-term bond performance at service conditions are lacking from the literature. Realistic testing techniques and correlating laboratory and field data remains a significant challenge. In this research, a comprehensive study has been conducted to evaluate three CFRP-strengthened bridge diaphragms extracted from the recently deconstructed Champlain Bridge in Montreal that have been exposed to aggressive environmental conditions for several years. The main objectives are: 1) to develop a comprehensive procedure to assess the long-term performance of CFRP-concrete interfaces of field structures using non-destructive and destructive testing techniques, and establish a large database to correlate non-destructive test (NDT) findings with bond strength data; 2) to assess the integrity of the CFRP-concrete interface using advanced sensing and destructive testing techniques, including the development of new test configurations to evaluate the CFRP-concrete interface under distinct loading directions; 3) to predict the bond behaviour and failure mechanisms through finite element numerical modelling of intermediate crack-induced debonding behaviour under various loading conditions; and 4) develop recommendations to ensure bridge safety and improve future maintenance and repair protocols.

The first phase of work included a detailed visual inspection combined with a series of advanced NDT methods. Several issues were identified including material incompatibility, discolouration due to corrosion, and inter-fibre cracks as well as fundamental problems arising from construction of the bridge diaphragms

and installation of the CFRP. The results of the NDT field testing techniques generally point to strong bond between the CFRP and concrete substrate with defects mainly concentrated around the anchorage strips, where four layers of CFRP strips were used in the manual wet lay-up installation.

In phase two, five different destructive/semi-destructive test methods were performed to investigate the effects of load orientation and test setup on bond behaviour and the degree to which bond may be compromised by field defects. Single mode loading protocols comprised of the direct-tension pull-off test on 490 samples, two single shear-lap test setups (newly designed and conventional), and a double shear-lap configuration. Mixed mode loading was achieved using flexural beam tests. The direct tension pull-off confirmed NDT results, showing that approximately 96% of the tested CFRP pull-off samples exhibited failure in the concrete substrate, indicating good bond durability. The debonding strains from the single mode and mixed mode tests were significantly lower than code predictions.

The efficiency of the novel designed test setups proposed and utilized in this thesis were calibrated through separate pilot tests. A newly designed and pilot tried variable angle peel test included in the appendix of this document is proposed to investigate the interfacial peel strength of the CFRP-concrete interface at 15 to 60 degrees peel angles (Fowai et al., 2022). During the various experimental stages, damage progression was monitored and characterized by incorporating advanced optical techniques such as 2-dimensional and 3-dimentional digital image correlation (DIC) and distributed fibre-optic sensors (DFOS), as well as strain gauges. Finally, experimental data obtained were used as input parameters for the development and calibration of a detailed finite element (FE) model. The FEM modelling approach was validated against existing literature and was used to verify the experimental results from phase two and analyze how key parameters affect the performance and integrity of the CFRP-concrete bond of the structural elements.

List of Publications Based on this Research

Journals

I. **Issa Fowai*;** Martin Noël; Beatriz Martín-Pérez; Leandro Sanchez. *Assessment of CFRP-concrete interface integrity of Original Champlain Bridge diaphragms through non-destructive and semi-destructive testing".* Journal of Composites for Construction, Special Collection CICE 2023 (Invited paper published). https://doi.org/10.1061/JCCOF2.CCENG-4698

II. **Issa Fowai***; Martin Noël; Jacob Yager; Beatriz Martín-Pérez, Leandro Sanchez; Mark F. Green; Neil A. Hoult. *Strain distribution and debonding behaviour of CFRP sheets with different anchorage lengths from a decommissioned concrete bridge.* Submitted.

III. **Issa Fowai*;** Martin Noël; Mohammad Esmaili; Beatriz Martín-Pérez; Leandro Sanchez. *Bond performance of deteriorated CFRP-concrete interface under different shear-lap configurations: A Champlain Bridge case study*. Construction and Building Materials. CONBUILDMAT-D-25-03086. https://doi.org/10.1016/j.conbuildmat.2025.142002

IV. **Issa Fowai***; Martin Noël; Beatriz Martín-Pérez; Leandro Sanchez. *FEM simulation approaches of debonding in CFRP-Retrofitted Concrete: A Case Study of the 57-year-old Champlain Bridge from Montreal*. Submitted.

Conferences

I. **I. Fowai***; M. Noel; M. Esmaili; B. Martin-Perez; L. Sanchez (CICE 2025, Lisbon Portugal). *Impact of test configurations and field defects on debonding mechanisms in deteriorated CFRP-concrete interfaces from the decommissioned Champlain bridge*. (*Paper Accepted*). Paper 1514

II. **I. Fowai***; M. Noel; B. Martin-Perez; L. Sanchez (CICE 2025, Lisbon Portugal). *Assessment of CFRP-concrete bond interface from the deconstructed Champlain bridge- A comparison of single and mixed mode behaviour*. (*Paper Accepted*). Paper 1127

III. **I. Fowai***; M. Noel; B. Martin-Perez; L. Sanchez (CICE 2023). *Condition assessment of FRP-strengthened concrete bridge diaphragms using non-destructive testing*. 11th International Conference on FRP Composites in Civil Engineering, July 23-26, Rio de Janeiro, Brazil. https://doi.org/10.5281/zenodo.8066158

IV. **I. Fowai***; M. Noel; B. Martin-Perez; L. Sanchez (CICE 2023). *Integrity assessment of CFRP-concrete interface on externally strengthened bridge diaphragms using direct tension pull-off*. 11th International Conference on FRP Composites in Civil Engineering, July 23-26, Rio de Janeiro, Brazil. https://doi.org/10.5281/zenodo.8092062

V. **I. Fowai***; M. Noel; B. Martin-Perez; L. Sanchez (2022). *Evaluation of interfacial debonding of fibre-reinforced polymer using variable angle peel test*. 11th International Conference on Bridge Management, Safety and Management, July 1-15, Barcelona, Spain.

*_Corresponding author

Acknowledgements

I wish to extend my sincere and profound appreciation to my supervisor and mentor, Professor Martin Noel, for the unyielding support rendered throughout the various stages of this endeavor. Professor Noel's patience and consistent guidance were instrumental in turning this aspiration into a reality. His knowledge and expertise in the research domains were crucial to the timely completion of this project, ensuring a wide array of future research prospects. I am forever grateful for his understanding and support amidst the toughest hurdles of this journey. Working with him has been a privilege, fostering personal and professional growth. Furthermore, I would like to express my sincere gratitude to co-supervisors Professors Beatriz Martin-Perez and Leandro Sanchez for their invaluable recommendations and comments that shaped the overall success of this work. Their expertise in the field of numerical/structural and microanalysis guided me in producing the first ever comprehensive work on this topic. Special recognition is offered to the members of the thesis committee, Professors Hassan Aoude, Elena Dragomirescu, Vahid Sadeghian, and Pedram Sadeghian.

Acknowledgement is extended to Drs. Gamal Elnabelsya and Muslim Majeed for their technical assistance during my tenure at the University of Ottawa. Their expertise is greatly valued and critical to timely completion of this project. Many experts in machinery at the University of Ottawa contributed to bringing my conceptual designs into a reality, a note of thanks is therefore directed towards James Kent, Alexandre Vendette, Jacques Audet and Paul Burberry from the machine shop for their dedicated support and enthusiasm in facilitating the fabrication of the various setups used in this research. Gratitude is expressed to Chris Parkes from Hanco, among the many gracious Canadians encountered during this journey.

The collaborative rapport and encouragement of research colleagues significantly enriched this profound academic voyage. I am thankful to Aws Hasak, Zainab Al-Faesly, Abdullah Abodrahim, Abdul Watfa, Seyed Alireza Alavi, Hamidreza Asgharigharakheili, Osamah Mahmood, Mina Javankhoshraftar, Mohammed Skalli, all members of the Noel's research group, Dana Tawil, Leah Kristufek, Esmaeil Morshedi, Bita Hosseinian, Jacob Yager, and all the Mitacs interns that I worked with over the years. I am

thankful for the undergraduate volunteers; Mingliang Hong, Huan Ju, and Yuchen Yang and all uOttawa Co-op students. My apologies to all direct and indirect contributors not mentioned; I remain grateful for your support.

I want to express my gratitude to my mentor, Professor Mark F. Green, at Queen's University, for the research collaboration and mentorship he provided over the duration of my Ph.D. I am also grateful to Professor Daniel Cardoso at the Pontifical Catholic University of Rio de Janeiro and his research group for their generous hospitality and support during my research trip to Brazil.

I would like to express my deepest gratitude to the Department of Civil Engineering at the University of Ottawa for fostering an environment where I could thrive and providing the generous funding that allowed me the opportunity to excel in my research. The holistic experience of this journey was made possible through financial support from the Natural Science and Engineering Research Council of Canada (NSERC) through the Vanier Canada Graduate Scholarship and the Indigenous and Black Engineering/technology (IBET) PhD program. This research and development project would not have been possible without the contribution and collaboration of The Jacques Cartier and Champlain Bridges Incorporated.

I would like to extend my heartfelt thanks to my wife, Kristina, whose unwavering support and belief in me have been my greatest source of strength throughout this journey. During the most challenging moments, when I lost track of my own thoughts, her encouragement and faith in my abilities kept me motivated, disciplined and focus. I am deeply grateful for her patience, love and understanding, which have and will always be vital to my success.

Dedication

This work I dedicate to my wife and soulmate, Kristina Shcheglova, and son, Leomaris Fowai, for their unwavering patience, strength, and courage. Their presence in my life provided me with the necessary fortitude to bravely confront any challenges that came my way.

Table of Contents

List of Figures

List of Tables

Chapter 1 - Introduction

1.1 General

The ageing of bridge infrastructure is one of the critical challenges faced by the engineering sector in Canada. Damage resulting from structural deterioration, changes in load requirements, deficiencies in construction, vehicle collisions, and corrosion of reinforcement due to excessive use of de-icing salts in the winter seasons have contributed to a reduction in the service life of major Canadian bridge networks. The Champlain Bridge (CB) in Montreal epitomizes this trend, showing signs of extensive deterioration over its service life and undergoing multiple stages of rehabilitation and strengthening. Five years prior to the CB replacement, multiple layers of CFRP strips were externally bonded to the concrete diaphragms to provide the much-needed shear reinforcement following corrosion-induced cracking.

In these bond-critical applications, the efficiency of the rehabilitation—which depends on the proper transfer of predominately shear stresses between individual layers of the CFRP composite material or between the CFRP composite material and the concrete substrate—is governed by the behaviour and performance of the adhesive interface (or bond-line). However, our knowledge about the long-term performance of CFRP retrofits mainly comes from laboratory tests on small-scale samples under controlled conditions. In the field, externally bonded CFRP materials are exposed to fluctuating moisture levels and harsh temperature cycles, which can reduce their durability and degrade the CFRP-concrete bond. Furthermore, the ongoing deterioration of the underlying concrete is hidden behind the CFRP layer, effectively masking any visual warning signs of potential structural failure.

A comprehensive assessment of this critical bond interface requires a combination of non-intrusive, optical, multi-directional destructive structural testing, detailed numerical modelling, and microscopic analysis to accurately characterize and predict the performance and integrity of the bond-line. These innovative and practical approaches will not only provide qualitative and quantitative information about the condition of the strengthened components from a real field structure but will help better understand design requirements, refine code design approaches, and assess the long-term potential of CFRP as a means of retrofitting deteriorating bridges in Canada and beyond.

To the author's knowledge, no single study prior to this research program has attempted to undertake such a comprehensive and holistic approach to correlate material behaviour and deterioration, visual inspection, NDT, and a wide range of traditional and novel test methods for a detailed understanding of CFRP-concrete bond behaviour, nor has any condition assessment of CFRP-strengthened bridges in the field included such a rigorous combination of test methods. Central to this research program is the development of a deeper understanding of the damage progression in bond-critical applications under different stress states to improve the design and service life of CFRP-strengthened concrete structures. The primary objective of this thesis and all companion publications is not to expect bridge engineers or inspection practitioners to adopt the holistic approach proposed in this research, but rather to use it as a tool to provide specific management recommendation for similar crumbling infrastructures.

1.2 Overview of Champlain Bridge Research at the University of Ottawa

This thesis is based on research within a larger interdisciplinary project focused on a recently deconstructed bridge in central Canada. The goal is to develop a framework for diagnosing and predicting problems in a prominent Canadian bridge that has experienced premature deterioration. The findings of this research will contribute to the development of a comprehensive decision-making strategy for addressing other deteriorating infrastructure. The research team at the University of Ottawa was provided with twenty-eight full-scale bridge components, as indicated in Table 1.1. These original bridge elements were distributed among four PhD students, each focusing on specific aspects such as material damage assessment, structural assessment, and predictive numerical modelling. The following paragraphs provide a general overview of the various streams of work undertaken in this research program.

Table 1.1-Full-scale bridge elements contributed from bridge owner

Element	Number of samples	Dimensions of samples
Edge & Intermediate girders	6	5 m segments
Piers	6	1 m segments
Cap beams	5	1 m segments
Infill slabs	8	2 m x 3 m slabs
FRP-strengthened diaphragms	3	1.95 m segments

Stream A: Material Damage assessment

This section of the project focuses on a detailed diagnosis of the physicochemical, mechanical, and microscopic damage in the different concrete elements shown in Table 1.1. Specific tasks include crack indexing, chemical analysis, stiffness damage test, damage rating index, image analysis and scanning electron microscopy (SEM). Analytical models to study the prognosis of the detected mechanism from the diagnosis will also be developed.

Stream B: Structural assessment of girders

In this part of the project, the focus will be on investigating how the deterioration mechanisms present in the bridge girders have affected their shear behaviour and overall performance. Six post-tensioned girder segments will be tested to failure and nonlinear finite elements models will be developed with calibrated as-is material properties from experimental testing.

Stream C: Structural assessment of infill slabs

This stream investigates the performance of corroded infill slabs from the bridge. The experimental work consists of flexural testing of sixteen slab panels under a three-point bending setup. Data from material testing in stream A will be used to calibrate and develop nonlinear finite element model that will focus on validating the experimental work and used for parametric studies to simulate the performance of the slabs under different levels of damage.

Stream D: Structural assessment of diaphragms

The current thesis is centered on the research from this stream of the project involving three CFRP shear-strengthened diaphragms. Specifically, this work will focus on evaluating the CFRP-concrete bond interface which is critical to ensuring structural integrity, durability, and performance of the strengthened members. The study will investigate key fundamental parameters such as the bond strength after prolonged exposure to several environmental conditions in the field, deformation characteristics, failure modes and interface debonding mechanisms to measure the load transfer and damage progression between the CFRP and concrete. The three diaphragms underwent visual inspection and various non-destructive testing to detect debonding signs. Additionally, five different destructive testing methods were employed to holistically quantify the performance and integrity of the CFRP-concrete

interface. To validate the experimental work and analyse key factors impacting the short and long-term performance of externally bonded CFRP, a detailed FE model was developed taking into account the material deterioration.

Stream E: Predictive numerical modelling

Stream E of the project will develop a global finite element model for the multi-span superstructure system, exploring load-sharing characteristics and the bridge behaviour under various loading and deterioration scenarios. The model will also consider the different stages of rehabilitative work on the bridge components. Specifically, this global model will account for changes in member stiffness affecting load distribution. The model will aim to provide knowledge on the residual capacity of similar bridges leading to improved management frameworks for resilient bridges that can withstand similar harsh environmental conditions.

1.3 Overview of the Champlain Bridge and CFRP-strengthening scheme

The Original Champlain Bridge was opened to traffic in 1962 and closed in 2019, lasting for a much shorter life span than required by current standards. The structure was exposed to harsh environmental conditions that proved detrimental to the short- and long-term durability of the original structure, potentially compromising the integrity of the FRP strengthening systems undertaken in the final decades of the bridge's service life. The annual climate varies from warm humid summers to several months of freezing winter. In Montreal, the temperature can fluctuate from -27 degrees Celsius in January to 36 degrees Celsius in July, with an annual average temperature of 7 degrees Celsius. Multiple freeze-thaw cycles and excessive use of de-icing salt in the winter months are common for structures in this region of Canada. The bridge's location over the St. Lawrence River also contributes to increased humidity for the structure. This 3.44 km long bridge was located over the St. Lawrence River in Montreal. The bridge comprises three main sections: two concrete sections on either approach end (accounting for a total of 50 spans) and a seven-span cantilevered steel truss in the middle, referred to as Section 6 (Taylor, 2013). An overview of the bridge sections is shown in Figure 1.1. A typical approach span of the Champlain Bridge showing all six lanes of traffic can be seen in Figure 1.2. The approach spans in Sections 5 and 7 are simply supported reinforced concrete systems with seven 3.07 m deep precast post-tensioned

girders spaced at 3.72 m. A highly integrated structural system was obtained by post-tensioning the infill slabs (in the transverse direction), with the diaphragm at the level of the girder flange (Taylor, 2013). Four post-tensioned trapezoidal diaphragms (two placed at the pier locations and two intermediate diaphragms) were distributed along each of the concrete spans to increase the stiffness of the girders. The thickness of the concrete diaphragms varied from 210 mm to 220 mm. A typical post-tensioned diaphragm was reinforced with five internal post-tensioning tendons, each comprised of 12 strands having a diameter of 7 mm. These tendons were horizontally placed; hence, their contribution to shear capacity was achieved indirectly through axial compression in the concrete.

Figure 1.1- Overview of various sections (Taylor, 2013)

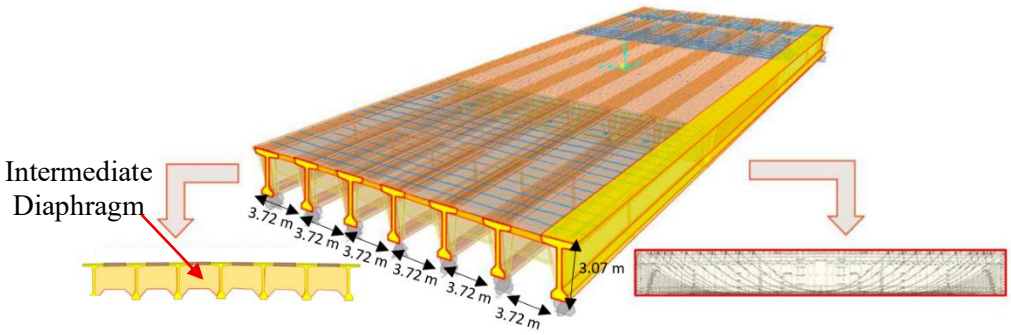

Figure 1.2 - A typical approach span (sections 5 or 7) (Taylor, 2013)

The majority of the FRP repair works on the Champlain Bridge were undertaken to improve shear capacity of girders and diaphragms (Figure 1.3) (Stantec, 2018). The purpose of the bridge diaphragm is primarily to transfer in-plane shear forces and vertical loads from traffic to the girders (Figure 1.3). The shear strengthening configuration on Champlain Bridge components mostly employed a practical U-wrap scheme (the sheets are continuous around the member's bottom), and the sheets were oriented perpendicular to the axis of the beams. As seen in Figure 1.3, two horizontal strips were provided as

anchorage strips with the sole purpose of preventing/delaying premature debonding of the vertical sheets. No mechanical anchors were observed on the bridge diaphragms. Although mechanical anchors can enhance the bond between the CFRP and concrete, and prevent debonding, their installation would have require drilling into the deteriorated concrete, which poses a heightened risk of inducing additional cracking in the aged concrete.

Major structural repairs to address significant integrity issues of the original Champlain Bridge started 24 years after its initial construction, with the scope and number of repairs increasing over time. The observed problems were atypical for a bridge of that age, and escalating maintenance costs reflected severe deterioration and heightened public safety concern. In 2011, the Government of Canada announced plans to construct a new bridge to replace the aging original Champlain Bridge. The Champlain bridge was 49 years old by then and had experienced significant deterioration, necessitating substantial investment to repair and replace (Domingue & Le Goff, 2017). The diaphragms under consideration were strengthened in the winter of 2014 (5 years before the decommissioning of the bridge). Considering the timeline of the CFRP retrofit, the subsequent dismantling of the original Champlain bridge, and the construction of the new Samuel de Champlain Bridge, which started in June of 2015, it is reasonable to deduce that the extensive CFRP retrofitting applied to the secondary structural members, such as the diaphragms, in 2014 was primarily intended to maintain the structural integrity, improve public safety concerns and to keep the existing bridge accessible to traffic during the construction of the adjacent cable-stayed replacement. It remains uncertain whether the bond degradation issues associated with the CFRP retrofit on the bridge components, as identified and reported in this research, contributed to the decision to close the original bridge four days after the opening of the new bridge (Samuel de Champlain bridge. However, the experimentally observed strain level for a high strength concrete strengthened with CFRP under various directional loads indicate substantial deterioration of the concrete elements. The three concrete diaphragms extracted from the decommissioned bridge to assess the bond performance of the FRP-repairs after five years of field exposure are shown in Figure 1.4.

Figure 1.3 – Typical CFRP strengthening schemes a) Girders b) Diaphragm with load transfer path shown in red arrows (Stantec, 2018)

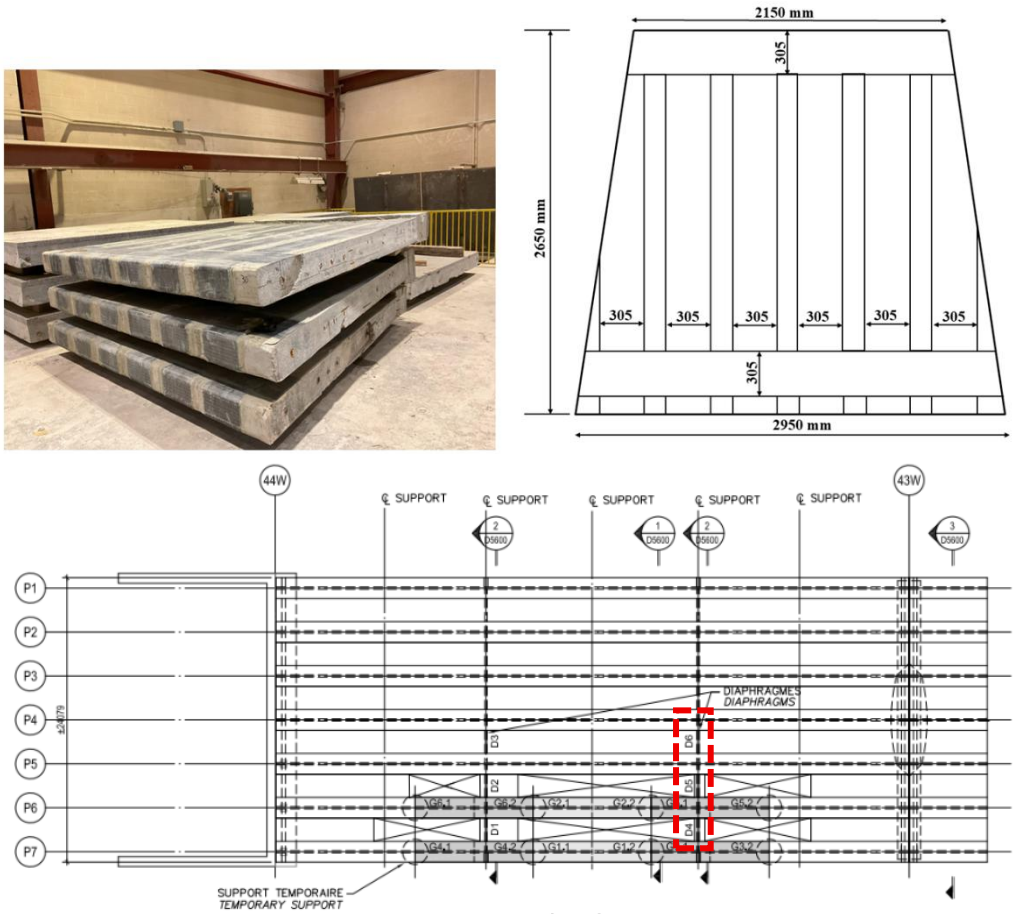

Figure 1.4-Extracted bridge diaphragms, dimensions and location (D4, D5, D6) in the bridge structure shown in dotted red rectangle

1.4 Evaluation of FRP-concrete bond

Common applications for externally bonded composites on bridge structures include flexural strengthening, shear strengthening, and column confinement as shown in Figure 1.5. The FRP is applied to the tension zone with fibres oriented in the longitudinal direction for flexural strengthening (Figure 1.5). In contrast, for shear strengthening, the FRP strips are used in such a way that the fibres are

oriented transverse to the longitudinal axis (Baggio et al., 2014). These FRP sheets can be applied on the concrete substrate as a single or multi-layer composite. Many of these externally bonded composite repairs on bridge structures are considered bond critical. In this scenario, the integrity of the bond (adhesion) between the composite and the concrete substrate is critical for proper stress transfer, since there are no redundant load paths for the stress to follow should the bond become compromised. Thus, knowledge on the long-term performance, bond behaviour, and failure mechanisms of the interface is crucial to understanding the behaviour of not only the strengthened component but to the overall structural response of the bridge.

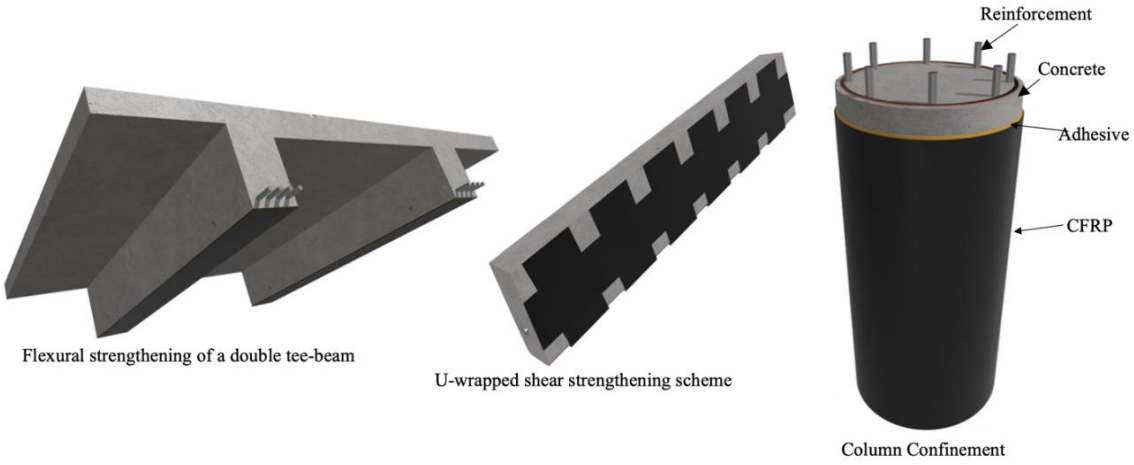

Figure 1.5 - Various strengthening schemes for externally bonded CFRP

The investigation of CFRP-concrete bond through conventional laboratory methods such as shear lap, direct tension pull-off test, and classical bending tests have been studied in detail (Allen & Atadero, 2012; Au & Büyüköztürk, 2006; Dai et al., 2004a; Halabe et al., 2020; Mata & Atadero, 2014; Smith & Teng, 2002). However, a comprehensive comparison of these various test methods and their ability to simulate stress conditions in real structural elements is noticeably absent from the literature. Whereas standard field tests do not accurately represent the stress states that develop under realistic loading conditions, existing laboratory methods are not practical for condition assessment of existing structures, and the results of one test type cannot be easily or directly correlated to the results from another test setup. Furthermore, the assessment of various NDT technologies for defect identification in deteriorated concrete members with externally bonded strengthening systems is limited in the literature. Thus, a

need exists for the development of practical knowledge on the limitation of current NDT techniques in defect identification and characterization of deteriorated concrete members.

In an effort to collect data on the bond that develops at the CFRP-concrete interface, previous researchers have focused on evaluating the failure mechanism and bond strength under either mode I (tensile) or mode II (shear) loadings (Banthia et al., 2009; Eveslage et al., 2010; Mazzotti et al., 2008; Pallempati et al., 2016), despite the fact that bond failures in real structural members are more likely to result from combined loading. The complexity, time, and cost of custom designing a novel test setup with capability to account for both modes of loading have precluded detailed examinations of the effects of load orientation and test setup on bond behaviour. Furthermore, almost all existing models for predicting the behaviour of the FRP-concrete bond have been developed assuming the absence of defects/deterioration at the bond line where a uniform stress transfer may be idealized. The implications of field defects on bond stress-slip response is noticeably missing from the literature.

1.5 Research Objectives

The use of CFRP as a bonded repair material for ageing and deteriorated bridge infrastructure has progressively increased over the past few decades. Many of these critical bridge structures in Canada are found in areas either susceptible to freeze-thaw cycling or other extreme environmental exposure conditions (snow and rain, frequent temperature fluctuations, and excessive use of de-icing salt). These natural and manmade conditions can result in changes in behaviour over time which should be monitored to guarantee the integrity of the structure. The long-term performance of external FRP strengthening systems is sensitive to the process by which the material was stored, handled, mixed, installed, and cured (Mirmiran, 2004). However, documentation on the long-term performance of externally bonded CFRP composites on actual in-service structures is rare in the literature. Therefore, knowledge about CFRP materials' long-time behaviour (durability) and the bond between the composite and the concrete substrate is of vital importance. Development of an innovative multi-level approach to evaluate and predict the long-term bond performance of deteriorating critical bridges retrofitted with

CFRP is crucial to extending the integrity and the service life of other crumbling bridge networks in similar environments. Through a comprehensive assessment of the Champlain Bridge diaphragms, this research aims to establish a holistic and invaluable field data on the long-term bond performance of externally bonded CFRP composite materials on bridge structures. This study aims to address the following questions:

- How do externally bonded CFRP systems perform in actual field conditions in Canada and to what extent does underlying damage contribute to a reduction in structural capacity?
- How can we assess the condition of CFRP strengthening systems and the underlying concrete without damaging the structure?
- How can we predict future performance and improve rehabilitation strategies to extend the service lives of ageing structures in aggressive environments?

To answer the above questions, the following specific objectives will be targeted:

01) Develop a comprehensive procedure to determine the state of deterioration at the CFRP-concrete interface.
02) Identify and quantify defects, including their location and distribution, at the CFRP-concrete interface across the three diaphragms.
03) Evaluate the effectiveness of various non-destructive testing (NDT) methods such as digital tapping, hammer tapping, and infrared thermography in the condition assessment of CFRP-strengthened concrete members. Discuss the limitations of these NDT techniques and provide recommendations where feasible.
04) Create an extensive database correlating NDT result with bond strength results obtained from semi-destructive field tests on the CFRP-concrete interface.
05) Implement advanced sensing techniques such as distributed fibre optic sensors and digital image correlations to study the distribution of strains under loading as an indication of the long-term performance of the CFRP-concrete bond interface.

06) Investigate the integrity of the bonded interface between the CFRP and the concrete through a wide range of destructive test methods, including development of new testing configurations to evaluate the CFRP-concrete interface under mode II or mixed mode loading conditions.
07) Establish cohesive material laws and use analytical models to predict the shear stress-slip relation of the deteriorated CFRP-concrete interface under various directional loading.
08) Develop and validate robust 3D FEM models to investigate delamination at the CFRP-concrete interface caused by intermediate crack-induced debonding under mode II and mixed mode conditions using cohesive zone material laws.
09) Evaluate the effect of various parameters, such as concrete properties and geometrical factors, on bond behaviour.
10) Develop guidelines for improved rehabilitation measures for critical concrete infrastructure in Canada.

1.6 Research Methodology

A methodological approach has been developed following a detailed literature study assessing the state-of-the-art pertaining to bridges strengthened with CFRP materials and identification of important research gaps. The research proposed herein aims to adopt a holistic approach of evaluating the long-term bond performance of externally bonded CFRP on a concrete bridge. The research approach includes three phases. The principal steps that will be undertaken to achieve the above-mentioned objectives are summarized below:

Task 01: In phase one, a detailed visual inspection in combination with advanced NDT methods were conducted on all CFRP-strengthened diaphragms. The visual inspection helped to qualitatively identify areas of surface defects. Thereafter, NDT techniques including infrared thermography (IRT), coin tapping, and digital tap testing (DTT) were used to investigate the subsurface defects. During the tapping and infrared scanning process, debonded regions were marked and the location and estimation of the area of delamination on the CFRP strips for a given surface was recorded and sketched. Besides the above-mentioned NDTs that were dedicated to evaluating the condition of the bond between the

CFRP strips and the underlying concrete, the rebound hammer, ultrasonic pulse velocity, and resonant frequency test were also conducted to assess the uniformity and hardness of the underlying concrete. This task aims to address objectives 01, 02 and 03.

Task 02: In phase two of the research, the three full-size diaphragms extracted from the Champlain Bridge were distributed among five different destructive tests. This stage of the laboratory investigation focused on assessing the effect of both loading directions and test setup on bond performance of the diaphragms at the presence of field defects. These different destructive test methods were employed to develop new correlations covering a wide range of realistic stress cases. These include the classic field test (direct tension pull-off test), bending test (interfacial shear and tension), customized shear lap test (for new single and double shear-lap tests), and conventional shear-lap tests. A variable angle peel test setup included in the appendix was designed and proposed for evaluating the peel resistance of the CFRP-concrete interface under mixed-mode loading. Objectives 04 to 07 will be accomplished through Task 02.

Task 03: In phase three of the work, the data obtained from the destructive tests and material testing such as the concrete compressive and tensile strengths, as well as bond stress-slip values, are used as input parameters for a detailed finite element (FE) model that can be used to analyze bond behaviour (strength and deformation performance) of CFRP-strengthened components. The experimental bond stress-slip values enable the evaluation of interfacial response of the CFRP-concrete interface by allowing the modeling of the bond interface between the CFRP and the concrete substrate using contact elements in ANSYS APDL software. The validity of the FE models built in this research were then compared against data from the literature and the experimental tests (beam test samples and shear-lap tests) in this study. The established models were used to simulate the bond interface and the damage process at the CFRP-concrete interface as a function of key parameters such as concrete strength, effective length, and bond width. Task 03 focuses on achieving objectives 08 and 09.

This integrated methodological approach covering Tasks 01 to 03 will collectively address objective 10.

1.7 Thesis Organization

This thesis is structured into eight chapters:

Chapter two offers a comprehensive literature review on various non-destructive techniques applicable to the condition assessment of in-situ concrete structures externally retrofitted with CFRP. It also investigates different structural tests developed by researchers for characterizing bond performance and analytical models predicting CFRP-concrete interfacial bond behaviour. Chapter three focuses on characterizing the as-is mechanical properties of the concrete, and CFRP composites, essential for modeling the CFRP-concrete debonding failure at the interface.

Chapter four presents the procedure and results of a comprehensive condition assessment through visual inspection, non-destructive and direct tension pull-off tests. This chapter and the subsequent three chapters are structured as stand-alone publications which have either been published or submitted to reputable journals. Chapter five presents the experimental procedure and results from the investigation of the CFRP-bond behaviour using the novel designed single shear-lap test setup, conventional single shear-lap setup, and double shear-lap setup. The chapter discusses the proposed bond-slip relationship derived from the experimental work and highlights the stress and strain behaviour of the deteriorated CFRP-concrete interface in a typical mode II loading condition. The chapter further discussed the deficiencies in current models using experimental data.

In Chapter six, the strain distribution and debonding behaviour under mixed mode loading conditions is presented based on the results of flexural beam tests. Chapter seven presents the procedure and results of the numerical analysis and validates them against the experimental data from the literature and the current study. Concrete, prestressing steel, and FRP composite are calibrated against the corresponding experimental materials properties. In addition, a parametric study using the proposed finite element model is conducted to investigate the impact of various parameters on CFRP-concrete bond performance. Chapter eight summarizes the conclusions and recommendations drawn from this research. It also highlights future research opportunities that can further build upon the findings of this study.

1.8 References

Allen, D. G., & Atadero, R. A. (2012). Evaluating the long-term durability of externally bonded FRP via field assessments. *Journal of composites for construction*, *16*(6), 737-746.

Au, C., & Büyüköztürk, O. (2006). Peel and shear fracture characterization of debonding in FRP plated concrete affected by moisture. *Journal of composites for construction*, *10*(1), 35-47.

Baggio, D., Soudki, K., & Noel, M. (2014). Strengthening of shear critical RC beams with various FRP systems. *Construction and Building Materials*, *66*, 634-644.

Banthia, N., Abdolrahimzadeh, A., & Boulfiza, M. (2009). Field assessment of FRP sheets-concrete bond durability. International Conference on Sustainable Built Environment Infrastructures in Developing Countries ENSET Oran (Algeria),

Dai, J.-G., Ueda, T., Sato, Y., & Hadiyono, J. (2004a). Dowel resistances of bond interfaces between FRP sheets and concrete. Proceedings of the second international conference on FRP composites in civil engineering, Adelaide, Australia,

Domingue. R, & Le Goff. P (2017). Report 4-Replacing Montreal's Champlain Bridge-Infrastructure Canada.

Eveslage, T., Aidoo, J., Harries, K. A., & Bro, W. (2010). Effect of variations in practice of ASTM D7522 standard pull-off test for FRP-concrete interfaces. *Journal of Testing and Evaluation*, *38*(4), 424-430.

Halabe, U. B., Joshi, R. M., & GangaRao, H. V. (2020). Nondestructive Testing of FRP Composite Structural Components and FRP Rehabilitated Bridge using Digital Tap Testing. *Journal of Multidisciplinary Engineering Science and Technology (JMEST)*, *7*(1).

Mata, O. R., & Atadero, R. A. (2014). Evaluation of pull-off tests as a FRP–concrete bond testing method in the laboratory and field. *Practice Periodical on Structural Design and Construction*, *19*(2), 04014001.

Mazzotti, C., Savoia, M., & Ferracuti, B. (2008). An experimental study on delamination of FRP plates bonded to concrete. *Construction and Building Materials*, *22*(7), 1409-1421.

Mirmiran, A. (2004). *Bonded repair and retrofit of concrete structures using FRP composites: recommended construction specifications and process control manual* (Vol. 514). Transportation Research Board.

Pallempati, H., Beneberu, E., & Yazdani, N. (2016). Evaluation of external FRP-concrete bond in repaired concrete bridge girders and columns. *Innovative Infrastructure Solutions*, *1*(1), 1-8.

Smith, S. T., & Teng, J. (2002). FRP-strengthened RC beams. I: review of debonding strength models. *Engineering structures*, *24*(4), 385-395.

Stantec. (2018). *Rapport d'inspection 2018 – Volume 1 : Inspection annuelle des sections 5 et 7 – Version finale* (0309098564). 3549).

Taylor, B. a. (2013). *Champlain Bridge Approach Spans, Edge Girder Condition Assessment and Rehabilitation Requirement*.

Chapter 2 - Literature review

2.1 Introduction

The application of bonded composite materials offers significant benefits for bridge rehabilitation due to their corrosion-resistant nature, ease of installation, minimal maintenance requirements, and high strength-to-weight ratio. Nevertheless, it is important to recognize that all engineering materials degrade over time when exposed to harsh environmental conditions. The establishment of an interface between the concrete and the bonded CFRP during the installation of composite materials plays a crucial role in governing the short-term and long-term structural performance of the repaired components (Coronado, 2006). Given the widespread use of CFRP materials to strengthen concrete bridges in Canada, gaining a comprehensive understanding of their long-term performance under real field conditions is imperative. Visual inspection serves as an economical initial step in condition assessment and structural evaluation. However, it is essential to prioritize methods that can minimize or mitigate the subjective nature of visual inspection. The Canadian Highway Bridge Design Code (CSA-Group, 2019), National Cooperative Highway Research (NCHRP) Report 514 (Mirmiran, 2004), and American Concrete Institute (ACI) Committee 440 (ACI, 2023b) have all identified acoustic sounding (hammer and coin tap test) and infrared thermography (IRT) as potential NDT techniques for bonded FRP composites. Researchers have also explored destructive bond tests to establish data on the bond behaviour and the mechanisms of load transfer of the concrete-CFRP interface. These tests include shear lap test, beam bending test, peel-off test, punching peel test, and the standardized direct tension pull-off test. This research review summarizes various intrusive and non-intrusive methods applied to assess the bond mechanism of CFRP-concrete interface and highlights the key areas to which the current detailed research will contribute.

2.2 Structural members strengthened with FRP

Over the past four decades, the practice of strengthening new, old, and damaged concrete structures using externally bonded CFRP has become increasingly prevalent. This approach followed the prior practice of bonding steel plates to concrete surfaces to improve the flexural and shear capacities.

Nevertheless, concern including corrosion risk, limitations on delivery length and conformity to concrete geometry, and the substantial weight of steel plates gave rise to the use of externally bonded CFRP for concrete retrofitting. The strengthening of concrete members using externally bonded CFRP can be classified as either bond critical applications or contact critical applications. In bond critical applications, the transfer of stresses from the concrete to the externally bonded CFRP occurs via the bond line interface, the effectiveness of the repair depends primarily on the integrity and performance of the bond between the CFRP and concrete. Conversely, in contact critical applications, effective repair hinges on intimate confining contact (bearing pressure) between the CFRP and concrete. CFRP concrete strengthening have been extensively conducted on various structural elements in both laboratory and in-situ settings. Retrofitted structural members have included reinforced concrete slabs (Al-Rousan et al., 2012; Enochsson et al., 2007; Mosallam & Mosalam, 2003; Soudki et al., 2012), reinforced concrete beams/girders (Bukhari et al., 2010; Miller et al., 2001; Täljsten, 2003; Tavakkolizadeh & Saadatmanesh, 2003), concrete columns (Fitzwilliam & Bisby, 2010; Moshiri et al., 2015; Parvin & Brighton, 2014), shear walls (Altin et al., 2013; Lombard et al., 2000; Woods et al., 2017) etc.

One of the earliest examples of CFRP field retrofitting occurred in Switzerland, where the Ibach bridge was strengthened with three 150 mm wide x 5000 mm long CFRP laminates (Meier, 1995). As pointed out by Meier (Meier, 1995), this 1969 bridge experienced a 39 m damaged span mainly due to inappropriate core boring work on the bridge, which led to severe damage to the prestressing tendons. Vehicle load testing validated the effectiveness of this early repair work. In Japan, the application of CFRP for seismic retrofitting gained prominence following earthquake disaster (Fukuyama & Sugano, 2000; Wu et al., 2007). In Canada, the establishment of the Intelligent Sensing for Innovative Structures (ISIS Canada) in 1995 amplified the nation's interest and research capabilities in the field of FRP, and its recognition as a leader in this field is undeniable. Important lessons have been learned about the application of FRP in bridge design and strengthening since the publication of their first manual, obtainable from the Structural Innovation and Monitoring Technologies Resource Centre website (SIMTrec, 2008). Noteworthy pioneering projects involving externally bonded FRP composites on Canadian bridges are outlined in Table 2.1. The application of FRP strengthening on reinforced concrete

bridges has significantly increased following these early field applications, attributable to research and developments in Canada and internationally.

Table 2.1-Pioneering projects of Externally Bonded FRP in RC Bridges in Canada

Bridge	Strengthening Method(s)	Built	Retrofitted	Reference
Champlain Bridge (Montreal)	FRP composites were used to increase confinement of a 4-meter-long pier with a diameter of 1.37 m. Nine layers of glass FRP were used.	1962	1996	(Rizkalla & Labossiere, 1999)
Country Hills Boulevard Bridge (Calgary)	Bridge deck strengthened for negative bending with CFRP strips. Thin bridge deck was strengthened to carry design live loading at the time of rehabilitation.	1975	1997	(Hutchinson et al., 2003)
Maryland Bridge (Manitoba);	Shear strengthening. I shaped AASHTO precast prestressed girders were strengthened with CFRP sheets	1969	1999	(Rizkalla & Labossiere, 1999)
John Hart Bridge (B.C)	Shear strengthening of 84 girder ends. Shear capacity was increased by 15 to 20% using CFRP.	Early 1960's	1999	(Hutchinson et al., 2003)
Leslie Street bridge on Highway 401 (Toronto);	Column deteriorated due to corrosion from de-icing salt. Three columns were rehabilitated using a combination of concrete grout, polyethylene and GFRP wraps.	1960s	1996	(Banthia et al., 2010; Sheikh & Homam, 2004)
St. Etienne de Bolton (Sherbrooke);	9 out of 12 deteriorated columns were confined with GFRP and CFRP.	1962	1997	(Banthia et al., 2010)

Many research studies have been conducted to assess how FRP can enhance the service life of reinforced concrete structures (Beydokhti & Shariatmadar, 2016). While a significant portion of these research studies focused on small-scale tests, a considerable number also have been conducted on large scale concrete members (Afefy et al., 2013; Baggio et al., 2014; Bakht & Mufti, 1998; Grace et al., 2004; Loudon & Bell, 2010; Neale, 2000; Rizkalla & Labossiere, 1999).

In a 2010 laboratory work, Ludovico et al. (Di Ludovico et al., 2010) investigated five full-scale prestressed concrete (PC) I-shaped girders of dimensions 13 m x 1.05 m. Amongst the five specimens, four were intentionally damaged to simulate a vehicle collision, and two of those damaged components were further strengthened with CFRP laminates. The research aimed to evaluate the damaged PC beams'

flexural behaviour as a function of the number of strands damaged and then assess the FRP laminates' efficiency as a retrofitting technique. A four-point bending configuration was employed, and LVDTs were then used to monitor the rotation and the strains during the testing. Based on their experimental work, the authors made the following conclusions: 1) flexural capacity can decrease by 20 and 26%, respectively, given a 17 and 33% loss of strands; 2) restoring the ultimate flexural capacity of the undamaged PC components using CFRP laminates requires prevention of fibre debonding; and 3) CFRP laminates increase both the stiffness and flexural moment capacity of the damaged PC specimens.

In a similar endeavour by the structural laboratory of Queensland University in Australia, de Waal et al., 2017 (de Waal et al., 2017) assessed two FRP strengthening techniques on three 60-year-old decommissioned PC bridge decks to determine their potential in improving the flexural capacity and flexural stiffness. One of the three specimens was used as a reference specimen without FRP strengthening, while the other two were each strengthened with four 8 m long CFRP pultruded plates and three 8 m long adhesively bonded GFRP I-beams, respectively. Abaqus finite element modelling tool was also used to approximate the peeling force near the GFRP I-beam termination points. The test specimens were tested under 4-point bending with a spreader beam at the midspan. All three specimens were in sound condition (uncracked) before testing. Visual cracks occurred at a load of 107 kN for the reference component, which then ultimately failed due to the crushing of concrete at an ultimate load of 200 kN. The CFRP-strengthened deck's flexural capacity was increased by 54%, while the deck with GFRP I-beam had a 105% increase with reference to the control specimen. It was therefore concluded that both schemes significantly improved the nonlinear portion of the deflection curve. Also, the authors pointed out the effectiveness of both techniques due to the lack of debonding.

2.3 Non-destructive condition assessment of FRP-strengthened bridges

As discussed in the previous chapter, when concrete members are strengthened with externally bonded composite materials, the short and long-term performance of the strengthened substrate relies significantly on the strength and stiffness of the bond at the CFRP-concrete interface. Thus, evaluating

and inspecting this interface without compromising the bond is critical. Contrary to the condition assessment of ordinary reinforced concrete structures, for CFRP composites externally bonded to concrete structures, only a limited number of NDT techniques exist. IRT and acoustic sounding (coin tapping, hammer tapping, and digital tap testing) are methods that have been used to supplement the available destructive testing methods for large CFRP-strengthened structures. This summary highlights several promising NDT methods, and the specialized equipment required to conduct the condition assessment of the bond interface of CFRP-strengthened concrete structures.

2.3.1 Visual inspection and associated challenges

The focus of a visual inspection is to provide documentation on the type and extent of the problem and investigate what causes the distress and how the structure can be restored (Noel, 2020). Visual inspection provides a history of construction, loading, and exposure conditions. In addition, the document usually includes information such as the description of the structure (name, location, member types, and photographs) and state of materials used (e.g., gross sectional loss for both steel and concrete). These baseline data are critical to monitoring the structure's performance over time. A visual inspection helps detect distress and deterioration at an earlier stage which can facilitate repair. However, a visual inspection can only be conducted on accessible surfaces of the concrete structure, and this becomes a problem for strengthened structures where the CFRP layer hides the concrete substrate (Figure 2.1).

Various signs of distress at the bond line (interface between concrete and CFRP) such as cracks (width and patterns), voids, stains, leaking, and chemical interventions cannot be seen until the CFRP is removed/replaced or deterioration becomes visible on the surface of the composite materials. Visual inspection and observation are usually the first steps in evaluating reinforced concrete structures. It is the most recommended inspection method by various guidelines including ACI Committee 440 (ACI, 2023b) and the National Cooperative Highway Research Program (Mirmiran, 2004). However, a gap in knowledge exists with respect to how the visual inspection of composite structures should be executed. Bridge inspectors usually rely on their knowledge and experience of inspecting conventional concrete structures to inspect retrofitted concrete bridges with externally bonded FRP composites. It is

worth mentioning that there is a comprehensive document on field inspection of in-service FRP bridge decks (Telang, 2006). However, their behaviour and load transfer mechanisms are dissimilar to bonded composite materials.

Regardless of the level of training, bridge inspectors of FRP repairs should fundamentally search for visual signs of damage and defects such as scratches, cracks (in both fibre and concrete), discolouration due to chemical reactions (from corrosion product or ultraviolet radiation (UV) exposure), blistering and voids, delamination (split between layers of fibres), and debonds (separation at the fibre-concrete interface). The concrete surface accessibility issues regarding the visual inspection of CFRP-strengthened members were apparent in the decommissioned Champlain Bridge (Figure 2.1).

The extent of corrosion underneath the CFRP was challenging to assess. Corrosion from steel plates in Section 5 of the bridge extended to the CFRP protective cover on a beam in Figure 2.2. However, the inspectors could not fully understand the extent of this deterioration to the bond interface and the substrate without removing the protective coating. Figure 2.3 shows delamination of the protection covers on a beam in Section 5 (Span: 22W-23W) with a delaminated area of more than 16000 mm^2 (Stantec, 2018). In the absence of this protective layer, the CFRP interface is exposed to attacks from UV, aggressive fluid (e.g., melted de-icing salt); contamination of the epoxy by humidity, rain or dirt which can also weaken the bond interface and exacerbates damage associated with progressive ageing over time.

The 2018 inspection also revealed air bubbles in excess of 16000 mm^2 on one of the worst affected girder strips from span 23W-24W of Section 5 of the bridge (Figure 2.4). These air bubbles trap leaking fluid (Figure 2.5) which during the freeze-thaw cycles leads to further delamination. During the visual inspections of CFRP-strengthened members, the length and area of the defects (delamination, voids, or discolouration) were estimated. However, given that the depth of the damage is unknown, the marking size on the defect areas does not correspond to the actual size of the damage in the composite or the strengthening layer.

Figure 2.1-Examples of various kinds of inspected defects on CFRP-strengthened elements of the Champlain Bridge (Stantec, 2018)

Figure 2.6 depicts schematic of air bubbles detected in the diaphragms. The size of these air pockets ranges from 20 mm x 100 mm to 160 mm x 650 mm (Stantec, 2018).

Figure 2.2 - Corrosion leading to discolouring of CFRP protective layer (4W-5W) (Stantec, 2018)

These irregularities could be attributed to a deficiency in construction/installation practices (e.g., lack of uniform pressure to remove entrapped air, installing and curing during unfavourable weather) or as a result of much more extensive damage beyond the strengthened layer due to overloading or environmental interventions. In addition to the air bubbles, cracks due to corrosion of post-tensioning tendons visibly propagating behind the CFRP sheets are shown in Figure 2.7.

Figure 2.3 - Detachment of CFRP protective cover (Section 5; 22W-23W) (Stantec, 2018)

Figure 2.4 -Air bubbles observed on girder 2 of Span 23W-24W of the CB (Stantec, 2018)

Figure 2.5-Stained protective coat due to leakage (Stantec, 2018)

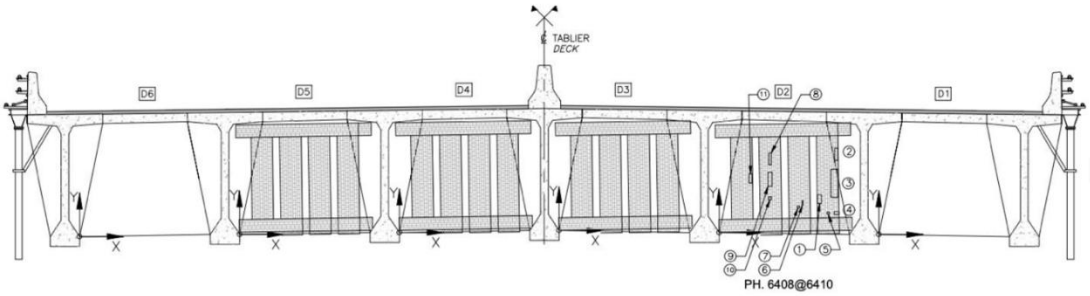

Figure 2.6 - Air bubbles detected on interior diaphragms (Section 5; span 19W-20W) (Stantec, 2018)

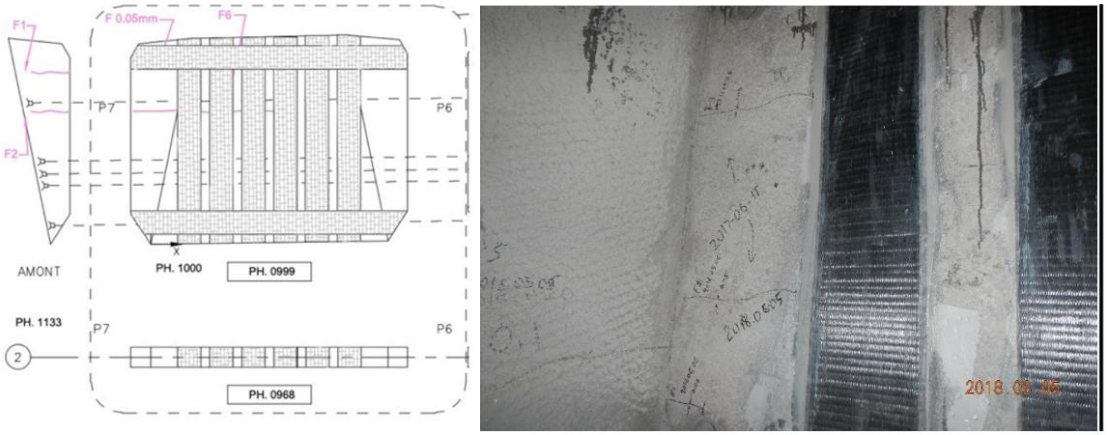

Figure 2.7- Crack propagation in a diaphragm of section 5 (Stantec, 2018)

The above images emphasize the need for regular global and localized visual inspections. However, although the visual inspection is generally economical (requiring inexpensive equipment such as flashlight, measuring tape, and magnifying glass), the main drawback is that inspection data is subjective and prone to human misinterpretations (Riad, 2017). Hence, other NDT techniques such as those outlined below should complement the visual inspection. These advanced NDT techniques allow the inspector and the bridge owners to track the propagation of these various forms of damage over time.

2.3.2 Infrared Thermography

In recent years, the use of infrared thermography (IRT) has gained considerable popularity in the inspection of civil infrastructure due to its capability to accurately and efficiently characterize flaws within the bonded CFRP composite (Tashan & Al-Mahaidi, 2012). In civil engineering applications, IRT cameras are commonly used to diagnose problems before significant damage occurs or to inspect

whether a repair material was installed properly (Mtenga et al., 2001). The process relies on the variation of heat transfer within a given object with both sound and defective regions.

The process of heat transfer is achieved through conduction, convection, or radiation (Hing, 2006). Radiation is heat transfer that is due to the emission of electromagnetic waves. By the first law of thermodynamics, this heat energy will transfer from hotter areas to colder regions until a temperature equilibrium is approached. As distinguished by their wavelength, infrared radiation (IR) is part of the electromagnetic spectrum below visible light. Every object above absolute zero temperature emits radiation (Hing, 2006). The radiated energy of the surface is captured as digital images which is measured by an IR camera. According to Stefan-Boltzmann's expression, the intensity of this radiation depends on the object's temperature and an inherent surface property known as emissivity (reflective property of the materials when compared to a blackbody) given by Equation 2.1:

$$E = \varepsilon \sigma T^4 \qquad \text{Equation 2.1}$$

Where: E is the radiant energy emitted by the surface at all wavelengths ($^{W}/_{m^2}$), ε is the emissivity of the inspected material, σ is Stefan-Boltzmann constant ($\frac{W}{m^2 K^4}$) and T is the temperature (in Kelvin).

Equation 2.1 shows that a slight elevation in the object's temperature will result in a substantial increase in the radiant energy. The emissivity is the rate at which the object emits radiation in comparison to a perfect hypothetical blackbody that has an emissivity value of 1. Concrete has a high emissivity value while the emissivity value of CFRP composites have been found to range between 0.77 to 0.84 with an average of 0.8 (Starnes et al., 2003). In the analysis of thermographic images, it is important to specify the reflective properties (emissivity) of the materials being viewed, because according to Equation 2.1 different materials may emit radiation at different rates even if their temperature is constant. For instance, a thermal image of an externally bonded CFRP wrap on a concrete structure may show different temperature values of the CFRP wrap and the concrete even though both materials may be subjected to the same temperature due to the difference in their emissivity values. However, commercial

IR cameras now have the capability to adjust/regulate the emissivity value during the post-processing phase of thermography using advanced software. In principle, if there is a void or delamination within the concrete (between the CFRP strengthening layer and the substrate or within thin layers of CFRPs), then a layer of air is present that alters the material's thermal conductivity (Figure 2.8).

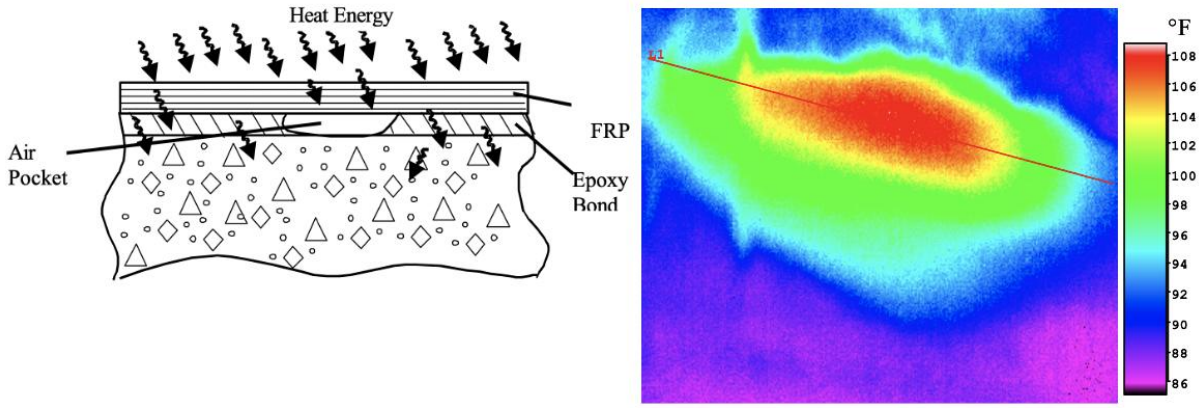

Figure 2.8 - bond line defect identification a) Typical heat transfer around subsurface defect b) Detected defect observed via thermography (Mtenga et al., 2001)

Therefore, these subsurface anomalies (voids, debonds, delamination, or water infiltration) will alter heat flow within the concrete and, hence, lead to differences in surface temperature. Areas above the voids (separated concrete) or cracks warm up faster than the defect-free areas (Starnes et al., 2003). By measuring these variations in surface temperature, the position of the subsurface defects can be determined. The measurement or data collection is conducted in one of two ways. Qualitative test results are captured in the form of thermal images depicting potential delaminated regions. The qualitative IR inspection also focuses on temperature differences as opposed to specific temperature values within the CFRP sheets. The qualitative inspection is a quick and easy approach to track the progression of the defect within the bonded CFRP material. Quantitative measurements, on the other hand, use precise temperature values of a specific defect or potential defect to analyse the deteriorated regions and estimate the total delaminated area. The apparatus for this test consists of an infrared camera, heat source (including solar loading), and data analysis tool such as a computer equipped with the necessary image processing software.

The advantage of the IRT as a viable NDT method for bonded repairs using CFRP composites can be attributed to the ability for large areas of a structure to be scanned within a very short period of time

compared to other available test methods. IRT can be used for both in-situ assessment and laboratory work. IRT is a contactless NDT method that is easily repeatable and is labour efficient. Moreover, for field assessments, this test can be completed without obstructing the flow of traffic. IRT allows for the estimation of the total delaminated area of the strengthened component and aids in keeping track of the progression of these defect regions within the repaired structure. However, the efficacy of the IRT method is subjective to camera grade/specifications, heating source, and post-processing technique adopted (Ghosh & Karbhari, 2011b). For instance, using robust post-processing techniques with capability to efficiently remove background noise can be favoured when a poor IRT technique is used to excite the specimen (Yumnam et al., 2021).

The first step of an infrared inspection involves the establishment of a thermal gradient. The development of temperature differentials can be accomplished considering the size and environmental conditions around the inspected structure. Two separate approaches are used when conducting IRT inspection: active or passive approaches (Yumnam et al., 2021). Active thermography involves the transfer of heat to the inspected surface through the use of external heating (halogen heat lamps, electric/gas heaters, heat guns, and heating blankets) or cooling sources (liquid nitrogen, liquid carbon dioxide, and cold water) and transient heat transfer occurs (Hing, 2006). This method is suitable for small-to-medium scale laboratory specimens. For inspection of large in-situ structures, the passive approach which relies on the existing temperature difference of the structure (or derived from solar loading) is used.

Regardless of the approach used one of the following methods must be employed: a) the surface of the CFRP is heated and the inspector monitors the surface temperature during the heating process, b) the surface is heated and the inspector observes the surface while it cools down or c) the opposite side of the inspected surface is heated and observation of the surface of interest is made as the heat is conducted through the material (Hing, 2006). For civil structures several different factors affect the heat transfer in concrete structures under ambient condition. These factors include wind effect, ambient temperature changes, and solar loading. A limitation of the IRT testing method is that in instances where the depth

of the defects is of concern, the infrared camera cannot be used since it only provides information on voids' planar dimensions. On the other hand, its sensitivity to temperature variation means depending on the heat intensity, defects can be left undetected. It is, therefore, a good practice to verify IRT results with other applicable NDT such as tap testing.

While laboratory experiments have demonstrated the effectiveness of IRT as a reliable NDT technique for inspecting CFRP composites bonded to concrete, these relevant experimental studies have focused on embedding artificial defects in the strengthened layer (Galietti et al., 2007; Hu et al., 2002; Tashan & Al-Mahaidi, 2014; Valluzzi et al., 2009b). The same approach is typical for research on composite bridge decks found in (Brown & Fox, 2010; Halabe et al., 2006; Halabe et al., 2007). An earlier study by Halabe et al. demonstrated that IRT is capable of detecting subsurface defects between concrete columns and different types of FRP materials (Halabe et al., 2008). This qualitative research involved the inspection of twelve small-size laboratory samples with embedded air-filled and water-filled debonds of varying sizes and field testing of in-service timber railroad bridge piles wrapped with glass FRP (GFRP) composites.

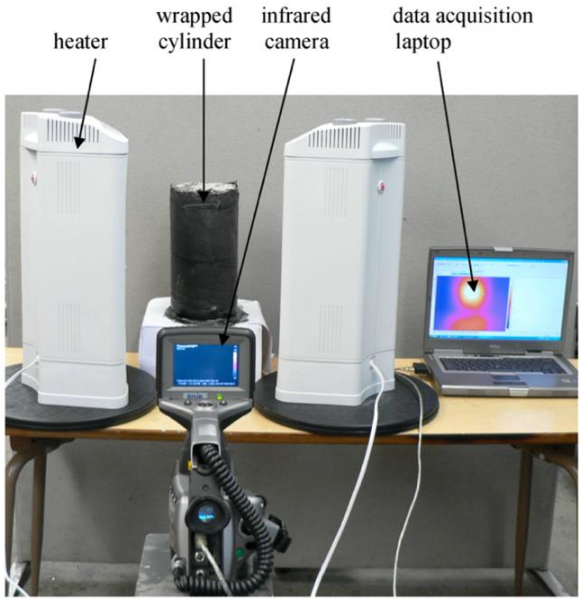

Figure 2.9 - IRT setup in laboratory (Halabe et al., 2008)

During the 70 second heating period of the laboratory samples, using two 1500W quartz tower heaters shown in Figure 2.9, the data acquisition or image collecting process was initiated immediately after

the heaters were switched on and continued a few minutes after the heating sources were turned off. All the water- and air-filled voids were easily identified as hot spots; that is, regions above the defect areas showed temperature readings much higher than the defect-free regions

Brown and Hamilton completed an IRT study on small-scale laboratory specimens followed by four full-scale AASHTO Type II concrete girders that were loaded to failure (Brown & Hamilton III, 2003). The girders were strengthened with varying layers (single to four layers) of FRP strips. Prior to testing, vehicle impact was simulated in the girders by cutting multiple prestressing tendons. CFRP and GFRP were then applied to increase the flexural capacity of the damaged girders and IRT was conducted after installation of the composite materials and at various stages of loading and post-failure to capture the effect of loading on the debonded area. In their study, three heat sources were investigated: 500W halogen lamp, infrared heating lamps (125W), and a photographer's flash. The inspection carried out on both the small-scale specimens and the full-size AASHTO Type II girder concluded that IRT is efficient in evaluating the condition of the bond interface between the bonded CFRP wraps and the concrete substrates. They found that the photographer flash was only effective in identifying defects within a single layer of carbon-fiber. The study also concluded that IRT performed poorly for detecting deeper defects. Infrared analysis of the pixel-by-pixel temperature data showed that the effectiveness of the IRT method in detecting subsurface defects decreased as the laminate thickness increased. A similar investigation of double-tee (DT) concrete beams retrofitted with carbon-FRP wraps was performed by Mtenga et al. (Mtenga et al., 2001). In their approach, heat guns were used as the primary source of heat to detect voids. They concluded that IRT is an essential method for quality assurance in structures retrofitted with bonded composite materials.

Miceli et al. demonstrated the use of IRT for monitoring the health of FRP bridge decks (Miceli et al., 2001). Analysis of the infrared images revealed the usefulness of IRT in detecting debonds and delamination in the FRP decks. However, surface anomalies such as staining and non-uniform wear caused complications in data interpretation. The authors also highlighted the inaccuracy of IRT in the

estimation of defects with moisture contents. Hu et al. used IRT method to detect voids of different sizes that were embedded at the interface between the FRP and the concrete (Hu et al., 2002). The defects were created by cutting pieces of plastic. The researchers were able to detect subsurface defects even when the heat source was placed at a distance of 20 metres from the test specimens.

In an in-situ condition assessment, IRT was used to detect bonding defects on a strengthened bridge located over the Doubs River in France, shown in Figure 2.10 and Figure 2.11. The bridge was built in the 1960s with three distinct and independent sections (two access spans and a main central structure) (Taillade et al., 2012). A visual inspection in the 1990s revealed extensive transverse cracking of the lower slabs on the mid-span girders, which warranted CFRP strengthening. IRT was then used to detect defects within the strengthened system.

Figure 2.10 - In-situ Infrared bridge inspection a)View of strengthened regions (left), b) mounted lift-platform (right) (Taillade et al., 2012)

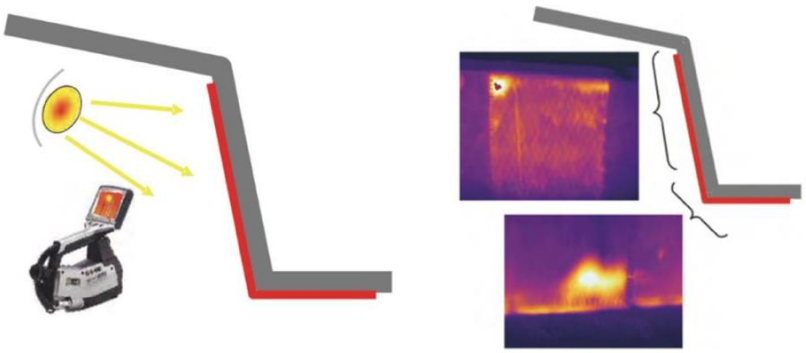

Figure 2.11 - Test schematic and defects within bonded CFRP (Taillade et al., 2012)

The authors discovered both wrapping defects and gluing defects. The test schematic and detected defects are shown in Figure 2.11. Taillade et al. (Taillade et al., 2012) pointed out that the main

challenge of the IRT inspection was the accessibility to the FRP bonded areas. In this case, a truck-mounted lift platform was used, as shown in Figure 2.10.

There is still a lack of test data on the application of IRT to investigate the long-term field performance of in-service CFRP-strengthened bridge elements where defect locations and sizes are unknown before the inspection. Furthermore, there are no existing specifications for IRT inspection of bond repairs using CFRP composite and this has led to inconsistency in the IRT approach amongst researchers. Throughout available literature variation in heating sources, distance from heat source to the inspected surface, and the duration of heat exposure differs immensely. Determining the heating limits is significant for a proper IRT analysis.

2.3.3 Digital Tap Testing

The tap testing methods (traditional coin tap and the electronic hammer tap) are simple and cost-effective NDT techniques for condition assessment of critical infrastructure retrofitted with externally bonded composite materials. Tap testing methods in combination with the previously mentioned IRT are reliable approaches for detecting subsurface anomalies without compromising the integrity of the FRP-strengthened structure. Both the IRT and the tap testing techniques complement each other and provide the inspector with confidence in their inspection results. The tap testing techniques discussed herein can be conducted for quality assurance of new installation and inspection of in-service structures strengthened with CFRP composite materials, which can further prompt repair.

The traditional coin tap (Figure 2.12a) is the simplest and cheapest widely used tap testing method for inspection of FRP composites. However, the traditional coin tapping approach is inherently subjective, operator-dependent, and prone to interference from the test surroundings. Demands from the industry to quantify test results and eradicate the subjectivity of this approach has led to the development of new technology. The digital tap testing resolves the ambiguity of the coin tap results. The digital tap test (DTT) hammer shown in Figure 2.12b is another technology transfer from the aerospace industry to

civil infrastructures. This device, also known as the Rapid Damage Detection Device (RD3), was developed by the Boeing Defense and Space Group for detailed inspection of composite materials used for aircrafts. The device comprises a lightweight hammer equipped with an accelerometer; the hammer head is connected to the handheld module via a cable, as shown in Figure 2.12. In addition, the handheld module contains digital logic components and a liquid crystal digital display powered by a portable rechargeable 9-volt battery. The accelerometer within the hammerhead is built to translate the force-time pulse generated after each tap into a voltage pulse. The inbuilt programmable array logic integrated circuit (PAL IC) measures and displays the pulse width at half amplitude on the display screen in microseconds. The force-time pulse is related to the localized stiffness of the inspected material. As a result, regions of surface defects such as debonds or delamination will produce a wider force-time pulse response than the sound areas (Figure 2.13) and a larger value will be displayed on the LCD screen (Georgeson et al., 1996).

Figure 2.12- Acoustic tapping devices a) Traditional coin tap test b) Digital tap testing hammer used on the CB Diaphragms

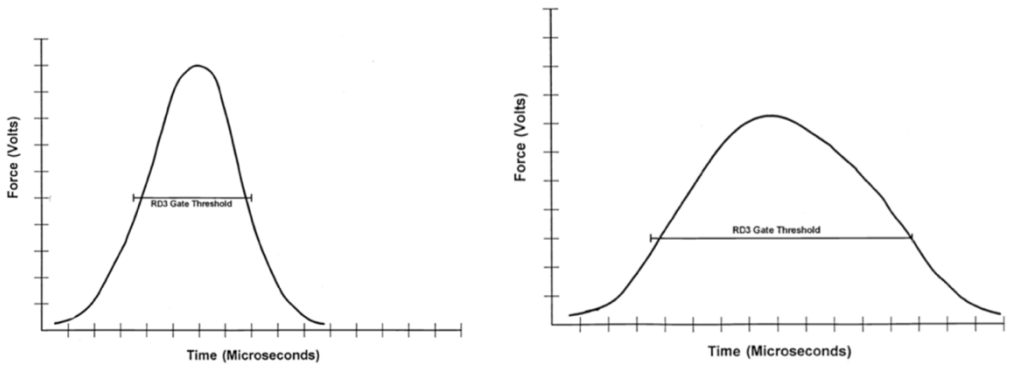

Figure 2.13 - Digital hammer typical force-time pulse a) Force-time pulse over sound region b) over defective area (Georgeson et al., 1996)

In general, the technique involves knocking the surface of the composite laminate/sheets with a small hammer, and the electronic device attached to this hammer will display a number in microseconds for each tap. The change in the number readings will help detect areas of voids and delamination within the composite. First, a tap number range is set for sound areas of the structure. Then, the rest of the area is tapped, and any number that is ten percent greater than that of the readings of the sound areas is deemed a defective area (Halabe et al., 2020). After every single tap, a light tap should be made to reset the display reading to zero before proceeding to the subsequent tapping spot. The displayed number is generally independent of the tapping force; however, if the tap is too light, erroneous readings are likely, and an excessively hard tap may damage the tapping sensor (Joshi, 2018).

Limited literature is available on the application of digital tap testing on CFRP laminates/sheets bonded to concrete structures. However, in a recent laboratory and field study work by Halabe et al. (Halabe et al., 2020), findings from laboratory specimens with varying thickness shows that DTT technique was only effective for defects at shallow depth, such as debonds in thin CFRP wraps and the technique was not able to detect delamination in thick FRP members. Moreover, their field testing results on Whiteday Bridge concrete box-beam bridge in West Virginia (Figure 2.14) showed the potential of the DTT technique in detecting voids and delamination in thin FRP wraps. Tap results of the Whiteday Bridge, which was retrofitted with CFRP due to corrosion of the prestressing strands, were well within the 10% margin for readings from the debonded and sound areas. The authors concluded that the DTT method is a quick and convenient technique, but is unable to detect delamination for thicknesses greater than 5 mm.

Figure 2.14 -Whiteday Creek Bridge a) before repair b) After CFRP repair (Joshi, 2018)

In summary, although coin tapping has its inherent drawback, a more time efficient approach for inspection of large composite structures strengthened with CFRP composites should start with coin tap testing since the method can help narrow down the defective area and the accuracy of the result can be checked by both the digital tap test and IRT.

2.4 FRP Bond Tests

2.4.1 Direct tension pull-off test

Over the years researchers have conducted various NDT and destructive testing methods, mainly in laboratory settings, to understand the performance of the bond between composite materials and concrete. The pull-off test stands out as the most popular semi-destructive or destructive evaluation method that can be conducted both in the laboratory and the field to assess the bond strength between the CFRP and the concrete substrate.

Several variations of pull-off test exist (ASTM, 2004, 2021b; ASTMD4541, 2017), all of which are used to measure the tensile capacity of an overlayed material on the concrete substrate. The version of direct tensile pull-off test specific to bonded FRP composites is currently standardized in ASTM D7522 (ASTM, 2021b). The testing apparatus (loading fixture with a minimum diameter of 2 inches and pull-off tester) and configuration with the FRP-substrate interface is seen in Figure 2.15. Other required equipment includes a circular hole cutter, a timer to control the loading rate (required for manual versions of the machine), and a fixture bonding adhesive (epoxy). As shown in Figure 2.16 the pull-off testing system determines the maximum tensile force that the concrete-CFRP interface can withstand before failure. Failure is expected to occur within the weakest plane of the strengthened system. Since the tensile capacity of the underlying concrete is expected to be much lower than the tensile strength of the structural adhesive at the bond interface, failure is expected to occur within a few millimetres into the concrete adjacent to the strengthened layer. The testing procedure generally includes scoring through the CFRP sheet or laminate into the concrete using a core drill to a total depth of 6 mm to 12 mm. The surface of the isolated area is then cleaned, sanded using medium-grit sandpaper, and rinsed

with solvent. To avoid compromising the bond surface, the cleaned surfaces should be allowed to dry out properly before proceeding with the next step. The circular metallic dolly is then adhesively bonded perpendicular to the FRP sheet. After that, the pull-off tester is attached to the metallic dolly and aligned through a threaded hole at the centre of the dolly (loading fixture).

Figure 2.15 - Direct tension pull-off testing apparatus

According to ASTM D7522 (ASTM, 2021b), an applied normal stress of less than or equal to 1 MPa/min is gradually applied until the dolly (loading fixture) detaches with a portion of either material. The operator should ensure that the arrangement of the pull-off tester is kept at this perpendicular location throughout the test as depicted in Figure 2.16. The load which is recorded at the time of failure/rupture is known as the maximum bond force. The pull-off bond strength is calculated by simply dividing the peak force by the area of the dolly, as shown in Equation 2.2:

$$\sigma_p = \frac{4F_p}{\pi D^2} \qquad \text{Equation 2.2}$$

In this expression, σ_p is the pull off strength or the tensile capacity of the bond, F_p is the peak load obtained at failure, and D represents the diameter of the testing disc. A recent version of the pull-off tester shown in Figure 2.15 can automatically calculate the peak load and bond stress and allows the

user to input the failure mode, which can later be extracted in a comma-separated values (CSV) file or excel file.

It is worth noting that ASTM D7522 (ASTM, 2021b) does not specify a requirement for the minimum strength for the direct tension pull-off test. ACI 440.2R-17 (ACI, 2023b), however, requires that a minimum of 1.4 MPa be considered acceptable and failure should occur in the concrete substrate. Seven common modes of failure (Figure 2.17) are defined by (ASTM, 2021b) to interpret the potential cause of failure. The failure modes can be adhesive (occurs at the interface), cohesive (coating fails within the layer which leaves the same coating on both the loading fixture and the concrete specimen), or a combination of both.

Failure Mode A reflects the most undesirable failure mode as the failure occurs at the interface between the FRP and the loading fixture. This failure mode indicates that an inappropriate workmanship was executed, or inadequate epoxy was used to fix the loading fixture to the concrete substrate and provides no useful data.

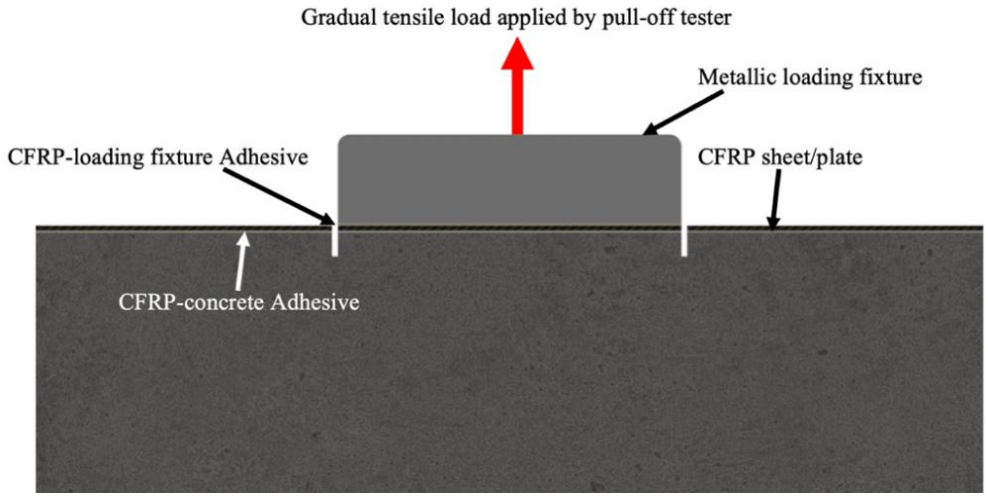

Figure 2.16 - Loading direction of bond interface during pull-off test

Failure modes B through F are premature failure modes commonly encountered. Finally, mode G is a cohesive failure in the concrete, which is the desired mode of failure. This failure indicates that the full

potential of the bond between the FRP and the concrete was utilized before failure since the bond that exists between the FRP, and the concrete substrate is stronger than the tensile capacity of the concrete.

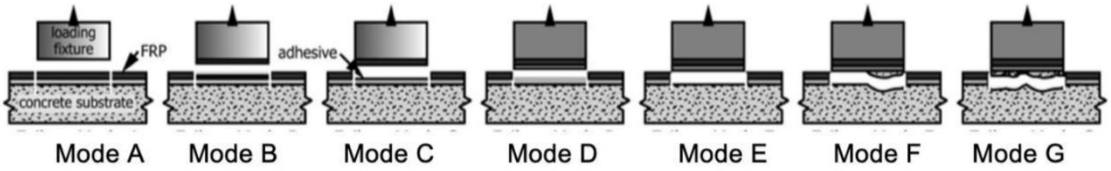

Figure 2.17 - FRP-concrete bond failure modes under pull-off test (ASTM, 2021b)

The direct tension pull-off test has been implemented in many laboratory settings to evaluate the bond behaviour between bonded composite materials and concrete substrate (Eveslage et al., 2010; Fazli et al., 2018; Karbhari & Ghosh, 2009; Mata & Atadero, 2014) and a few researchers have used the pull-off test method to examine the long-term bond durability of CFRP composite bonded to bridge structures in-service (Allen & Atadero, 2012; Banthia et al., 2009; Banthia et al., 2010; Pallempati et al., 2016). Banthia et al. (Banthia et al., 2010) used the pull-off test method to assess the durability of the bond of CFRP and GFRP repairs on four Canadian bridges after several years in service. These bridges were selected to represent a wide range of environmental exposure conditions, length of service, and different types of externally bonded FRP materials from various suppliers. A summary of the bridges investigated in this project is provided in Table 2.2.

Upon chiselling the protective coating, the pull-off test was conducted on random arbitrary locations on columns except in the case of the shear-strengthened girders from the Maryland bridge in Manitoba, where the pull-off test was conducted near the support where maximum shear is expected to occur.

Table 2.2-Canadian Bridges investigated by Banthia et al. (2010)

Bridge	Year Built	Year Repaired	Type of composite Used	Bridge Location
Safe Bridge	1955	2001	Sprayed GFRP	Vancouver, BC
St. Ètienne	1962	1997	GFRP and CFRP	Québec
Leslie Street Bridge	1960	1996	CFRP wraps	Toronto, ON
Maryland Bridge	1969	1999	CFRP wraps	Winnipeg, MB

These pull-off tests were performed using ASTM C1583 (ASTM, 2004), an older specification used prior to ASTM D7522. The average bond strength given in Figure 2.18 for all the bridges ranged from 0.83 MPa to 3.54 MPa. Interestingly, these two values were obtained from different columns on the same St. Ètienne Bridge in Quebec. However, the authors concluded that while the bond between these structures and the externally applied composite materials after being exposed to more than a decade of harsh environmental conditions remains adequate, they highlighted the need to develop innovative approaches for restoring the degraded bond.

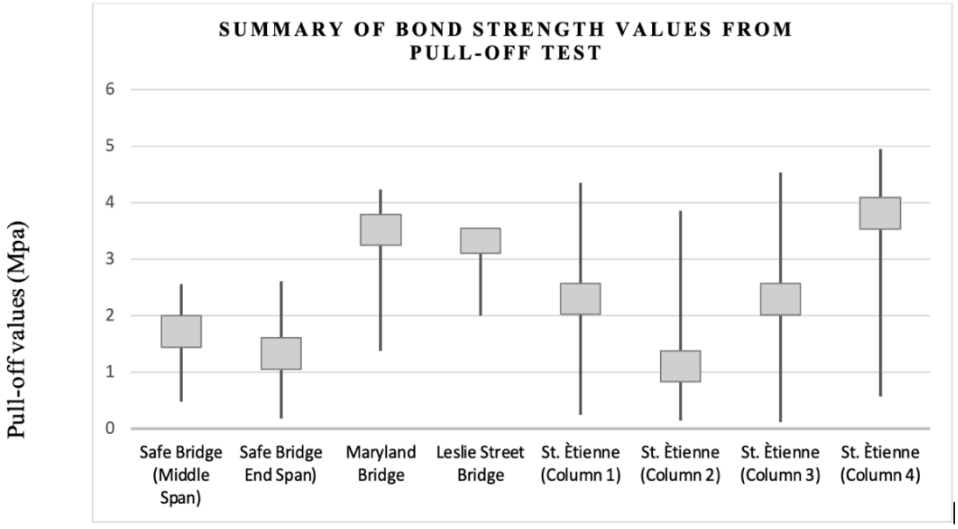

Figure 2.18 - Direct tension pull-off values obtained for various bridges (Banthia et al., 2010)

One limitation in this study is that it is impossible to judge what material (concrete, FRP, or the adhesive) controlled the bond strength since the failure modes were not reported by the authors. Furthermore, the research failed to present the compressive strength of the concrete from the various bridges assessed and so the influence of this parameter on the pull-off test results is not clear. Based on the results presented in Figure 2.18, it was impossible to understand if the results are due to the quality of the original repair or a consequence of bond degradation over the years.

The pull-off test is an economical and quick testing procedure with the added advantage of being deployable on-site as opposed to the other available destructive testing methods solely efficient for laboratory setting. However, the direct tension pull-off test is labour-intensive in scoring through the concrete substrate and surface preparation is critical to obtaining accurate results. Furthermore, test

results can be significantly affected by slight misalignment between the sample and the loading axis (Eveslage et al., 2010; Mata & Atadero, 2014; Pallempati et al., 2016). Considerable care should be taken during the drilling process. The depth of the drilled core should be limited to not more than 12 mm to avoid interference with any internal reinforcement and avoid the introduction of excessive torsional or thermal stresses that can be generated during the drilling process. In addition, the test evaluates the bond performance in a direction that is not a realistic representation of the loading condition of the FRP during service Figure 2.16. Moreover, the pull-off test procedure can be challenging for round surfaces in columns and piers. Therefore, several precautions should be observed when conducting pull-off tests on bonded FRP repairs to curb the variability in test results.

2.4.2 Shear lap tests

The role of the bond interface between the composite and the concrete substrate is generally to transfer shear stresses from the concrete member to the externally bonded FRP sheets (Ueda & Dai, 2005). Thus, there have been several experimental studies of the local interfacial shear bond behaviour at the FRP-concrete interface to study parameters such as the bond strength, effective bond length, interfacial energy, and the local bond-slip relation (Au & Büyüköztürk, 2006; Chataigner et al., 2011; D'Antino & Pellegrino, 2014; López-González et al., 2012; Mazzotti et al., 2008; Mukhtar & Faysal, 2018; Ueda & Dai, 2005). A popular laboratory approach commonly performed to evaluate the interfacial shear bond characteristics between the FRP, and the concrete substrate is the shear-lap test which can be categorized as single or double shear lap test depending on the number of bonded surfaces. A simplified sketch of different shear lap test configurations in available literature is shown in Figure 2.19.

It was previously stated by Mukhtar and Faysal that various test setups could lead to differences in results even for the same quantity and type of laminate (Mukhtar & Faysal, 2018). In the single shear testing technique, tensile force is applied to only one laminate or embedded reinforcing steel on either side of the substrate while in the double shear bond test the tensile force is applied to two components (López-González et al., 2012). Among the two approaches, the single shear-lap test is the most commonly used due to its simplicity (López-González et al., 2012). Regardless of the test configuration

(single or double shear), the shear lap test can generally only be performed in the laboratory and pure shear is hardly achievable partially due to load eccentricity or imperfection on the concrete surface. No standardized requirement exists with respect to the bonded length or width of the composite in these test configurations and researchers have typically tailored the test setup to meet project-specific objectives.

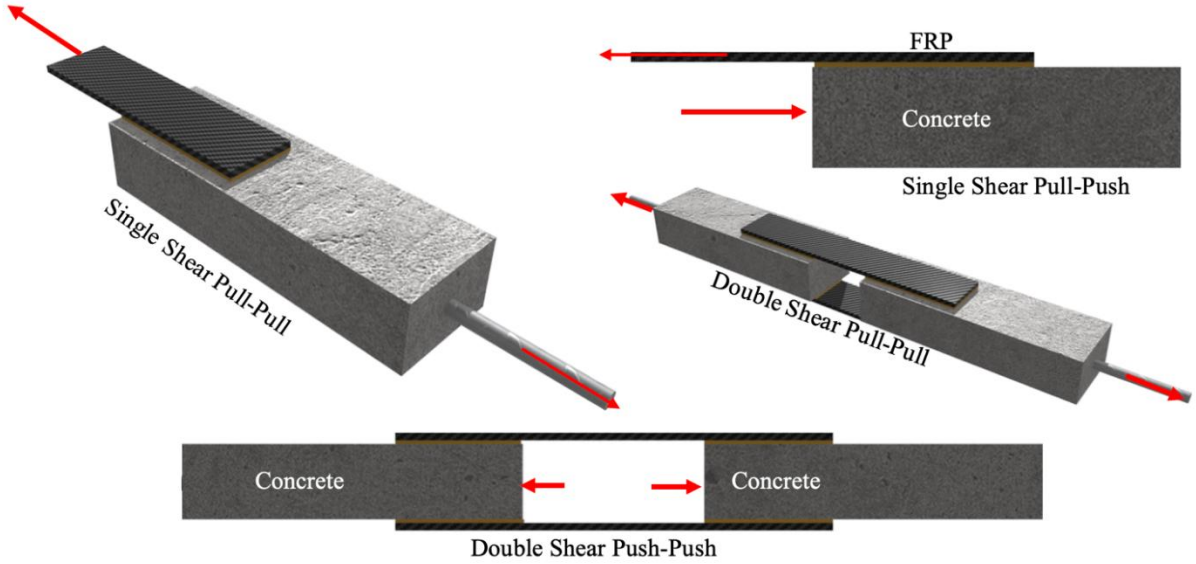

Figure 2.19 - Different shear-lap test configurations for characterisation of FRP-concrete bond layer

Chataigner et. al (Chataigner et al., 2011), used a single lap shear test to investigate the failure mode, ultimate capacity, strain distribution, and influence of edge condition in FRP composites. In this experiment, the authors developed a near-end supported single-shear test that was originally intended to be for the assessment of shear bond properties of steel-to-concrete joints. Contrary to the common technique of using a universal testing machine, a 100 KN-capacity hydraulic jack as shown in Figure 2.20 was used to apply the load. Both CFRP plates and laminates were used to strengthen the substrates.

The mode of failure (cohesive failure in concrete) was unaffected by the strengthening process (plates or sheet). However, a difference in failure mode was noticed depending on whether the specimen was bonded to the edge of the slab or bonded 50 mm away from the edge. Figure 2.21 shows that specimens bonded to the edge showed a detached concrete on the CFRP after failure.

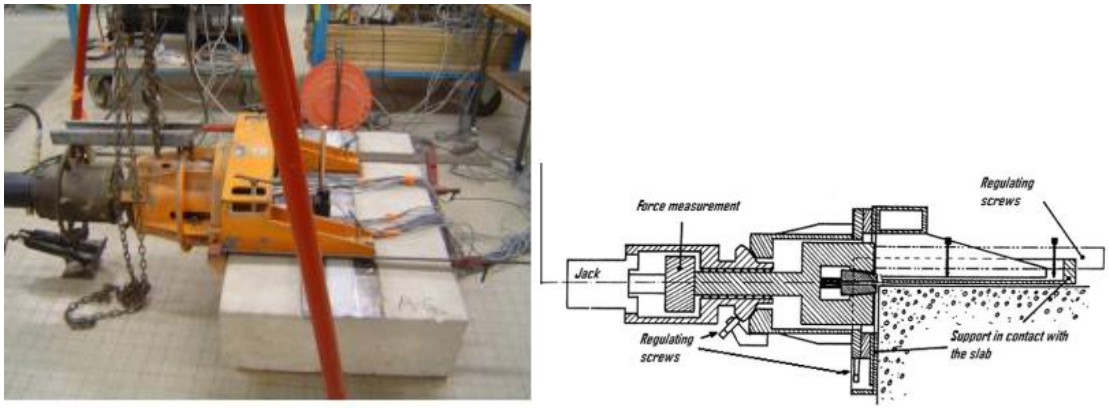

Figure 2.20 -Test set up and machine (Chataigner et al., 2011)

The ultimately load capacity of the joint was found to greatly be dependent on the type of strengthening approach adopted in Figure 2.22. However, both strengthening processes showed similar behaviour (linear and near-constant load plateau). Based on results obtained from the strain profiles (Figure 2.23), the bond transfer length was estimated between 100 and 200 mm. The higher stiffness material (CFRP plates) had a higher transfer length than the CFRP sheets.

Figure 2.21 - Failure surfaces for a) 50 mm gap from the edge b) bonded to the edge (Chataigner et al., 2011)

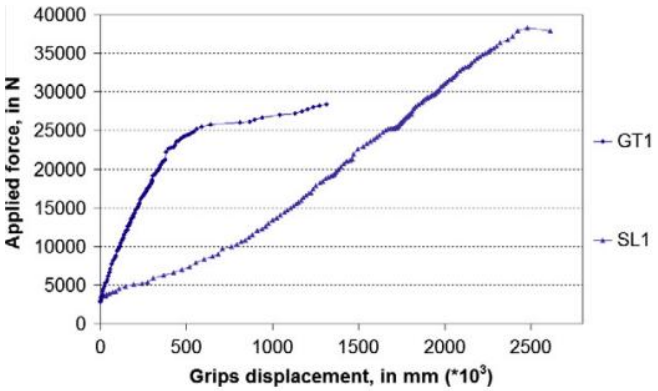

Figure 2.22 - Load-displacement curve of a typical CFRP sheet (GT1) and Plate (Chataigner et al., 2011)

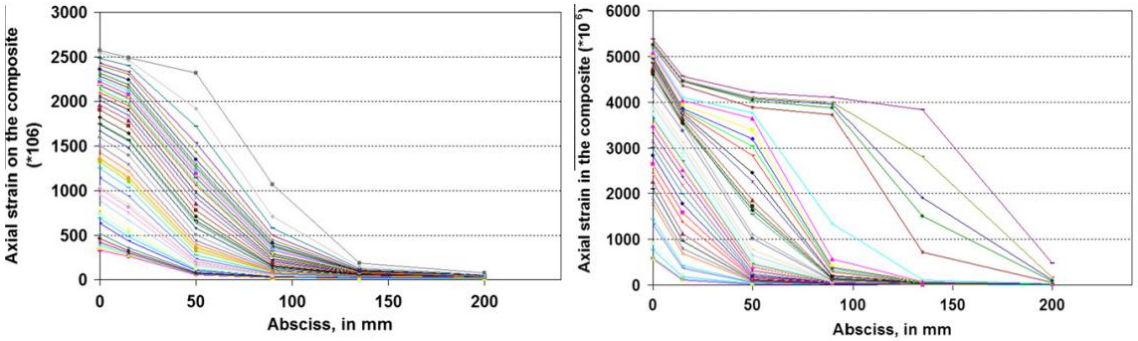

Figure 2.23 - Lap length strain profiles for a) CFRP plates b) CFRP sheet (Chataigner et al., 2011)

Li et al. (Li et al., 2023) conducted a detailed investigation to assess the impact of interface defects on the bonding behavior between FRP and concrete interfaces. The authors used Teflon tapes to replicate the discontinuities that can arise at the CFRP-concrete bond line.

Using 30 concrete prisms of rectangular cross-section, the specimen was prepared with varying size and shapes of defects (circular, oval and squares) ranging from one to nine defects. Analysis of strain data obtained through 3D digital image correlation techniques revealed a notable reduction in axial strain in the vicinity of defects, particularly in specimens where defect areas exceeded 5%. For instance, as the defect size increased from 10% to 25%, the strain on the CFRP sheet at the defect location decreased from 0.004 to 0.002. This decline in strain indicates a diminished capacity of the interface to transfer shear stresses. Specimens with smaller defect sizes exhibited constant strain across the bonded width, while increasing the defect sizes led to strain heterogeneity at the edges.

Li et al. (Li et al., 2023) noted that when the defect area was less than 5%, the influence of defects on interface shear stress transfer was minimal, with the reduction in debonding load similar to the fluctuation seen in traditional interface debonding processes. Moreover, regarding defect shape, circular and oval defects were observed to have more detrimental effect on bond performance compared to square defects. The authors also highlighted that defect concentration significantly impacted the bond strength.

2.4.3 Beam tests

The load transfer between the CFRP sheet and the concrete occurs through the interface bond layer as mentioned earlier. For a concrete member strengthened with CFRP sheet for flexure or shear, failure (in the form of debonding) in the bond layer may result in a brittle fracture of the structural member (Ueda & Dai, 2005). It is therefore important to understand all the possible modes of failure and their influence on the ultimate capacity of the strengthened concrete member, since these different failure modes alter the ultimate load at failure. The failure modes of CFRP-strengthened concrete members have been well-researched (Gao et al., 2007; Smith & Teng, 2002; Teng & Chen, 2007; Ueda & Dai, 2005; Wu & Niu, 2000). While contradictions exist on the definitions for classifying these failure modes, the testing approach through flexural bending tests have been consistent among researchers.

Ueda and Dai (Ueda & Dai, 2005) classified bond failure for flexural strengthened members to consist mainly of plate-end debonding (also known as concrete cover separation), which occurs from high normal and shear stresses at the end of thick bonded CFRP laminates but seldom for thin CFRP sheets, anchorage failure due to insufficient anchorage length, and intermediate crack induced debonding initiating from flexural and flexural-shear cracks. Smith and Teng (2001) identified the six failure modes shown in Figure 2.24.

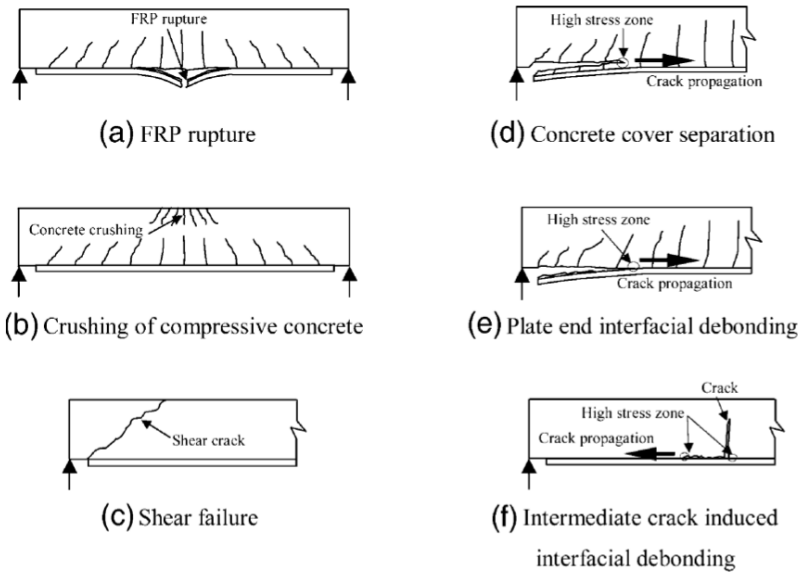

Figure 2.24 - Various failure modes of CFRP strengthened concrete members under flexure (Smith & Teng, 2002)

In terms of shear-strengthened beams the common mode of failure identified by researchers are CFRP rupture and CFRP debonding. The latter mode of failure is highlighted by shear critical beams investigated by Baggio et al. (Baggio et al., 2014). These various modes of failure have been demonstrated by researchers using the conventional four-point or three-point bending test setup such as that shown in Figure 2.25.

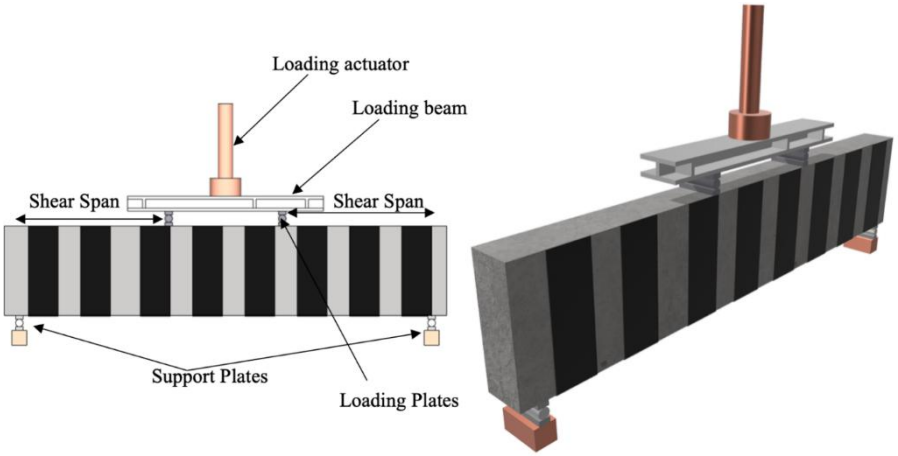

Figure 2.25 - Schematic sketch of conventional four-point flexure test

Baggio et al. (Baggio et al., 2014) conducted beam tests to determine the capacity of nine shear-critical beams strengthened with different commercially available composite materials. These simply supported beams with a clear span of 2200 mm between supports and a shear span of 900 mm on either side of the beam were subjected to four-point loading under a displacement control condition of 0.3 mm/min. Three modes of failure comprising of shear failure, shear failure with debonding, and flexural failure with crushing of the concrete were observed as shown in Figure 2.26. The load displacement curves depicted a minimum ultimate load of 223 KN for the control beam (without external strengthening) which failed in shear by diagonal tension. A minimum and maximum of 32 and 75 percent increase in ultimate capacity was obtained for the strengthened beams in comparison with the ultimate capacity of the control specimen. Their predicted values using code-based approaches and the values obtained from experimental work were in close agreement.

Figure 2.26 - Failure modes observed by [8]: a) Diagonal tension failure of control specimen b) debonding c) flexural failure (Baggio et al., 2014)

2.4.4 Punching peel test

In the early 2000s, a new application of bonding FRP composites on the bottom surface of tunnel linings or elevated bridges to prevent the falling or spalling of deteriorated concrete materials became popular in Japan (Dai et al., 2004a; DAI et al., 2004b; WU et al., 2000; Wu et al., 2005a; Wu et al., 2005b) Figure 2.27.

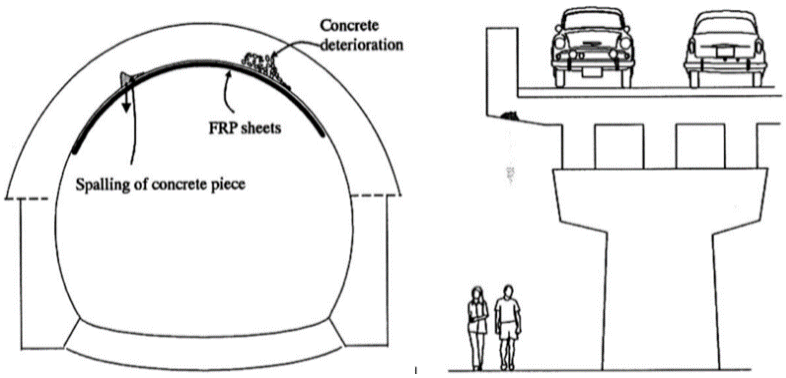

Figure 2.27 - Schematic of concrete spalling from tunnel lining and slab of viaducts (Wu et al., 2005a)

As shown in Figure 2.27 the CFRP-concrete interface in these strengthening schemes is subjected to both tensile and shear stresses simultaneously (mixed mode loading). This state of stress is representative of the actual loading condition of many field structures strengthened externally with CFRP materials. Few experimental studies were undertaken to investigate the CFRP-concrete interface under this particular mixed mode loading condition and most of the detailed published literature are in the local language (Japanese). In these experimental endeavours, two types of test methods were developed to help characterize the bond interface (DAI et al., 2004b; WU et al., 2000; Wu et al., 2005a). The first type of test is a beam-type dowel test, in which unidirectional FRP sheets are bonded on the soffit of a notched concrete beam and the second is a slab-type punching shear test (Figure 2.28) which is mostly undertaken with a bidirectional FRP sheet bonded to the bottom of the slab.

Among the limited available literature in this field, Dai et al. (Dai et al., 2004a) used the beam-type test to perform a detailed investigation on the effect of several parameters (such as concrete strength, CFRP stiffness, adhesive etc.) on the dowel resistance of the bond interface on eleven strengthened beams with cross-sectional dimensions of 150 mm x 150 mm and a span length of 900 mm (Figure 2.28).

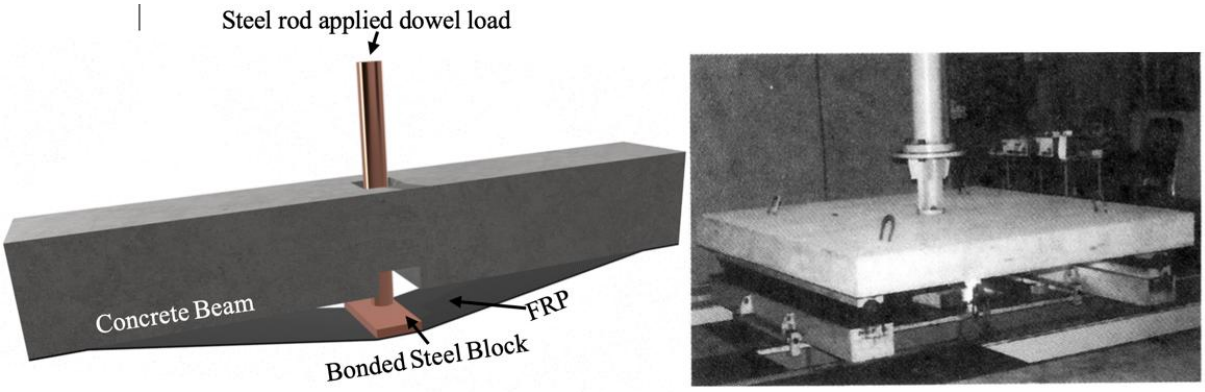

Figure 2.28 - Schematic diagram of beam-type dowel test and slab-type dowel test (Wu et al., 2005a)

In the test procedure, the CFRP was directly subjected to the dowel force through a 30 mm diameter vertical rod that was connected to the universal testing machine similar to the arrangement shown in the beam-type setup in Figure 2.28. A steel block of dimensions 45 x 60 x 30 mm was bonded to the 60 mm wide CFRP sheet and a ball hinge was set between the rod and steel plate. The effects of various

parameters on the dowel resistance are shown in dowel force versus crack mouth open displacement (CMOD) graphs presented in Figure 2.29. Figure 2.29 shows that the interface dowel resistance increased by nearly 28% with increase in the compressive strength of the concrete from 23.4 MPa to 42.1 MPa, while the lower elastic modulus adhesives resulted in higher dowel force resistance. Figure 2.30 depicts the effect of FRP stiffness on the dowel force resistance for a given pre-set unbonded length between the FRP and the substrate. At the initial peeling stage, the dowel resistance increased with the increase in material stiffness. This observation was more pronounced when a shorter pre-set unbonded length of 2.5 mm was set between the FRP and the concrete. Overall, two different modes of failure (in the concrete and the adhesive) were observed with the most common failure occurring a few millimeters into the concrete just adjacent to the bond line.

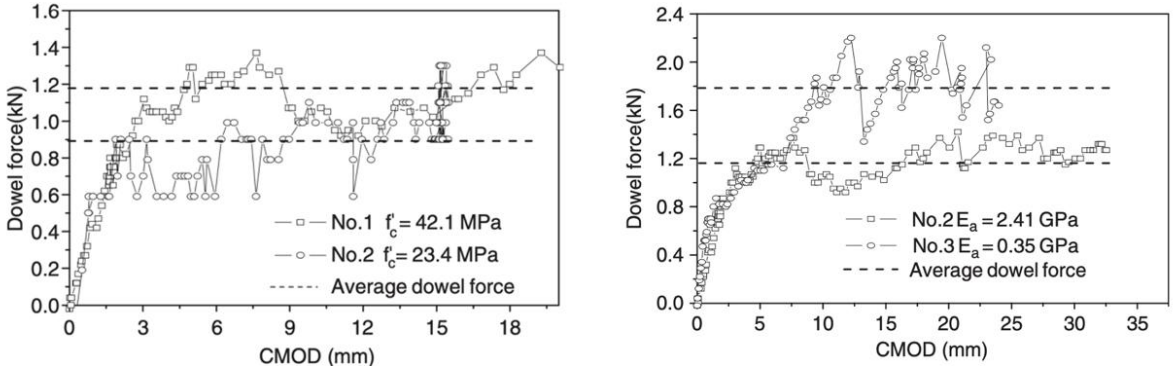

Figure 2.29 - Dowel force versus crack mouth open displacement (CMOD): a) Effect of concrete strength on dowel resistance b) Effect of adhesive on dowel resistance (Dai et al., 2004a)

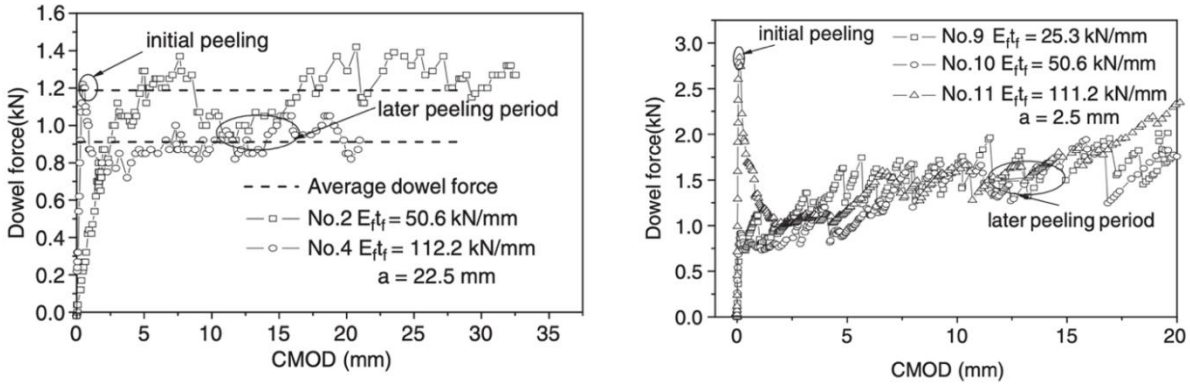

Figure 2.30 - Dowel force versus crack mouth open displacement (CMOD)Effects of FRP stiffness on dowel resistance a) pre-set un-bonded length a =22.5 mm b) a=2.5 mm (Dai et al., 2004a)

There is a lack of comprehensive literature on the bond behaviour of FRP-concrete interfaces when subjected to dowel forces such as those imposed by delaminated concrete pieces. A wide range of values

have been reported for the maximum dowel force and current literature have failed to investigate the effect of the interfacial fracture energy on the peel angle.

2.4.5 Variable angle peel-off test

The premature debonding of FRP sheets may be produced by a significant flexural or flexural-shear crack in the member's span. Under that condition, the relative vertical displacement of the crack's opposites sides will induce mixed mode loading on the FRP sheet (Figure 2.31). Understanding the strength of the adhesion or the interfacial fracture energy is critical to the success of the composite behaviour of the repaired structure. One of the less widely used adhesion tests is the peel-off test. In general, a peeling test involving a rigid material (concrete) and a relatively flexible material (FRP sheets) can be performed by pulling the flexible material away from the rigid one (Figure 2.32). The greatest amount of force required for peeling per unit width of the laminate bonded to the substrate is regarded as the peeling strength of the bond between the FRP-concrete interface. Karbhari and Engineer designed a practical peel test to study the bond strength at the FRP-concrete interface under mixed-mode loading conditions at different interface peeling angles (Karbhari et al., 2003; Karbhari & Engineer, 1995; Karbhari & Engineer, 1996; Xie & Karbhari, 1997). Figure 2.33 shows the configuration and setup of the proposed test.

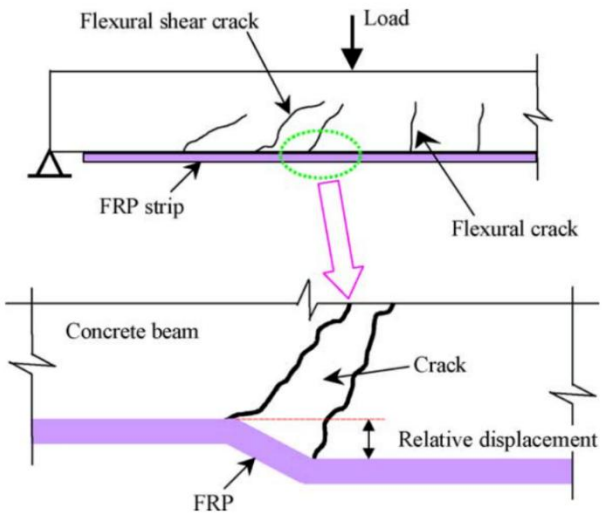

Figure 2.31-State of FRP at the tip of intermediate crack (Yao et al., 2005)

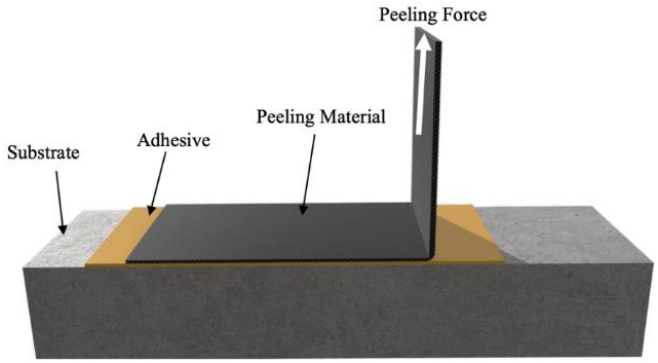

Figure 2.32 - Schematic diagram of vertical angle peel test

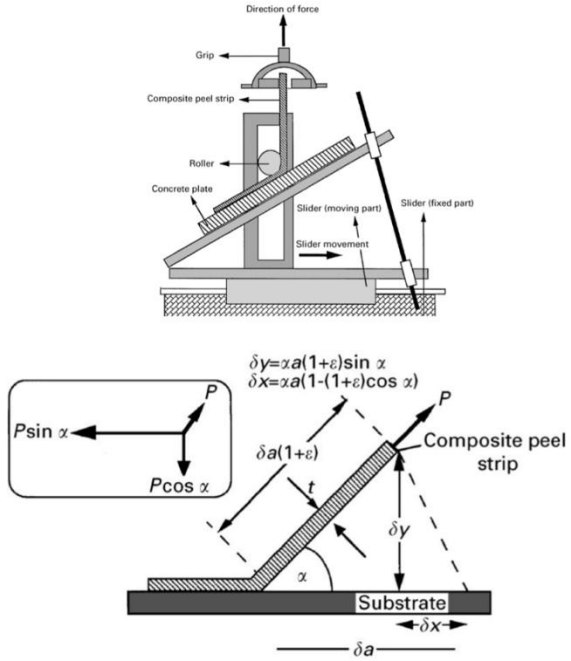

Figure 2.33 - Top to Bottom: Schematic of peel test setup and geometrical mechanics (Karbhari & Engineer, 1995)

Besides the fact that it can represent the mixed-mode of failure encountered by strengthened structures during service, other advantages of this test method include the controlled rate of failure and the fact that the peel force is directly related to the work of detachment (Karbhari et al., 2003; Karbhari & Engineer, 1995; Karbhari & Engineer, 1996; Xie & Karbhari, 1997). Even though the test was not oriented towards a particular application of FRP strengthening, it enables the evaluation of both the opening mode G_I (work of the normal traction) and the sliding mode G_{II} (work of the shear traction). In Figure 2.33, a thin strip of unidirectional carbon fibre is bonded to the concrete substrate and a peel force is applied to the end of the sheet at a predetermined angle. A peel angle of 45 degrees was

suggested by Karbhari & Engineer, and an angle above 60 degrees was shown to cause severe cracks of the composite strips during the peeling (Karbhari & Engineer, 1996). A detailed analysis of the test is presented in (Karbhari et al., 2003; Karbhari & Engineer, 1995; Karbhari & Engineer, 1996; Xie & Karbhari, 1997).

From Figure 2.33, when a length of δa is peeled away at a constant angle of α from the concrete, the point of application of force *P* will travel a distance of δa (1 + ϵ), where ε is the tensile strain in the FRP (in the direction of the fibre). The work input by the force P can therefore be calculated as the product of the magnitude of *P* and the distance travelled $P\delta a$ (1 + ϵ). In the absence of other external forces, the expression of the energy equilibrium is given in Equation 2.3.

$$P\delta_a(1+\varepsilon) = \delta_a WtU + Pcos\alpha\delta_a + Gw\delta_a \qquad \text{Equation 2.3}$$

In this expression, w and t represent the width and thickness of the strip, respectively, and *U* (Equation 2.5) is the strain energy density at a strain of ε (Equation 2.4). $Pcos\alpha\delta_a$ is therefore the work done by the horizontal components of the applied load *P* and G (Equation 2.6) is the fracture energy required to peel a bonded area of $w\delta_a$.

$$\varepsilon = \frac{P}{wtE} \qquad \text{Equation 2.4}$$

$$U = \frac{\sigma\varepsilon}{2} = \frac{P^2}{2W^2tE} \qquad \text{Equation 2.5}$$

$$G = \frac{P}{w}(1 - cos\alpha) + \frac{P^2}{2w^2tE} \qquad \text{Equation 2.6}$$

In a more recent endeavour (Kim & Horwitz, 2021), Kim and Horwitz modified the peel test to investigate the out-of-plane peeling of the CFRP-concrete interface at elevated temperatures (up to 150 degrees Celsius). Peel tests were conducted on 54 concrete blocks—the concrete blocks measured 75 mm wide by 50 mm deep by 280 mm long. The research affirms the vulnerability of the FRP-concrete interface under variable angle loading and temperatures exceeding the glass transition temperature of

the epoxy adhesive were found to cause a substantial reduction in the interface's capacity due to the softening of the interface (Figure 2.34). However, the implication of peel angles less than 30 or greater than 60 degrees was not studied. The peeling failure of the CFRP-concrete bond interface was captured with an IRT camera as depicted in Figure 2.35.

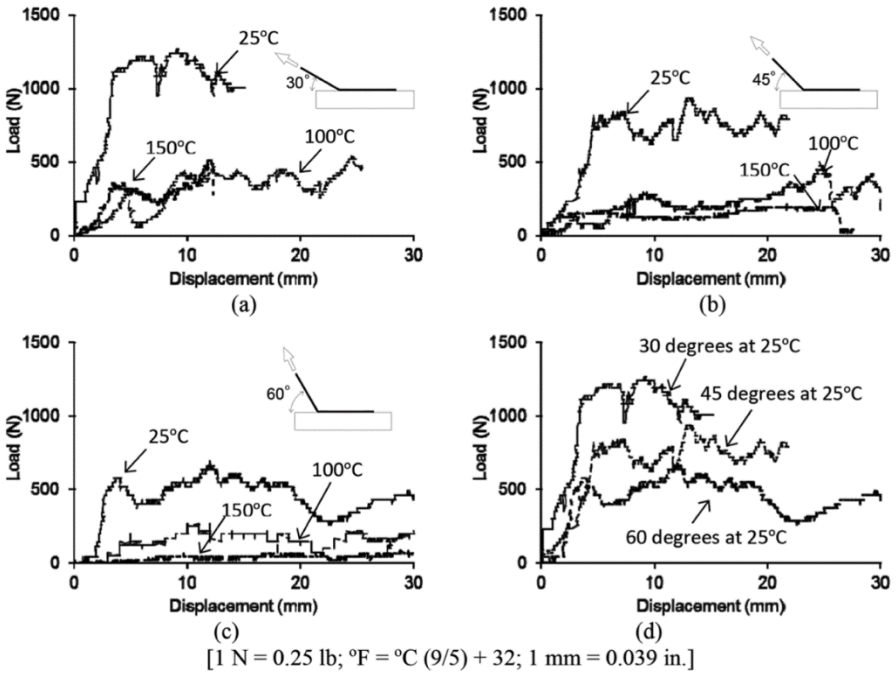

Figure 2.34 - Load-displacement relation at different peel angles (Kim & Horwitz, 2021)

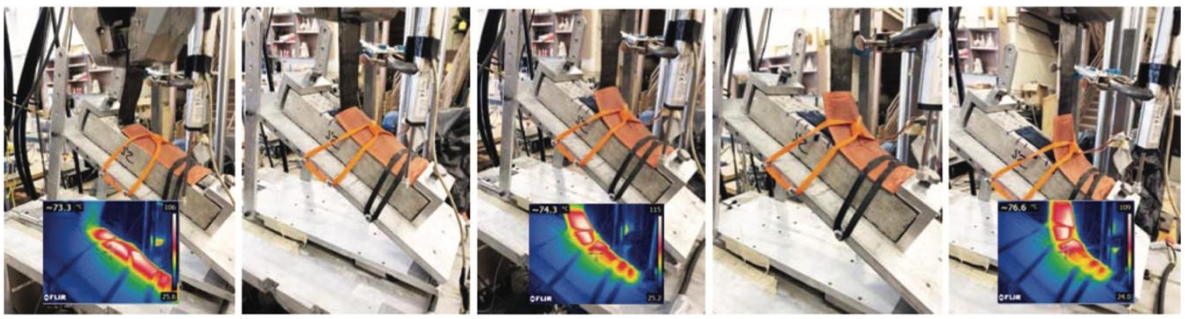

Figure 2.35 - Peeling sequence at 60 degrees angle under 75 degree Celsius (Kim & Horwitz, 2021)

2.5 Analytical modelling of bond at the CFRP-concrete interface

The tension developed in bonded FRP materials is transferred to the concrete substrate primarily through shear stresses in the adhesive. Shear stress-slip relationship therefore becomes an important topic for many researchers (Ueda & Dai, 2005). Many analytical models have been proposed to account for the influence of parameters such as effective bond length, concrete strength, and interfacial fracture

energy on the average shear bond strength or the ultimate shear strength (Blaschko et al., 1998; Chen & Teng, 2001; Holzenkämpfer, 1994; Maeda, 1997; Neubauer & Rostasy, 1997; Täljsten, 1994; Tanaka, 1996; Yoshizawa, 1997; Yuan & Wu, 1999; Yuan et al., 2001). These models are normally based solely on data collected and analysed from experimental work in the literature (empirical), fracture mechanics, or simplified expressions to facilitate design as highlighted in the flowchart below (Figure 2.36).

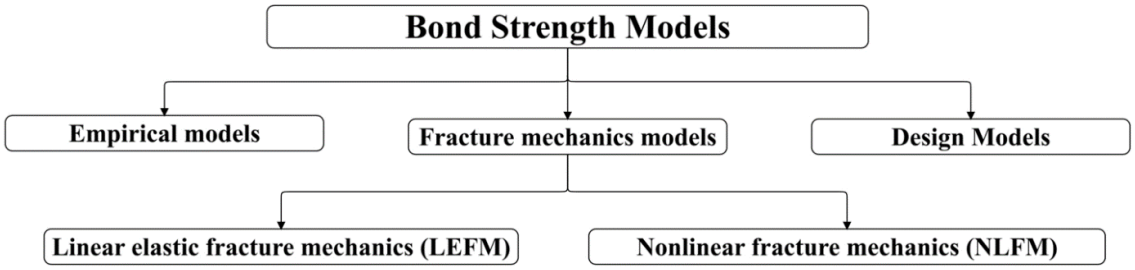

Figure 2.36 - Classification of present shear bond strength model for FRP bonded to concrete

The following subsections will highlight selected bond strength models and their limitations. Most of the fracture mechanics models are based on modified work by Holzenkampfer (Holzenkämpfer, 1994), and a significant difficulty exists in accessing the original work by the authors (in German).

2.5.1 Yoshizawa model

Based on a series of double shear lap tests conducted by Yoshizawa (Yoshizawa, 1997), an empirical expression was proposed that presents a relationship between the full bonded length of the FRP and the average shear stress at failure given by Equation 2.7:

$$\tau_u = 5.88 L_p^{-0.669} \qquad \text{Equation 2.7}$$

In this expression, L_p is the entire bonded length in millimeters and τ_u is the average shear stress in MPa. Yoshizawa's model, however, fails to consider critical parameters that affect bond strength such as the stiffness of the composite, concrete strength, or effective bond length. A similar empirical model that neglects these critical bond parameters was also presented by Tanaka (Tanaka, 1996).

2.5.2 Maeda et al.'s model

Maeda et al. (Maeda, 1997) put forward a more developed empirical model that takes into account the effect of the effective bonded length and the stiffness of the composite. The ultimate force which is given as the product of the average bond strength and the effective bond area is given in Equation 2.8 to Equation 2.10:

$$P_u = \tau_u * b_p L_e \qquad \text{Equation 2.8}$$

$$\tau_u = 11.02 * 10^{-6} E_p t_p \qquad \text{Equation 2.9}$$

$$L_e = e^{6.13 - 0.580 ln E_p t_p} \qquad \text{Equation 2.10}$$

In Equation 2.8 to Equation 2.10, P_u is the ultimate force in Newton, τ_u is the average shear bond strength, b_p is the bonded width, and L_e is the effective bond length beyond which an increase in bond strength is not experienced. E_p and t_p are the modulus of elasticity and thickness of the FRP, respectively.

2.5.3 Blaschko et al.'s model

Based on Holzenkampfer's nonlinear fracture mechanics (NLFM) work, Blaschko at al. presented a modified version of the model that included the effective bond length (Blaschko et al., 1998; Chen & Teng, 2001), given by Equation 2.11:

$$P_u = \begin{cases} 0.78 b_p \sqrt{2 G_f E_p t_p} & if\ L_p \geq L_e \\ 0.78 b_p \sqrt{2 G_f E_p t_p} \frac{L_p}{L_e}\left(2 - \frac{L_p}{L_e}\right) & if\ L_p < L_e \end{cases} \qquad \text{Equation 2.11}$$

The parameters in this fracture mechanics model are defined as those in the previous mentioned empirical equations. Equation 2.11 shows the expression for the ultimate force. The effective bond length L_e in mm, fracture energy G_f ($N.mm/mm^2$), are given in Equation 2.12 and Equation 2.13 and the geometric parameter K_p is presented in Equation 2.14:

$$L_e = \sqrt{\frac{E_p t_p}{4 f_{ctm}}}$$ Equation 2.12

$$G_f = C_f k_p^2 f_{ctm}$$ Equation 2.13

$$k_p = \sqrt{1.125 \frac{2 - b_p/b_c}{1 + b_p/400}}$$ Equation 2.14

In the above equations, f_{ctm} is the average surface tensile strength of the concrete, C_f is a constant derived from linear regression analysis of shear lap tests. b_p and b_c are the width of the bonded composite and the concrete, respectively. This model included many key parameters to predict the shear bond strength between FRP and concrete.

2.5.4 Taljsten's model

Based on Holzenkampfer model and the modified model from Blaschko, Taljsten (Täljsten, 1994), developed a simplified NLFM model (Equation 2.15 and Equation 2.16) that ignored the concept of effective bond length:

$$P_u = \sqrt{\frac{2 E_p t_p G_f}{1 + \alpha_T}} b_p$$ Equation 2.15

$$\alpha_T = \frac{E_p t_p}{E_c t_c}$$ Equation 2.16

2.5.5 Yuan and Wu's model

A model similar to Taljsten's was developed by Yuan and Wu (Yuan & Wu, 1999), which also excluded the concept of effective bond length but did include the effect of geometric parameters such as the width of the composite material and the concrete. The expression for the ultimate bond strength P_u is the same as that presented by Taljsten (Equation 2.15) but the coefficient α_T (Equation 2.17) was adjusted to include the width of the concrete and composite:

$$\alpha_T = \frac{E_p t_p b_p}{E_c t_c b_c}$$ Equation 2.17

2.5.6 Neubauer and Rostasy's model

Neubauer and Rostasy (Neubauer & Rostasy, 1997) developed a NLFM model that did not take into account the width of the concrete in formulating the expression for the maximum bond strength given by Equation 2.18 to Equation 2.20:

$$P_u \begin{cases} 0.64 K_P b_p \sqrt{E_p t_p f_{ctm}} & if\ L \geq L_e \\ 0.64 K_P b_p \sqrt{2 G_p E_p t_p f_{ctm}} \frac{L}{L_e}\left(2 - \frac{L}{L_e}\right) & if\ L < L_e \end{cases}$$ Equation 2.18

$$L_e = \sqrt{\frac{E_p t_p}{2 f_{ctm}}}$$ Equation 2.19

$$G_f = C_f f_{ctm}$$ Equation 2.20

Parameters L_e, G_f, f_{ctm}, E_p, t_p, K_P, b_p are defined as given in previous models.

2.5.7 Chen and Teng's model

Chen and Teng (Chen & Teng, 2001), developed a more simplified practical model to predict the bond strength and effective bond length of FRP-concrete interface. The model accounts for parameters such as the effective bond length, tensile strength of concrete, and geometrical (width) ratio. The ultimate bond strength is given by Equation 2.21. An explanation of the various parameters in this model have been presented in the other highlighted models.

$$P_u = 0.427 \beta_p \beta_L \sqrt{f_c'} b_p L_e$$ Equation 2.21

The width ratio was defined according to Equation 2.22:

$$\beta_p = \sqrt{\frac{2 - b_p/b_c}{1 + b_p/b_c}}$$ Equation 2.22

The coefficient β_L accounts for the ratio of the effective length to the total bonded length.

$$\beta_L = \begin{cases} 1 & if\ L \geq L_e \\ sin\dfrac{\pi L}{2L_e} & if\ L < L_e \end{cases}$$ Equation 2.23

The effective bond length was expressed as given in Equation 2.24:

$$L_e = \sqrt{\frac{E_p t_p}{\sqrt{f_c'}}}$$ Equation 2.24

2.6 Numerical modelling of bond at the CFRP-concrete interface

In recent years, researchers have proposed various numerical modelling procedures to complement experimental investigations and enable the evaluation of different parameters that affect the bond performance between the CFRP and concrete through parametric studies (Arduini et al., 1997; Chansawat et al., 2001; Tedesco et al., 1999). Furthermore, the flexibility of the finite element method means comprehensive studies to predict the failure mechanism of RC members strengthened with CFRP can be conducted within a minimal time and budget. However, numerical modelling of the nonhomogeneous behaviour of concrete in combination with the anisotropic behaviour of the CFRP sheets is a difficult challenge and researchers have disagreed on the best modelling approach. Researchers have simulated concrete elements strengthened with FRP using three main approaches embedded in the various available commercial software such as ABAQUS: the smeared crack approach, discrete crack model, and the concrete damaged plasticity model (CDP).

In the discrete approach, the debonding is modelled as a crack of zero width that propagates along the bond surface. Even though this approach is numerically economical, it requires a prior understanding of the crack path, and besides, interfacial crack propagation rarely occurs (Coronado & Lopez, 2010). This method is ideal for modelling debonding that occurs along the surface formed between two adjacent materials (Coronado, 2006). However, in a more realistic scenario, the crack path during FRP debonding continuously changes direction, and these cracks can propagate within the concrete.

In the smeared crack method, the damage process that occurs during the failure of the laminate-substrate interface is smeared in a band of fixed width (Coronado & Lopez, 2010). Moreover, the orientation of the crack plane is not restricted (Rots & Blaauwendraad, 1989). The material properties such as modulus of elasticity, tensile strength, compressive strength, stress-strain curve, softening curve, and the Poisson ratio of the concrete, epoxy, and FRP are crucial for the accuracy of the finite element analysis. These properties are obtained from a series of material testing. The CDP is a material model embedded in the software that allows users to define the elastic and plastic properties in addition to the damage properties (compression and tension damage) of plain and reinforced concrete.

A detailed review of the literature shows that majority of the numerical analysis work on concrete elements strengthened with CFRP are performed assuming a perfect bond between the concrete and the CFRP sheet or plate which makes it difficult to replicate the debonding failures that are sometimes observed during experimental work (Arduini et al., 1997; Chansawat et al., 2001; Tedesco et al., 1999). Moreover, no literature is available on a single detailed finite element model that could validate multiple experimental loading conditions.

Obaidat et al. (Obaidat et al., 2010) used commercially available finite element model tool Abaqus to highlight the benefits of modelling the interface between the concrete substrate and the CFRP using two different models. The first model assumed a perfect bond between the concrete and the CFRP. However, in the second model, the bond interface was modeled using cohesive zone model. Shown in Figure 2.37 is the simple bilinear relationship used in the cohesive zone model to define the traction-separation. In this bilinear relationship, τ_{max} represents the peak shear stress of the adhesive, k_0 is the local stiffness of the adhesive, δ_0 and δ_f are the opening displacement at peak stress and fracture respectively. G_{cr} is the energy required to open a unit crack (interfacial fracture energy). These numerical models were also used to analyse the effect of bonded length on the ultimate load capacity (Figure 2.38). The numerical simulation results were then validated against experimental work on eight beams presented in (Obaidat et al., 2011).

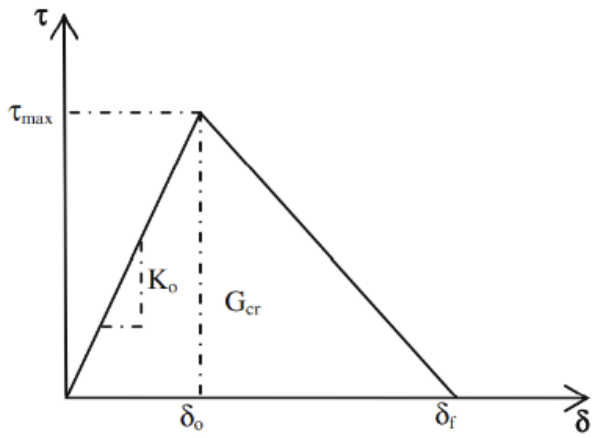

Figure 2.37 - Constitutive law used to define the traction-separation of the adhesive (Obaidat et al., 2010)

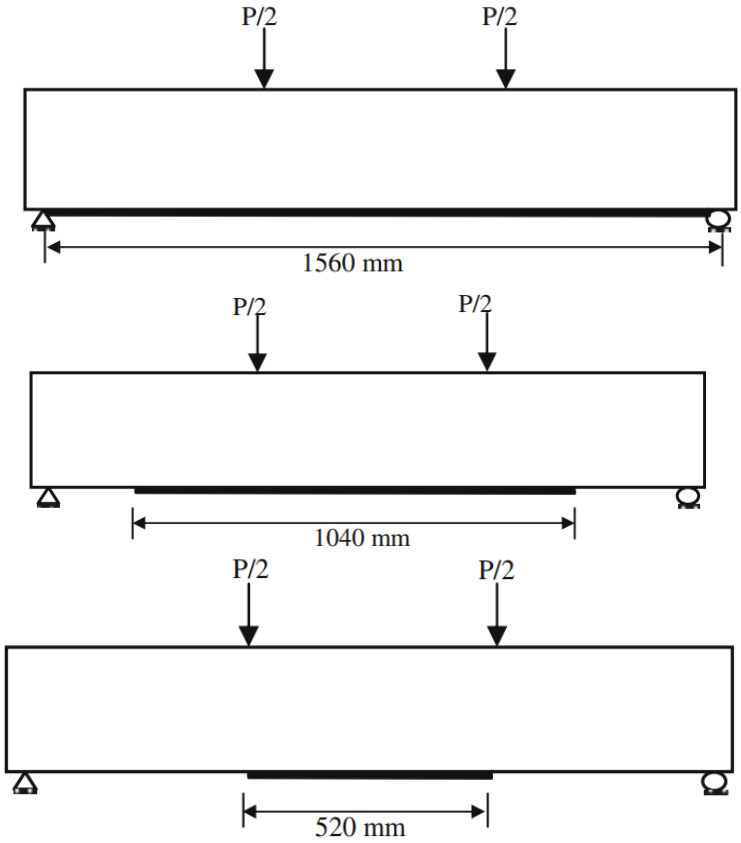

Figure 2.38 - Different bonded length investigated (Obaidat et al., 2010)

In these models, a plastic damage constitutive model was used to model the concrete and elastic-perfectly plastic behaviour was assumed for the steel, while the CFRP was modeled as a linear elastic material. In modelling, 4-node linear tetrahedral elements were used to model all three materials (concrete, internal steel, and CFRP) while a cohesive interface element was used for the adhesive. Due to symmetry, only a quarter of the beam was modeled (Figure 2.39).

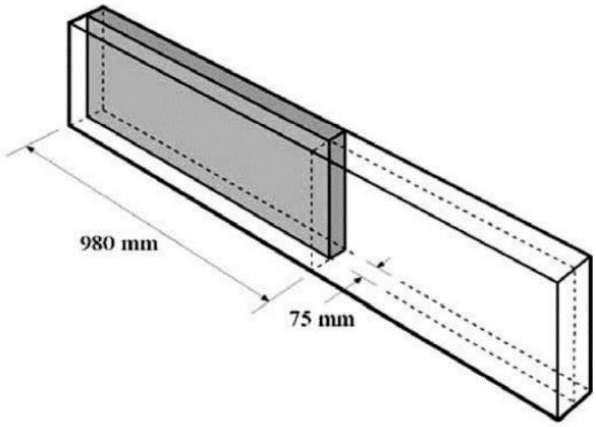

Figure 2.39 - Geometry and meshed elements (Obaidat et al., 2010)

Comparison of finite element results and experimental data showed a good agreement for the control beam (unstrengthened) with a slight overestimation of capacity from the finite element model (Figure 2.40).

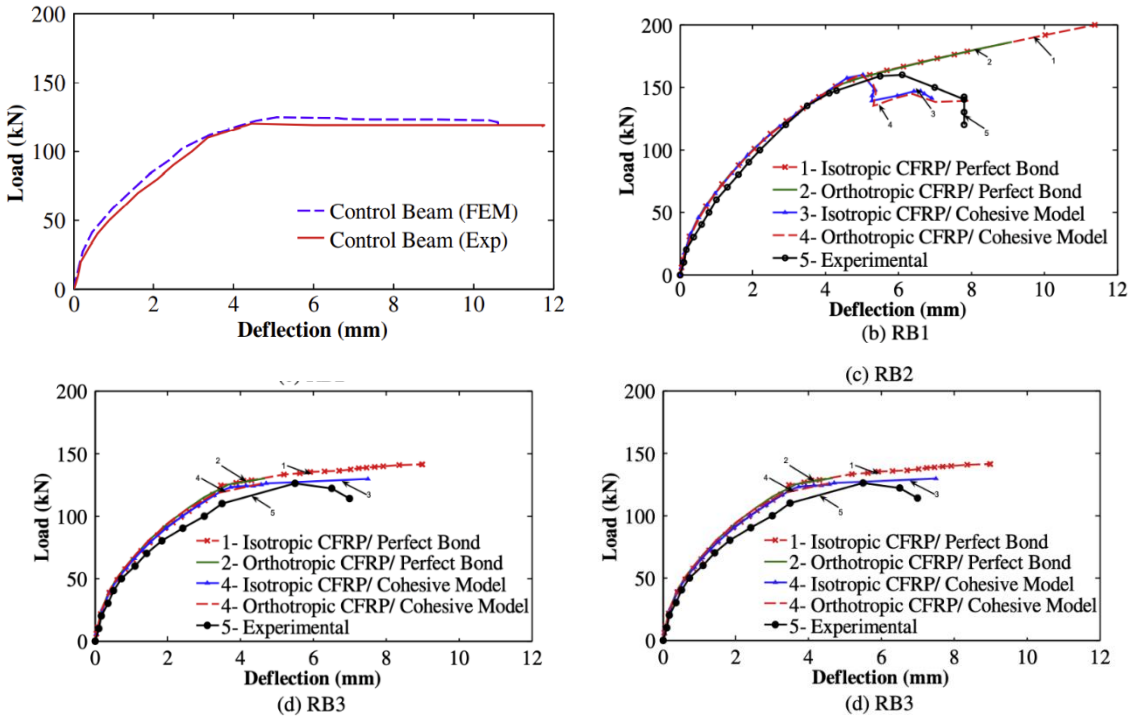

Figure 2.40 - Load-deflection curve for experimental versus FEM (Obaidat et al., 2010)

The authors observed an increase in maximum load with increasing CFRP bond length; however, the effective bond length was not mentioned. In other words, the length beyond which negligible increase in maximum strength is observed was not provided. Regarding the interface model approach the following observations were made:

- Prior to cracking, the cohesive zone model and the perfect bond model showed similar load-deflection behavior.
- The stiffness of the beams was then overestimated after cracking in the perfect bond model and the model failed to capture the softening behavior of the beam.
- The overestimation of the stiffness in the post-cracking phase led to rupture of the CFRP instead of the debonding that was experienced in the experimental work.
- Cohesive zone modeling of the interface gave good agreement with the experimental work.

Besides the more established commercial numerical modeling tools such as ANSYS, ABAQUS, MSC MARC and ADINA, there have been several numerical modeling studies (Gergely et al., 2019; Salgado & Guner, 2019; Wong, 2001) on reinforced concrete members strengthened or repaired with externally bonded CFRP using a University of Toronto in-house 2-dimensional nonlinear finite element tool known as Vector2 (Wong et al., 2013). Vector2 and its complementary software versions (Vector3 to Vector5) are based on theoretical work undertaken by Vecchio and Collins (Vecchio & Collins, 1986). The software incorporates realistic material constitutive models for concrete, steel, and the externally bonded composite material and provides a better approach to model the bond interface between the CFRP and concrete using link and contact elements as the bond elements between the rectangular or triangular element concrete and the CFRP truss elements. These link or contact elements allow the relative slippage between the CFRP and concrete substrate through predefined bond stress-slip models.

Wong (Wong, 2001) used Vector2 to predict the structural response on concrete members strengthened with varying types of composite materials. Inclusion of imperfect bond was achieved using bond elements (link and contact) in combination with different bond stress-slip models (linear elastic and elastic-plastic). The research involved experimental testing of three shear-critical beams externally bonded with CFRP materials at the University of Toronto and the numerical validation of those experimental tests in addition to other experimental programs carried out by other researchers in the literature. The original experimental work of the other researchers validated by Wong's numerical simulations are presented elsewhere in (El-Refaie et al., 2001; Zarnic et al., 1999). The approach of

modeling the CFRP-concrete interface involves creating double nodes in the concrete and CFRP at locations were the CFRP is attached to the concrete element, thereafter a four-node contact element or two node link element is used to define the interface. The bond properties are then applied to the interface while the reinforcement properties are used for the CFRP. It is essential to note that the debonding failure mode is extremely sensitive to the reference points or bond stress-slip constitutive law used in the Vector2 program.

The first set of Wong's FE validation was performed on beams and slabs originally tested by Zarnic et al. (Zarnic et al., 1999). The beams had cross-sectional dimensions 200 mm by 300 mm with a length of 3250 mm and the slabs were 800 mm by 120 mm with identical length as the beams. Table 2.3 shows the various elements used in the modeling and a typical mesh of the strengthened components are shown in Figure 2.41. A perfect bond was assumed for the interaction between the concrete and internal steel. Stirrups were smeared throughout the components.

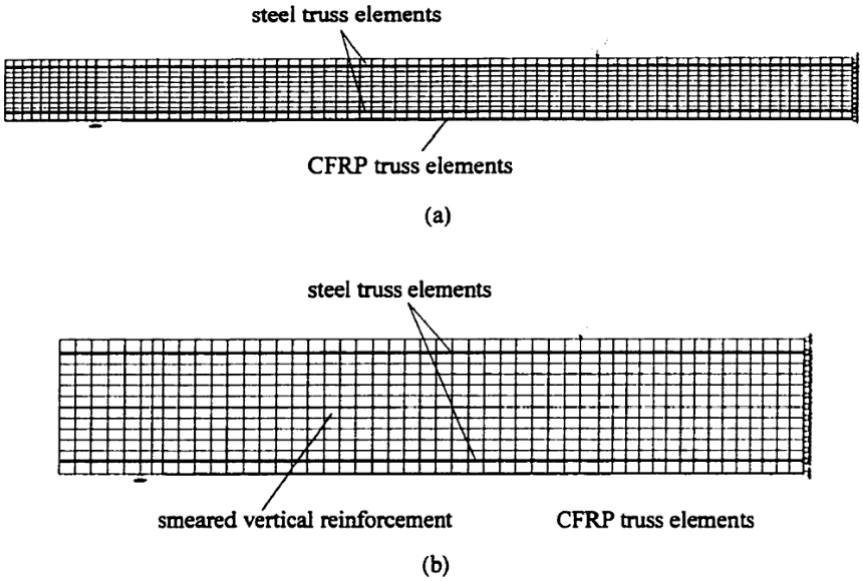

Figure 2.41 - Meshed slab and beam respectively (Zarnic et al., 1999)

From the FE analysis of the different slab models presented in Table 2.4, it was determined that a maximum bond stress-slip value of 3 MPa was optimal in capturing the debonding failure experienced in the experimental work.

Table 2.3- Element used in modelling the Zarnic Beams and Slabs

	Concrete	Internal Steel	CFRP	Bond Interface
Beam	588 Rectangular elements	98 Truss elements	42 Truss elements	43 link or 42 contact
Slab	847 Rectangular elements	154 Truss elements	65 Truss elements	66 link or 65 contact

Table 2.4 - Results obtained for the Zarnic slab modeled (Zarnic et al., 1999)

Bond Element Type	Constitutive Relation	Ultimate bond stress (MPa)	Maximum Load (kN)	Deviation from Exp. Load (%)	Mid-span Deflection at Max. load (mm)	Deviation from Exp. Deflection (%)
Contact	Linear elastic	2.0	55.0	-10.3	38.3	-17.4
		2.5	57.8	-5.72	44.3	-4.58
		3.0	58.2	-5.07	45.5	-1.99
		3.5	64.4	5.04	56.7	22.1
		4.0	65.2	6.35	57.6	24.1
		4.5	65.0	6.02	57.2	23.3
	Elastic-plastic	3.0	75.8	23.6	81.6	75.8
Link	Linear elastic	2.5	56.4	-8.01	44.3	-4.56
		3.0	59.2	-3.44	49.0	5.57
	Elastic-plastic	3.0	73.2	19.4	78.6	69.3
Perfect Bond	NA	NA	81.6	33.1	92.4	99.0

At a bond stress-slip value of 3 MPa a good agreement was observed between the two different bond elements used (contact and link). However, the contact element predicted load capacity and deflections much closer to the experimental value (63 kN) for the linear elastic bond stress-slip assumption. The perfect bond (no slippage) assumption between the concrete and CFRP yielded an overestimated value of 33%. Similar observation was made by the author regarding the beam models where the perfect bond assumption overestimated the ultimate load and deflection by 19% and 66% respectively.

The second model validated by Wong (Wong, 2001) was a set of five continuous beams originally tested at the University of Bradford, United Kingdom, by El-Refaie (El-Refaie et al., 2001). The full-scale beams had cross-sectional dimensions of 150 mm by 250 mm with a length of 8500 mm. The beams were internally reinforced with 4-16 mm diameter rebars evenly distributed at the top compression level and bottom tension region. The model approach for the composite strengthened beams involved the fundamental steps described above in the Zarnic beams/slabs. Due to symmetry in dimensions, loading and support conditions and to reduce computational time, only half of the length of the beam was modeled. Therefore, in the modeled portion, the beam was restrained with vertical rollers in the direction perpendicular to the axis of symmetry. The geometrical detail of the beam is shown in Figure 2.42. The load-deflection curves of the modeled specimens are shown in Figure 2.43. It was observed that using contact or link elements to model the interface between the concrete and CFRP led to almost identical results shown in the negligible differences for the load-displacement behaviour.

A detailed step-by-step approach of Wong's model is available in (Wong, 2001). The author's observations reaffirm the importance of modeling the bond interface to accurately predict the structural response of concrete members externally strengthened with CFRP materials. The work of Wong concluded that while accurate results can be obtained by using link or one-dimensional contact elements, higher order contact elements are generally preferred.

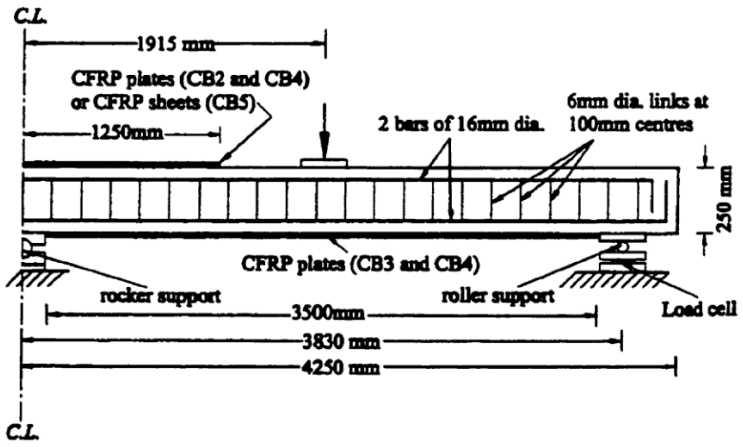

Figure 2.42 - Load and Support condition of the El-Refaie Beams (El-Refaie et al., 2001)

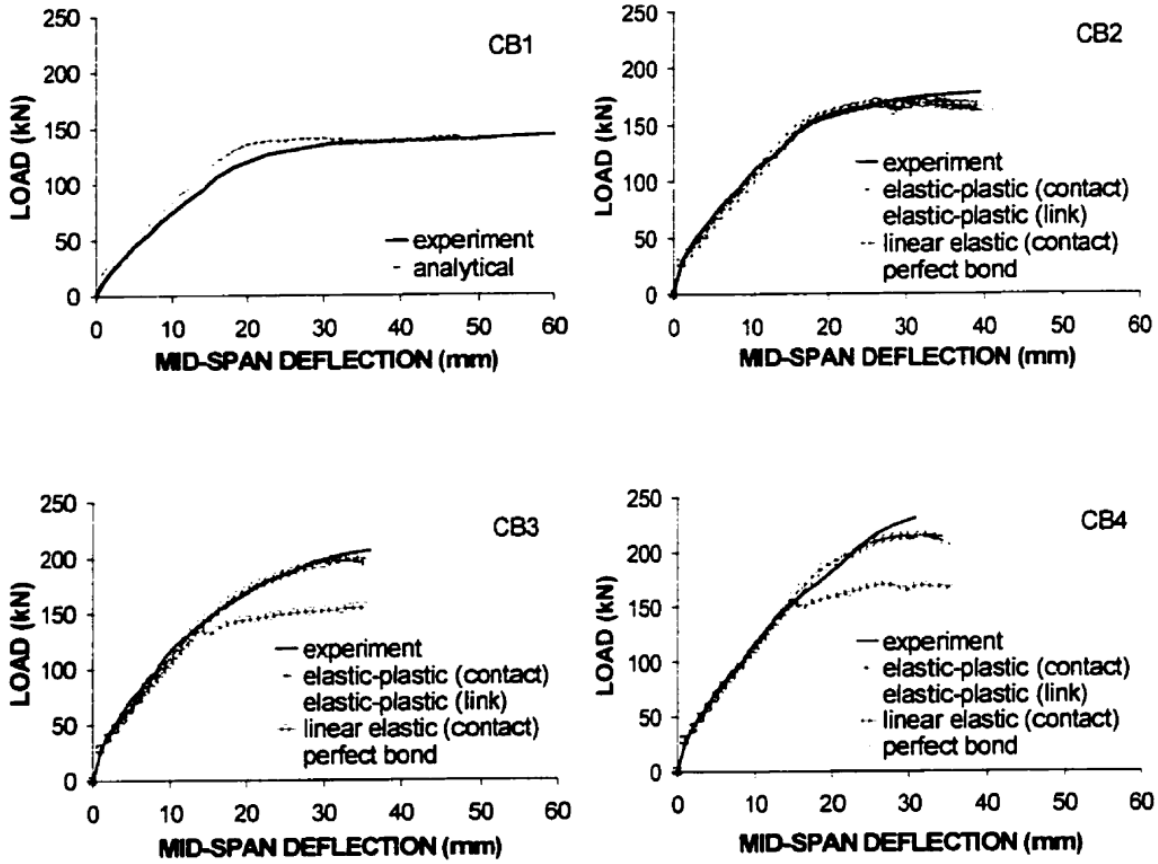

Figure 2.43 - Load-displacement for the FEM analysis of the El-Refaie beams (El-Refaie et al., 2001)

2.7 Summary and research gaps

Research on the bond between externally bonded CFRP and concrete has advanced significantly, especially regarding its application in structural strengthening and repair of bridge infrastructures. The existing literature has primarily concentrated on either the NDT approaches outlined in Section 2.3 or on different types of bond tests discussed in Section 2.4 for evaluating bond integrity. There is a notable deficiency of multilevel studies that integrate various evaluation protocols, including series of NDTs, multi-directional bond tests and numerical simulations and particularly in structural elements built with high-strength concrete.

Over the past few decades, most of the laboratory investigations on the use of externally bonded CFRP have been conducted on sound concrete without considering some of the common deterioration present in existing structures that are subjected to fluctuating environmental conditions during service. The interaction between CFRP systems and deteriorated concrete/patch materials remain inadequately addressed within current studies. Real field scenarios, which may include debonded regions of unknown size and location, add complexity to the detection capability of the available NDT techniques (coin tapping or infrared). In addition, laboratory findings often neglect real-world complexities encountered in practice, including the interactions between repair materials used for patching or resurfacing deteriorated concrete and the variability in workmanship, particularly related to installation and curing under cold weather conditions.

Furthermore, structural tests are usually conducted on small samples and correlations between various test setups and between lab and field testing are not available. Accelerated laboratory tests designed to assess how factors such as moisture, humidity, and temperature fluctuations influence the CFRP-concrete bond over time poorly correlates with real-world exposures. This discrepancy necessitates extended field validation, especially for strengthened structures that are exposed to extreme temperatures cycles. The implications of these factors on bond degradation and overall structural performance remain inadequately understood.

The research objectives and research methodology described in Chapter 1 targets the following identified research gaps:

- Characterization of bond performance of field structures externally retrofitted with CFRP
- Lack of literature on testing techniques that mimic realistic loading and failure conditions
- Comprehensive comparison of laboratory and standard field test
- Reliability of results obtained from the standard field (direct tension pull-off) test with laboratory test methods
- Results correlation remains a challenge. Limited research is available on how the deterioration of the bond line affects bond performance in real-world structures.
- Numerical simulations assuming perfect bond is a common practice in the literature but is not always appropriate especially when assessing the bond between deteriorated concrete and CFRP systems.
- Most significantly, a single multi-stage approach that includes destructive and non-destructive testing, microanalysis, numerical simulation is absent in the literature for both laboratory specimen and field structures.

The comprehensive interdisciplinary work proposed herein aims to provide robust data to address the above-mentioned limitations in the field of externally bonded CFRP for retrofitting of concrete bridges.

2.8 References

ACI. (2023b). Guide for the design and construction of externally bonded FRP systems for strengthening concrete structures. In (pp. 1-112).

Afefy, H. M. E.-D., Mahmoud, M. H., & Fawzy, T. M. (2013). Rehabilitation of defected RC stepped beams using CFRP. *Engineering structures*, *49*, 295-305.

Al-Rousan, R., Issa, M., & Shabila, H. (2012). Performance of reinforced concrete slabs strengthened with different types and configurations of CFRP. *Composites Part B: Engineering*, *43*(2), 510-521.

Allen, D. G., & Atadero, R. A. (2012). Evaluating the long-term durability of externally bonded FRP via field assessments. *Journal of composites for construction*, *16*(6), 737-746.

Altin, S., Anil, Ö., Kopraman, Y., & Kara, M. E. (2013). Hysteretic behavior of RC shear walls strengthened with CFRP strips. *Composites Part B: Engineering*, *44*(1), 321-329.

Arduini, M., Di Tommaso, A., & Nanni, A. (1997). Brittle failure in FRP plate and sheet bonded beams. *ACI structural journal*, *94*(4), 363-370.

ASTM. (2004). Standard test method for tensile strength of concrete surfaces and the bond strength or tensile strength of concrete repair and overlay materials by direct tension (pull-off method). In: West Conshohocken PA.

ASTM. (2021b). Standard test method for pull-off strength for FRP laminate systems bonded to concrete substrate. In *ASTM D7522*. West Conshohocken, PA.

ASTMD4541. (2017). Standard test method for pull-off strength of coatings using portable adhesion testers. *ASTM International: West Conshohocken, PA, USA*.

Au, C., & Büyüköztürk, O. (2006). Peel and shear fracture characterization of debonding in FRP plated concrete affected by moisture. *Journal of composites for construction*, *10*(1), 35-47.

Baggio, D., Soudki, K., & Noel, M. (2014). Strengthening of shear critical RC beams with various FRP systems. *Construction and Building Materials*, *66*, 634-644.

Bakht, B., & Mufti, A. A. (1998). Five steel-free bridge deck slabs in Canada. *Structural engineering international*, *8*(3), 196-200.

Banthia, N., Abdolrahimzadeh, A., & Boulfiza, M. (2009). Field assessment of FRP sheets-concrete bond durability. International Conference on Sustainable Built Environment Infrastructures in Developing Countries ENSET Oran (Algeria),

Banthia, N., Abdolrahimzadeh, A., Demers, M., Mufti, A., & Sheikh, S. (2010). Durability of FRP-concrete bond in FRP-strengthened bridges. *Concrete International*, *32*(8), 45-51.

Beydokhti, E. Z., & Shariatmadar, H. (2016). Strengthening and rehabilitation of exterior RC beam–column joints using carbon-FRP jacketing. *Materials and Structures*, *49*(12), 5067-5083.

Blaschko, M., Niedermeier, R., & Zilch, K. (1998). Bond failure modes of flexural members strengthened with FRP. Second International Conference on Composites in InfrastructureNational Science Foundation,

Brown, J., & Fox, T. (2010). Development of a nondestructive evaluation method for FRP bridge decks. Thermosense XXXII,

Brown, J. R., & Hamilton III, H. (2003). NDE of Reinforced Concrete Strengthened with Fiber-Reinforced Polymer Composites using Infrared Thermography. *Proc. InfraMation*, 149-154.

Bukhari, I., Vollum, R., Ahmad, S., & Sagaseta, J. (2010). Shear strengthening of reinforced concrete beams with CFRP. *Magazine of concrete research*, *62*(1), 65-77.

Chansawat, K., Kachlakev, D. I., Miller, T. H., & Yim, S. C. (2001). FEA of the Horsetail Creek Bridge Strengthened with FRP Laminates. INTERNATIONAL SAMPE SYMPOSIUM AND EXHIBITION,

Chataigner, S., Caron, J.-F., Benzarti, K., Quiertant, M., & Aubagnac, C. (2011). Use of a single lap shear test to characterize composite-to-concrete or composite-to-steel bonded interfaces. *Construction and Building Materials*, *25*(2), 468-478.

Chen, J. F., & Teng, J. (2001). Anchorage strength models for FRP and steel plates bonded to concrete. *Journal of Structural Engineering*, *127*(7), 784-791.

Coronado, C. A. (2006). Characterization, modeling and size effect of concrete-epoxy interfaces.

Coronado, C. A., & Lopez, M. M. (2010). Numerical modeling of concrete-FRP debonding using a crack band approach. *Journal of composites for construction*, *14*(1), 11-21.

CSA-Group. (2019). Canadian Highway Bridge Design Code. In *CSA S6:19*.

D'Antino, T., & Pellegrino, C. (2014). Bond between FRP composites and concrete: Assessment of design procedures and analytical models. *Composites Part B: Engineering*, *60*, 440-456.

Dai, J.-G., Ueda, T., Sato, Y., & Hadiyono, J. (2004a). Dowel resistances of bond interfaces between FRP sheets and concrete. Proceedings of the second international conference on FRP composites in civil engineering, Adelaide, Australia,

DAI, J., Ueda, T., & Sato, Y. (2004b). Dowel Effects on Interface Shear Bond Force Transfer in Concrete Beams Strenthened with FRP Sheets. *Proceedings of JCI*, *25*.

de Waal, L., Fernando, D., Cork, R., & Foote, J. (2017). FRP strengthening of 60 year old pre-stressed concrete bridge deck units. *Engineering structures*, *143*, 346-357.

Di Ludovico, M., Prota, A., Manfredi, G., & Cosenza, E. (2010). FRP strengthening of full-scale PC girders. *Journal of composites for construction*, *14*(5), 510-520.

El-Refaie, S., Ashour, A., & Garrity, S. (2001). Strengthening of reinforced concrete continuous beams with CFRP composites. In *Structural Engineering, Mechanics and Computation* (pp. 1591-1598). Elsevier.

Enochsson, O., Lundqvist, J., Täljsten, B., Rusinowski, P., & Olofsson, T. (2007). CFRP strengthened openings in two-way concrete slabs–An experimental and numerical study. *Construction and Building Materials*, *21*(4), 810-826.

Eveslage, T., Aidoo, J., Harries, K. A., & Bro, W. (2010). Effect of variations in practice of ASTM D7522 standard pull-off test for FRP-concrete interfaces. *Journal of Testing and Evaluation*, *38*(4), 424-430.

Fazli, H., Yassin, A. M., Shafiq, N., & Teo, W. (2018). Pull-off testing as an interfacial bond strength assessment of CFRP-concrete interface exposed to a marine environment. *International Journal of Adhesion and Adhesives*, *84*, 335-342.

Fitzwilliam, J., & Bisby, L. A. (2010). Slenderness effects on circular CFRP confined reinforced concrete columns. *Journal of composites for construction*, *14*(3), 280-288.

Fukuyama, H., & Sugano, S. (2000). Japanese seismic rehabilitation of concrete buildings after the Hyogoken-Nanbu Earthquake. *Cement and Concrete Composites*, *22*(1), 59-79.

Galietti, U., Luprano, V., Nenna, S., Spagnolo, L., & Tundo, A. (2007). Non-destructive defect characterization of concrete structures reinforced by means of FRP. *Infrared physics & technology*, *49*(3), 218-223.

Gao, B., Leung, C. K., & Kim, J.-K. (2007). Failure diagrams of FRP strengthened RC beams. *Composite structures*, *77*(4), 493-508.

Georgeson, G. E., Lea, S., & Hansen, J. (1996). Electronic tap hammer for composite damage assessment. Nondestructive Evaluation of Aging Aircraft, Airports, and Aerospace Hardware,

Gergely, V., Pop, M., Campian, C., & Chira, N. (2019). Finite element modelling of different strengthening strategies for reinforced concrete deep beams. IOP Conference Series: Materials Science and Engineering,

Ghosh, K. K., & Karbhari, V. M. (2011b). Use of infrared thermography for quantitative non-destructive evaluation in FRP strengthened bridge systems. *Materials and Structures*, *44*(1), 169-185.

Grace, N. F., Roller, J. J., Navarre, F. C., Nacey, R. B., & Bonus, W. (2004). Load testing a CFRP-reinforced bridge. *Concrete International*, *26*(7), 51-57.

Halabe, U. B., Dutta, S. S., & GangaRao, H. V. (2008). NDE of FRP wrapped columns using infrared thermography. AIP Conference Proceedings,

Halabe, U. B., Joshi, R. M., & GangaRao, H. V. (2020). Nondestructive Testing of FRP Composite Structural Components and FRP Rehabilitated Bridge using Digital Tap Testing. *Journal of Multidisciplinary Engineering Science and Technology (JMEST)*, *7*(1).

Halabe, U. B., Roy, M., Klinkhachorn, P., & GangaRao, H. V. (2006). Detection of Air and Water-Filled Subsurface Defects in GFRP Composite Bridge Decks Using Infrared Thermography. AIP Conference Proceedings,

Halabe, U. B., Vasudevan, A., Klinkhachorn, P., & GangaRao, H. V. (2007). Detection of subsurface defects in fiber reinforced polymer composite bridge decks using digital infrared thermography. *Nondestructive Testing and Evaluation*, *22*(2-3), 155-175.

Hing, C. L. (2006). Nondestructive evaluation of fiber reinforced polymer bridge decks using ground penetrating radar and infrared thermography.

Holzenkämpfer, P. (1994). *Ingenieurmodelle des verbunds geklebter bewehrung für betonbauteile*. IBMB.

Hu, C., Shih, J., Delpak, R., & Tann, D. (2002). Detection of air blisters and crack propagation in FRP strengthened concrete elements using infrared thermography. Inframation-The Thermographer's Conference,

Hutchinson, R., Tadros, G., Kroman, J., & Rizkalla, S. (2003). Use of externally bonded FRP systems for rehabilitation of bridges in Western Canada. *ACI Special Publications*, *215*, 239-248.

Joshi, R. M. (2018). Nondestructive evaluation of FRP composite bridge componenets using infrared thermography and digital tap tesing.

Karbhari, V., Chin, J., Hunston, D., Benmokrane, B., Juska, T., Morgan, R., Lesko, J., Sorathia, U., & Reynaud. (2003). Durability gap analysis for fiber-reinforced polymer composites in civil infrastructure. *Journal of composites for construction*, *7*(3), 238-247.

Karbhari, V., & Engineer, M. (1995). Assessment of interfacial fracture energy between concrete and glass reinforced composites. *Journal of materials science letters*, *14*(17), 1210-1213.

Karbhari, V., & Engineer, M. (1996). Investigation of bond between concrete and composites: use of a peel test. *Journal of Reinforced Plastics and Composites*, *15*(2), 208-227.

Karbhari, V. M., & Ghosh, K. (2009). Comparative durability evaluation of ambient temperature cured externally bonded CFRP and GFRP composite systems for repair of bridges. *Composites part A: Applied science and manufacturing*, *40*(9), 1353-1363.

Kim, Y. J., & Horwitz, C. F. (2021). Out-of-Plane Peeling of Carbon Fiber-Reinforced Polymer-Concrete Interface at Elevated Temperatures. *ACI structural journal*, *118*(3).

Li, P.-D., Zhao, Y., Wu, Y.-F., & Lin, J.-P. (2023). Effect of defects in adhesive layer on the interfacial bond behaviors of externally bonded CFRP-to-concrete joints. *Engineering structures*, *278*, 115495.

Lombard, J., Lau, D. T., Humar, J. L., Foo, S., & Cheung, M. S. (2000). Seismic strengthening and repair of reinforced concrete shear walls. Proc., 12th World Conf. on Earthquake Engineering,

López-González, J. C., Fernández-Gómez, J., & González-Valle, E. (2012). Effect of adhesive thickness and concrete strength on FRP-concrete bonds. *Journal of composites for construction*, *16*(6), 705-711.

Loudon, N., & Bell, B. (2010). FRP strengthening of concrete road and rail bridges in the UK. *Magazine of concrete research*, *62*(4), 243-252.

Maeda, T. (1997). A study on bond mechanism of carbon fiber sheet. *FRPTCS3*, *1*, 279-286.

Mata, O. R., & Atadero, R. A. (2014). Evaluation of pull-off tests as a FRP–concrete bond testing method in the laboratory and field. *Practice Periodical on Structural Design and Construction*, *19*(2), 04014001.

Mazzotti, C., Savoia, M., & Ferracuti, B. (2008). An experimental study on delamination of FRP plates bonded to concrete. *Construction and Building Materials*, *22*(7), 1409-1421.

Meier, U. (1995). Strengthening of structures using carbon fibre/epoxy composites. *Construction and Building Materials*, *9*(6), 341-351.

Miceli, M., Horne, M. R., & Duke Jr, J. C. (2001). Health monitoring of FRP bridge decks. Advanced Nondestructive Evaluation for Structural and Biological Health Monitoring,

Miller, T. C., Chajes, M. J., Mertz, D. R., & Hastings, J. N. (2001). Strengthening of a steel bridge girder using CFRP plates. *Journal of Bridge Engineering*, *6*(6), 514-522.

Mirmiran, A. (2004). *Bonded repair and retrofit of concrete structures using FRP composites: recommended construction specifications and process control manual* (Vol. 514). Transportation Research Board.

Mosallam, A. S., & Mosalam, K. M. (2003). Strengthening of two-way concrete slabs with FRP composite laminates. *Construction and Building Materials*, *17*(1), 43-54.

Moshiri, N., Hosseini, A., & Mostofinejad, D. (2015). Strengthening of RC columns by longitudinal CFRP sheets: Effect of strengthening technique. *Construction and Building Materials*, *79*, 318-325.

Mtenga, P. V., Parzych, J. G., & Limerick, R. (2001). Quality assurance of frp retrofit using infrared thermography. In *Structures 2001: A Structural Engineering Odyssey* (pp. 1-8).

Mukhtar, F. M., & Faysal, R. M. (2018). A review of test methods for studying the FRP-concrete interfacial bond behavior. *Construction and Building Materials*, *169*, 877-887.

Neale, K. (2000). FRPs for structural rehabilitation: a survey of recent progress. *Progress in structural engineering and materials*, *2*(2), 133-138.

Neubauer, U., & Rostasy, F. (1997). Design aspects of concrete structures strengthened with externally bonded CFRP-plates. PROCEEDINGS OF THE SEVENTH INTERNATIONAL CONFERENCE ON STRUCTURAL FAULTS AND REPAIR, 8 JULY 1997. VOLUME 2: CONCRETE AND COMPOSITES,

Noel, M. (2020). *Rehabilitation of Concrete Structures-Lecture 1* (27). University of Ottawa.

Obaidat, Y. T., Heyden, S., & Dahlblom, O. (2010). The effect of CFRP and CFRP/concrete interface models when modelling retrofitted RC beams with FEM. *Composite structures*, *92*(6), 1391-1398.

Obaidat, Y. T., Heyden, S., Dahlblom, O., Abu-Farsakh, G., & Abdel-Jawad, Y. (2011). Retrofitting of reinforced concrete beams using composite laminates. *Construction and Building Materials*, *25*(2), 591-597.

Pallempati, H., Beneberu, E., & Yazdani, N. (2016). Evaluation of external FRP-concrete bond in repaired concrete bridge girders and columns. *Innovative Infrastructure Solutions*, *1*(1), 1-8.

Parvin, A., & Brighton, D. (2014). FRP composites strengthening of concrete columns under various loading conditions. *Polymers*, *6*(4), 1040-1056.

Riad, M. (2017). *Quantitative Non-destructive Evaluation (NDE) of FRP Laminate-Concrete Bond Strength*

Rizkalla, S., & Labossiere, P. (1999). Structural engineering with FRP-in Canada. *Concrete International*, *21*(10), 25-28.

Rots, J. G., & Blaauwendraad, J. (1989). Crack models for concrete, discrete or smeared? Fixed, multi-directional or rotating? *HERON, 34 (1), 1989*.

Salgado, R. A., & Guner, S. (2019). A Numerical Analysis Methodology for the Strengthening of Deep Cap Beams. *Special Publication*, *333*, 1-18.

Sheikh, S. A., & Homam, S. M. (2004). A decade of performance of FRP-repaired concrete structures. Proceedings of the ISIS-SHM 2004 Workshop. Winnipeg, Manitoba, Canada,

Smith, S. T., & Teng, J. (2002). FRP-strengthened RC beams. I: review of debonding strength models. *Engineering structures*, *24*(4), 385-395.

Soudki, K., El-Sayed, A. K., & Vanzwol, T. (2012). Strengthening of concrete slab-column connections using CFRP strips. *Journal of King Saud University-Engineering Sciences*, *24*(1), 25-33.

Stantec. (2018). *Rapport d'inspection 2018 – Volume 1 : Inspection annuelle des sections 5 et 7 – Version finale* (0309098564). 3549).

Starnes, M. A., Carino, N. J., & Kausel, E. A. (2003). Preliminary thermography studies for quality control of concrete structures strengthened with fiber-reinforced polymer composites. *Journal of materials in Civil Engineering*, *15*(3), 266-273.

Taillade, F., Quiertant, M., Benzarti, K., Dumoulin, J., & Aubagnac, C. (2012). Nondestructive Evaluation of FRP Strengthening Systems Bonded on RC Structures Using Pulsed Stimulated Infrared Thermography, In: Infrared Thermography, Chapter 9. In: InTech.

Täljsten, B. (1994). *Plate bonding: Strengthening of existing concrete structures with epoxy bonded plates of steel or fibre reinforced plastics* Luleå tekniska universitet].

Täljsten, B. (2003). Strengthening concrete beams for shear with CFRP sheets. *Construction and Building Materials*, *17*(1), 15-26.

Tanaka, T. (1996). Shear resisting mechanism of reinforced concrete beams with CFS as shear reinforcement. *Graduation Thesis, Hokkaido University, Japan*.

Tashan, J., & Al-Mahaidi, R. (2012). Investigation of the parameters that influence the accuracy of bond defect detection in CFRP bonded specimens using IR thermography. *Composite structures*, *94*(2), 519-531.

Tashan, J., & Al-Mahaidi, R. (2014). Detection of cracks in concrete strengthened with CFRP systems using infra-red thermography. *Composites Part B: Engineering*, *64*, 116-125.

Tavakkolizadeh, M., & Saadatmanesh, H. (2003). Strengthening of steel-concrete composite girders using carbon fiber reinforced polymers sheets. *Journal of Structural Engineering*, *129*(1), 30-40.

Tedesco, J. W., Stallings, J. M., & El-Mihilmy, M. (1999). Finite element method analysis of a concrete bridge repaired with fiber reinforced plastic laminates. *Computers & structures*, *72*(1-3), 379-407.

Telang, N. M. (2006). *Field inspection of in-service FRP bridge decks* (Vol. 564). Transportation Research Board.

Teng, J., & Chen, J. (2007). Debonding failures of RC beams strengthened with externally bonded FRP reinforcement: behaviour and modelling. Proceedings of the first Asia-Pacific conference on FRP in structures (APFIS 2007),

Ueda, T., & Dai, J. (2005). Interface bond between FRP sheets and concrete substrates: properties, numerical modeling and roles in member behaviour. *Progress in structural engineering and materials*, *7*(1), 27-43.

Valluzzi, M., Grinzato, E., Pellegrino, C., & Modena, C. (2009b). IR thermography for interface analysis of FRP laminates externally bonded to RC beams. *Materials and Structures*, *42*(1), 25-34.

Vecchio, F. J., & Collins, M. P. (1986). The modified compression-field theory for reinforced concrete elements subjected to shear. *ACI J.*, *83*(2), 219-231.

Wong, P., Vecchio, F., & Trommels, H. (2013). Vector2 & Formworks user's manual second edition. *University of Toronto, Canada*.

Wong, R. S. Y. (2001). *Towards modelling of reinforced concrete members with externally-bonded fibre reinforced polymer, FRP, composites*

Woods, J., Lau, D. T., Bao, X., & Li, W. (2017). Measuring strain fields in FRP strengthened RC shear walls using a distributed fiber optic sensor. *Engineering structures*, *152*, 359-369.

WU, Z., ASAKURA, T., YOSHIZAWA, H., YUAN, H., KOBAYASHI, A., & TAKAHASHI, T. (2000). EXPERIMENTAL AND ANALYTICAL STUDIES ON PEELING BEHAVIOR AND SPALLING RESISTANCE EFFECT OF EXTERNALLY BONDED CONTINUOUS FIBER SHEETS. *Doboku Gakkai Ronbunshu*, *2000*(662), 45-58.

Wu, Z., & Niu, H. (2000). Study on debonding failure load of RC beams strengthened with FRP sheets. *Journal of Structural Engineering*, *46*(3), 1431-1441.

Wu, Z., Wang, X., & Iwashita, K. (2007). State-of-the-art of advanced FRP applications in civil infrastructure in Japan. *Composites and Polycon*, *37*, 1-17.

Wu, Z., Yuan, H., Asakura, T., Yoshizawa, H., Kobayashi, A., Kojima, Y., & Ahmed, E. (2005a). Peeling behavior and spalling resistance of bonded bidirectional fiber reinforced polymer sheets. *Journal of composites for construction*, *9*(3), 214-226.

Wu, Z., Yuan, H., Kojima, Y., & Ahmed, E. (2005b). Experimental and analytical studies on peeling and spalling resistance of unidirectional FRP sheets bonded to concrete. *Composites science and technology*, *65*(7-8), 1088-1097.

Xie, M., & Karbhari, V. M. (1997). Peel test for characterization of polymer composite/concrete interface. *Journal of composite materials*, *31*(18), 1806-1825.

Yao, J., Teng, J., & Chen, J. F. (2005). Experimental study on FRP-to-concrete bonded joints. *Composites Part B: Engineering*, *36*(2), 99-113.

Yoshizawa, H. (1997). Analysis of debonding fracture properties of CFS strengthened RC member subject to tension. Non-Metallic (FRP) Reinforcement for Concrete Structures, Proc. 3rd Intern. Symp.,

Yuan, H., & Wu, Z. (1999). Interfacial fracture theory in structures strengthened with composite of continuous fiber. Proc., Symp. Of China and Japan: Sci. and Technol. of 21st Century, Tokyo, Sept,

Yuan, H., Wu, Z., & Yoshizawa, H. (2001). Theoretical solutions on interfacial stress transfer of externally bonded steel/composite laminates. *Doboku Gakkai Ronbunshu*, *2001*(675), 27-39.

Yumnam, M., Gupta, H., Ghosh, D., & Jaganathan, J. (2021). Inspection of concrete structures externally reinforced with FRP composites using active infrared thermography: A review. *Construction and Building Materials*, *310*, 125265.

Zarnic, R., Gostic, S., Bosiljkov, V., & Bokan-Bosiljkov, V. (1999). Improvement of bending load-bearing capacity by externally bonded plates. *Proc., CREATING WITH CONCRETE, Thomas Telford, London*, 433-442.

Chapter 3 – Mechanical properties of materials

3.1 Introduction

Due to the lack of detailed records regarding the as-is mechanical properties of the various materials, a series of tests were conducted prior to the bond tests described in Chapters 5 and 6 to assess the material properties of the bridge diaphragms. These material properties were used in both analytical calculations (involving either bond stresses, limiting debonding strains or effective bond lengths) and finite element numerical simulations of bond tests conducted on the bridge elements. Three concrete cores were extracted to evaluate the compressive strength of the concrete. In addition, 36 CFRP coupons were collected. All tests were performed under static loading conditions in accordance with standard testing methods established by the American Society for Testing and Materials (ASTM).

Due to the thin thickness of the patch material (5-10 mm) and the presence of multiple cracks in regions of the diaphragm soffits with thicker mortar, the mechanical properties of the patch mortar under uniaxial tension and compression could not be directly examined in this study (Figure 3.1).

Figure 3.1-Cracks in patch materials

3.2 Material testing

3.2.1 Concrete

Three concrete cylindrical cores extracted were tested in compression following ASTM C39 (ASTM, 2021a) to obtain the compressive of the diaphragms (Figure 3.2).

Figure 3.2-Concrete cores extracted from Diaphragm #1

The average diameter of the three cylinders was 95 mm, and the height was 200 mm.

3.2.2 CFRP coupons

To evaluate the CFRP material's mechanical properties, 36 coupon samples were extracted from Diaphragm #1. Eighteen coupons were tested following ASTM D3039 (ASTM, 2017) to determine the tensile properties of the composite materials, four of which exhibited desirable failure modes and were used to determine the material properties. These samples were carefully extracted using an angular grinder, mallet, and concrete chisels, taking care not to damage the CFRP itself (Figure 3.3). Extracted samples were cut into coupons of 300 mm in length by approximately 25.4 mm in width. Before testing, 6-mm thick aluminum tabs with bevel ends were designed, ground, and bonded to the coupons for even stress distribution and minimizing stress concentrations over the grip region (Figure 3.4).

To minimized damage to the final 300 mm coupon samples, the extracted CFRP was longer than the required 300 mm length (see Figure 3.3). Gentle scoring was done on the marked areas where the CFRP coupon was to be cut, and aggressive cutting methods were avoided. No heat was used during this process to prevent damage to the adhesive. Any concrete residue on the extracted CFRP strips at the bond line were carefully removed with an angle grinder and sandpaper before attaching the 6 mm aluminum tabs to the ends of the coupons.

An electrical resistance strain gauge was installed at mid-height on one side of the samples (flat surface obtained after grinding of bond line) while the other surface was speckled for digital image correlation. A universal testing machine operating at 2 mm/min was used to complete the coupon tests.

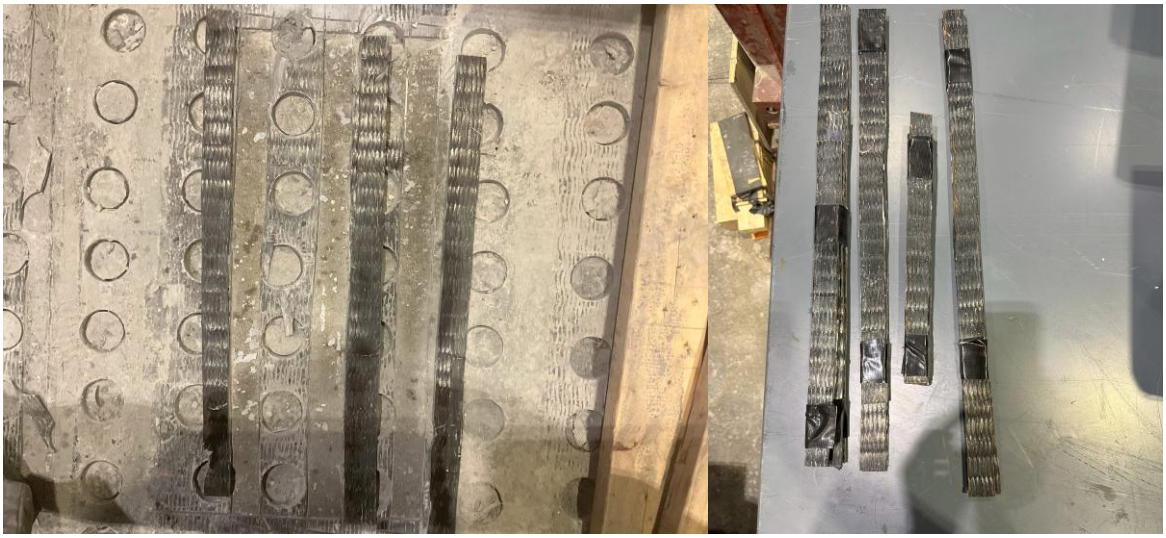

Figure 3.3-Extraction of CFRP coupon from bridge diaphragm

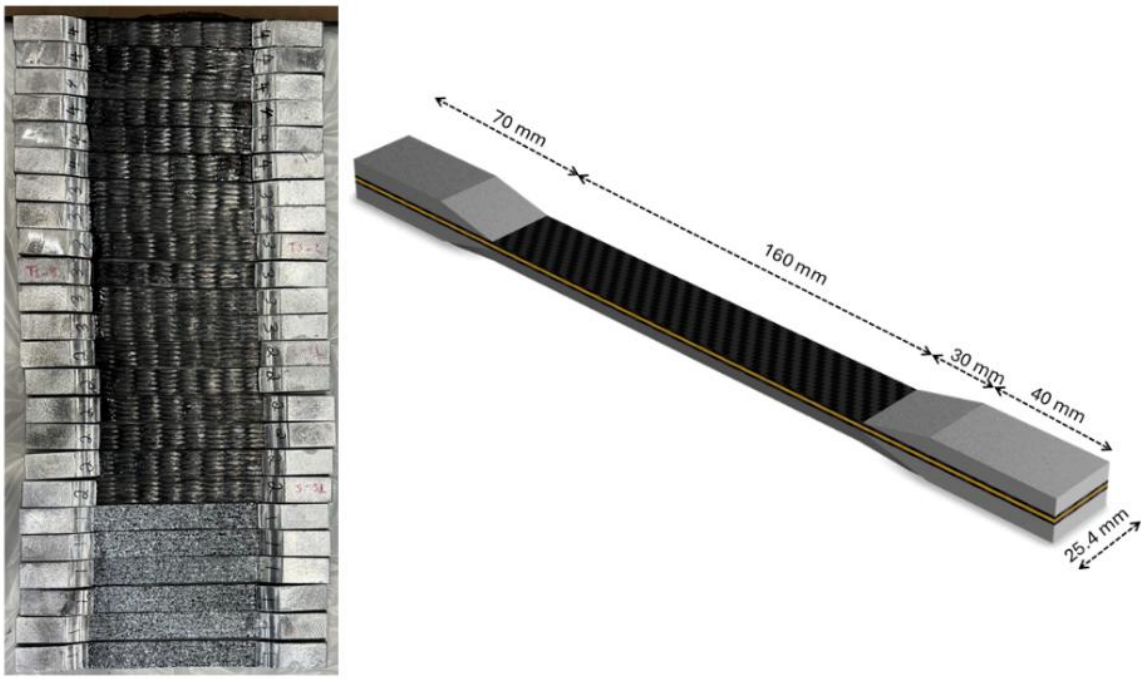

Figure 3.4-Extracted samples and coupon dimensions

3.3 Results

3.3.1 Concrete

The compressive strength of the underlying concrete substrate obtained from the average of the three core samples (77.7 MPa, 75.0 MPa and 74.9 MPa) was 75.9 MPa (standard deviation of 1.30 MPa), and the estimated cracking strength of the concrete obtained is 3.48 MPa (CSA-Group, 2019).

3.3.2 CFRP coupons

Table 3.1 and Figure 3.5 present the experimentally determined material properties of the double-layered CFRP sheets. The manufacturer design properties for a single layer with a thickness value of 1.7 mm per layer are as follows: the tensile strength, modulus of elasticity and elongation at break are 855 MPa, 49.6 GPa, and 1.7%, respectively.

The discrepancy between the measured tensile strength of the CFRP coupons extracted from the deconstructed bridge elements and the design values provided by the manufacturer can be attributed to potential premature failure due to misalignment of test setup (grips). This angular deviation between the coupon and tensile axis of the machine induces unintended transverse stresses. In additional, harsh environmental conditions experienced by the structure during its service life could possibly be a secondary contributing factor. As discussed in Chapter 4, the potential for microcracks along the fiber direction, which were observed during the condition assessment, can contribute to reduced performance characteristics. In addition, if the bond between the individual fibers is compromised as a result of exposure to humidity, freeze-thaw cycles, moisture or subzero temperatures during initial curing, then a misalignment of fibers can adversely affect the reported tensile strength in addition to imperfection accumulated over the installation process. However, it is essential to recognize that the performance of the CFRP-concrete interface, which is the primary focus of this comprehensive research, depends more significantly on the adhesive properties between the CFRP and the concrete than on the tensile strength of the CFRP itself.

Considering the extent of deterioration in the 60-year-old concrete, failures in bond tests, as described in subsequent chapters, predominantly manifested as debonding rather than CFRP rupture. This

indicates that the behaviour of the adhesive is critical, suggesting that the tensile strength of the CFRP is not a significant factor in bond performance. In other words, the mechanism of load transfer observed in the debonding process is largely determined by bond strength rather than the ultimate tensile strength of the CFRP. Once the bond fails, the CFRP loses its efficacy, independent of its material properties.

It is also important to note that current engineering design considerations are focused on bonding conditions, knowing that a strong interface can mitigate the overall reliance on the tensile properties of the CFRP. Bond-slip models as will be discussed in Chapter 5 prioritize interfacial shear stress and concrete properties over CFRP tensile strength.

Table 3.1-Double-layer CFRP sheet properties (as-is)

	Coupon 1	Coupon 2	Coupon 3	Coupon 4	Average Values	Standard Deviation
Tensile strength (MPa)	542.4	556.8	588.2	642.0	582.4	38.2
Elongation at break (%)	0.93	1.17	1.31	1.03	1.11	0.15
Modulus of elasticity (GPa)	56.13	49.64	50.29	50.14	51.55	2.65
Length (mm)	300	300	300	300	300	-
Width (mm)	25.4	25.4	25.4	25.4	25.4	-
Thickness (mm)	3.68	3.56	3.39	3.29	3.48	0.15

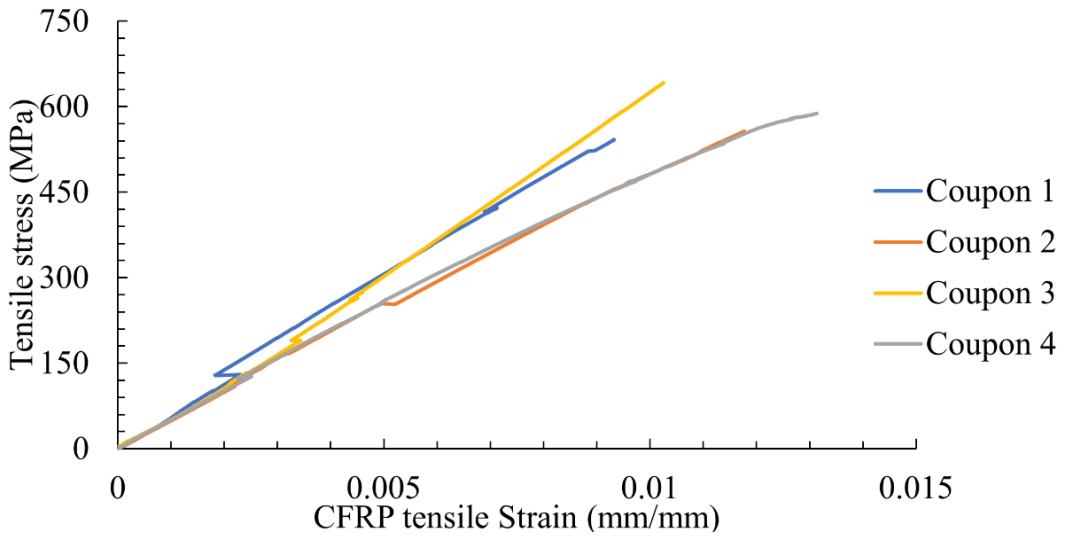

Figure 3.5-Stress-strain curves for unidirectional coupons

3.4 Summary

This chapter presented the mechanical material properties of the different materials (concrete and CFRP) from the extracted bridge diaphragm. These material properties served as essential input parameters for the calibration and validation of the finite element models of the experimental tests.

3.5 References

ASTM. (2017). Standard Test Method Tensile Properties of Polymer Composite Materials. In *ASTM D3039*. West Conshohocken, PA: ASTM.

ASTM. (2021a). Standard Test Method for Compressive Strength of Cylindrical Concrete Specimens. In *ASTM C39*. West Conshohocken, PA.

CSA-Group. (2019). Canadian Highway Bridge Design Code. In *CSA S6:19*.

Chapter 4 - Condition assessment through non-destructive and semi-destructive testing[1]

4.1 Abstract

Externally bonded fiber-reinforced polymer (FRP) composites have been widely adopted for the rehabilitation of aging bridge infrastructure in recent decades. The major reasons for the utilization of these materials in bridge rehabilitation include strength, durability, lightweight nature, design flexibility, and quick installation. However, deterioration of the bonded interface between the concrete substrate and the FRP—or between individual layers of a multi-layer composite—can significantly impact the structural performance of the strengthened member or system. Thus, it is necessary to evaluate the effectiveness and accuracy of condition assessment techniques to ensure satisfactory performance over the intended service life of the structure. This paper presents a visual inspection and detailed assessment of three full-size diaphragms from the Champlain Bridge in Canada. The diaphragms were strengthened with externally bonded CFRP sheets five years before the bridge was decommissioned as a result of extensive degradation after 57 years in service. The condition assessment includes non-destructive (acoustic tapping and infrared thermography) and semi-destructive (direct pull-off) testing to identify surface and subsurface issues including CFRP delamination, material incompatibility, discoloration due to corrosion, inter-fiber cracks, and fundamental problems arising from the construction of the bridge diaphragms and installation of the CFRP. Results of 490 pull-off tests, comprising the largest single database of its kind to-date, generally confirmed the results of non-destructive tests which aimed to locate hidden defects behind the strengthening layers. Microscopy of failed surfaces provide additional insights into the condition of the bond line in defective regions.

[1] A version of this chapter has been published as: Issa Fowai, Martin Noël, Beatriz Martín-Pérez, Leandro Sanchez (2024). *Assessment of CFRP-concrete interface integrity of Original Champlain Bridge diaphragms through non-destructive and semi-destructive testing*. Journal of Composites for Construction, Special collection CICE 2023 (invited paper). https://doi.org/10.1061/JCCOF2.CCENG-4698

4.2 Practical Applications

Premature deterioration of bridges is one of the critical challenges faced by the engineering sector in Canada. One such structure is the Original Champlain Bridge in Montreal, which exhibited signs of significant damage to structural components including the girders, deck, diaphragms, and foundation elements. Following a series of extensive but ultimately unsuccessful rehabilitative measures, the historic Champlain Bridge was eventually replaced at a cost to taxpayers of over $4 billion (CAD). The primary goal of this study is to investigate and understand the performance and integrity of the CFRP strengthening technique applied to three diaphragms in the bridge through various non-destructive and semi-destructive methods.

Even though CFRP are commonly used to strengthen bridges globally, comprehensive studies on their long-term bond performance are lacking from the literature. This paper presents findings from an assessment of the condition of the CFRP strengthening system using visual inspections and non-destructive testing (NDT), followed by semi-destructive direct tension pull off tests on one diaphragm. The outcomes of this work will be beneficial in understanding the advantages and limitations of various NDT techniques for assessing damage in critical concrete members strengthened with CFRP.

4.3 Introduction

Bridges are highly complex transportation infrastructure that require proper maintenance and regular inspections to prevent premature deterioration and unnecessary repairs, particularly in aggressive environments. Even with strict construction and prioritized, planned maintenance practices, bridges are expected to experience time-dependent deterioration from various factors such as corrosion of internal steel reinforcement, environmental conditions (multiple freeze-thaw cycles, humidity, and chemical attacks), overloading, and design flaws. In Canada alone, the Canadian Infrastructure Report Card (CIRC) estimated that the extrapolated replacement cost of bridges exhibiting signs of deterioration and deficiencies was $37 billion in 2016 (Infrastructure, 2016). Thus, immediate rehabilitative interventions are crucial to mitigate further deterioration and ensure the longevity of these structures.

Traditional retrofitting schemes such as concrete section enlargement, externally bonded steel plates, or external post-tensioning are often impractical due to the added self-weight or need for mechanical anchorages that can compromise the integrity of the concrete substrate (Obaidat et al., 2011). Externally bonded carbon fiber-reinforced polymer (CFRP) sheets are an attractive solution with proven durability in harsh environmental conditions and have a negligible effect on member size or weight (Benzarti et al., 2011; Fazli et al., 2018; Green et al., 2000; Hao et al., 2024; Karbhari & Ghosh, 2009; Mikami et al., 2015) In addition, the retrofitting process can be completed with minimal or no disruptions to the service flow (traffic). Many of these CFRP retrofitting works are undertaken to increase the shear and flexural capacity of deteriorated bridge elements (Obaidat et al., 2011). In these bond-critical applications, the efficiency of the rehabilitation—which depends on the proper transfer of stresses between the CFRP composite material and the concrete substrate—is governed by the behavior of the CFRP-concrete interface and the properties of the concrete cover (Karbhari & Ghosh, 2009). CFRP sheets are typically installed using the wet lay-up technique, which is a manual and multi-stage process with the inherent capability of introducing defects in the form of voids and pores at the various stages of work. Additionally, while in service, the externally bonded CFRP materials may also be exposed to fluctuating moisture levels and harsh temperature cycles that can potentially reduce their durability and degrade the CFRP-concrete bond (Hao et al., 2024). Furthermore, in these externally bonded applications, the ongoing deterioration of the underlying concrete and at the CFRP-concrete interface is hidden behind the CFRP layer, effectively masking any visual warning signs of potential structural failure (Fowai et al., 2023b).

Most studies on the long-term durability of CFRP retrofits are conducted in laboratory settings with small-scale samples subjected to highly aggressive exposure conditions to achieve accelerated deterioration, while field data on major structural elements under the synergistic effect of fluctuating environmental conditions and service loads are limited (Fowai et al., 2022; Ghosh & Karbhari, 2011a; Halabe et al., 2006; Harries & Sweriduk, 2016; Milev & Tatar, 2023; Tatar & Brenkus, 2021). Similarly, most research studies investigating the damage assessment of internal defects have been conducted on

sound concrete with artificial defects in the laboratory (Brown & Hamilton III, 2003; Galietti et al., 2007; Ghosh & Karbhari, 2011b; Halabe, 2013; Mac et al., 2020; Mtenga et al., 2001; Starnes et al., 2003; Valluzzi et al., 2009a; Yumnam et al., 2021). However, actual field conditions, including pre-existing damage, presence of surface patch materials, and debonded regions of unknown size, location, and depth add complexity to the detection capability of available non-destructive testing (NDT) techniques. Thus, comprehensive studies on the long-term performance of the CFRP-concrete interface in externally strengthened field structures are needed to ensure a long-lasting solution for aging infrastructure.

Previous studies report that the presence of defects (surface and subsurface damage or voids) plays a vital role in the overall durability performance of the bond between externally bonded FRP and concrete in composite retrofitted concrete structures (Büyüköztürk et al., 2013; Cawley & Adams, 1989; Ghosh et al., 2005; Kaiser & Karbhari, 2004; Kaiser et al., 2004; Malla et al., 2023; Milev & Tatar, 2023; Tatar & Brenkus, 2021). Identifying and characterizing these defects and their potential effects on FRP-retrofitted concrete members was the subject of an in-depth discussion provided by (Ghosh et al., 2005). The study concluded that the classification of defects should be based on their location, size, and density relative to the overall strengthening area. Defect criticality was assessed based on five classifications: aesthetic, quality control critical, structural performance, short-term durability, and long-term durability. Small voids or surface discontinuities up to 6.4 mm were considered non-serious unless near edges. Defects sized from 6.4 to 32 mm require low-pressure epoxy injection. Minor defects with diameter between 32 and 152 mm should be cut and patched with the same type of FRP, extending at least 25 mm on all sides. Defects larger than 152 mm are critical to structural integrity and may necessitate complete removal and reapplication of the entire FRP system. The authors also suggested that certain defects, such as localized porosity, surface scratches, or single broken fibers have a negligible effect on material properties. The research found that current field methodologies like visual inspection and surface tapping are not sufficient for evaluating rehabilitation schemes. These methods should only be used as initial inspections. Instead, they recommended utilizing alternative techniques like ultrasound, thermography, and shearography as suitable options for future implementation and study. While the

above-mentioned techniques are valuable for assessing the bond between FRP and different substrates, their field application is limited by environmental conditions, accessibility, and equipment mobility. (Cawley & Adams, 1989) conducted a study on defect types and the various NDT techniques for composites and bonded joints and concluded that ultrasonic methods are very sensitive to defect detection in composites; however, the need for expensive probe systems limits their use (Cawley & Adams, 1989).

The condition assessment of retrofitted concrete bridges in most jurisdictions is relatively frequent (biennial) and mainly involves visual inspection (including the review of available engineering documents) and a range of NDT methods that may include low-cost acoustic methods (hammer and coin sounding) or high-quality equipment such as infrared thermographic cameras (Halabe et al., 2020). Evaluation of the NDT data can provide significant insight into the location of the bridge distress and allow for the estimation of the in-plane dimensions (size and shape), orientation, and total debonded area of identified defects. The continuous monitoring of the progression of these identified flaws can indirectly reduce the probability of failure of critical bridge members by prompting timely additional repair interventions. While these NDTs have proven useful in identifying defects, they each possess inherent disadvantages which should be adequately understood (Ghosh et al., 2005). In the condition assessment of multi-layer composite-strengthened elements, for instance, determining the actual location/depth of the weak interface within the different layers is still a limitation for cost-effective NDT techniques.

Several researchers have adopted the semi-destructive pull-off test method to evaluate the bond quality between externally bonded composites and concrete under ambient temperature in the laboratory following accelerated aging tests or in field settings (Allen & Atadero, 2012; Banthia et al., 2010; Benzarti et al., 2011; Harries & Sweriduk, 2016; Milev & Tatar, 2023; Pallempati et al., 2016). In situ, the test has been extensively adopted for quality control as standardized in ASTM D7522 (ASTM, 2021b). Two primary outputs are generated from the test: the tensile bond capacity and failure mode. The failure modes, which are fully described in ASTM D7522 (ASTM, 2021b), can be an adhesive

failure (at the interface), cohesive (within an individual material), or a combination of both (mixed mode). A cohesive failure in the concrete indicates that the bond between the FRP and the concrete substrate is stronger than the tensile capacity of the concrete. However, the acceptable bond strength for current design provisions is quite low, ranging from 1.38 MPa in (ACI, 2023a) to 1.5 MPa (CSA-Group, 2019). Even though the test method is an easily repeatable means of quantifying the bond between the FRP and concrete, available literature discussing the use and reliability of the pull-off test for the assessment of in-service structures is relatively scarce. In most studies, the small number of test samples makes it difficult to confirm the extent and variation of deterioration in the retrofitted member. Furthermore, in some of these studies, the strength of the underlying concrete that ideally controls failure is not provided, and the mode of failure and the number of samples were not specified, which makes the interpretation of results challenging.

Based on an assessment of available literature, it is evident that previous research has not thoroughly investigated the variability of field-applied CFRP-concrete bond strength in service using a large number of pull-off test results, nor correlated these results with NDT methods, visual inspection, and forensic analysis. Data is particularly scarce pertaining to the field performance of repairs applied to large structural members from aging concrete structures, and a detailed comparison of different NDT methods is absent from the literature. This research aims to bridge the gap by providing a comprehensive condition assessment of three deteriorated diaphragms from a Canadian bridge that underwent external strengthening with CFRP five years before the bridge was decommissioned as a result of extensive degradation following 57 years in service. The assessment includes visual inspection, tap testing (acoustic sounding), infrared thermography, and the testing of 490 pull-off specimens—the largest single database of its kind to-date—to assess the integrity and performance of the CFRP-concrete interface. Microanalysis was subsequently performed to gain extensive insights into the condition of the bond line between the concrete and CFRP, as well as between the multiple layers of CFRP sheets.

4.4 Materials and experimental methods

This study includes a detailed visual inspection and NDT assessment of three full-size deteriorated bridge diaphragms, followed by pull-off testing on one of the three diaphragms to validate NDT findings both in bond strength and shift in failure modes, as well as microanalysis of pull-off samples.

4.4.1 Overview of the bridge, environmental exposure, and material details

Section 1.3 provides a detailed overview of the original Champlain bridge, its environment, and the rationale for CFRP retrofitting. The diaphragms under consideration were strengthened in the winter of 2014 (5 years before the decommissioning of the bridge). It is worth noting that cold winter temperatures are not optimal for proper curing of epoxy resins. Figure 4.1 shows the strengthening layout of the three diaphragms; each diaphragm was shear-strengthened with six double-layer vertical

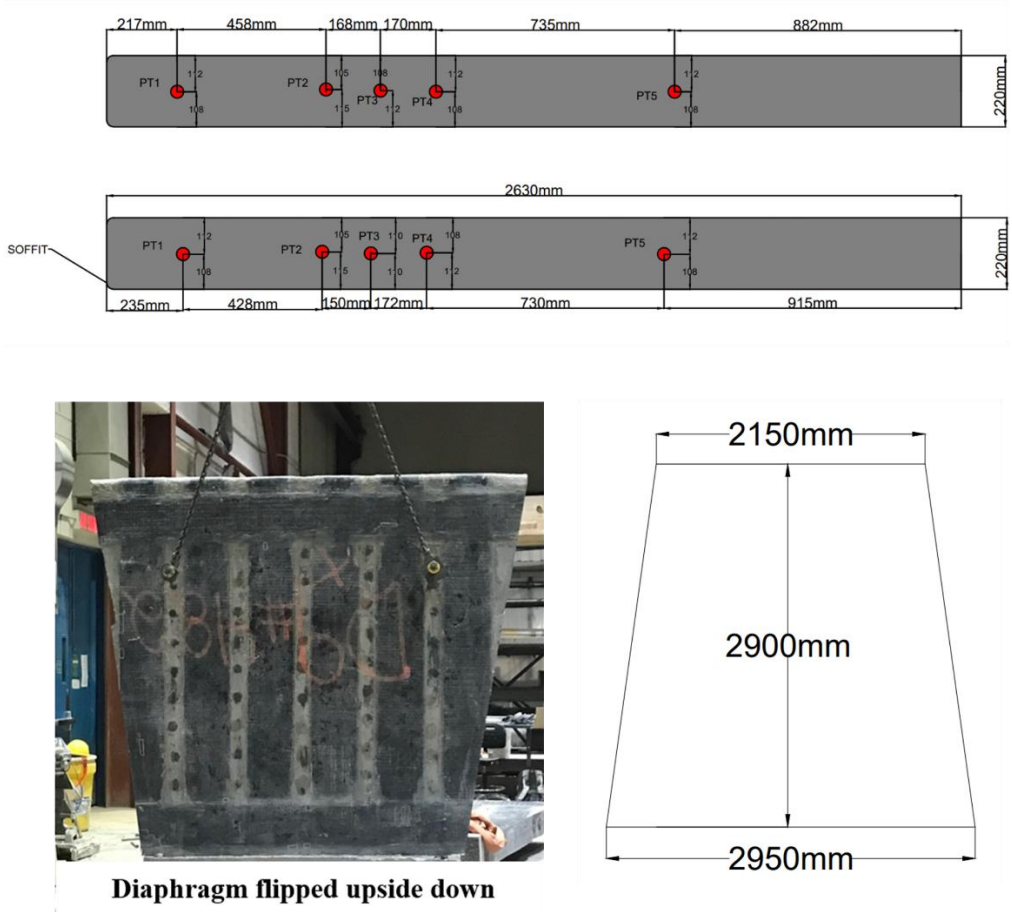

Figure 4.1-As-is geometrical dimensions of diaphragms a) Tendon spacing side view b) Plan view

CFRP strips (in a U-wrap configuration) with a width of approximately 305 mm and spaces between each strip ranging from 135 mm to 150 mm. Additionally, two double-layer horizontal strips were installed as anchorages at the bottom (a few millimetres from the soffit) and the top of the diaphragms to prevent premature debonding of the vertical U-wraps. CFRP coupons were extracted for material testing; the thickness of the coupons (two layers) ranged from 3.2 mm to 3.5 mm.

4.4.2 Non-destructive testing methods and equipment

Visual inspection was the first step in the condition assessment for each element. The visual inspection aimed at verifying the as-is geometrical dimensions and reinforcement locations, as well as identifying external signs of deterioration. All surfaces of each diaphragm were thoroughly examined to identify size, shape, and texture of surface anomalies. Two 50-mm diameter holes were drilled approximately 750 mm from the soffit of the diaphragms in the concrete strip to facilitate lifting and flipping of the 4-ton concrete diaphragms by an overhead crane (Figure 4.1). Following the visual inspection, a conventional coin tapping approach was used to locate subsurface anomalies. The procedure involved using a coin to impact the surface of the CFRP wraps on the diaphragms (Figure 4.2).

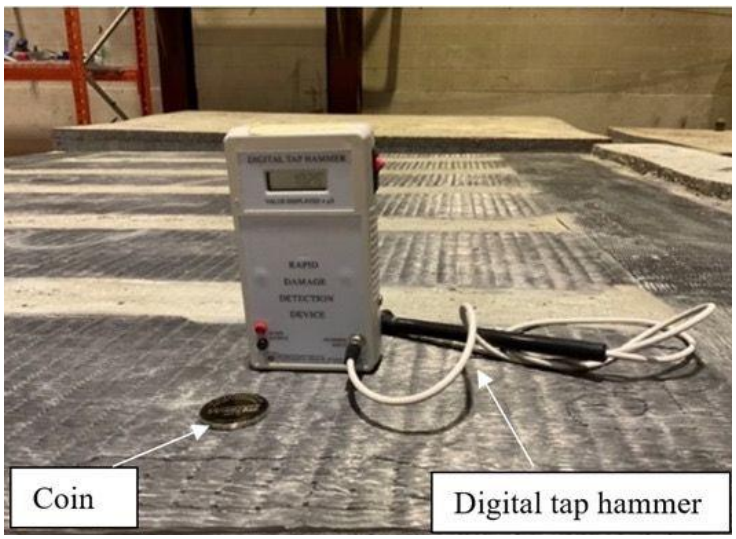

Figure 4.2-NDT equipment for acoustic sounding

Based on the local stiffness of the tapped area, debonded regions were identified and the estimated area of delamination on the CFRP strips for a given surface was recorded and sketched. Under controlled conditions in the laboratory, the surface of each strip of CFRP was completely coin tapped a minimum

of four times per strip. A time consuming but reliable step which involved tapping on and between individual stitches of fibers on the strips was adopted. This approach proved to be an efficient method for pin-pointing smaller defects. The coin tapping technique was also used to locate delamination in the concrete, especially at critical locations such as the diaphragm-girder joints.

Infrared thermography was then performed on all three diaphragms using a FLIR high resolution T650sc handheld infrared camera and four 1500 W external heaters connected in series on a wooden frame. The infrared technique exploits the thermal patterns emitted by the various materials to detect defects. Uniform heating was maintained at a distance of 1 m by positioning the wooden frame along the length of each individual CFRP strip and later moving the frame across the length of the diaphragms to capture the entire surface area. The heating durations of the strips were set to 30 s, 60 s and 120 s. Radiometric images of temperature values were captured as soon as the heaters were crane-lifted a substantial distance above the strip or totally removed from the surface of the diaphragm. The heating method used in infrared thermography, whether external heaters, heating blankets, or passive (ambient) heating directly affects the accuracy and sensitivity of defect detection through thermal contrast. Active heating methods, such as heaters or blankets, offer better control and improved sensitivity. On the other hand, passive heating is simpler but less reliable for detecting defects. Battery or electrically powered mat or blankets placed directly on the surface provide flexibility, but the heating elements/coils must be spaced closely enough to ensure uniform heating. It is worth pointing out that prior to performing the heating technique mentioned above, previous efforts to use heating blankets or passive heating while the components were stored outdoors presented several challenges and did not produce reliable results.

Finally, an automated Wichitech digital tap hammer shown in Figure 4.2 was used to cross validate the results from the coin tap testing and the infrared thermography. The tapping apparatus consists of a calibrated handheld hammer. This low-cost instrumented hammer measures the duration of the hammer impact pulse in microseconds and displays it on a screen. The displayed value is influenced by the hardness of the tapped area. To identify defects, first a defect-free area is tapped to establish a baseline and any subsequent tap value exceeding the baseline value by more than 10% is recorded as a defective

area. The principle and general operational procedure for the digital tap hammer developed by Boeing can be found in available literature (Georgeson et al., 1996; Halabe et al., 2020).

Lastly, computerized tomography scanning was performed on selected cylindrical samples obtained from the pull-off testing described in the following section. A high-resolution Phoenix nano CT scanner equipped with a DXR-250 digital detector and a 130 kV X-ray source was used for this test (Dilonardo et al., 2020; Lunardelli et al., 2022; Pejryd et al., 2014; Qiu, 2020; Zhuang et al., 2022). Samples were securely fixed in the machine, and the area of interest was centred within the scanning field. The parameters used during the scanning process are presented in Table 4.1.

Table 4.1-Scanning parameters used for Micro-CT scanning

X-ray voltage	X-ray current	Exposure time	Voxel size	No. of Images
130 $\boldsymbol{kV}$	200 μA	333 μs	30 μm	1200

4.4.3 Pull-off test method and equipment

To study the effect of the identified defects on the bond quality between the composite and the concrete substrate, the direct tension pull-off test was conducted. 490 pull-off samples from a single surface of one of the diaphragms were extracted to validate the NDT findings both in terms of strength and failure surface as per ASTM D7522 (ASTM, 2021b). 391 tests were conducted on the CFRP-strengthened areas of the diaphragms, referred to as the CFRP-tested samples, while 99 tests were conducted between the CFRP strips which are referred to as the concrete strip samples. The latter group does not include the possibility of adhesive failures and is intended only to increase the sample size of the concrete cohesive failures for statistical analysis. The difference between the means of each group was analysed using the analysis of variance (ANOVA) method.

In this study, the pull-off samples were drilled using both the wet and dry/hot scoring approaches using a diamond drill. The wet drilling method involves the utilization of water to reduce heat generation at the composite interfaces throughout the drilling process, whereas dry/hot drilling was performed without water cooling. A wooden plate with a 50-mm diameter hole was used to constrain the drill from

sliding during the coring process. All the bonded surfaces (CFRP and loading disc) were first abrasively cleaned with medium-grit sandpaper. Thereafter, compressed air was used to free the surfaces of all dust, laitance, and foreign inhibitors, and acetone was later applied to clean the surface of any further impurities before the discs were bonded to the specimens. Specific details regarding sample preparation, loading rate, and data analysis can be found in ASTM D7522 (ASTM, 2021b). A schematic of the test setup is shown in Figure 4.3.

To conduct the direct tension pull-off test, a pull-off tester, a loading fixture, and an epoxy adhesive are utilized. The loading fixture is securely attached to the isolated test sample using epoxy paste, and a threaded bolt is used to connect the loading disc and the pull-off tester. Following the guidelines from ASTM D7522 ((ASTM, 2021b)), the pull-off test was performed at a controlled rate of 1 MPa/min until the dolly (loading fixture) separated from the sample, carrying a portion of either the FRP or concrete. To ensure pure tension on the bonded area, the pull-off tester was maintained perpendicular to the test surface throughout the testing process. In this study, the Proceq DY-225 device was employed, which automatically records the peak load and calculates the bond strength (Figure 4.3).

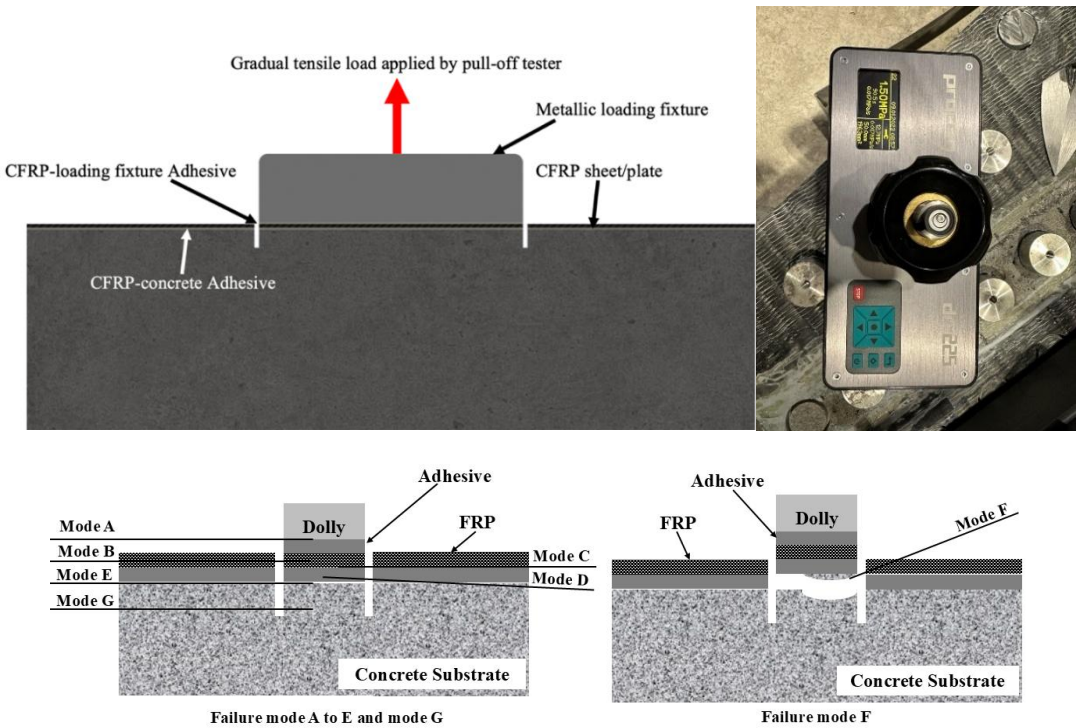

Figure 4.3-Pull-off testing set up a) Loading direction b) Pull-off testing apparatus c) FRP-concrete bond failure modes under pull-off test (ASTM 2021)

4.4.4 Material testing

Three concrete cores were extracted from the diaphragms and tested in compression in accordance with ASTM C39 (ASTM, 2021a). The compressive strength of the underlying concrete substrate obtained from the average of three core samples (77.7 MPa, 75.0 MPa and 74.9 MPa) with an average diameter of 95 mm and height of 200 mm was 75.9 MPa (standard deviation of 1.30 MPa) and the estimated cracking strength of the concrete obtained from Equation 4.1 is 3.48 MPa (CSA-Group, 2019).

$$f_{cr} = 0.4\sqrt{f_c'} \qquad \text{Equation 4.1}$$

To evaluate the mechanical properties of the CFRP material, a total of 36 coupon samples were extracted from one of the diaphragms. Eighteen coupons were tested following ASTM D3039 (ASTM, 2017) to determine the tensile properties of the composite materials, four of which exhibited desirable failure modes and were used to determine the material properties. These samples were carefully extracted using an angular grinder, mallet, and concrete chisels, taking care not to damage the CFRP itself. Extracted samples were cut into coupons of 300-mm length by approximately 25.4-mm width. Before testing, 6-mm thick aluminium tabs with bevel ends were designed, ground, and bonded to the coupons for even distribution of stress and minimizing stress concentrations over the grip region.

An electrical resistance strain gauge was installed at mid height on one side of the samples (flat surface obtained after grinding of bond line) while the other surface was speckled for digital image correlation. A universal testing machine operating at 2 mm/min was used to complete the coupon tests. Table 4.2 presents the experimentally determined material properties of the double layered CFRP sheets. The manufacturer design properties for a single layer with thickness value of 1.7 mm per layer are as follows: the tensile strength, modulus of elasticity and elongation at break are 855 MPa, 49.6 GPa, and 1.7%, respectively.

Table 4.2-Double-layer CFRP sheet properties (as-is)

	Coupon 1	Coupon 2	Coupon 3	Coupon 4	Average Values	Standard Deviation
Tensile strength (MPa)	542.4	556.8	588.2	642.0	582.4	38.2
Elongation at break (%)	0.93	1.17	1.31	1.03	1.11	0.15
Modulus of elasticity (GPa)	56.13	49.64	50.29	50.14	51.55	2.65
Length (mm)	300	300	300	300	300	-
Width (mm)	25.4	25.4	25.4	25.4	25.4	-
Thickness (mm)	3.68	3.56	3.39	3.29	3.48	0.15

4.5 Results and discussion

The NDT techniques used were effective in identifying anomalies in the CFRP composite materials and concrete substrates of the diaphragms. Although similar types of defects were observed across all diaphragms, the severity of these flaws varied. The time of initiation of the damage in the composite materials during the structure's service life remains unknown due to a lack of documentation on these identified problems.

4.5.1 Visual Inspection

In bonded repairs using FRP composites, the interface between materials is prone to cracking or separation due to factors like thermal incompatibility or relative movement of strengthened components due to discontinuity at joints. One of the main issues observed during the visual inspection in this research was the bond-separation issues between the underlying concrete substrate and the patch mortar that was used to repair the concrete surface prior to bonding the CFRP wraps (Figure 4.4). This damage might have occurred due to inadequate mechanical interlocking (surface roughening) between the patch mortar and concrete substrate during installation and curing resulting in complete separation between the two materials.

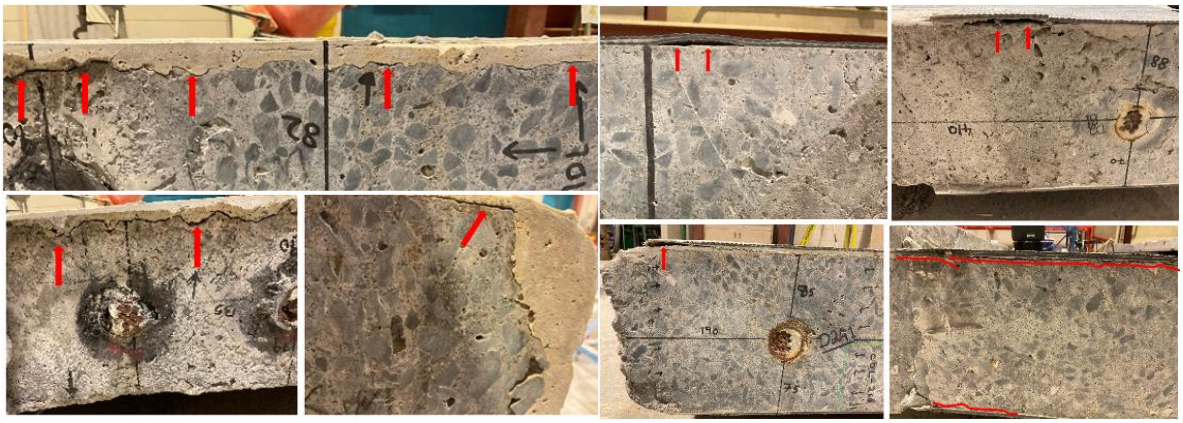

Figure 4.4-Interfacial delamination at mortar-concrete interface and CFRP-concrete interface a) Separation at mortar-concrete interface b) Delamination at CFRP-concrete interface

Variation in thermal expansivity may also lead to differential movement between the repaired area and the surrounding concrete. To prevent separation of the mortar from the deteriorated concrete substrate, several best practices should have been implemented. These include focusing on surface preparation and profiling to improve mechanical adhesion, application of appropriate bonding agent between the mortar and concrete, selecting mortar mixes that are compatible with the aged concrete in terms of thermal expansion, mechanical properties and chemical composition to minimize interfacial stresses, and proper curing to prevent premature drying, shrinkage and bond failure.

Additionally, severe cracks were observed in areas where multiple patch materials were used in the same location. The incompatibility between materials compromises stress transfer and exacerbates damage progression during normal service loading and environmental changes. Thus, to reduce the risk of debonding and potential cracking that could compromise the structural integrity, it is crucial that patch mortar, underlying concrete, and FRP material deform as a composite system. Interfacial separation between the various materials was also observed at the concrete-CFRP interface through the saw-cut edges of the diaphragms shown in Figure 4.4. These separations can lead to reduced load-carrying capacity and limit the effectiveness of the CFRP strengthening, as well as increase vulnerability to degradation from moisture ingress, and chemical exposure.

Multiple cracks aligned parallel to the fibers in the U-wrapped sheets and anchorage strips were also observed in these bridge samples (Figure 4.5). These cracks were positioned near the cold joint between

the diaphragm and girder, where uneven stress distribution is probable due to variation in member stiffness. These parallel cracks in the CFRP indicate a loss of load transfer between the fibers and the saturating matrix. Although these cracks are unlikely to affect the immediate load-carrying capacity of the strengthened diaphragm, exposure of the CFRP to moisture infiltration, chemical attack, and environmental degradation could reduce the long-term durability of the repair work. Premature cracking in the fibers may also result from poor workmanship during installation, such as curing the CFRP at low winter temperature, which can make the matrix more brittle. If the bond between individual fibers is compromised due to inadequate fiber saturation, exposure to freeze thaw cycles and subzero temperatures can cause fiber misalignment. This misalignment can facilitate crack propagation with the CFRP strip under service loads, further undermining the bond integrity over time.

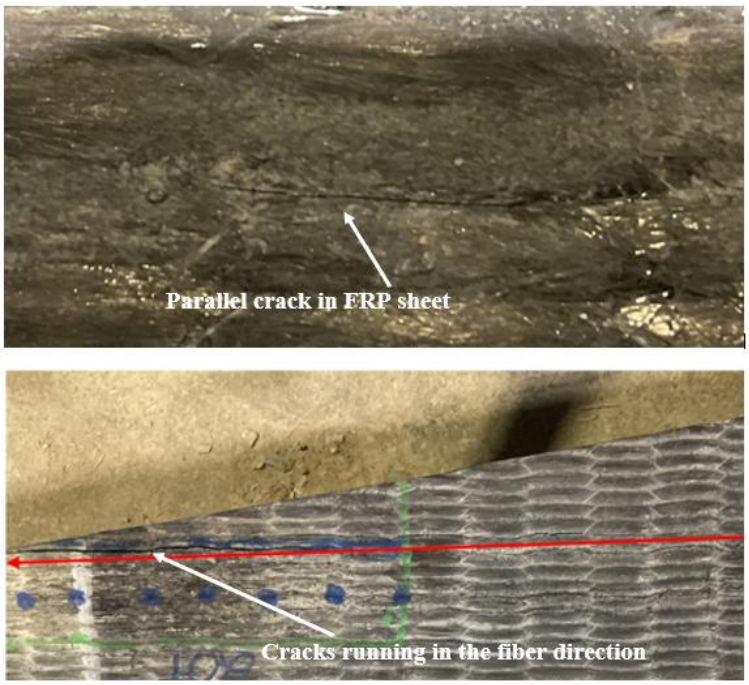

Figure 4.5-In-service cracks running parallel to fiber direction a) Parallel cracks in CFRP sheet b) Crack running in the fiber direction near the cold joint

In the concrete, severe cracks were observed at the joint between the diaphragms and the girder which may have been initiated by the corrosion of the reinforcing tendons. These cracks, along with minor horizontal cracks branching from them, may have contributed to the interfacial debonding at the CFRP-concrete interface (Figure 4.6). Several cracks on the sides of the diaphragms (girder-diaphragm joints) were picked up by the AI crack detection software used for the crack inspection (Figure 4.6); however, the software did not detect any cracks on the concrete gaps between the CFRP strips. A hand-held

magnifying glass also did not identify clear signs of damage in the concrete/mortar regions between the strips.

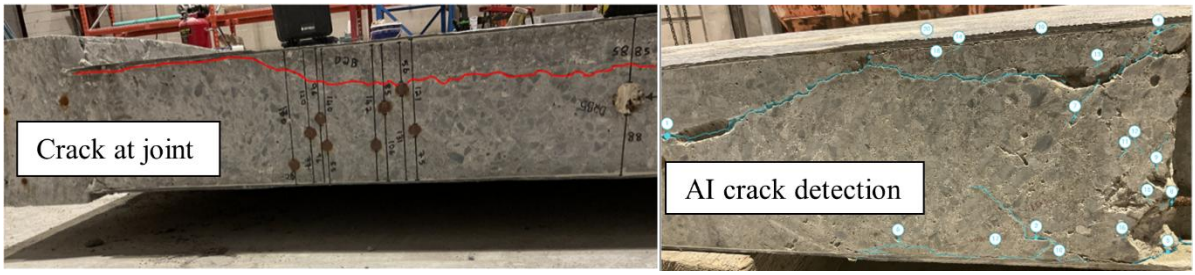

Figure 4.6-Severe cracks at diaphragm-girder joints a) 1.5-m long crack at the cold joint b) Spalled concrete and cracks detected by the INSPECT AI software

During the inspection of the full-scale diaphragms, random dispersion of air voids was visible at the CFRP-concrete interface, within cured fibers, and between layers of strips. Although most of these defects were minor issues that could have been avoided during the installation process, the presence of multiple overlapping layers of strips increased the risk of void formation because additional adhesive materials are required to fill the gaps between each layer. The accumulation of these minor flaws can lead to the formation of larger voids within the composite material, potentially disrupting the transfer of stresses between the layers of CFRP strips or between the strips and the underlying concrete substrate. Additionally, these voids can trap substances that could be detrimental to the long-term durability of the epoxy adhesive used.

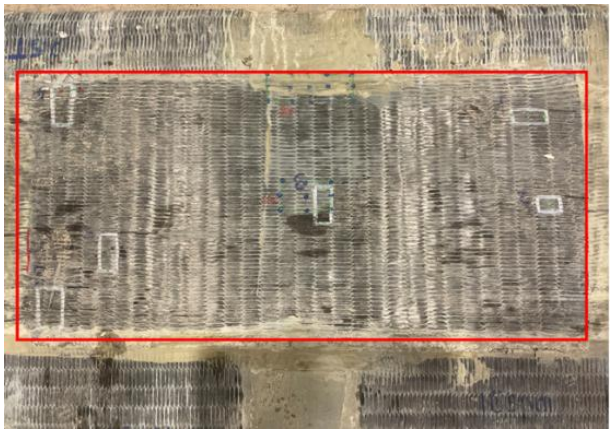

Figure 4.7-Short anchorage strip used to fix debonds

It is important to minimize the issue of void formation to ensure proper performance and longevity of the bond between the repair materials. Short anchorage strips, approximately 650 mm in length, were observed near the diaphragm's soffit, as depicted in Figure 4.7**.** While not certain, it is possible that

these shorter anchorage strips were utilized during the installation to address debonding problems on the main anchorage strips.

The inspection also uncovered potential construction errors that can hasten deterioration in critical structural components. The random arrangement of internal steel reinforcement, as seen in Figure 4.8, revealed instances of overlapping bars or insufficient concrete cover. Consequently, corrosion in one reinforcing bar will inevitably spread to nearby reinforcements. Moreover, when reinforcement is placed too close to the surface without concrete cover, it accelerates corrosion, resulting in surface cracking that compromises the integrity of the CFRP-concrete system.

Figure 4.8-Random placement of rebars without sufficient spacing or concrete cover a) side A of diaphragm #3 b) side B of diaphragm #3

During the retrofitting of these bridge diaphragms, the potential issue of loose fibers being pulled out from the free edges of the strips during resin infiltration was effectively addressed. This careful installation procedure was observed across all CFRP strips on the three diaphragms. However, use of excessive epoxy led to the formation of hard bubbles on multiple vertical shear strips at the chamfered corners of all the diaphragms. Though these defects may appear as harmless aesthetic imperfections, they typically result from the excessive use of primers, potentially causing inadequate stress transfer between the composite and the concrete.

While visual inspections are relatively inexpensive, the subjective nature of the approach remains a major disadvantage. Limitations of the human eye, obstructed access, and lapses in judgement means that flaws may remain unnoticed after the inspection. This is further complicated in FRP-strengthened members where signs of debonding may not be visibly detectable from the surface.

4.5.2 Acoustic Sounding and Infrared Thermography

The total delaminated area estimated from the coin tapping method shows that 2.8 percent of the total bonded area of Diaphragm II (D5 in Figure 1.4) experienced delamination, the highest proportion among the examined surfaces (Figure 4.9). This is nearly twice the total delaminated area identified by coin tapping on each surface of Diaphragm I. It is not clear from the reports obtained from the bridge management corporation which direction this surface of the diaphragm was facing and whether the direction had any impact on this delamination prior to curing of the CFRP. The opposite surface of Diaphragm II, however, had the minimum delaminated area identified by coin tapping of 0.8 percent. The estimation of the percentage of defective area by the coin tapping method on the bonded CFRP regions indicated that only a small fraction of the total bonded area in all three diaphragms was detached from the concrete substrate, suggesting that the majority of the bonded area was in good condition.

The coin tapping NDT results also revealed debonded regions ranging in size from 500 mm^2 to 26,000 mm^2. These defective areas are categorized as small to large defects according to ACI (ACI, 2017) guidelines. Following ACI (ACI, 2017)) acceptance guidelines for wet layup systems, delaminations smaller than 1,300 mm^2 are considered allowable as long as the defect-free areas account for over 95 percent of the strengthened region and there are no more than 10 such delaminations per square meter. Delamination less than 16,000 mm^2 may be treated with epoxy injection or ply replacement depending on their size, distribution and location. For large delaminations exceeding 16,000 mm^2, selective cutting and installation of overlapping sheets should be considered. In accordance with ACI (ACI, 2017)) acceptable guidelines, 62 percent of all defects identified by coin tapping are categorized as medium defects, exhibiting sizes within the range of 1300 mm^2 to 16000 mm^2 (Figure 4.9b). Five defects were

classified as “large”; however, selective cutting and installation of overlapping sheets at these locations was not implemented on the diaphragms while in service.

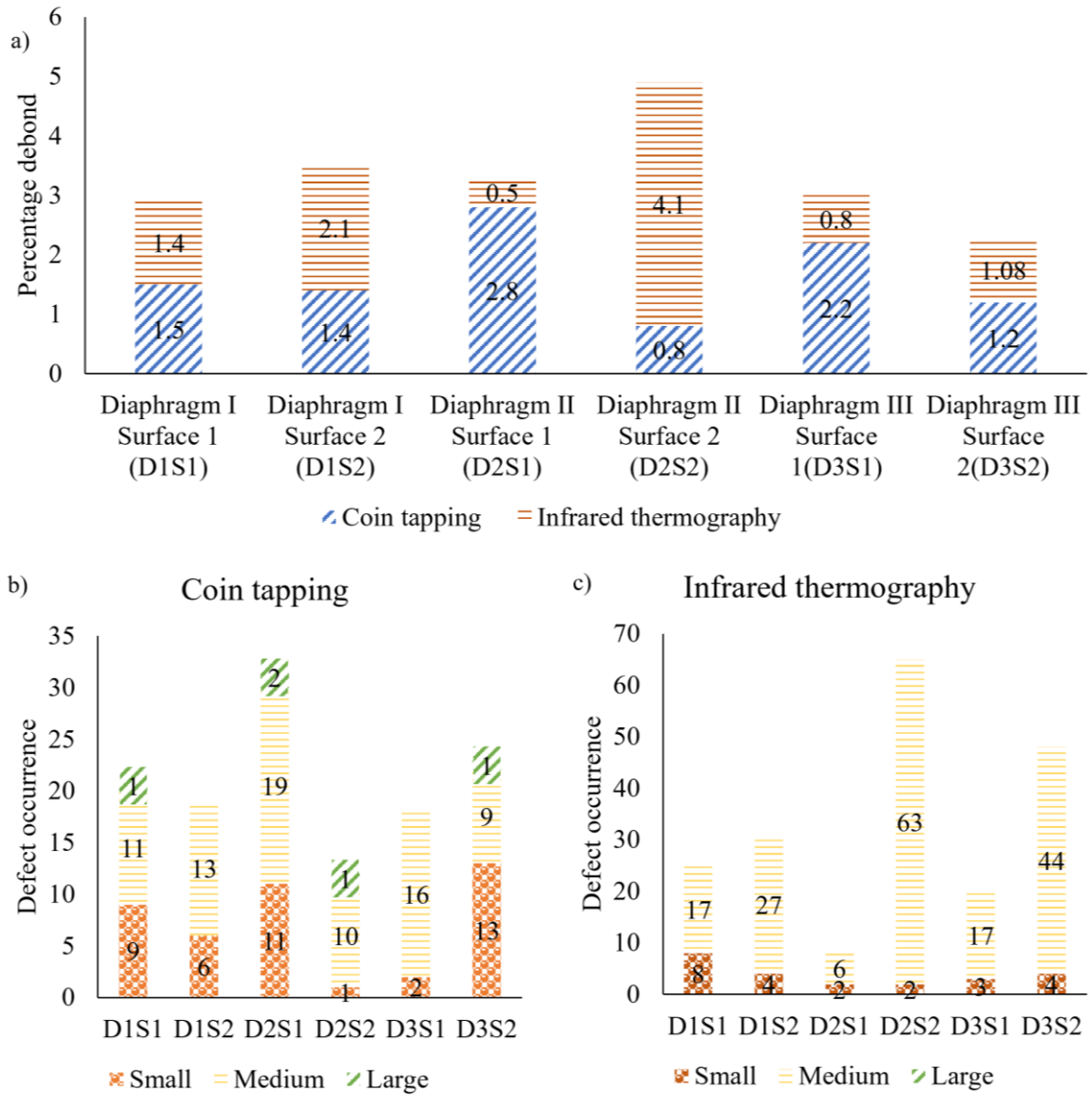

Figure 4.9-Comparison of defects detected by the coin tapping and additional debonds detected by infrared NDT method a) Percentage of debonds detected b) Defect occurrence from coin tapping and infrared thermography

The initial passive infrared thermography inspection conducted on all three diaphragms at an outdoor storage site in Ottawa during the winter did not reveal any defects, likely due to the low ambient temperature. However, subsequent use of infrared thermography in the laboratory was able to detect additional problems that went unnoticed by the conventional coin tapping in the lab setting (Figure 4.9). The additional defects detected by infrared thermography corresponded to 0.5% to 4.1% of the total CFRP surface area of each diaphragm surface. Interestingly, the infrared camera detected few additional

defects on Surface #1 of Diaphragm II (8 defects comprising 0.5% of the total surface area) and a high number of defects on Surface #2 of the same diaphragm (65 defects comprising 4.1% of the total surface area). This discrepancy between the infrared and coin tapping for Diaphragm II may be related to the depth of the anomaly that is detected, stiffness variations, and operator dependence. In a multi-layer application such as the installation on the bridge diaphragms, it is also expected that higher CFRP thickness will diminish the accuracy of these NDT methods due to changes in thermal and acoustic properties. The infrared camera is sensitive to any slight variation in heat transfer between sound and unsound regions, whereas the coin tapping is subjective and more sensitive to local stiffness of the defective area. If a significant portion of concrete is attached to a defective area (i.e., the delamination is further from the surface), then it would be challenging for the coin tap to give an accurate distinctive sound upon tapping. Planned future destructive testing of segments of these diaphragms will confirm if these results may be indicative of the depth and/or degree of deterioration present at each location. It is worth noting that no additional "large" defects were identified using infrared thermography. Infrared thermography offers objective and repeatable inspection, particularly over large areas, making it more reliable for detecting defects in composite repairs. Its effectiveness is further improved by optimal heating, which enhances defect visibility in the repair.

Figure 4.10 schematically illustrates the size and location of the localized delaminated areas identified using the conventional coin tapping and infrared thermography for one of the inspected diaphragms. The results showed that the tapping test was, in general, effective in locating subsurface defects with the externally bonded CFRP wraps, especially in a low-noise environment like the structural laboratory where the tests were conducted. The delamination issues detected were primarily concentrated on the anchorage strips. The complexity of the stacking process in the anchorage zones where four layers of CFRP were installed increased the likelihood of defects in these regions of the diaphragms.

In infrared thermography, the defective areas manifest as distinctive hot spots in thermal images and can be efficiently analyzed using commercial software (i.e., Research IR) to enhance identification

(Figure 4.11). By analyzing the thermal contrast and temperature distribution across the CFRP strengthened structure, abnormalities such as moisture ingress could also be identified.

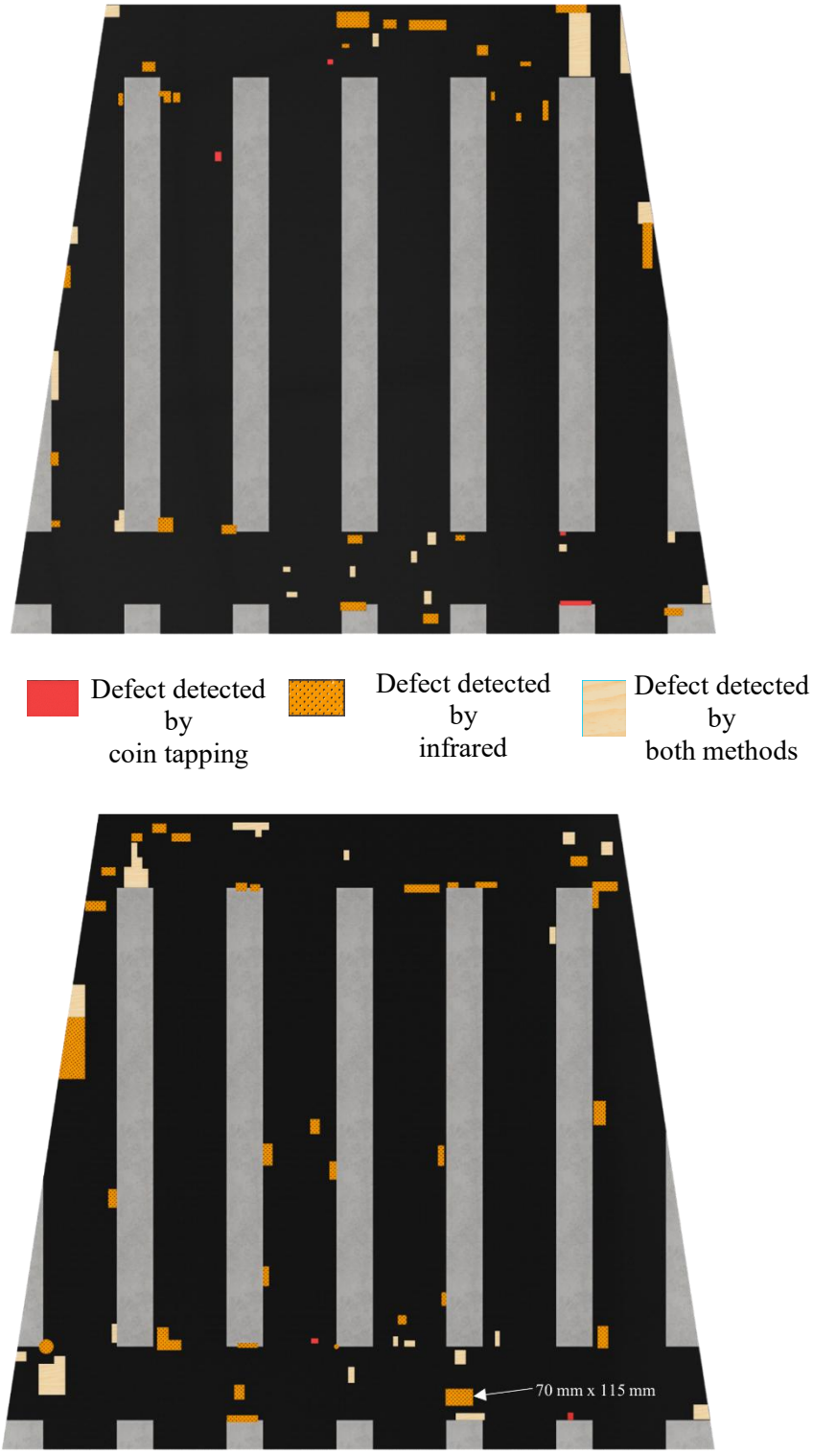

Figure 4.10-Typical defect layout for diaphragm #1 a) Defects on surface 1 b) Defect on surface 2

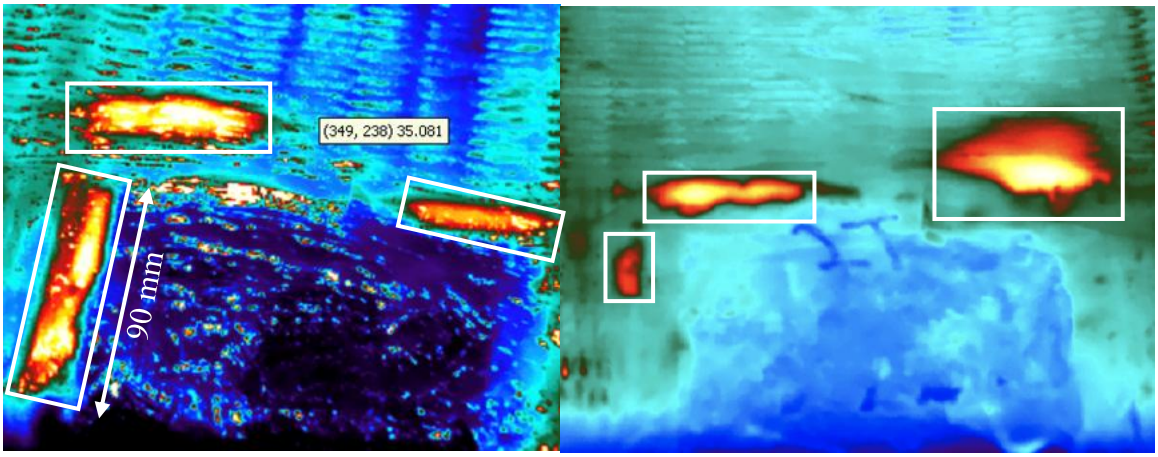

Figure 4.11-Defects identified by infrared thermography

During the inspection of the bridge diaphragms, the benefits of infrared thermography as a modern inspection technique were evident. It allowed for scanning large surface areas in a short period, proving highly repeatable and labor-efficient. However, infrared thermography as used in-situ has some limitations. It primarily provides information on the planar dimensions of flaws, making it less effective in determining the depth of defects. Additionally, its sensitivity to temperature variations means that depending on heat intensity, some defects may go unnoticed, especially in cold weather where heat contrast between the target object and its surroundings is low. Factors such as non-uniform heating, reflections from the test surroundings, and camera quality should be given considerable attention. However, the major limitations of the coin tapping approach include inconsistency in results depending on local stiffness of tapped area and the lack of information on defect depth.

Digital tap testing, on the other hand, proved to be quick and convenient. However, it was inconsistent in verifying defective spots within regions identified by the coin and infrared thermography. The baseline readings for the ten spots tapped on the sound areas on the various diaphragms are listed in Table 4.3 and a detailed list of digital tap readings of the defects for Diaphragm II is shown in Table 4.4. A value of a tapped area 10 percent greater than the values in Table 4.3 (i.e., greater than 1285 microseconds) was considered confirmation of a defective area. As shown in Table 4.3**,** unsatisfactory results were obtained in that some defects previously identified by the coin tapping and infrared thermography were not confirmed by the digital tap test. While the infrared and coin tapping tests can

be used independently for condition assessment of concrete structures retrofitted with CFRP composites, the digital tap test, originally developed for thin-walled FRP-only materials used in the aerospace industry, was found to be less reliable for this application. In the case of large structural elements, it is important to note that performing coin tapping can be highly labor-intensive and reliant on the operator's hearing abilities for accurate interpretation of results.

Table 4.3-Digital tap values of sound regions

Diaphragm I		Diaphragm II		Diaphragm III	
Surface 1	Surface 2	Surface 1	Surface 2	Surface 1	Surface 2
1141	1072	1077	1076	1021	1154
1160	1033	1101	1077	1033	1139
1078	1027	1130	1058	1029	1072
1123	1070	1098	1072	1024	1151
1056	1030	1064	1067	1022	1104
1155	1030	1083	1063	`1036	1038
1168	1055	1145	1048	1031	1164
1133	1023	1114	1025	1035	1091
1086	1042	1075	1035	1024	1062
1129	1028	1132	1086	1037	1109
Average 1122.9	1041.0	1101.9	1060.7	1029.2	1108.4
Standard Deviation 37.7	18.2	27.6	19.5	6.1	43.1

Table 4.4-Digital tap readings for Diaphragm II surface 1

Debond #	DTT readings	NDT detectability	Defect width (mm)	Defect length (mm)	Area ($\mathbf{mm^2}$)
1	1058-1375	Both	48	50	2400
2	1069-1156	Undetected	25	40	1000
3	1120-1356	Both	20	47	940
4	1042-1286	Coin	23	35	805
5	1109-1244	Undetected	28	53	1484
6	1044-1373	Both	35	125	4375
7	1202-1286	Both	18	70	1260
8	1001-1473	Both	35	65	2275
9	1088-1286	Both	17	70	1190
10	1018-1535	Both	45	222	9990
11	1109-1290	Coin	30	55	1650
12	1059-1243	Undetected	35	68	2380
13	1167-1333	Both	27	49	1323
14	1063-1308	Coin	40	90	3600
15	1128-1209	Both	23	46	1058
16	1154-1216	Undetected	26	68	1768
17	1207-1242	Undetected	26	68	1768
18	1165-1247	Undetected	20	55	1100
19	1201-1569	Both	26	113	2938
20	1103-1348	Coin	25	30	750
21	1067-1878	Both	87	205	17835
22	1103-1145	Undetected	25	60	1500
23	1080-1328	Coin	37	46	1702
24	1138-1322	Both	25	48	1200
25	1403	Coin	16	25	400
26	1122-1268	Both	25	70	1750
27	1053-1172	Undetected	125	385	48125
28	1189-1318	Both	47	61	2867
29	1162-1210	Undetected	50	75	3750
30	1201-1257	Undetected	100	120	12000
31	1153-1299	Both	18	130	2340
32	1275-1309	Both	25	35	875

4.6 Pull-off results for Diaphragm I

4.6.1 Failure modes

The pull-off test results obtained in terms of the failure modes and bond strength are shown in Figure 4.12. While the majority of the samples experienced the ideal concrete cohesive failure, several other failure modes were also observed, indicating varying levels of deterioration at the bond-line (Figure 4.13). From the CFRP-strengthened samples, 96% of test samples exhibited a desirable failure mode within the concrete (Mode G). The portion of concrete material remaining attached to the loading disc

after failure varied significantly, without any clear correlation with bond strength or level of deterioration.

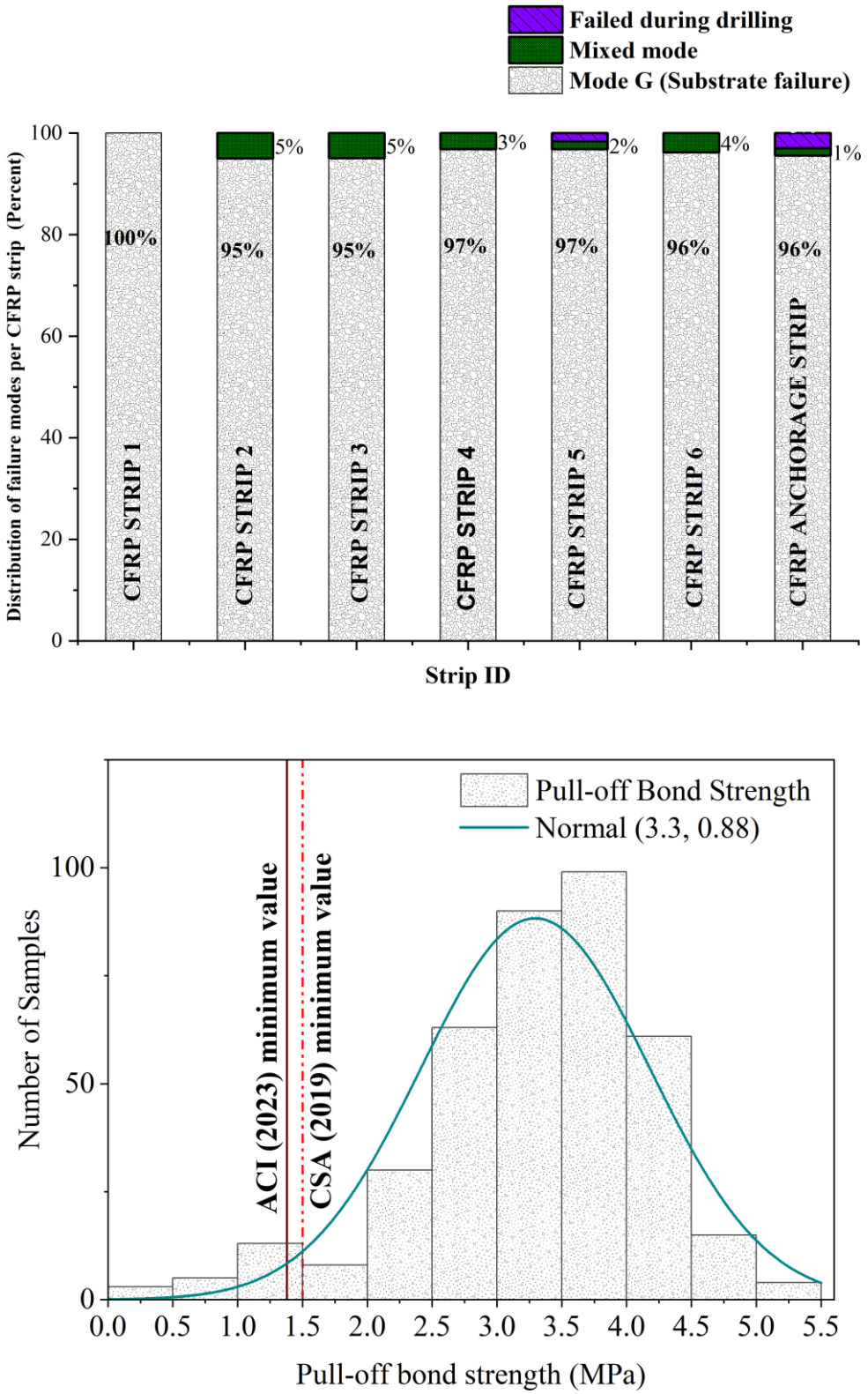

Figure 4.12-Pull-off failure modes and bond strength distribution for CFRP strengthened regions a) Observed failure modes b) Pull-off bond strength distribution

The observed failures, other than the substrate failure, were characterized by either: 1) failure at the interface between the first and the second layer of CFRP sheet, indicating degradation of the adhesive bond line between the layers and hence a disruption in stress transfer (Figure 4.13); or 2) failure at the interface between the concrete and the first layer of the CFRP sheets. Three samples failed during the drilling process (Figure 4.13c**)**, coinciding with previous identification of these samples as defective regions through NDT approaches. This premature failure is characterized by a complete separation at the interface between the first layer of CFRP and the concrete. Thus, stress transfer between the concrete and the CFRP at these locations was compromised and could lead to progressive debonding under service load conditions. Three percent of samples showed a mixed mode failure within multiple materials depending on the level of deterioration.

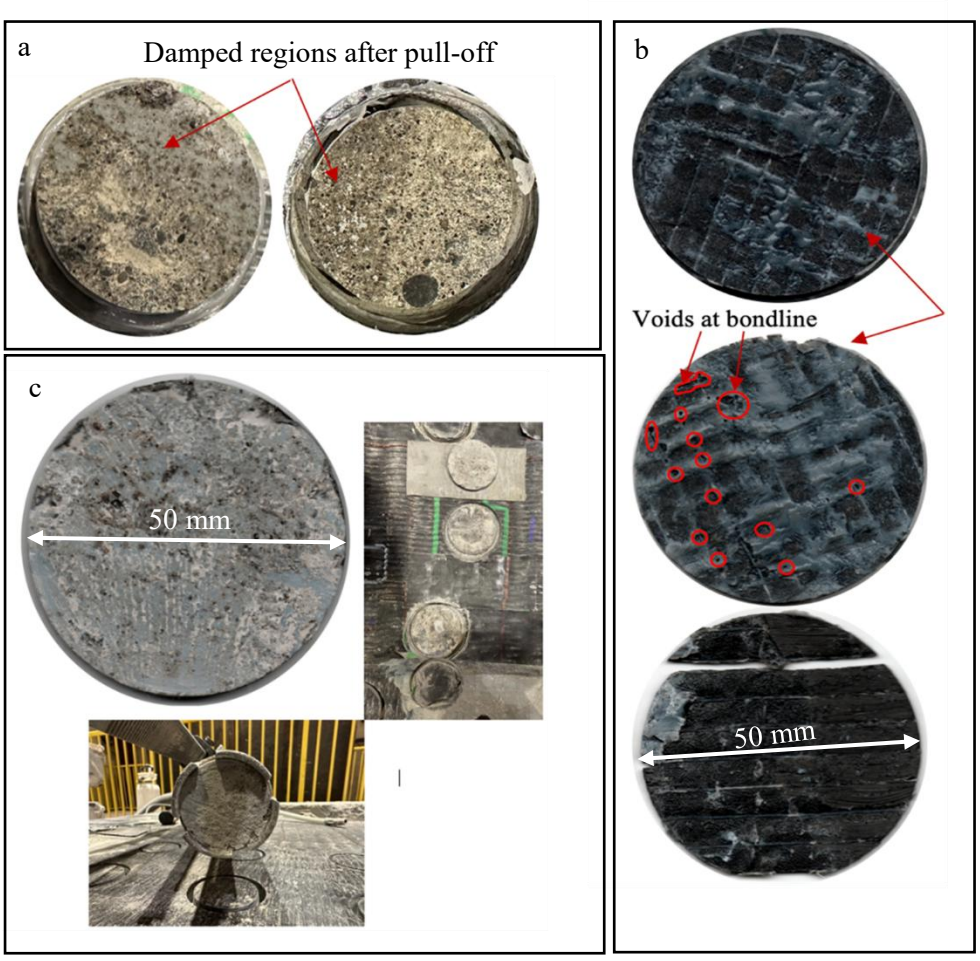

Figure 4.13-Pull-off failure modes a) A typical sample showing dampness at bond-line b) bond-line failure observed between individual layers of composites c) Debonding of defective sample during drilling

Samples that did not experience substrate failure (Mode G) typically demonstrated lower bond strength values (Figure 4.14b).

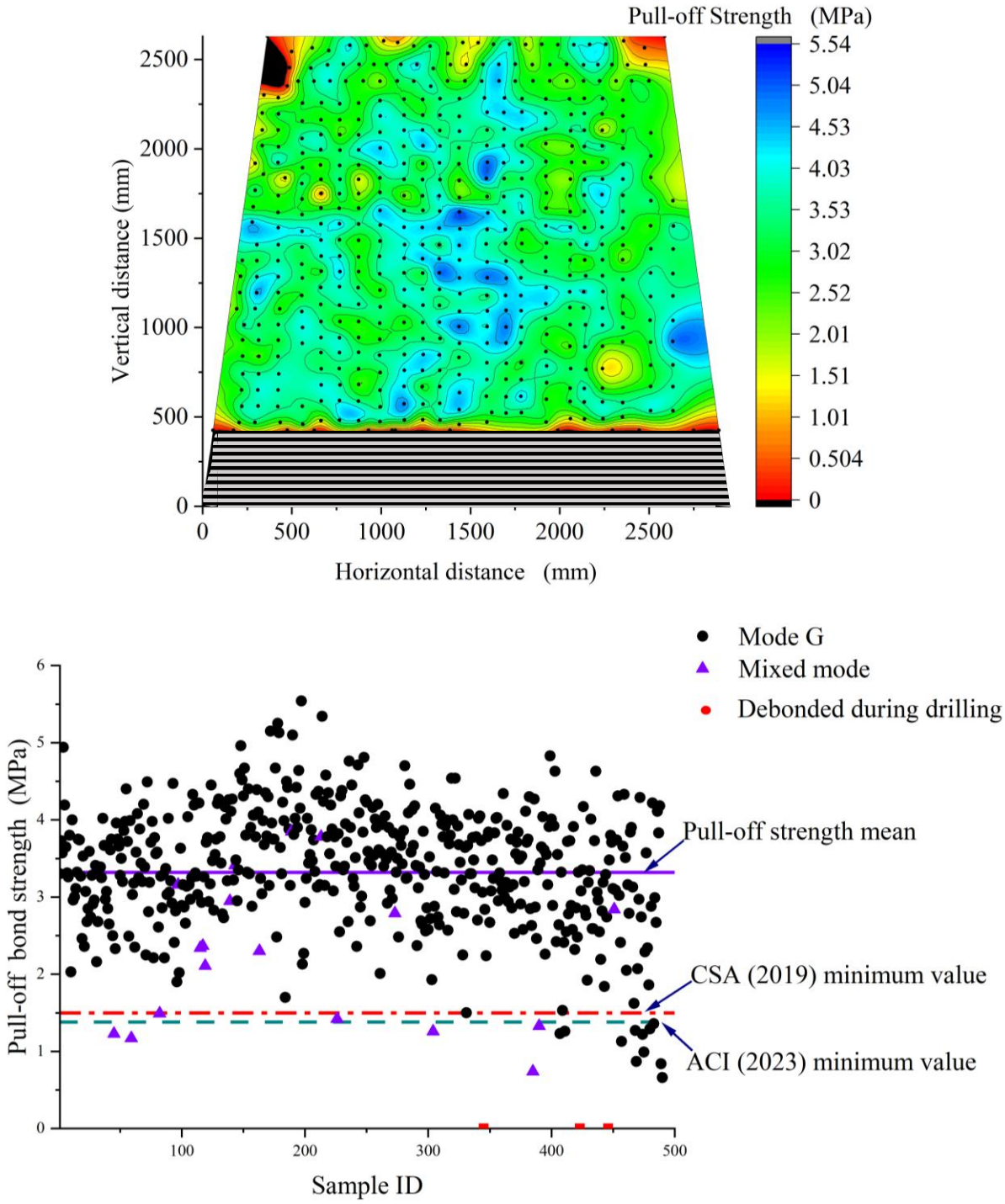

Figure 4.14-Statistical distribution of all bond strength and failure mode a) Contour map for statistical distribution of bond strength over the surface b) Proportion of failure mode by bond strength

None of the 490 samples in this study exhibited brooming failure of the fiber materials, commonly seen in accelerated aging tests in laboratory settings. Interlaminar cohesive failure between the layers of CFRP sheet as shown in Figure 4.13b was observed in three samples which may be attributed to insufficient epoxy resin usage or inadequate resin curing during installation. Bond deterioration at the transition zone (bond line) between the top and first layer can also be caused by infiltration of water and other substances. Over time, the absorbed moisture can lead to plasticization of the epoxy adhesive, weakening the intermolecular bond and reducing material properties. In addition, the presence of voids at the bond line affects the level of moisture accumulation between the layers, and during freeze-thaw or subzero weather conditions, volumetric expansion and contraction worsens the bond between the CFRP sheet layers.

The quality of workmanship during the initial strengthening phase is a key factor in understanding the bond deterioration of strengthened structures. The curing phase of the thermosetting epoxy used in this installation is sensitive to ambient temperature. It is important to note that the CFRP installation work on the evaluated bridge components was done during the winter period with an ambient temperature of less than 10 degrees Celsius which may have affected the required curing duration for the resin used. The lack of documentation makes it challenging to discern if compensation was made in terms of the pot life or curing condition under this unfavorable installation scenario. Moistened or damp concrete at the CFRP-concrete interface of failed samples was noticed after the detachment of test samples (Figure 4.13a).

4.6.2 Pull-off bond strength

The bond strength values obtained from this single-mode loading, testing the bond capacity perpendicular to the principal tensile strength of the CFRP, exhibited significant variations even for closely located areas. These variations are primarily caused by inherent heterogeneity in the concrete and patch mortar materials, including aggregate variation, misalignment, stress concentration, and microcracks. However, when considering in-situ structural elements that have undergone multiple

retrofitting interventions and experienced fluctuating weather conditions, the scattering of pull-off values arises from additional factors that compromise structural integrity.

In this research, out of 490 tested samples, bond strength values ranged from 0 MPa (for NDT-identified defective zones) to 5.54 MPa for a sound bond (Figure 4.14b) with more than 94% of pull-off test results exceeding the minimum values of 1.38 MPa and 1.5 MPa recommended by ACI and CSA (ACI, 2023a; CSA-Group, 2019), respectively (Figure 4.14). This is attributed to the fact that code-prescribed general thresholds are not a function of the strength of the concrete in the repair work. It is worth noting that the pull-off strength value is essentially an indicator of the quality of the concrete substrate and interface; it does not provide a quantitative value of the interface shear strength, and the minimum values prescribed in provision documents are conservative for high strength concrete such as that used in the diaphragms of this study. Considering the significant increase in experience with FRP strengthening over the last few decades, it may be appropriate to revisit prescriptive approaches to quality assurance of FRP rehabilitation. Performance-based guidelines that consider the type of application and material properties of concrete and FRP system could allow for more efficient use of materials while also ensuring that best practices are followed during installation.

The statistical distribution of the pull-off strength values showed a coefficient of variation (COV) of 27% and a mean bond strength value of 3.3 MPa for the 391 CFRP-tested samples. Among the 99 concrete strip samples, the mean bond strength value and COV were 3.4 MPa and 19%, respectively. These findings indicate a slight reduction in bond strength values for the CFRP-tested region, likely due to decreased bond performance associated with adhesive failures at the CFRP-concrete interface or interlaminar areas for some samples. However, statistical data analysis using analysis of variance (ANOVA) shows that the reduction in mean values between the test results in the CFRP and the concrete strip samples was determined to be statistically insignificant at the 0.05 significance level.

Figure 4.14 visually represents the spatial distribution of bond strength across the entire surface. Degradation in bond strength is primarily concentrated around the anchorage strip where multiple layers

of composite materials were installed and at the edges of the diaphragm connecting with the main load-carrying member (the girder) of the superstructure. Six of the extremely low bond values were obtained from the anchorage strip at locations with defects identified by NDT. The mean bond strength value for the anchorage strip was found to be 19% lower than the overall mean of the CFRP-strengthened regions; however, at the 0.05 significance level in analysis of variance (ANOVA) the means were deemed not significantly different.

Consistent with NDT results, the pull-off samples with identified flaws from the NDT approach showed a reduced value in the bond strength and prevailing delamination of the CFRP material. . Interestingly, these defective regions' average bond strength value (1.55 MPa) was still slightly above the code-prescribed minimum value.

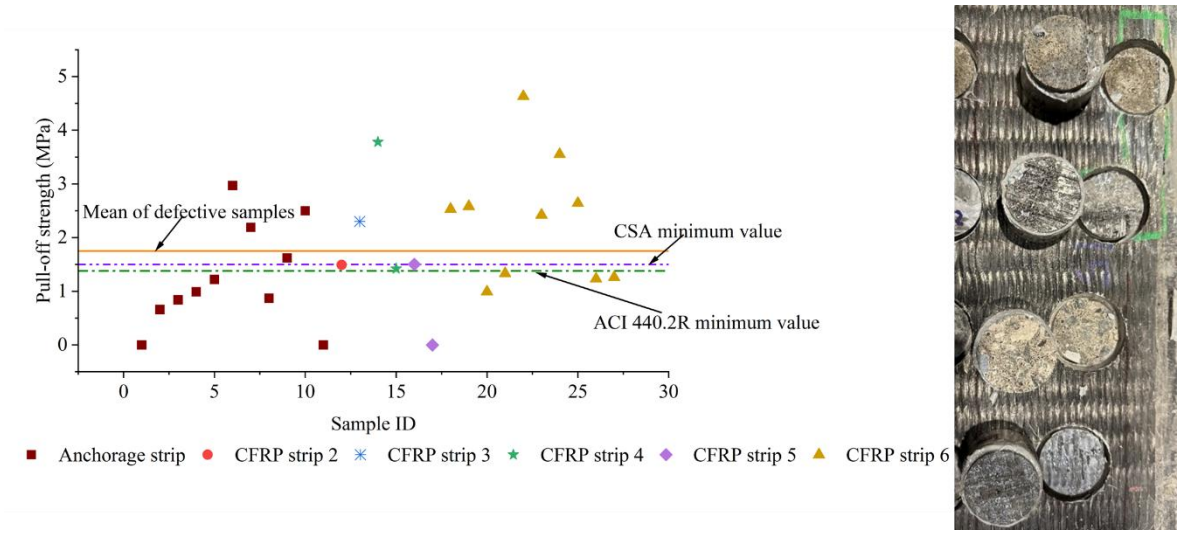

Figure 4.15-NDT validation in anchorage strip a) Pull-off strength of known defect areas on various strips b) typical delamination failure

The poor bond at these locations is evident in Figure 4.15 and Figure 4.16. The prevailing failure mode in these regions was a mixed-mode delamination of CFRP occurring at different layers of the composite (Figure 4.15b and Figure 4.16): a) Failure at the interface between the first layer and the second layer of CFRP sheets, which indicates a deterioration of the adhesive between the two layers of sheet and a discontinuity in stress transfer; and b) mixed mode failure at the interface between the concrete and the first layer of the CFRP sheet. Notably, values as low as 1.13 MPa were obtained during the pull-off test in locations that were not identified as defective by NDT. Among these values, four were below the

(CSA-Group, 2019) limit of 1.5 MPa. One low-strength result was correctly identified using infrared thermography but was missed using acoustic tapping techniques.

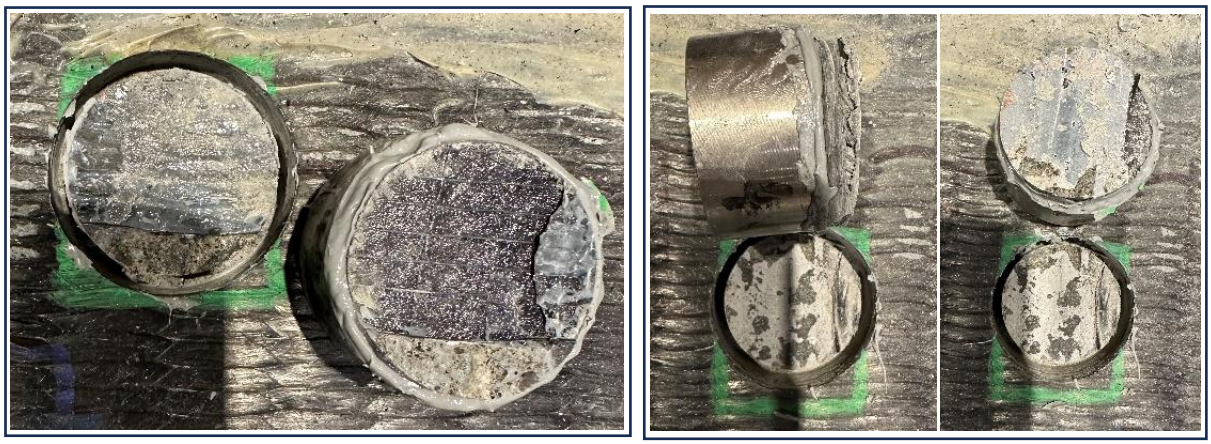

Figure 4.16-Pull-off failure surface showing mixed mode failure at different layers of the material a) Separation between layer 1 and layer 2 b) Separation between multiple layers

According to Figure 4.17, the ANOVA showed that the interaction between the failure mode and drilling method was insignificant. The COV of the two drilling approaches (wet and hot drilling) were 22.7% and 22.8%, respectively. At a 95% confidence level, the null hypothesis of equal mean is acceptable, with the mean values 3.24 MPa for the wet drilling and 3.37 MPa for hot drilling (p-value of 0.16). However, for pull-off tests requiring deeper drilling depth, the impact of thermal stresses on the bond behavior should be carefully considered.

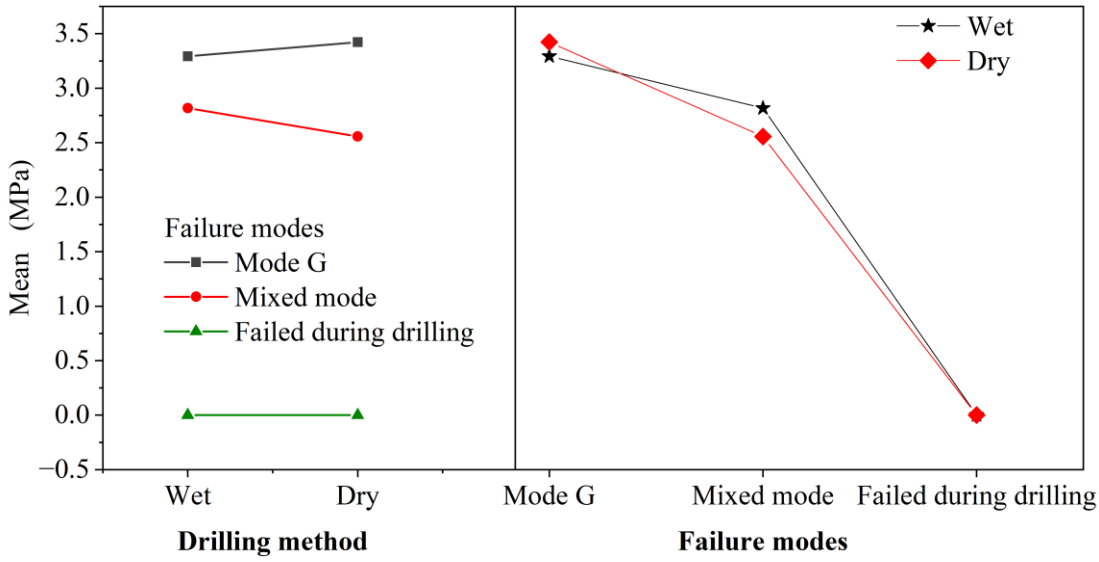

Figure 4.17-Effect of drilling approach on bond test results

Heterogeneity of the underlying concrete is a critical factor contributing to the dispersion in bond strength values. However, in field structural components, the variance can also be attributed to inconsistencies in the construction and installation process, as well as the presence of patch materials and surface cavities as shown in Figure 4.18. These various anomalies, such as the use of different patch materials, unfilled cavities during surface preparation, inconsistencies during construction (such as misplaced metal strips), and the presence of joints with uneven stress distribution, can individually or collectively impact failure strength and fracture propagation in the strengthened substrate. In bond-critical applications, the adherence and compatibility of the patch material to the underlying concrete substrate through mechanical interlock or chemical bonds are crucial factors.

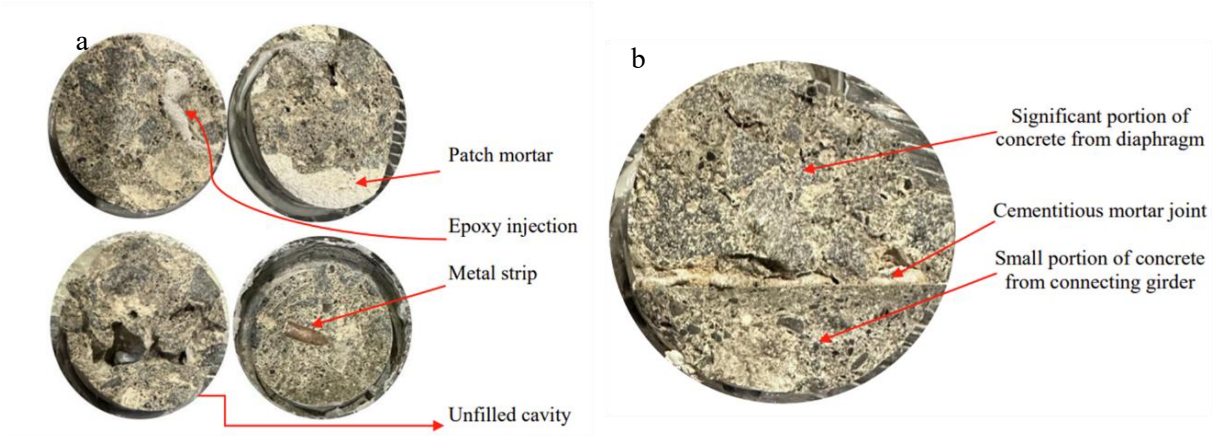

Figure 4.18-Rationale for additional variability in pull-off test results a) Typical anomalies in repaired concrete b) Discontinuity at joint

The micro-CT (volume scanning through tomography) of the pull-off samples revealed defects and deficiencies at the bond lines that occurred during the installation process (Figure 4.19). These included voids and pores at the different interfaces, such as between CFRP layers and the CFRP-concrete interface. Micro-CT scanned images also showed the distribution of voids and cracks within the concrete. This qualitative microanalysis emphasizes the influence of workmanship on the quality, reliability, and performance of externally bonded composite repair systems. Further investigation of differences in microstructure can potentially provide insights into the potential reasons behind variations in pull-off bond strength values and failure modes and enhance our knowledge to optimize the design and installation of CFRP composite materials for external retrofitting.

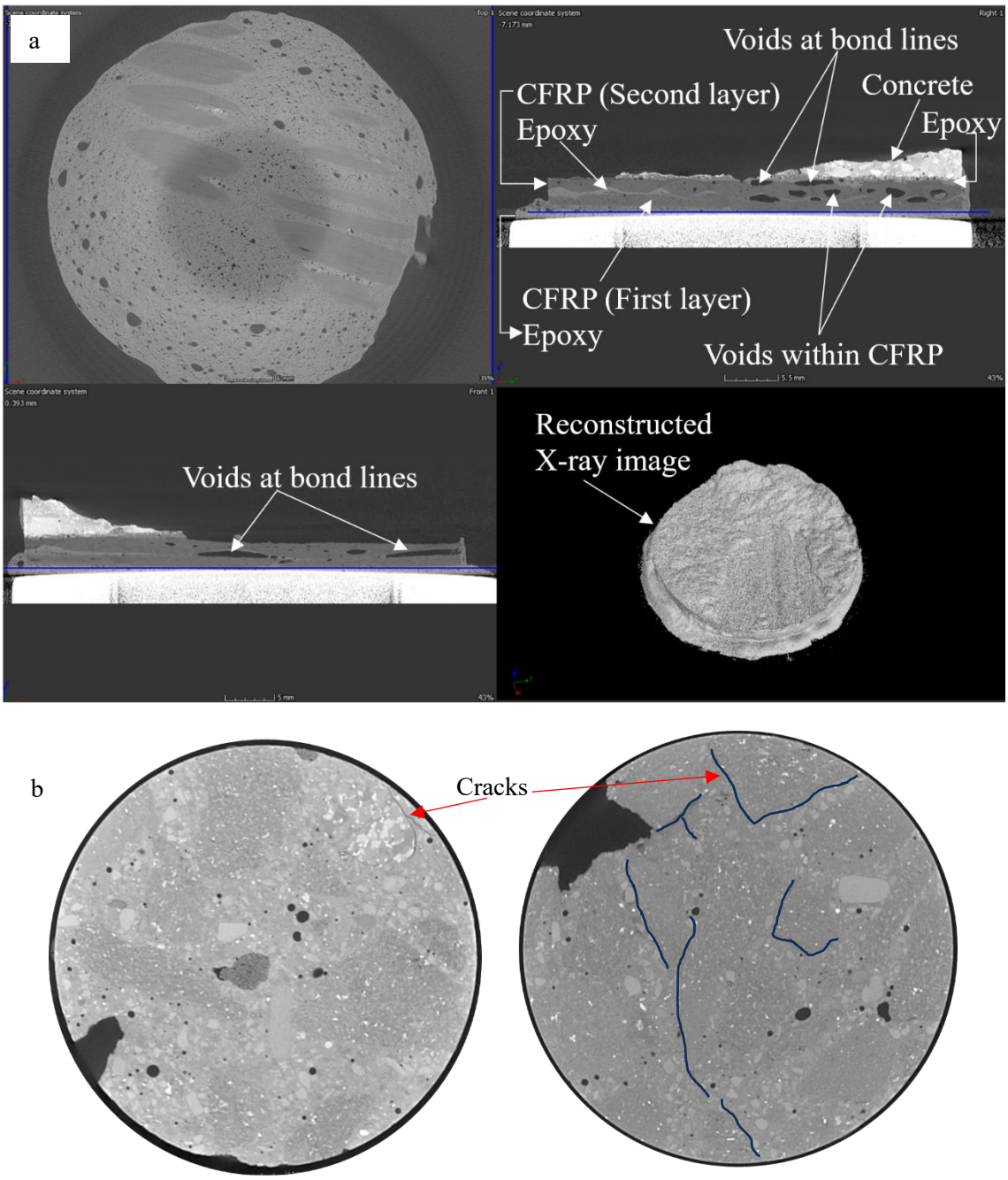

Figure 4.19-Reconstructed volume from micro-CT scan of pull-off sample a) voids at various interfaces b) Void and crack distributions in concrete

4.7 Conclusions

This study conducted a holistic assessment of three CFRP-strengthened concrete bridge diaphragms from the Original Champlain Bridge, a major structure within the Canadian bridge network. Various in-situ NDT methods for condition evaluation, such as localized and area scanning techniques, were

employed. The single largest database of direct tension pull-off test data was provided to establish a correlation between bond integrity and NDT results after five years under the synergistic effect of service load and fluctuating harsh environmental conditions. It is important to note that the structural implications of defects at the CFRP-concrete interface remain poorly understood and not well addressed in literature. Additional research to link interface integrity with structural performance, which is essential to move from condition assessment to structural evaluation, is currently ongoing by the authors. Based on the findings, the following conclusions can be drawn.

- Through visual inspection and various NDT measurements, defect concentration was observed at locations where more than two layers of CFRP strips were used in the manual wet lay-up installation, such as anchorage strips, as well as near joints where significant force transfer occurred.
- NDT assessment found that over 95% of the bonded area remained intact after nearly six years of exposure to aggressive environmental conditions. Nevertheless, some large-size defects were identified that would require repair according to current guidelines.
- Results of the 490 direct tension pull-off tests generally confirmed the results of NDT. Low strength results were obtained at defective locations identified by NDT, although in some cases the pull-off strength was still higher than code minimums. In a few instances, low strength results were also obtained at locations that were not flagged by NDT. In general, infrared thermography was found to be more reliable to detect hidden defects than acoustic sounding methods.
- Depending on the level of deterioration at the bond-line, different fracture surfaces were observed during pull-off testing: adhesive failure between layers, mixed mode failure between concrete and CFRP, and separation during drilling. In this study, approximately 96% of tested CFRP pull-off samples from deteriorated concrete diaphragms exhibited failure in concrete, demonstrating a relatively good bond between CFRP and concrete under extensive exposure to service loads and harsh climate conditions.

- Bond strength results were found to be influenced by inconsistencies in construction and installation processes, as well as the presence of substantial patch cementitious materials.
- The minimum pull-off strength values prescribed by current codes may be significantly lower than the actual pull-off strength. However, owing to the various factors affecting consistency in pull-off strength values, performance standards should consider concrete type and application to reflect real-world conditions.

4.8 References

ACI. (2017). Guide for the design and construction of externally bonded FRP systems for strengthening concrete structures. In (pp. 1-112).

ACI. (2023a). Design and Construction of Externally Bonded FiberReinforced Polymer (FRP) Systems for Strengthening Concrete Structures—Guide (ACI PRC-440.2-23). In. Farmington Hills, MI, 2023: American Concrete Institute.

Allen, D. G., & Atadero, R. A. (2012). Evaluating the long-term durability of externally bonded FRP via field assessments. *Journal of composites for construction*, *16*(6), 737-746.

ASTM. (2017). Standard Test Method Tensile Properties of Polymer Composite Materials. In *ASTM D3039*. West Conshohocken, PA: ASTM.

ASTM. (2021a). Standard Test Method for Compressive Strength of Cylindrical Concrete Specimens. In *ASTM C39*. West Conshohocken, PA.

ASTM. (2021b). Standard test method for pull-off strength for FRP laminate systems bonded to concrete substrate. In *ASTM D7522*. West Conshohocken, PA.

Banthia, N., Abdolrahimzadeh, A., Demers, M., Mufti, A., & Sheikh, S. (2010). Durability of FRP-concrete bond in FRP-strengthened bridges. *Concrete International*, *32*(8), 45-51.

Benzarti, K., Chataigner, S., Quiertant, M., Marty, C., & Aubagnac, C. (2011). Accelerated ageing behaviour of the adhesive bond between concrete specimens and CFRP overlays. *Construction and Building Materials*, *25*(2), 523-538.

Brown, J. R., & Hamilton III, H. (2003). NDE of Reinforced Concrete Strengthened with Fiber-Reinforced Polymer Composites using Infrared Thermography. *Proc. InfraMation*, 149-154.

Büyüköztürk, O., Taşdemir, M. A., & Crawford, K. (2013). Non-Destructive Testing of FRP-Structural Systems Applied to Concrete Bridges. Nondestructive Testing of Materials and Structures,

Cawley, P., & Adams, R. (1989). Defect types and non-destructive testing techniques for composites and bonded joints. *Materials science and technology*, *5*(5), 413-425.

CSA-Group. (2019). Canadian Highway Bridge Design Code. In *CSA S6:19*.

Dilonardo, E., Nacucchi, M., De Pascalis, F., Zarrelli, M., & Giannini, C. (2020). High resolution X-ray computed tomography: A versatile non-destructive tool to characterize CFRP-based aircraft composite elements. *Composites science and technology*, *192*, 108093.

Fazli, H., Yassin, A. M., Shafiq, N., & Teo, W. (2018). Pull-off testing as an interfacial bond strength assessment of CFRP-concrete interface exposed to a marine environment. *International Journal of Adhesion and Adhesives*, *84*, 335-342.

Fowai, I., Noël, M., Martin-Perez, B., & Sanchez, L. (2022). Evaluation of interfacial debonding of fibre-reinforced polymer using variable angle peel test. In *Bridge safety, maintenance, management, life-cycle, resilience and sustainability* (pp. 2526-2532). CRC Press.

Fowai, I., Noël, M., Martín-Pérez, B., & Sanchez, L. (2023b). *Condition assessment of FRP-strengthened concrete bridge diaphragms using non-destructive testing* 11th International Conference on FRP composites in civil engineering, Rio de Janeiro.

Galietti, U., Luprano, V., Nenna, S., Spagnolo, L., & Tundo, A. (2007). Non-destructive defect characterization of concrete structures reinforced by means of FRP. *Infrared physics & technology*, *49*(3), 218-223.

Georgeson, G. E., Lea, S., & Hansen, J. (1996). Electronic tap hammer for composite damage assessment. Nondestructive Evaluation of Aging Aircraft, Airports, and Aerospace Hardware,

Ghosh, K., Karbhari, V. M., Kaiser, H., Navada, R., & Lee, L. (2005). *Methods for Detecting Defects in Composite Rehabilitated Concrete Structures*.

Ghosh, K. K., & Karbhari, V. M. (2011a). Use of infrared thermography for quantitative non-destructive evaluation in FRP strengthened bridge systems. *Materials and Structures*, *44*, 169-185.

Ghosh, K. K., & Karbhari, V. M. (2011b). Use of infrared thermography for quantitative non-destructive evaluation in FRP strengthened bridge systems. *Materials and Structures*, *44*(1), 169-185.

Green, M. F., Bisby, L. A., Beaudoin, Y., & Labossière, P. (2000). Effect of freeze-thaw cycles on the bond durability between fibre reinforced polymer plate reinforcement and concrete. *Canadian Journal of Civil Engineering*, *27*(5), 949-959.

Halabe, U. (2013). Non-destructive evaluation (NDE) of composites: techniques for civil structures. In *Non-Destructive Evaluation (NDE) of Polymer Matrix Composites* (pp. 483-517e). Elsevier.

Halabe, U. B., Joshi, R. M., & GangaRao, H. V. (2020). Nondestructive Testing of FRP Composite Structural Components and FRP Rehabilitated Bridge using Digital Tap Testing. *Journal of Multidisciplinary Engineering Science and Technology (JMEST)*, *7*(1).

Halabe, U. B., Roy, M., Klinkhachorn, P., & GangaRao, H. V. (2006). Detection of Air and Water-Filled Subsurface Defects in GFRP Composite Bridge Decks Using Infrared Thermography. AIP Conference Proceedings,

Hao, Z.-H., Zeng, J.-J., Chen, G.-M., Dai, J.-G., & Chen, J.-F. (2024). Durability of FRP-to-concrete bonded joints subjected to 110 months accelerated laboratory and field exposure. *Engineering structures*, *305*, 117681.

Harries, K., & Sweriduk, M. (2016). Factors affecting direct tension pull-off test results of materials bonded to concrete. *Advances in Civil Engineering Materials*, *5*(1), 353-370.

Infrastructure, C. (2016). Canadian infrastructure report card-informing the future. In.

Kaiser, H., & Karbhari, V. (2004). Non-destructive testing techniques for FRP rehabilitated concrete. I: a critical review. *International Journal of Materials and Product Technology*, *21*(5), 349-384.

Kaiser, H., Karbhari, V., & Sikorsky, C. (2004). Non-destructive testing techniques for FRP rehabilitated concrete. II: an assessment. *International Journal of Materials and Product Technology*, *21*(5), 385-401.

Karbhari, V. M., & Ghosh, K. (2009). Comparative durability evaluation of ambient temperature cured externally bonded CFRP and GFRP composite systems for repair of bridges. *Composites part A: Applied science and manufacturing*, *40*(9), 1353-1363.

Lunardelli, M., Leusmann, T., & Lowke, D. (2022). Importance of Concrete Mesoscale Structure on Bond-Slip Behavior of Externally Bonded CFRP Strips. *Journal of composites for construction*, *26*(5), 04022057.

Mac, V. H., Huh, J., Doan, N. S., Shin, G., & Lee, B. Y. (2020). Thermography-based deterioration detection in concrete bridge girders strengthened with carbon fiber-reinforced polymer. *Sensors*, *20*(11), 3263.

Malla, P., Khedmatgozar Dolati, S. S., Ortiz, J. D., Mehrabi, A., & Nanni, A. (2023). Damage and Defects in Fiber-Reinforced Polymer Reinforced and Strengthened Concrete Elements. *Journal of composites for construction*, *27*(4), 04023035.

Mikami, C., Wu, H.-C., & Elarbi, A. (2015). Effect of hot temperature on pull-off strength of FRP bonded concrete. *Construction and Building Materials*, *91*, 180-186.

Milev, S., & Tatar, J. (2023). Durability Assessment of the First Externally Bonded FRP Repair of a Publicly Owned Bridge in the United States after 26 Years of Service. *Journal of composites for construction*, *27*(5), 04023049.

Mtenga, P. V., Parzych, J. G., & Limerick, R. (2001). Quality assurance of frp retrofit using infrared thermography. In *Structures 2001: A Structural Engineering Odyssey* (pp. 1-8).

Obaidat, Y. T., Heyden, S., Dahlblom, O., Abu-Farsakh, G., & Abdel-Jawad, Y. (2011). Retrofitting of reinforced concrete beams using composite laminates. *Construction and Building Materials*, *25*(2), 591-597.

Pallempati, H., Beneberu, E., & Yazdani, N. (2016). Evaluation of external FRP-concrete bond in repaired concrete bridge girders and columns. *Innovative Infrastructure Solutions*, *1*(1), 1-8.

Pejryd, L., Beno, T., & Carmignato, S. (2014). Computed tomography as a tool for examining surface integrity in drilled holes in CFRP composites. *Procedia CIRP*, *13*, 43-48.

Qiu, Q. (2020). Imaging techniques for defect detection of fiber reinforced polymer-bonded civil infrastructures. *Structural Control and Health Monitoring*, *27*(8), e2555.

Starnes, M. A., Carino, N. J., & Kausel, E. A. (2003). Preliminary thermography studies for quality control of concrete structures strengthened with fiber-reinforced polymer composites. *Journal of materials in Civil Engineering*, *15*(3), 266-273.

Tatar, J., & Brenkus, N. R. (2021). Performance of FRP-strengthened reinforced concrete bridge girders after 12 years of service in coastal Florida. *Journal of composites for construction*, *25*(4), 04021028.

Valluzzi, M., Grinzato, E., Pellegrino, C., & Modena, C. (2009a). IR thermography for interface analysis of FRP laminates externally bonded to RC beams. *Materials and Structures*, *42*, 25-34.

Yumnam, M., Gupta, H., Ghosh, D., & Jaganathan, J. (2021). Inspection of concrete structures externally reinforced with FRP composites using active infrared thermography: A review. *Construction and Building Materials*, *310*, 125265.

Zhuang, X., Ma, J., Liu, F., Dan, Y., Huang, Y., & Jiang, L. (2022). Characterization of hydrothermal aging induced voids in carbon fiber reinforced epoxy resin composites using micro-computed tomography. *Polymer Degradation and Stability*, *206*, 110198.

Chapter 5 -Bond performance of deteriorated CFRP-interface under single mode loading[1]

5.1 Abstract

Carbon fiber-reinforced polymer (CFRP) has been adopted as an alternative to externally bonded steel for structural retrofitting; however, the long-term performance of CFRP composites in actual in-service applications remains under-explored. Laboratory experiments on pristine CFRP samples indicate improved structural capacity and highlight the adverse impact of premature debonding. This study aims to gather essential field data regarding the performance of CFRP composites on deteriorated 57-year-old concrete through 27 concrete samples subjected to three distinct mode II (in-plane shear) loading conditions. The samples were extracted from the diaphragms of the recently deconstructed Champlain Bridge in Canada. To test the field samples, modified single and double lap shear configurations were developed that eliminated the need for directly gripping the CFRP sheets, and the results were subsequently compared to a more conventional single lap shear test. The influence of existing defects on bond behaviour and the effect of test configuration on interface performance under single-mode loading were evaluated. Three-dimensional digital image correlation (DIC) was employed to capture full-field in-plane and out-of-plane displacement data, thereby addressing the strain measurement challenges in bonded interfaces and confirming the occurrence of mode I deformations (out-of-plane peeling) during debonding. Experimental strain measurements at failure predominately ranged from 2500 to 3400 microstrain, with a maximum of 4739 microstrain, which is approximately 56% of the debonding strain predicted by ACI PRC-440.2.23. The strain limit set by the Canadian Highway Bridge Design Code (CAN/CSA S6:19) exceeded the maximum experimental strain by 27%. Results indicated that the double lap shear test provided more consistent peak loads, while the single lap shear configuration exhibited greater variability. The bond stress-slip behaviour along the length of the CFRP sheet was found to vary significantly; an analytical comparison of experimental data with existing

[1] A version of this chapter has been published as: Issa Fowai, Martin Noel, Mohammad Esmaili, Beatriz Martin-Perez, and Leandro Sanchez (2025). *Bond performance of deteriorated CFRP-concrete interface under different shear-lap configurations: A Champlain Bridge case study*. Journal of Construction and Building Materials.

cohesive zone models demonstrated a strong correlation with local bond stress-slip results in certain regions that reached high levels of bond stress. In contrast, other regions showed both lower peak stresses and lower stiffness than predicted by most models, which may be attributed to local deterioration or defects at the CFRP-concrete interface.

5.2 Introduction

The application of externally bonded composite materials such as carbon fiber-reinforced polymer (CFRP) for repairing deficient civil concrete infrastructure is anticipated to rise due to the significant reduction in composite material costs and increased familiarity among engineers with repair processes. Extensive laboratory studies have spurred international efforts to create guidelines and codes for standardizing the repair process with composite materials (ACI, 2023a; CSA-Group, 2019; FIB, 2020). Earlier research in Canada and elsewhere has focused on bond strength and failure modes between externally bonded composite materials and concrete, primarily using laboratory-prepared samples with pristine material properties (Baggio et al., 2014; Bizindavyi et al., 2003; Green et al., 2000; Hao et al., 2024; Kabir et al., 2017; Li & Leung, 2016; Tomlinson & Fam, 2015; Yun & Wu, 2011). These studies demonstrate that adhesive quality, concrete surface preparation, and curing conditions critically affect bond strength under accelerated ageing and standard conditions (Benzarti et al., 2011; Karbhari & Ghosh, 2009; Leone et al., 2009). Additionally, these laboratory research studies have highlighted the necessity of addressing the brittle debonding between the elastic CFRP composite material and concrete, leading to design guidelines specifying debonding strain limits, debonding loads, and anchorage systems to delay or mitigate premature debonding (ACI, 2023a; CSA-Group, 2019; FIB, 2020). Researchers have also used several destructive and non-destructive techniques to enhance the understanding of the interaction between externally bonded CFRP and concrete. Different non-destructive testing (NDT) methods, such as coin tapping, hammer tapping, or infrared thermography, are significant in detecting localized and global bond defects. Structural testing methods to assess the CFRP-concrete bond strength have included direct tension pull-off tests (Harries & Sweriduk, 2016), variations of shear-lap tests (Aiello & Leone, 2008; Ueda et al., 1999), and beam tests (Khalifa & Nanni,

2002). Integrating NDT findings with bond integrity data from structural tests (Fowai et al., 2025a; Fowai et al., 2025c; Fowai et al., 2025e) represents an emerging area of research in composite repair that will be further developed with NDT data fusion and digital twin technologies.

Peng et al. (Li et al., 2023) utilized three-dimensional digital image correlation (DIC) to examine how artificial defects in the epoxy layer affect the interfacial bond behaviour between CFRP and concrete. The study found that defects smaller than 5% of the effective bond area had a limited impact on the CFRP-concrete interface performance, whereas a higher concentration of defects significantly reduced load-bearing capacity. Defect shape, size, and location were all found to affect interfacial bond behaviour. Specifically, a 5% defect area resulted in an 8.5% reduction in strength, and a 25% defect area caused a 27% drop in ultimate load. No change in ultimate slip was observed for defect areas up to 15%. A load capacity reduction model was proposed, showing a strong correlation with experimental data.

Ao et al. (Zhou et al., 2017) conducted experiments on flexural beams with artificial defects, revealing that deep beams showed greater sensitivity to interfacial defects than normal beams. The authors found that defects in the shear span critically reduce strength more than those in the constant moment region. Specifically, a 6000 mm^2 interfacial defect in the mid-span led to reduced load capacity of 5%, 0.9%, and 0.3% for beam lengths of 0.5 m, 3 m, and 6 m, respectively. In contrast, defects in the shear span resulted in load capacity reduction of 46.9%, 11.8% and 5.6% for the same beam lengths.

Despite substantial progress in laboratory studies on small-scale samples, there exists a lack of knowledge/studies on the dissimilarity between a pristine concrete specimen retrofitted with new CFRP in the lab and a real in-service structure with pre-existing deterioration retrofitted with CFRP after several years or decades of exposure to ambient environmental conditions (de Waal et al., 2017; Milev & Tatar, 2023; Tatar & Brenkus, 2021). Among several points to note, deteriorated concrete typically exhibits a compromised surface characterized by cracking, spalling, and overall loss of material integrity, which can adversely affect the bond strength between the old concrete and the new CFRP (Allen & Atadero, 2012). Also, moisture infiltration or contamination before CFRP application may

further diminish bond strength. Deteriorated concrete is more susceptible to ongoing degradation over time, potentially leading to earlier bond failure compared to pristine concrete. The risk of material incompatibility between the old concrete and retrofitting materials increases if surface preparation and thermal compatibility guidelines are not followed. The cumulative effect of these factors on bond behaviour must be addressed, as achieving full composite strength between old concrete and new CFRP can be challenging.

Several other research questions warrant investigation, particularly given that debonding is intrinsically linked to the strain limit in concrete under loads. For instance, it has not been established whether existing analytical models to estimate critical bond parameters, such as effective bond length, maximum shear stress, and slip, remain valid for in-service structures retrofitted after an extended period of degradation. Therefore, it is essential to develop a database assessing the durability of the bond between deteriorated concrete exposed to in-service loads and varying environmental conditions and retrofitted with pristine CFRP materials (de Waal et al., 2017; Fowai et al., 2023b; Fowai et al., 2025e; Fowai, 2023, 2024; Milev & Tatar, 2023; Tatar & Brenkus, 2021). This knowledge will enhance the calibration of current analytical models (Chen & Teng, 2001; Ferracuti et al., 2007; Yuan et al., 2004) and numerical studies (Chen & Pan, 2006) regarding the CFRP-concrete interface, ultimately improving design guidelines related to material strength reduction factors and other key design parameters.

A comprehensive literature review indicates a predominance of studies focusing on the bond between CFRP and normal-strength concrete (De Lorenzis et al., 2001; Lu et al., 2005; Nakaba et al., 2001), with limited investigations addressing the bond characteristics between high-strength concrete and CFRP where debonding failure mode may shift from cohesive failure in concrete to failure in the adhesive. Ongoing research into externally bonded CFRP systems applied to ultra-high-performance concrete (UHPC) present a promising area for structural rehabilitations. However, further research is essential to optimize their performance across various structural applications. Zhang et al. (Zhang et al., 2024a) used both experimental methods and finite element numerical simulations to examine the effect of temperatures (room temperature, 120% Tg, 150% Tg and 160% Tg, where Tg is the glass transition

temperature) on the debonding behaviour of adhesive bond between CFRP and UHPC. The authors reported a significant reduction in the load capacity; approximately 44% to 74 % as the temperature rose from room temperature to 1.2 Tg and 1.5 Tg respectively. At 1.6 Tg, the load capacity decrease was similar to that observed at 1.5 Tg. The study also demonstrated that the temperature influences the failure mode of debonding and the propagation of damage between the different material layers. At room temperature, a complete debonding failure occurred at the interface between the CFRP and concrete at the adhesive layer. At 120% Tg, a mixed -mode debonding was observed, wherein separation at the adhesive-concrete interface was noticed at the ends of the plate, while the middle section of the beam exhibited debonding at adhesive-CFRP interface. At 1.5 Tg and 1.6 Tg, the sharp characteristic brittle debonding sound diminished, as significant softening of the adhesive occurred, leading to a debonding primarily at the adhesive-CFRP interface. In a related study, Zhang et al. (Zhang et al., 2024b), conducted a comparative analysis under cyclic loading, assessing UHPC beams versus normal strength concrete beams strengthened with CFRP plates. The specimens were categorized into two groups: unstrengthened and strengthened with one layer of CFRP plates. Each group was further divided into three subcategories based on the height of UHPC used. The first subcategory in both groups was composed entirely of normal strength concrete with a compressive strength of 31 MPa. The second subcategory contained beams that were casted using a combination of normal strength concrete and UHPC, with or without externally bonded CFRP. In this category, the concrete in the tension zone of the beams were replaced with UHPC while the compression zone was fabricated with normal strength concrete. The final subcategory included beams either with or without CFRP plates cast entirely from 116 MPa UHPC. The results showed that replacing the 200 mm tension zone of the conventional 300 mm high beams with UHPC led to an increase in both the cracking load and ultimate load by 33% and 26%, respectively. For beams constructed entirely of UHPC, the cracking load and ultimate load increased by 78% and 49%, respectively. The application of CFRP plates substantially enhanced the load-bearing capacity of the normal strength concrete beams, while the effect was less pronounced in the UHPC beams. The use of UHPC in the tension zone resulted in wider cracks compared to the denser cracking observed in samples of normal strength concrete.

Test configurations on bond behaviour between CFRP and concrete under mode II loading have skewed towards conventional pull-push single shear-lap test setup (Carloni & Subramaniam, 2010; Chataigner et al., 2011; Li et al., 2023). However, no universally accepted test configuration exists for evaluating the CFRP-concrete bond under mode II loading. Aiello and Leone (Aiello & Leone, 2008) examined the interface behaviour of externally bonded FRP and concrete through flexural beams, single-shear-lap and double-shear-lap test setups. Their findings revealed comparable average bond strengths across all three setups, with beam samples showing higher bond strength values than the shear-lap tests. Double-shear lap specimens produced higher bond stress values than single-shear-lap tests. Meanwhile, the single shear-lap tests show high scatter in results. A review by Savoia and Ferrutti (Mazzotti et al., 2009) indicated that, although beam tests typically yield higher bond strength values, double-shear-lap tests are expected to exhibit lower debonding strength than single-shear tests. The authors attributed this observation to the inherent asymmetry of the double shear-lap specimens during damage progression, which usually experiences failure initiation on one side of the specimen. However, issues such as eccentricity and compressive stresses in concrete clamping of push-pull single shear-lap tests have not been sufficiently addressed (Brosens, 2001).

This paper aims to experimentally and analytically investigate the bond behaviour between deteriorated high-strength concrete bridge diaphragms and CFRP sheets through single-mode loading conditions. The experimental investigation will provide further knowledge on the in-service performance of the CFRP strengthened system after being in service for more than five years. The bridge discussed here was a major path of international trade between Canada and the United States, and research findings on the condition assessment and the bond behaviour under mixed mode loading are presented in companion studies (Fowai et al., 2025e; Issa Fowai et al., 2025). This study investigates the CFRP-concrete bond under three different shear lap configurations: a new single shear-lap, conventional, and double shear-lap setup. The maximum transferable load, strain and bond stress distribution in deteriorated concrete elements strengthened with CFRP is discussed. Optical DIC is used to provide full-field displacement and strain measurement data.

5.3 Overview of the Champlain Bridge

The bridge from which the shear-lap samples used for single mode loading were cut was the 57-year-old decommissioned bridge from Montreal, which had undergone strengthening with CFRP wraps at various intervals during its service life. Detailed accounts of the bridge and its deconstruction rationale are available in section 1.3 of this dissertation, along with findings from the thorough condition assessment of the extracted bridge diaphragms before the current structural tests on the bond behaviour of the composite materials used in the repair (Fowai, 2023, 2024). One of the bridge diaphragms was cut into blocks for the shear lap tests described in this study (see Figure. 5.1).

a) Sketch of shear-lap cut b) Cuts for double shear-lap specimens

Figure. 5.1. Shear-lap sample extracting from bridge diaphragm

5.4 Experimental program and test set-up

Various configurations of single and double shear-lap tests can yield data on the performance of CFRP-concrete bond. The lack of standardized or calibrated testing methods hampers the comparison of results across different studies. In addition, many laboratory setups require a free-hanging portion of the FRP to apply the tensile loads to the FRP. In this study, due to the unavailability of a free-hanging portion of the FRP for gripping, steel clamping systems were designed to induce shear in different shear-lap configurations. Two single shear-lap setups and one double shear-lap setup were used to experimentally evaluate 27 concrete prisms cut from the deconstructed bridge elements. A specimen naming convention in the form of X-Y has been adopted, where X corresponds to the type of shear-lap test, and Y corresponds to the sample number. For example, SS-S1 refers to the new single shear-lap specimen number 1, whereas DS-S7 indicates double shear-lap specimen number 7, and CSS-S3 represents conventional single shear-lap specimen number 3. Figure. 5.2 shows the various shear-lap bond tests

and sample gripping or clamping systems, while Figure 5.3 and Figure. 5.4 depict NDT identified defects and the tests in progress, respectively. All samples were tested under displacement control at a rate of 0.005 mm/s.

5.4.1 New single shear-lap set-up (stage 1)

In the initial single shear-lap tests, ten concrete prisms (300 mm x 500 mm x 220 mm) were gripped with a custom steel clamping system to apply shear stress to the CFRP-concrete interface. A rigid steel clamping system with four angle plates was bolted to a universal testing machine via four steel connector plates (see Figure. 5.2(a) and 5.4(c). This new single shear-lap setup shown in Figure 5.2 was designed to address the absence of free-hanging FRP from the bridge specimens, which is typically required in the conventional single shear-lap tests.

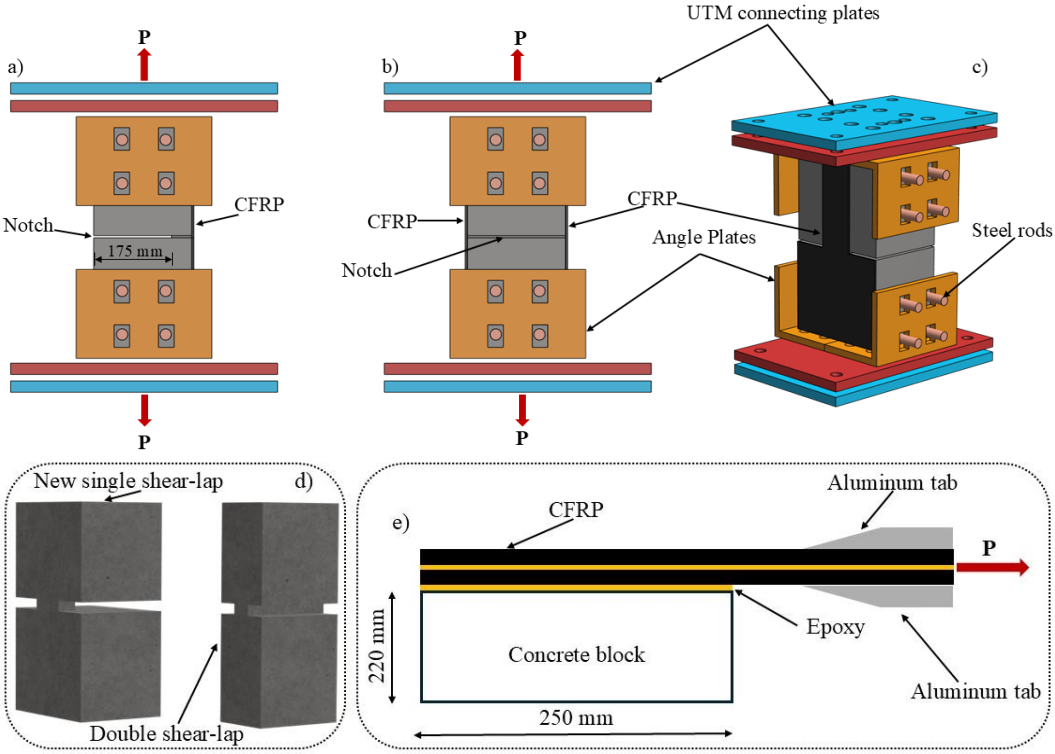

Figure. 5.2. Shear-lap setups a) Side view of new single shear-lap b) Side view of double shear-lap c) Isometric view of new single shear-lap test d) exaggerated view of notch condition in new single and double shear-lap tests se) Conventional single shear-lap

Each angle plate featured four slots on the side, and specimen preparation included drilling eight holes in the concrete blocks, which were epoxy-grouted with steel rods. The front face of the specimen was externally strengthened with two layers of 300 mm wide CFRP strips. A horizontal cut was introduced

at mid-height from the rear of the sample extending approximately 175 mm towards the front face to facilitate the formation of a crack in the concrete during tensile loading with the purpose of inducing debonding at the mid-height of the specimen. The bonded width above the notch was reduced to ensure failure in the reduced-width area (150 mm x 250 mm for the first four samples and 100 mm x 250 mm for the remaining six samples). The full-width region (at the bottom of the notch) served as anchorage. The horizontal notch was extended on both sides of the reduced-width CFRP. Failed specimens from this stage of testing were further trimmed to obtain smaller concrete prisms used for the conventional shear-lap tests discussed below.

Defects and debonded regions in concrete structures externally bonded with CFRP are known to have impacts on the durability and load bearing capacity of the retrofitted structure. The local strain distribution over and around defective regions in an externally bonded composite may be complex depending on defect type, size, and applied load. Defects can create stress concentrations and reduce the load-carrying capacity. In the case of defects at the FRP-concrete interface, the bond stress transfer is interrupted, and a lower strain gradient is expected (depending on the size of the defect relative to the sheet width). Before structural testing, thorough assessments of damage in the retrofitted bridge diaphragms were conducted using localized and global NDT methods (Fowai et al., 2025d). The evaluation involved a detailed visual inspection and a conventional coin-tapping approach, as well as infrared thermography and an automated Wichitech digital tap hammer to cross-validate the results from other methods (Fowai et al., 2025d).

The dimensions of defects identified in the shear-lap specimens varied, with size ranging from 20 mm x 40 mm in specimen SS-S9 to 35 mm x 110 mm in SS-S8 (see Figure 5.3). Some defects (voids, air pockets and debonds) were located outside the reduced width region, while others were present predominately within the full-width area and no major conclusions could be made regarding the impact of these defects on effective strain limits.

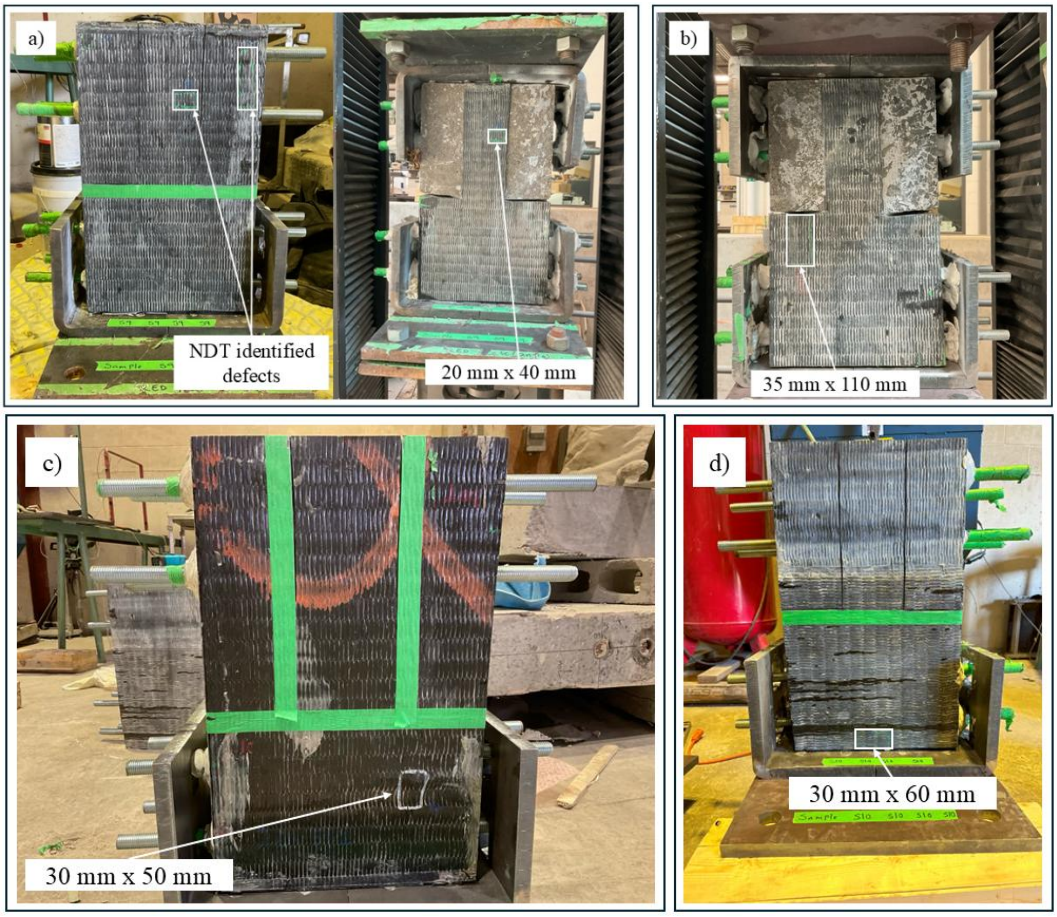

Figure 5.3-NDT identified defects in shear-lap specimens a) SS-S9 b) SS-S8 c) SS-S6 d) SS-S10

5.4.2 Conventional single shear-lap set-up (stage 2)

In stage 1 of testing, nine out of ten samples failed by debonding in the reduced width area as expected; the tenth sample exhibited a premature failure in the concrete and is not discussed further. The bottom "block" with the full-width CFRP sheet remained intact. This allowed the trimming of the intact block to create nine concrete specimens measuring 150 mm x 250 mm x 220 mm, each with a free-end length of 150 mm that could be directly gripped by the testing machine. The bonded width of the CFRP was reduced to 50 mm to avoid retesting pre-damaged areas. Figure. 5.4b depicts the conventional shear-lap tests (stage-2) in progress.

5.4.3 Double shear-lap set-up

An additional eight concrete prisms were cut from the diaphragms for the double shear-lap samples, measuring 150 mm x 500 mm x 220 mm. The width of the CFRP on both the front and back of the

blocks was reduced to 50 mm. A horizontal notch was provided on both sides of the bonded width to initiate a crack at the mid-height of the specimens under tensile loading. Since the DIC system could only capture one face of each test specimen, three strain gauges were installed on the back of six samples as shown on Figure. 5.4d : Gauge 1 (SG-1) was positioned 50 mm above the notch, Gauge 2 (SG-2)was placed at the notch height, and Gauge 3 (SG-3) was 50 mm below the notch. The customized angle plates from the shear-lap tests from Stage 1 were reused for the double shear-lap tests (see Figure. 5.2c).

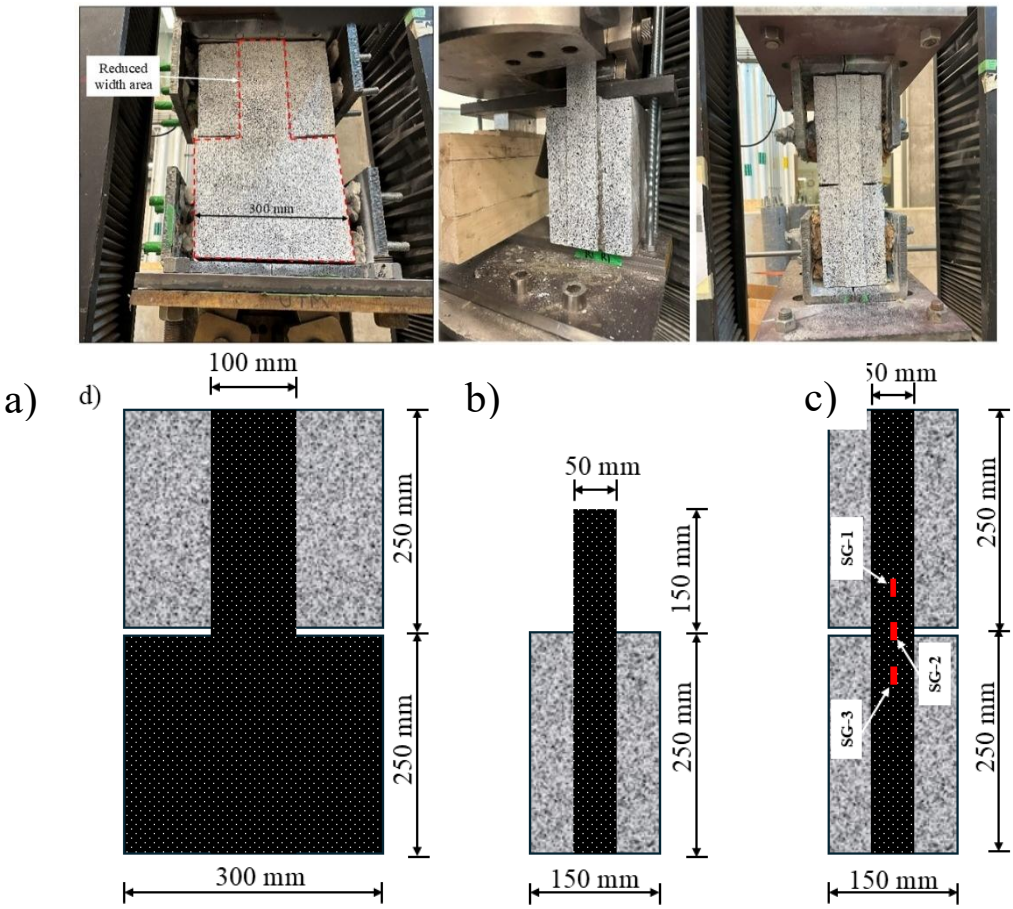

Figure. 5.4. Shear-lap tests in progress and specimen dimensions a) New single shear-lap b) Conventional single shear-lap c) Double shear-lap d) specimen dimensions

5.4.4 DIC set-up

DIC is a widely used technique in structural laboratories for measuring strain and displacement (Carloni & Subramaniam, 2010). In this study, full-field 3D DIC data was obtained using two high-resolution cameras synchronized to capture stereo images of specimens under load. These cameras were mounted on a single frame and configured with narrow-band blue lights to reduce ambient light interference. The 3D setup allows for the evaluation of the out-of-plane displacement of the specimens during testing.

Figure. 5.5 shows the 3D setup in the laboratory and the general steps involved, from surface preparation to data interpretation. The process involved the application of a high-contrast speckle pattern on the specimen surface: a base layer of white paint followed by random black patterns. The cameras were positioned on the frame at an angle of 25 degrees, as recommended by the manufacturer, with uniform illumination provided by the blue lights on tripods. The setup included data acquisition systems linked to a computer via ethernet cable, facilitating camera control and data recording. In scenarios of excessive ambient light, shielding of the test frame can be used to minimize shadows and reflections. Initial calibration is performed, and the quality of the speckle is checked for data accuracy. Future calibration for the same test setup is necessary only if the camera parameters (angle between cameras, camera focus and aperture, etc.) have changed. However, the quality of the speckle pattern should be checked before every test. Data acquisition starts when a reference image without load is captured first, and continuous images are captured at specified intervals during the loading stages. The cameras are synchronized to track the displacement of the speckle pattern throughout the test to establish the displacement field, which is then used to compute the surface strain of the specimen. In this study, continuous DIC images were captured every two seconds.

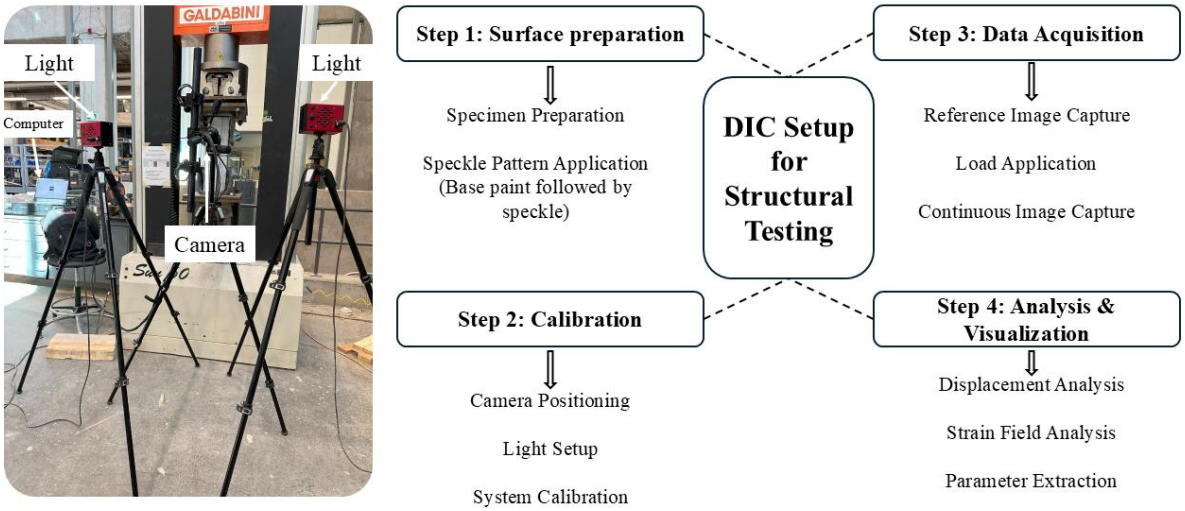

Figure. 5.5. 3D DIC setup and general steps involved in DIC measurements

5.4.5 Material properties

Three concrete cores were extracted from the diaphragms and tested in compression in accordance with ASTM C39 (ASTM, 2021a). The compressive strength of the underlying concrete substrate obtained

from the average of three core samples (77.7 MPa, 75.0 MPa and 74.9 MPa) with an average diameter of 95 mm and height of 200 mm was 75.9 MPa (standard deviation of 1.30 MPa), and the estimated cracking strength of the concrete obtained from Equation 5.1 is 3.48 MPa (CSA-Group, 2019). The elastic modulus of the concrete based on CSA provision is 38,020 MPa (CSA-Group, 2019).

$$f_{cr} = 0.4\sqrt{f_c'} \qquad \text{(Equation 5.1)}$$

To evaluate the CFRP material's mechanical properties, 36 coupons were extracted from one of the diaphragms. Eighteen coupons were tested following ASTM D3039 (ASTM, 2017) to determine the tensile properties of the composite materials, four of which exhibited desirable failure modes were used to determine the material properties. These samples were carefully extracted using an angular grinder, mallet, and concrete chisels, taking care not to damage the CFRP itself. Extracted samples were cut into coupons of 300 mm in length by approximately 25.4 mm in width. Before testing, 6-mm thick aluminum tabs with bevel ends were designed, ground, and bonded to the coupons for even stress distribution and minimizing stress concentrations over the grip region (see Figure. 5.6). To minimized damage to the final 300 mm coupon samples, the extracted CFRP was kept sufficient longer than the required 300 mm length (see Figure. 5.6a). Gentle scoring was done on the marked areas where the CFRP coupon was to be cut, and aggressive cutting methods were avoided. No heat was used during this process to prevent damage to the adhesive.

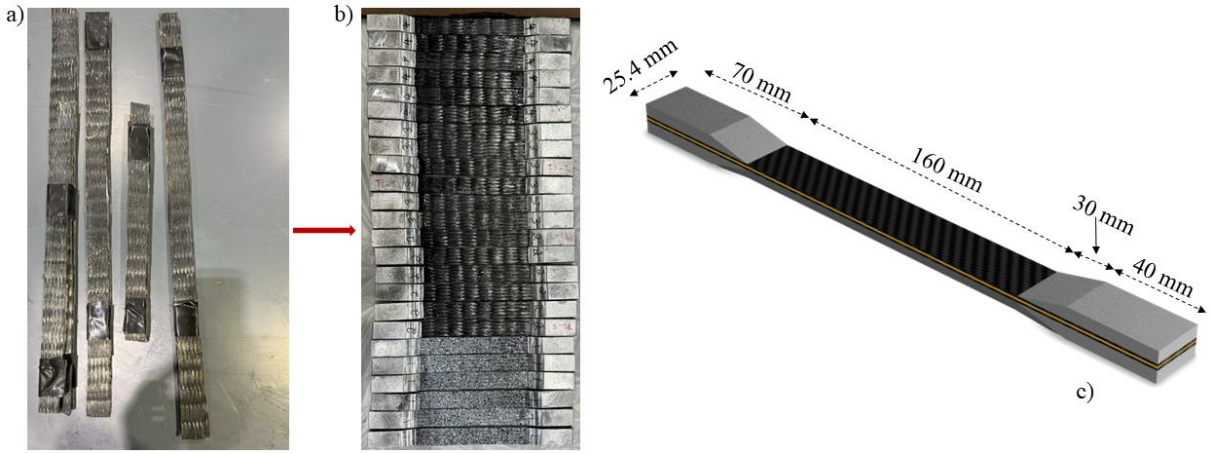

Figure. 5.6. Extracted samples and coupon dimensions

Any concrete residue on the extracted CFRP strips at the bond line were carefully removed with angle grinder and sandpaper before attaching the 6 mm aluminum tabs to the ends of the coupons. An electrical resistance strain gauge was installed at mid-height on one side of the samples (flat surface obtained after grinding of bond line), while the other surface was speckled for digital image correlation.

A universal testing machine operating at 2 mm/min was used to complete the coupon tests. Table 5.1 presents the experimentally determined material properties of the double-layered CFRP sheets based on measured thickness. The manufacturer's design properties for a single layer with a nominal thickness value of 1.7 mm per layer are as follows: the tensile strength, modulus of elasticity, and elongation at break are 855 MPa, 49.6 GPa, and 1.7%, respectively.

Table 5.1. Double-layer CFRP sheet properties (as-is)

	Coupon 1	Coupon 2	Coupon 3	Coupon 4	Average	Standard Deviation
Tensile strength (MPa)	542.4	556.8	588.2	642.0	582.4	38.2
Elongation at break (%)	0.9	1.2	1.3	1.0	1.1	0.2
Modulus of elasticity (GPa)	56.1	49.6	50.3	50.1	51.6	2.7
Length (mm)	300.0	300.0	300.0	300.0	300.0	-
Width (mm)	25.4	25.4	25.4	25.4	25.4	-
Thickness (mm)	3.7	3.6	3.4	3.3	3.5	0.2

5.5 Experimental Results and Discussion

5.5.1 Failure modes

23 out of 27 of the specimens tested exhibited a bond-induced cohesive/adhesive failure with the failure plane passing through both the concrete substrate and the adhesive layer (Table 5.2). These failures were characterized by a thin, sporadic layer of concrete adhering to the debonded strip (Figure 5.7). More concrete residue was observed at specific locations: the notch in new single and double shear-lap tests and the loaded end in conventional single shear-lap configurations.

a) Concrete failure in reduced bonded width for SS-S10

b) Typical concrete failure conventional single shear-lap

c) Typical concrete failure Double shear-lap

Figure 5.7-Failed samples from various shear-lap tests

Complete interface debonding without concrete residue was not observed, nor were any failed strips entirely covered with concrete substrates, contrasting with observations in lower to normal-strength concrete substrates (Czaderski et al., 2010; Li et al., 2023; Mabry et al., 2018).

Four specimens (three from new single shear-lap and one from double shear-lap) showed premature failure and were excluded from the result analysis. Premature failure was defined as localized concrete fracture or epoxy failure between the clamp and the steel rods. In new single shear-lap specimens, a premature fracture may have resulted from preexisting cracks or weak bonds between transverse prestressing tendons in the concrete prisms, causing in-plane rotation due to asymmetric stiffness (Figure 5.8).

Failure initiation occurred at the notch in new single and double shear-lap tests. Conventional pull-push single shear-lap tests experienced failure initiation at the loaded end, propagating towards the sheet end. In double shear-lap tests, bond interface collapse was not simultaneous on both bonded surfaces, but comparable strain measurements were observed via DIC and strain gauges on both sides. Load eccentricity was previously reported in the literature for double shear-lap tests with discontinuous concrete blocks held together by FRP strips on the two bonded surfaces (Mazzotti et al., 2009).

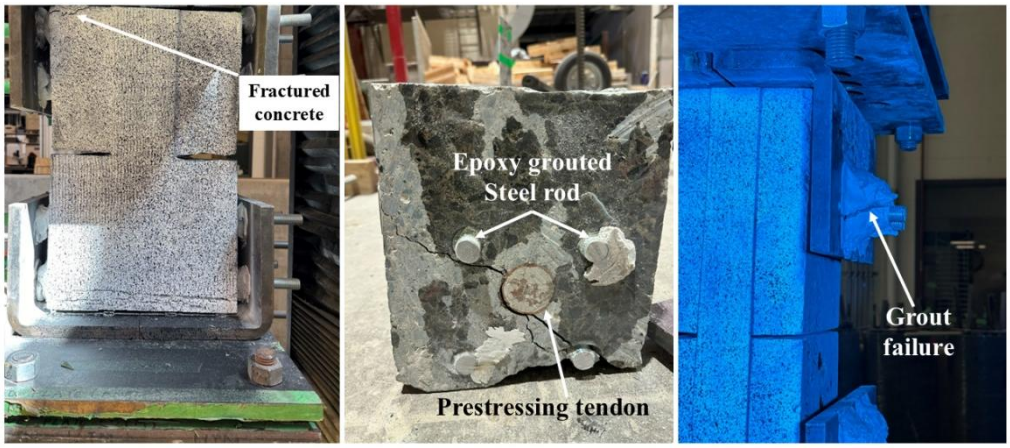

a) Localized concrete fracture b) Bond failure at tendon-concrete interface c) Epoxy failure

Figure 5.8-Premature concrete or grout failure

Table 5.2 summarizes experimental results for all specimens, excluding specimens that showed premature failure. Values in parenthesis for the double shear-lap specimens (DS-S1 to DS-S8) represent maximum strain readings from the electrical strain gauges.

Table 5.2-Summary of shear-lap results

Specimen[a]	CFRP width (mm)	P_u(kN)	P_u/b_f (N/mm)	Max CFRP strain (με)	Failure mode
SS-S1	150	45.9	306	2589	Substrate
SS-S2	150	32.8	219	2118	Substrate
SS-S3	150	39.9	266	2778	Substrate
SS-S5	100	60.1	601	–[b]	Substrate
SS-S6	100	30.0	300	–[b]	Substrate
SS-S7	100	38.5	385	2224	Substrate
SS-S9	100	44.0	440	2439	Substrate
CSS-S1	50	34.5	690	3359	Substrate
CSS-S2	50	26.6	532	3500	Substrate
CSS-S3	50	24.8	496	2712	Substrate
CSS-S4	50	25.8	516	3116	Substrate
CSS-S5	50	21.5	430	1617	Substrate
CSS-S6	50	21.1	422	3134	Substrate
CSS-S7	50	43.4	868	3619	Substrate
CSS-S8	50	30.6	612	4739	Substrate
CSS-S9	50	28.5	570	3034	Substrate
DS-S2	50	36.2	362	1774	Substrate
DS-S3	50	53.3	533	3301 (2800)	Substrate
DS-S4	50	49.4	494	3599 (3218)	Substrate
DS-S5	50	50.7	507	2925 (2221)	Substrate
DS-S6	50	51.1	511	2645 (2994)	Substrate
DS-S7	50	44.4	444	1372 (2103)	Substrate
DS-S8	50	48.6	486	–[b] (2159)	Substrate

[a]SS, CSS, DS-new single, conventional single and double shear-lap specimens
[b] DIC readings not available

5.5.2 Maximum load

Experimental results show mean ultimate loads of 41.6 kN, 28.5 kN, and 47.7 kN for the new single, conventional, and double shear-lap tests (two bonded surfaces), respectively. These average peak loads were in agreement with the maximum transferable loads found in accordance with the bond strength models of Chen & Teng (Chen & Teng, 2001) (Figure 5.9) for the conventional single shear-lap and double shear-lap tests. However, due to significant variability in the new single shear-lap tests, which is attributable to the out-of-plane rotations of these specimens, the prediction from the Chen & Teng model did not correlate well with the experimental load values observed for the 60-year-old deteriorated concrete specimens. The ultimate force is given by Equation 5.1. In these expressions, b_p and f_c' are the bond width and concrete compressive strength respectively.

$$\mathrm{P_u} = 0.427\beta_p\beta_l\sqrt{f_c'}b_pL_e \qquad \text{Equation 5.1}$$

The width ratio was defined according to Equation 5.2

$$\beta_\mathrm{p} = \sqrt{\frac{2 - {b_p}/{b_c}}{1 + {b_p}/{b_c}}} \qquad \text{Equation 5.2}$$

The coefficient β_L accounts for the ratio of the effective length to the total bonded length (Equation 5.3).

$$\beta_L = \begin{cases} 1, & if\ L \geq L_e \\ \sin\dfrac{\pi L}{2L_e}, & if\ L < L_e \end{cases} \qquad \text{Equation 5.3}$$

The effective bond length was expressed as given in Equation 5.4.

$$\mathrm{L_e} = \sqrt{\frac{E_p t_p}{\sqrt{f_c'}}} \qquad \text{Equation 5.4}$$

b_p and f_c' are the bond width and concrete compressive strength respectively.

Overall, increased bonded width in the new single and double shear-lap configurations correlated with higher peak loads. Increasing FRP width leads to an increase in the maximum load that the interface can carry; however, this relationship is not linear.

With a wider width, the new single shear-lap setup results also showed a lower unit load while the conventional pull-push single shear-lap specimens recorded higher unit loads (see Figure 5.9a). The new single shear-lap setup and conventional shear-lap exhibited greater variability in maximum transferable load, while double shear-lap specimens showed more consistent results. Despite efforts to restrain them, eccentricity in the new single shear-lap setup caused some out-of-plane rotation, which introduced bending moments to these samples; this effect is discussed in more detail later.

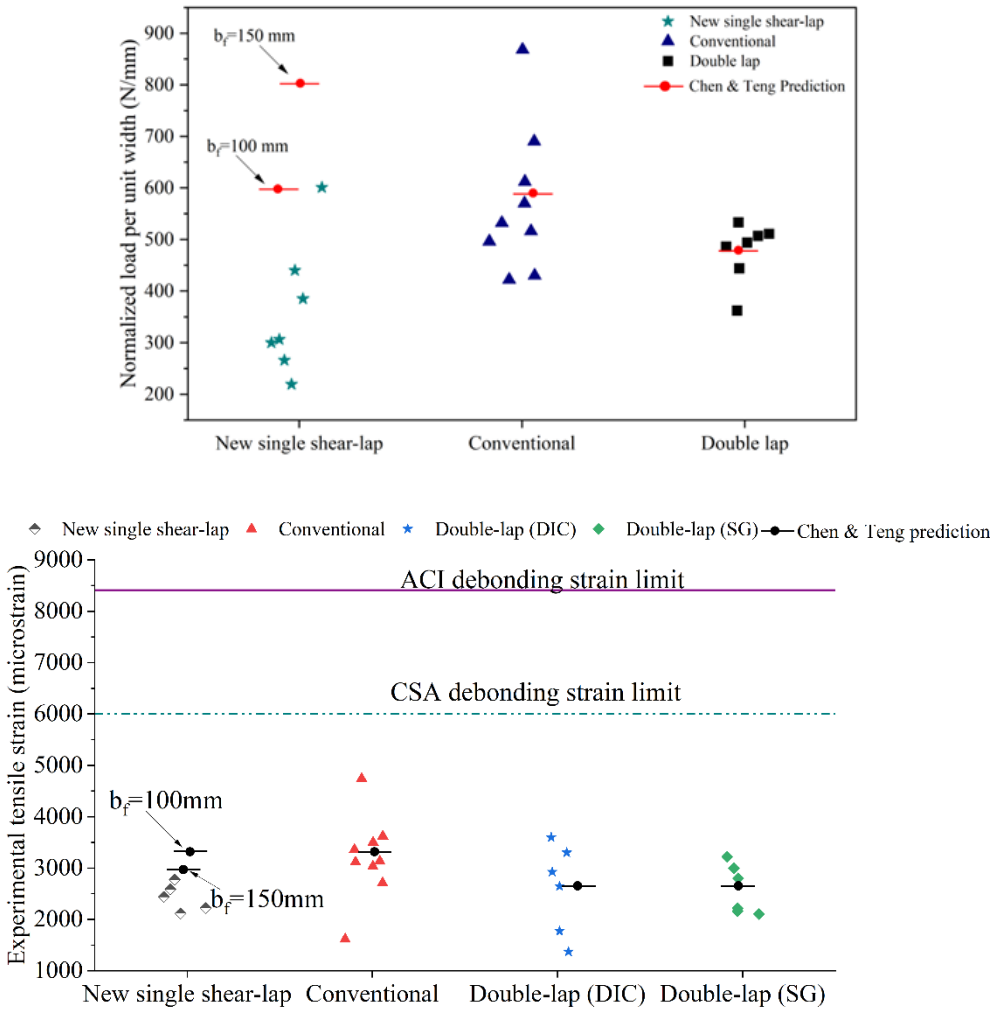

Figure 5.9-Correlation of experimental load and strain with prediction from existing analytical model a) Experimental unit load per tests b) Correlation of experimental strain with existing models

Out-of-plane displacement in shear-lap tests of CFRP-concrete interface is primarily attributed to the inherent eccentricity of the test setup. The out-of-plane displacement recorded during the shear-lap tests was measured using DIC data. The double shear-lap test showed the lowest displacement values. The out-of-plane displacement of the double shear-lap specimens was 1 mm less than the average of the conventional single shear-lap specimens (1.56 mm). On the other hand, the new single shear-lap setup yielded the highest out-of-plane displacement (8 mm) due to the specimens' out-of-plane rotation which was difficult to prevent.

A typical example of this out-of-plane displacement, illustrating the rotation for specimen SS-S9, is presented in Figure 5.10 and Figure 5.11. Figure 5.10a presents the contour plots of the out-of-plane displacement at various load levels leading up to failure in SS-S9, while Figure 5.11 depicts the rotational magnitude across the specimen's centreline at different load levels. The pronounced out-of-plane rotation in the new single shear-lap specimens is due to the asymmetrical test configuration shown in Figure. 5.2a and Figure. 5.4a. Because the FRP is bonded to only one side of the concrete, the opposite side is free to rotate, allowing the notch to function as a hinge. This asymmetry generates a bending moment during loading. Even with a well-designed rigid system, as illustrated in Figure. 5.2a and Figure. 5.4a, the bending moment in these specimens cannot be entirely eliminated without a relatively complex test setup. The out-of-plane bending induces additional stresses normal to the bonded interface (peeling), creating a local mixed-mode loading condition (shearing and peeling) for the CFRP-concrete interface. This peeling stress arising from the out-of-plane deformation can initiate or accelerate the debonding process.

It is important to note that the out-of-plane displacements for both the new single shear-lap and the double shear-lap tests were measured at the notch, while the conventional shear-lap measurements were taken at the start of the bonded length (from the loaded end).

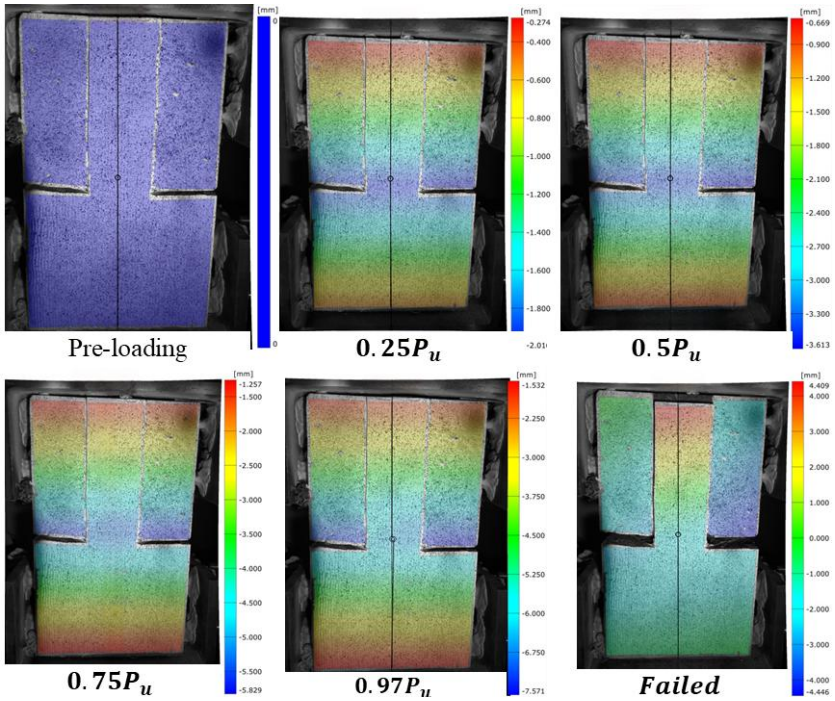

Figure 5.10-Contour of out-of-plane displacement for specimen SS-S9

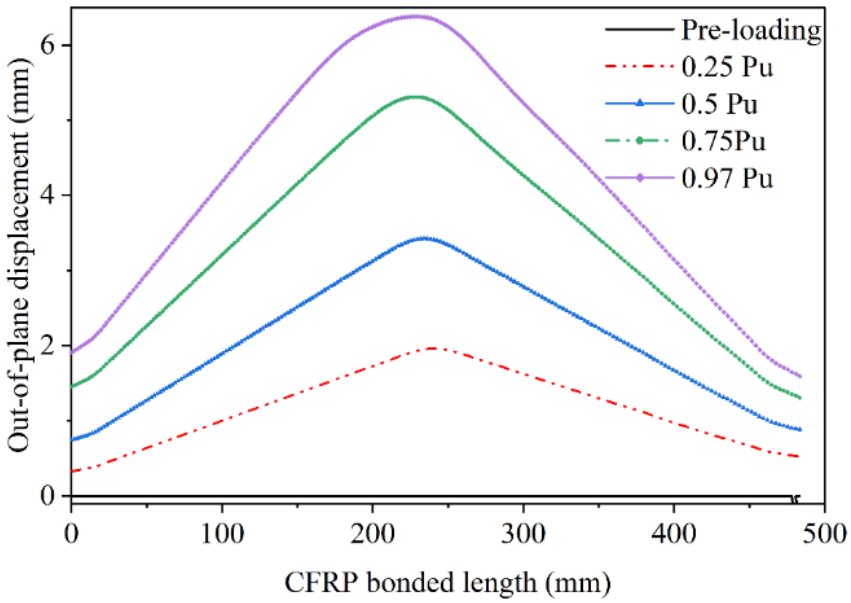

Figure 5.11-Magnitude of out-of-plane deformation for specimen SS-S9 at various load levels

5.5.3 Strain analysis along and across CFRP length

The tensile strain profile along the bonded length was derived from 3D DIC full-field strain data. The full-field DIC methods allow for the accurate evaluation of key interface parameters, including effective bond length, load transfer mechanism, and interface cohesive behaviour (bond stress and slip). The full-

field data also allows for assessing strain variation across the width of the CFRP throughout the debonding process.

Figure 5.12 shows strain variation for conventional single shear-lap tests, whereas Figure 5.13 depicts the strain distribution typical of the new single and double shear-lap configurations. The strain profile in Figure 5.12 indicates three different zones characterized by how stress or strain is distributed along the bonded interface at specific load levels. The identified zones include the debonded zone, where maximum tensile strain has plateaued and the CFRP has delaminated from the concrete substrate. This zone is followed by the stress transfer zone, marked by a rapid increase in CFRP strain from zero to maximum values, exhibiting a nonlinear strain distribution along the length of the CFRP. Beyond the stress transfer zone lies a region with low, constant strain, where minimal load transfer occurs. The strain in Figure 5.12 shows a progressive expansion of the stress transfer zone and the concurrent reduction of the unstressed region with increasing applied load. Based on Figure 5.12a, the following observations can be made: the initial transfer zone at 58-67 percent of ultimate load was approximately 135 mm, while the unstressed zone was 65 mm. This unstressed zone diminishes with increasing applied load as debonding propagates towards the free end. Near the ultimate state, the stress transfer length was 150-155 mm. The initial transfer length is defined as the distance needed for the strain in the transfer zone at low load levels (up to $0.7P_u$) to approach zero (Kabir et al., 2017; Leone et al., 2009). This increase in stress transfer zone between low load level and the ultimate load is reported in existing literature on shear-lap tests (Bizindavyi & Neale, 1999; Kabir et al., 2017; Leone et al., 2009).

The double shear-lap specimens showed a more symmetrical strain distribution relative to the notch location, as expected (see Figure 5.13). Figure 5.13 presents the strain behaviour for DS-S3 under various load increments, illustrating the debonding process and the shift in the stress transfer zone. The grey curve represents the strain along the centerline of the bonded width, while the red and blue depict the strain distribution 10 mm from each edge of the bonded width. The variation in strain measurement among these three lines indicates the non-uniform strain distribution along the bonded length during debonding. In Figure 5.13, the horizontal axis represents the distance from the CFRP end (above the

notch), while the vertical axis shows the measured experimental strain. The strain profile in Figure 5.13 shows debonding as a plateau with a low strain gradient, indicating a lack of stress transfer over the plateau region at a given load stage. The width of the plateau region increased throughout the test, and with increasing load, CFRP debonding shifted the active stress transfer zone symmetrically away from the notched location. The stress transfer length estimated on one side of the notch near the ultimate load was between 150-155 mm (see Figure 5.13).

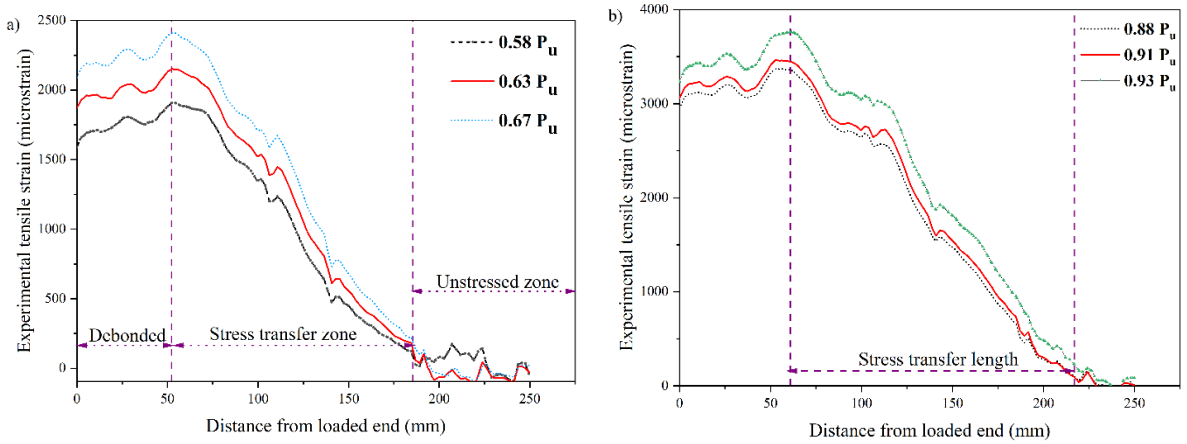

a) Centerline strain profile at low load levels

b) Centerline strain profile at high load levels

Figure 5.12-A typical strain profile for conventional single shear-lap specimens (CSS-S7)

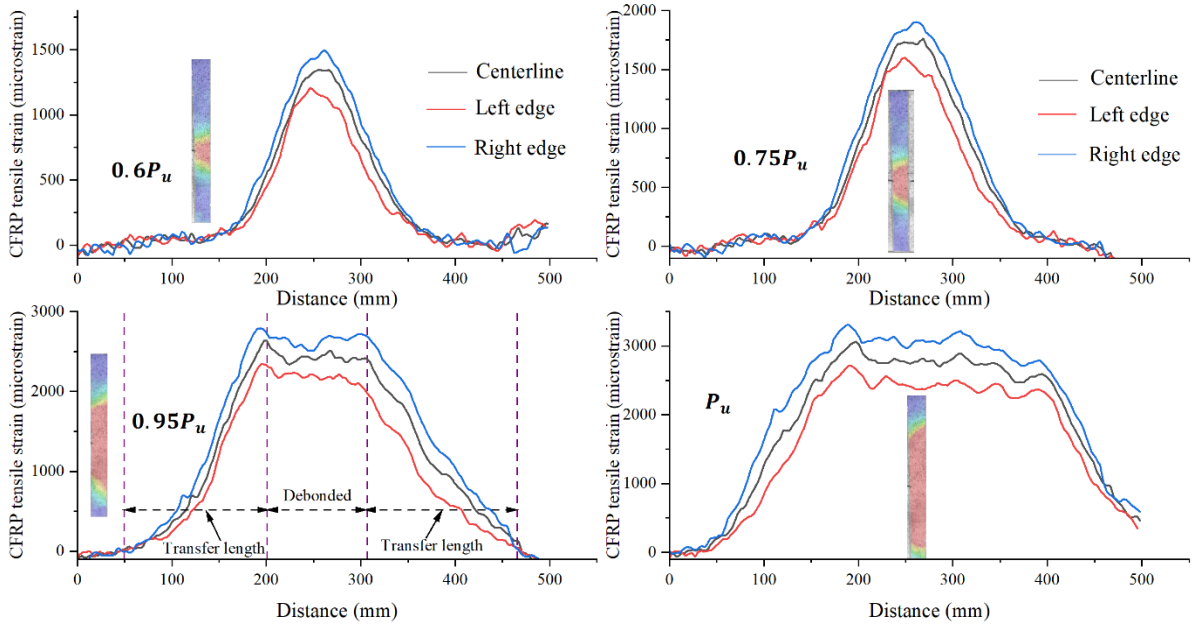

Figure 5.13-Typical strain profile for double shear-lap specimens (DS-S3) at various load levels

The maximum strain in Table 5.2 showed variability among the different shear-lap configurations. The conventional single shear demonstrated a mean strain that was 32 % greater than that observed in the new single shear-lap and 23% greater than in the double shear lap. This increased variability in the

conventional single shear-lap test can be attributed to the interface conditions, as the samples were taken from specimens previously tested under the new single shear-lap configurations. Consequently, any micro damage induced during that initial loading phase may contribute to increased variability during the conventional single shear-lap testing, in addition to pre-existing bond line degradation from service exposure.

Overall, strain results generally indicated higher peak strain values for the conventional pull-push single shear-lap setup (Table 5.2). The peak strain values from the double shear-lap tests were lower than those of the conventional single shear-lap tests yet higher than those of the new single shear-lap tests. The out-of-plane rotation-induced bending results in negative strain at the front face of the FRP, leading to reduced net strain measurements from the DIC. The average peak strain from the new single shear-lap tests was 2430 microstrain with a coefficient of variation (COV) of 11 percent (see Figure 5.9b and (Table 5.2). There is an observed discrepancy between the variability in peak strain and maximum load from the new single shear-lap tests. Importantly, the variability in strain calculated from experimental load data and material properties is expected to correlate with the variability ultimate load. This correlation arises because the approach provides an average strain over the entire bonded length of the CFRP sheet, without accounting for localized strain concentration or anomalies that may occur during testing. In contrast, strain measurement obtained from the DIC yield localized strain data, which accurately captures the non-uniform strain distribution. In addition, the DIC strain output will account for the bending effects on the CFRP sheet.

The conventional shear-lap tests yielded an average peak strain of 3203 microstrain and a COV of 26 percent. The double shear-lap tests showed an average peak strain of 2644 microstrain with a COV of 25 percent. The peak strain readings obtained from the strain gauges and the DIC for the same double shear-lap specimen showed good agreement. The variation in strain measurements from the DIC and strain gauges on the rear side of the double shear-lap tests can be attributed to the localized effects of the strain gauges or imperfections at the bonded interface. The DIC method collects data from the front surface of the specimen, while the strain gauges are positioned at the back. The experimental strains

mostly ranged from 2500 to 3400 microstrain, with the maximum observed strain of 4739 microstrain being approximately 56% of the value predicted by ACI PRC-440.2.23 for debonding strain (ACI, 2023b) (Equation 5.5). The strain limit specified in the Canadian Highway Bridge Design Code (CAN/CSA S6:19) surpassed the maximum experimental strain by 27 percent (CSA-Group, 2019) (Equation 5.6). Conversely, when the peak load derived from Equation 5.1 is used to compute corresponding strain, a strong correlation is achieved between experimental strain limits and those predicted by the Chen and Teng model. Both the ACI and CSA code equations and the Chen and Teng expression incorporate concrete compressive strength and FRP axial stiffness as key parameters. The difference in strain predictions in Figure 5.9b arises from the distinct approach of parameter consideration in these expressions. In the code equations, the calculated strain is proportion to $(f_c')^{0.5}$, while in the Chen and Teng model, it is proportional to $(f_c')^{0.25}$ when accounting for the effective bonded length (L_e). This indicates that while strain increases with concrete strength, the rate of increase differs between the two models. In addition, for longer bonded length, the inclusion of β_L in the Chen and Teng model does not affect the strain, whereas the geometric effects related to the CFRP-concrete width effect β_p do influences the strain calculation. Specifically, for a constant concrete width, β_p decreases as the FRP width increases; for instance, a change in CFRP width from 50 mm to 155 in a 300 mm wide concrete block results in a 20% reduction in β_p.

$$\varepsilon_{fd} = 0.41\sqrt{\frac{f_c'}{nE_{frp}t_{frp}}} \qquad \text{Equation 5.5}$$

$$\varepsilon_{frpe} = 0.41\sqrt{\frac{f_c'}{nE_{frp}t_{frp}}} \leq 0.006 \qquad \text{Equation 5.6}$$

In the above expressions, ε_{fd} and ε_{frpe} are the debonding strain and effective strain limits, respectively. The compressive strength of the concrete is denoted by f_c'; n, E_{frp} and t_{frp} represents the number of layers of sheets, the elastic modulus of FRP, and the thickness of FRP, respectively. Several factors influence the bond performance between externally bonded CFRP and concrete, including concrete

strength, CFRP axial stiffness, geometrical factors (bond length and width), CFRP-concrete width ratio, and the adhesive properties (Ueda & Dai, 2005). The ideal substrate failure mode at the CFRP-concrete interface is expected to depend on the limiting strain in the concrete, suggesting that deterioration in concrete quality or CFRP axial stiffness correlates with reduced strain capacity at the interface.

A preliminary comparison was conducted between peak strain measurements from the current research work on the deteriorated concrete bridge specimens and existing laboratory shear-lap specimens with pristine material properties (tested at ambient conditions) and similar specimen geometry found in the literature. Notably, research on high-strength concrete and CFRP under shear-lap testing is lacking. Therefore, selected laboratory studies with lower concrete compressive strength and CFRP axial stiffness than those in this research are used to evaluate the effect of concrete deterioration on peak strain values. Table 5.3 shows representative studies in which the concrete strength is less than or equal to 55% of the compressive strength of the specimens in this research. The mean experimental peak strain from Table 5.2 is 2798 microstrain which is 22-24% lower than the lowest strain values reported on lower strength concrete specimens from Liu et al. (Liu et al.) and Mukhtar (Mukhtar, 2024) in Table 5.3. While peak strains from the current study were significantly lower than the code values, the values in Table 5.3 from the existing literature with failure in concrete substrate exceeded the code limiting values calculated from Equation 5.5 based on the material properties used by the authors in respective studies. A modification coefficient of 0.76 was applied to convert the cube compressive strength of 26.5 MPa reported by Al-lami et al. (Al-Lami et al., 2020) to the equivalent cylinder strength (Liu et al.). It is important to note that factors like surface preparation quality for the selected laboratory samples from the literature and the deteriorated bridge specimens may differ. The purpose of the comparison was to emphasize that even with reduced concrete strength and CFRP axial stiffness, the laboratory specimens outperformed the specimen from the bridge elements in terms of ultimate strain capacity.

A vital bond parameter obtained from strain profiles is the variation of bond strength across the width of the bonded CFRP. Two width effects, specimen size and boundary effects, influence bond stress in the transverse direction. When the width of the CFRP is smaller than the concrete width, stress spreads

to neighbouring concrete, with local concrete stiffness and proximity to the CFRP edge influencing bond strength variation across the width (see Equation 5.2). This variation may also occur due to differences in bond anomalies at the CFRP edge. Figure 5.14 illustrates a typical strain variation across CFRP width for specimens CSS-S7, DS-S3 and SS-S9, indicating that a more uniform strain distribution is possible near the centerline of the CFRP width (see Figure 5.14a). The new single shear-lap specimens exhibited a significant strain gradient across the width promoted by the out-of-plane deformation effects present in these specimens (Figure 5.14b) and the larger bonded area that increased probability of weak points that may initiate debonding.

Table 5.3-Representative lab tests showing lower material properties with higher ultimate strain

Reference	f'_c (MPa)	$E_f t_f$ (GPa.mm)	b_f (mm)	L_f (mm)	b_c (mm)	Exp. peak strain ($\mu\varepsilon$)	Strain from Eq. 6 ($\mu\varepsilon$)
(Al-Lami et al., 2020)	26.5[c]	34.5	50.0	200.0	100.0	5400	3194
(Chajes et al., 1996)	36.4	110.2	25.4	203.2	228.6	4250	2356
(Liu et al.)	42.1	80.6	25.0	150.0	100.0	3693	2963
(Mukhtar, 2024)	41.3	66.7	60.0	300.0	150.0	3600	3226
(Ghaleh & Mostofinejad, 2022)	23.9	39.1	50.0	200.0	150.0	6000	3205
(Kabir et al., 2016)	36.6	26.4	40.0	150.0	200.0	8300	4828
(Kabir et al., 2016)	42.0	26.4	40.0	150.0	200.0	8000	5171
(Wu & He, 2019)	32.9	119.3	50.0	250.0	150.0	5500	2153

_[c] cube compressive strength

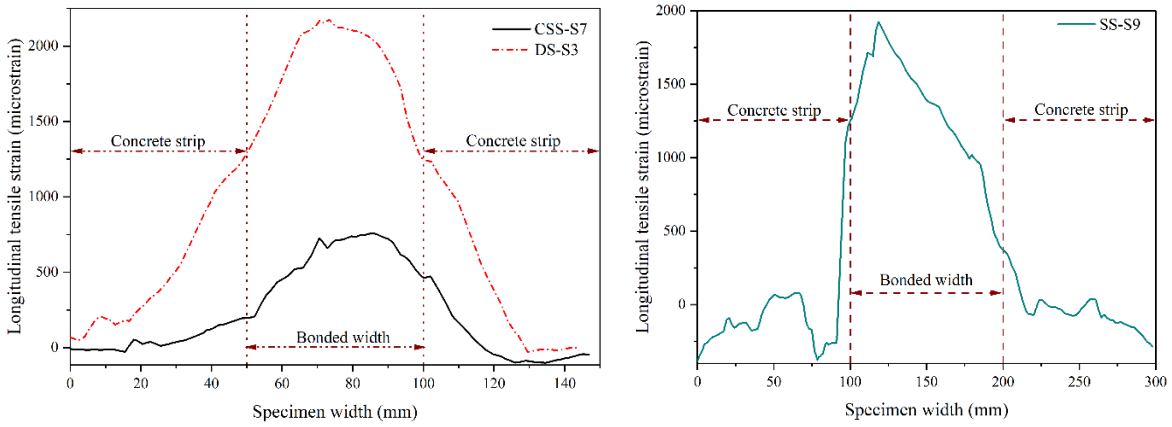

Figure 5.14-Strain variation across specimen width a) smaller width specimens b) wider width specimens

5.5.4 Bond strength distribution

The tensile force induced in the CFRP strip during loading is equilibrated by interfacial shear stress at the CFRP concrete interface, resulting from adhesive shear deformation. In assessing the bond behaviour during CFRP debonding from concrete, the interface shear bond capacity is, therefore, a crucial parameter. Debonding failure at the interface initiates when the shear bond capacity is exceeded. The maximum load capacity, as analyzed in section 5.5.2, relates directly with the CFRP width and the interfacial shear stress distribution along the bonded length, as expressed in Equation 5.7. The shear stress is hereafter referred to as bond stress.

$$P_u = \int_0^l \tau_{x(x)} b_f dx \qquad \text{Equation 5.7}$$

$$\tau = E_f t_f \frac{d\varepsilon}{dx} = \frac{E_f t_f (\varepsilon_j - \varepsilon_i)}{(x_j - x_i)} \qquad \text{Equation 5.8}$$

Where E_f is the elastic modulus of the CFRP, t_f is the total thickness of the CFRP, ε_j and ε_i are the strain readings at locations i and j, respectively. x_j and x_i are the locations (coordinates) of points i and j, respectively. The average bond stress between two points was calculated from the local strain gradient along the bonded length at the CFRP centerline (Equation 5.8). DIC used in the shear-lap tests provided closer measurement point spacing, leading to improved capture of stress distribution non-linearity compared to traditional strain gauges, which are typically spaced farther apart. The peak bond strength across the tests ranged from 4.1 to 7.9 MPa (Figure 5.15). The average experimental peak bond stress was closely correlated with peak bond stress model proposed by Lu et al. (Lu et al., 2005). In new single shear-lap and double shear-lap tests, shear stress distribution generally exhibited a positive magnitude on one side of the notch and a negative magnitude on the other, while in the conventional shear-lap configuration, a positive exponential decay of shear stress originated from the loading end. However, under the increased rotated in the new single shear-lap tests, strain behaviour under varying load levels did not allow for a reliable analysis of the bond stress -slip for these tests.

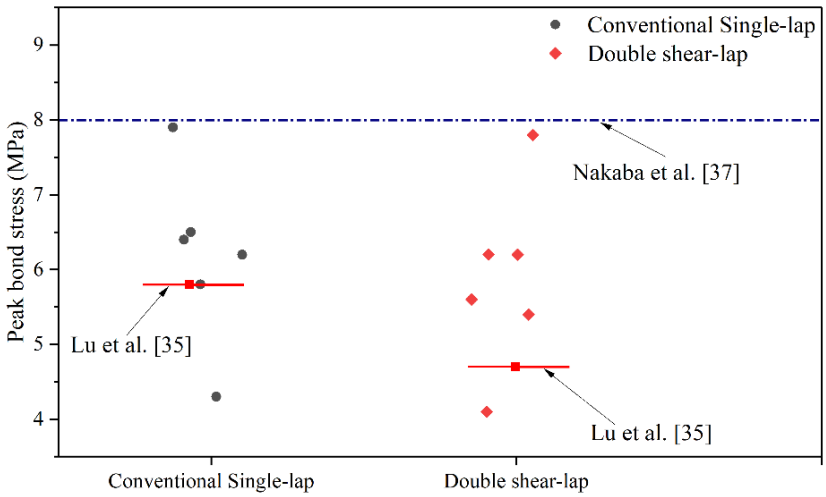

Figure 5.15-Peak shear bond stress across test methods

The experimental bond stress distribution is presented in Figure 5.16 and Figure 5.17. Similar shear stress behaviour was observed in the other tests; thus, only the results for specimen DS-S3 will be presented. Figure 5.16 and Figure 5.17 illustrate the distribution of shear stresses along the bonded length in specimen DS-S3 at various load levels. Under low load conditions (Figure 5.16), the experimental shear stress distribution was characterized by exponential softening and showed singular peaks that gradually shifted further from the notch location. In contrast, the shear stress distribution exhibited fluctuating peaks along the length as loads approached ultimate levels (Figure 5.17). This fluctuation in shear stress distribution near the ultimate load can be attributed to either crack condition/roughness during debonding or the presence of undetected local defects in the bond line, as in the case of the deteriorated concrete specimens in this research.

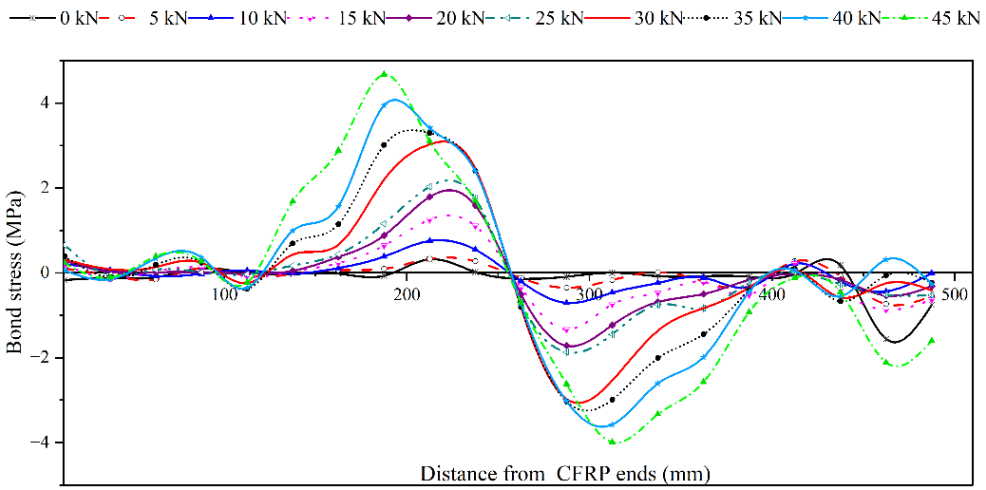

Figure 5.16-Bond stress distribution in double shear-lap specimens (at low to medium load levels)

In Figure 5.16, prior to debonding, shear stresses are expected to exhibit exponential decay, with CFRP-concrete bond line cracks emerging at peak shear stress, delineating distinct debonded zones in the pre-peak region and the uncracked bond line areas in the softening zone of the bond stress distribution. The evolution of the microcracks shifts the peak bond stress location away from the notch in the new single and double shear-lap tests or from the loaded end in the conventional single shear-lap tests until stress transfer is compromised by the formation of macrocracks in the concrete.

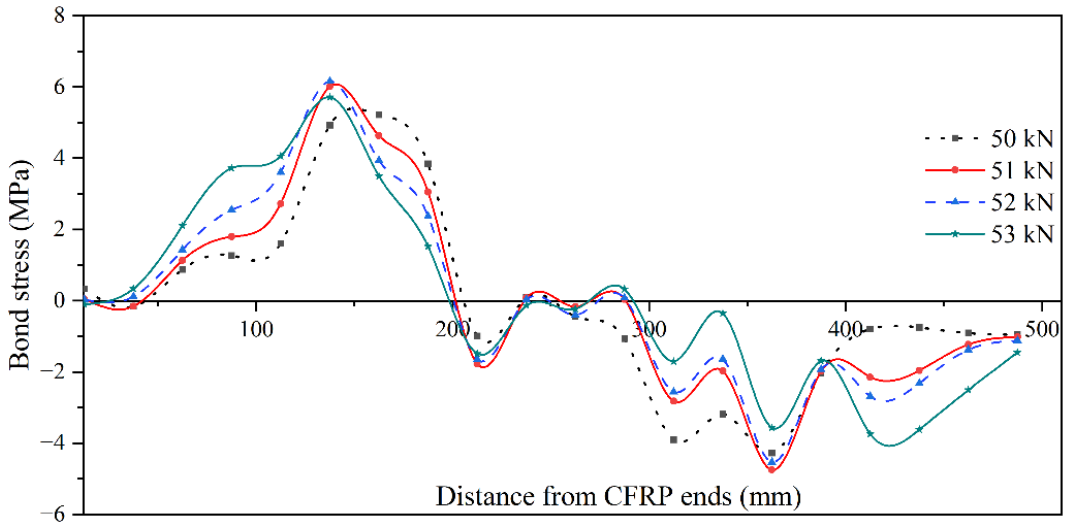

Figure 5.17-Bond stress distribution in double shear-lap specimens (around ultimate)

5.5.5 Analytical study and prediction from existing models

The CFRP-concrete interface bond stress transfer mechanism can be modelled using various stress-slip relationships found in the literature (Lu et al., 2005; Nelson et al., 2020; Nelson et al., 2024). These models predict the effective bond length necessary for proper stress transfer and allow the calculation of key parameters such as interfacial fracture energy (G). While linear or bilinear bond stress-slip relations are commonly used in earlier studies and for design purposes, experimental evidence suggests that the actual bond stress-slip relationship in shear tests more closely resembles an exponential function (Figure 5.18).

Limited research, if any, has been conducted correlating stress-slip relations from experimental work on deteriorated concrete structures retrofitted with CFRP and subjected to long-term in-service conditions. This section discusses the prediction of bond strength, effective bond length, and cohesive

bond stress-slip laws from existing literature with the experimental results from a deteriorated CFRP-concrete bond interface.

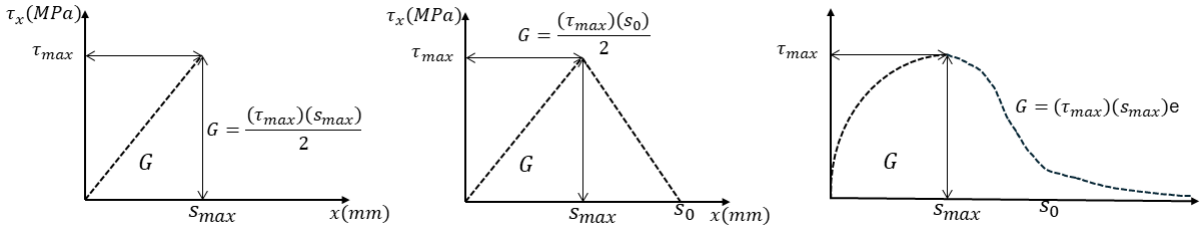

Figure 5.18-Common bond stress-slip curves in existing literature

Cohesive material law for interfacial bond fracture ($\tau - s$) and effective bond lengths

Figure 5.15 compares the maximum bond stress for specimens that experienced debonding. The bond stress used to establish the stress-slip relation was derived from the local strain gradient along the length of the CFRP (Equation 5.8), using Equation 5.11 to calculate the average slip between two points. The use of DIC in this study allowed for strain measurements every millimetre, offering improved insights into the non-linearity of the bond stress distribution. The experimental bond stress used in the bond stress-slip curves for DS-S3 shown in Figure 5.19, which represent the typical behaviour of the stress-slip behaviour, was determined using shear stress data at load increments of 5 kN up to 50 kN, followed by 1 kN increments (51 kN, 52 kN, and 53 kN). The local slip, defined as the relative displacement between CFRP and concrete in the loading direction (CFRP displacement minus the average displacement of a concrete strip at the same x position), was obtained from DIC data using three distinct approaches.

In the first method, the local experimental slip was calculated from the crack opening measurement at the notched location, assuming that the cumulative slip on either side of the notch equals the notch opening. The second approach integrated the strain distribution from the CFRP end to specific distances from the notch to obtain the local slip. This definition of

slip assumes that the strain in the concrete is negligible and can be considered as zero. The general expressions used for this integration are given in Equations 5.9 and 5.10.

$$s(x) = s(0) + \int_0^x \varepsilon(x)dx \qquad \text{Equation 5.9}$$

In Equation 5.9, $s(x)$ is the slip along the bonded length. $S(0)$, the slip at the free end of the FRP sheet is assumed zero. The local slip at a discrete location can obtained from the expression:

$$s_i = \frac{\Delta x}{2}(\varepsilon_0 + 2\sum_{j=1}^{i-1}(\varepsilon_j + \varepsilon_i)) \qquad \text{Equation 5.10}$$

Where the local slip at the location i is denoted by s_i, ε_0 is the strain at the far end of the CFRP, which is usually assumed to be zero. ε_j and ε_i are the strain at locations i and j, Δx is is the distance between the location i and j. The average slip between locations i and j used to establish the bond stress-slip relationship is given by Equation 5.11.

$$s_{j/2} = \frac{(s_i + s_j)}{2} \qquad \text{Equation 5.11}$$

In the third method for obtaining the bond stress-slip response, slip values were derived directly from DIC displacement data. In this method, the slip was calculated as the displacement differential between the CFRP and the concrete at identical positions along the CFRP bonded length. While there is a slight variation in the predicted slip, the general bond-slip behaviour is well captured by all three approaches. Table 5.4 summarises existing models for calculating the bond stress-slip relationship. These models were selected because they do not require knowledge of the adhesive layer thickness, which is often challenging to determine in experimental tests involving wet lay-up installations on decommissioned field structures with bonded CFRP. The peak bond stress and maximum slip are presented in Table 5.5. The experimental shear bond strength values for the conventional single shear-lap tests showed peak bond stress values ranging from 4.3 MPa to 7.9 MPa, with an average of 6.2 MPa. In comparison, the predictive models generally overestimated these values. The highest predicted value of 12.5 MPa (by

Ko et al.) substantially exceeded the maximum observed experimental value of 7.9 MPa. Conversely, the lowest prediction of 5.8 MPa (by Lu et al.) aligned more closely with the experimental average. For double shear-lap configurations, a similar trend of overestimation was observed in the predictive models. Experimental peak bond stress values for this test configuration ranged from 4.1 MPa to 7.8 MPa, with a mean of 5.9 MPa. The lowest predicted value of 4.7 MPa from Lu et al. showed better agreement with the experimental average and minimum. Comparison analysis indicated that the double shear-lap configuration with a wider bonded length of 100 mm exhibited slightly lower peak bond stress than the conventional single shear-lap configurations in the experimental results. The average peak slip obtained from the conventional single shear-lap and double shear-lap were 0.36 mm and 0.34 mm, respectively. It is important to note that predicted maximum slip values demonstrated considerable variability across different models. Due to the higher rotation in the new single shear-lap tests, strain behaviour under varying load levels did not allow for a reliable analysis of the bond-stress slip behaviour for these tests.

The stress-slip behaviour of CFRP bonded to concrete is a complex phenomenon governed by several factors including the properties of the concrete, the bonded length, the CFRP mechanical properties, and the surface profile of the concrete substrate. A typical comparison is made between the experimental observed stress-slip and the predicted values from established models in the literature. In Figure 5.19, the horizontal axis shows the slip between the concrete and CFRP in mm, while the vertical axis represents the bond stress developed at the CFRP-concrete interface. Experimental curves are presented for various distances from the notch in specimen DS-S3 (12 mm, 35 mm, and 112 mm). The locations are near the points where the shear stress peaked with better stress-slip behaviour (less randomness in strain distribution).

The stress-slip relationship is inherently location dependent, especially in the presence of defects. Depending on the size and distribution of defects relative to the bond length, defects will disrupt the interface transfers of shear stress (Li et al., 2023). Some analytical models in the existing literature can predict quite well the general behavior of the stress-slip response at locations where peak stress occurred.

Table 5.4-Summary of bond stress-slip models used in predicting interfacial cohesive material law

Model	Stress-slip parameters	Function of ascending branch	Function of descending branch
(Lu et al., 2005) Bilinear	$\tau_{max} = 1.5\beta_w f_t$ $\alpha = 1$ $s_1 = 0.0195\beta_w f_t$ $s_2 = \frac{0.616\beta_w^2\sqrt{f_t}}{\tau_{max}}$ $\beta_w = \sqrt{\frac{2 - {b_f}/{b_c}}{2 + {b_f}/{b_c}}}$	$\tau_{max}\frac{s}{s_1}$	$\tau_{max}\frac{s_2 - s}{s_2 - s_1}$
(Lu et al., 2005) Simplified	$\tau_{max} = 1.5\beta_w f_t$ $\alpha = 0.5$ $s_1 = 0.0195\beta_w f_t$ $\beta = \frac{1}{\frac{G_f}{\tau_{max}} - \frac{2s_1}{3}}$ $\beta_w = \sqrt{\frac{2 - {b_f}/{b_c}}{1 + {b_f}/{b_c}}}$ $G_f = 0.308{\beta_w}^2\sqrt{f_t}$	$\tau_{max}\left(\frac{s}{s_1}\right)^{0.5}$	$\tau_{max}e^{-\beta(s-s_1)}$
(Nakaba et al., 2001)	$\tau_{max} = 3.5f_c^{0.19}$ $s_1 = 0.065$	$\tau_{max}\left(\frac{s}{s_1}\right)(\frac{3}{2 + (\frac{s}{s_1})^3}$	$\tau_{max}\left(\frac{s}{s_1}\right)(\frac{3}{2 + (\frac{s}{s_1})^3}$
(Neubauer & Rostasy, 1999)	$\tau_{max} = 1.8\beta_w f_t$ $\alpha = 1$ $s_1 = s_2 = 0.202\beta_w$ $\beta_w = \sqrt{\frac{1.125(2 - {b_f}/{b_c})}{1 + {b_f}/{400}}}$	$\tau_{max}\left(\frac{s}{s_1}\right)^{0.5}$	$\tau_{max}e^{-\beta(s-s_1)}$
(Ko et al., 2014)	$\tau_{max} = 0.165f_c'$ $\alpha = 1$ $s_1 = 0.122 - 0.001f_c'$ $s_2 = 0.302 - 0.002f_c'$	$\tau_{max}\frac{s}{s_1}$	$\tau_{max}\frac{s_2 - s}{s_2 - s_1}$
(Savoia et al., 2003)	$\tau_{max} = 3.5f_c^{0.19}$ $s_1 = 0.051$	$\tau_{max}\left(\frac{s}{s_1}\right)(\frac{2.86}{1.86 + (\frac{s}{s_1})}$	$\tau_{max}\left(\frac{s}{s_1}\right)(\frac{2.86}{1.86 + (\frac{s}{s_1})^{2.86}}$

However, locations with discontinuities such as defects lead to reduced interface stiffness and induce non-linearity in the stress-slip response. The non-linear model by Nakaba et al. (Nakaba et al., 2001)

and the simplified model proposed by Lu et al. (Lu et al., 2005) accurately captured the trend of the experimental bond stress distribution (exponential softening). However, the model by Nakaba et al. overestimated the peak shear stress, on average. The bilinear model formulated by Ko et al. (Ko et al., 2014) also significantly overestimated the maximum experimental shear stress in Figure 5.15 by more than 58 percent.

Table 5.5-Summary of bond stress-slip predictions

	Conventional single shear-lap			Double shear-lap		
Model	τ_{max} (MPa)	s_0 (mm)	G	τ_{max} (MPa)	s_0 (mm)	G N/mm
Lu et al. Bilinear	5.8	0.3	0.7	4.7	0.2	0.5
Lu et al. Simplified	5.8	0.8	0.5	4.7	0.8	0.5
Nakaba	8.0	1.0	1.4	8.0	1.0	1.4
Neubauer & Rostasy	8.1	0.3	1.1	6.9	0.2	0.8
Ko et al.	12.5	0.2	0.9	12.5	0.2	0.9
Savioa et al.	8.0	1.0	1.2	8.0	1.0	1.2

Because of the significant discrepancy between the Ko et al. model and the experimental results, the bilinear stress-slip prediction reported in Table 5.5 was omitted from Figure 5.19 to maintain plot clarity. The significant discrepancy between the Ko et al. model and the experimental results arises from the model's heavy reliance on simple linear functions that depend on the concrete compressive strength to define the non-linear behaviour at the CFRP-concrete interface. The actual behaviour of the CFRP-concrete interface involves complex phenomena, including microcracking, aggregate interlock, and adhesive behaviour, which greatly affect bond performance, especially in deteriorated concrete. It is also worth noting that the Ko et al. model directly links the bond parameters such as maximum bond stress and slip to concrete compressive strength without considering the properties of the FRP material or geometrical factors like width effects.

The applicability of the Ko et al. model to high-strength concrete, as examined in this study, is not addressed in the existing literature. Consequently, the limitations of the model concerning high-strength and ultra-high-strength concrete strength have not been fully researched.

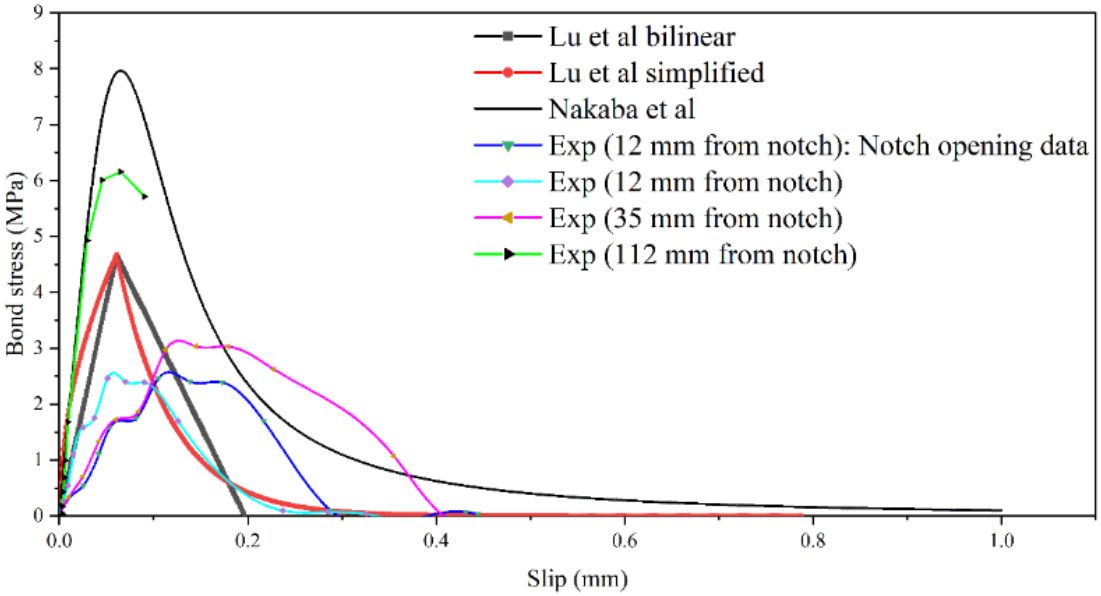

Figure 5.19-Bond stress-slip relation (Experimental v existing models) for specimen DS-S3

The effective bond length is a critical parameter in characterizing the bond behaviour of the CFRP-concrete interface. It represents the length over which most of the load transfer occurs between the CFRP and concrete. This length is typically defined as the distance from the fully debonded region to where the strain reduces to zero or 5% of the ultimate strain (Li et al., 2024) or the length over which 97% of the ultimate load is resisted (Yuan et al., 2004). Various models have been developed to calculate the effective bond length. The strain behaviour from the specimen rotation in the new single shear-lap setup hindered a reliable analysis of the effective bond length.

Table 5.6 shows the effective bond length calculated from the existing literature. From the expressions in Table 5.6, it can be inferred that the CFRP stiffness, concrete compressive strength and tensile properties influence the effective bond length and, subsequently, the bond stress-slip relationship. For bond lengths shorter than the effective bond length, stress is expected to only partially develop along the length of the CFRP. The closest correlation with the experimental results is obtained with the Chen and Teng model adopted by ACI PRC-440, with results differing by approximately 4 to 8% from the experimental value of 150-155 mm obtained for the conventional single shear-lap tests and double shear-lap tests. The strain behaviour from the specimen rotation in the new single shear-lap setup hindered a reliable analysis of the effective bond length.

Table 5.6-Existing effective length expressions used

Model	Equation	Effective bond length (mm)
(ACI, 2023a)	$L_a = \sqrt{\frac{E_f t_f}{\sqrt{f_c'}}}$	144
(Chen & Teng, 2001)	$L_e = \sqrt{\frac{E_f t_f}{\sqrt{f_c'}}}$	144
(CSA-Group, 2019)	$L_a = 0.5\sqrt{E_{frp} t_{frp}}$	212
(Institute, 2003)	$L_e = 1.89(E_f t_f)^{0.4}$	239
(Wu et al., 2009)	$L_e = 0.395\frac{(E_f t_f)^{0.54}}{f_c'^{0.09}}$	184
(Kanakubo et al., 2003)	$L_e = 0.7\sqrt{\frac{E_f t_f}{f_c'^{0.2}}}$	193
(Neubauer & Rostasy, 1997)	$L_e = \sqrt{\frac{E_f t_f}{2f_t}}$	161
(Niedermeier, 2000)	$L_e = \sqrt{\frac{E_f t_f}{4f_t}}$	114

5.6 Conclusions

This paper presents a study on the deteriorated CFRP-concrete interface from a decommissioned concrete bridge to address the knowledge gap between laboratory studies on pristine concrete samples and the performance of CFRP composites on deteriorated concrete from an actual in-service application. Twenty-seven concrete samples from a 57-year-old bridge were examined, focusing on the bond behaviour under shear. The study provides valuable data on the performance of CFRP-strengthened systems in terms of stress and strain behaviour for actual deteriorated concrete structures strengthened with CFRP. The following conclusions were found:

- The measured experimental strain was substantially lower than the code limits on the debonding strain. The observed strain was approximately 56% of the debonding strain limit set by ACI PRC-440, while the CAN/CSA S6:19 exceeded the peak experimental strain by 27%. Conversely, the failure loads and ultimate strain values were well-predicted using a model proposed by Chen and Teng.

- The peak strain values were slightly higher, on average, in the conventional shear-lap setup compared to the new single shear-lap and the double shear-lap tests. The average peak strain from the double shear-lap and conventional shear-lap tests were 2644 and 3203 microstrain, respectively, which was approximately 8.8% and 31.8 % higher than the average peak strain from the new single shear-lap test.
- The strain distribution across the width of the FRP sheet is not uniform. The strain along the centerline is generally higher than near the edges of the sheet.
- Double shear-lap tests provided a more consistent peak load with a (COV) of 11.2%, while the new single shear-lap and conventional shear-lap configurations showed greater variability with a (COV) of 23.9% and 24.5%, respectively.
- Although failure occurred at the notch in the new single-shear-lap and double shear-lap tests, out-of-plane rotation was unavoidable in the new single shear-lap tests, inducing bending and resulting in negative strain at the front face of the FRP. This led to a reduced net strain measurement from the DIC. The new single shear-lap specimens exhibited an average out-of-plane deformation of 8 mm.
- The new custom-designed set-up for shear-lap tests effectively characterizes the bond behaviour between FRP and concrete in the double shear-lap configuration, achieving an average out-of-plane displacement of 0.6 mm and a peak load variation of 11.2 %.
- Comparison of experimental results with existing literature indicates that laboratory-prepared specimens, which had lower concrete strength and CFRP axial stiffness, attained higher strain values than the deteriorated bridge specimens in this study.
- Comparison of the experimental bond stress-slip relationship with existing cohesive zone models showed a strong correlation of peak bond stress with the model by Lu et al. (Lu et al., 2005). In contrast, the model by Nakaba et al. (Nakaba et al., 2001) accurately represented bond stress-slip behaviour (exponential softening) but overestimated the peak bond stress.
- Chen and Teng's model for the effective bond length best captures the observed experimental stress transfer length with a difference of 4 to 8 percent.

- The analytical model by Ko et al. (Ko et al., 2014) that relies significantly on concrete material properties as the defining parameter for the bond stress-slip behaviour overestimated the peak bond stress by more than 58 percent.

5.7 References

ACI. (2023a). Design and Construction of Externally Bonded FiberReinforced Polymer (FRP) Systems for Strengthening Concrete Structures—Guide (ACI PRC-440.2-23). In. Farmington Hills, MI, 2023: American Concrete Institute.

ACI. (2023b). Guide for the design and construction of externally bonded FRP systems for strengthening concrete structures. In (pp. 1-112).

Aiello, M. A., & Leone, M. (2008). Interface analysis between FRP EBR system and concrete. *Composites Part B: Engineering*, *39*(4), 618-626.

Al-Lami, K., Colombi, P., & D'Antino, T. (2020). Influence of hygrothermal ageing on the mechanical properties of CFRP-concrete joints and of their components. *Composite structures*, *238*, 111947.

Allen, D. G., & Atadero, R. A. (2012). Evaluating the long-term durability of externally bonded FRP via field assessments. *Journal of composites for construction*, *16*(6), 737-746.

ASTM. (2017). Standard Test Method Tensile Properties of Polymer Composite Materials. In *ASTM D3039*. West Conshohocken, PA: ASTM.

ASTM. (2021a). Standard Test Method for Compressive Strength of Cylindrical Concrete Specimens. In *ASTM C39*. West Conshohocken, PA.

Baggio, D., Soudki, K., & Noel, M. (2014). Strengthening of shear critical RC beams with various FRP systems. *Construction and Building Materials*, *66*, 634-644.

Benzarti, K., Chataigner, S., Quiertant, M., Marty, C., & Aubagnac, C. (2011). Accelerated ageing behaviour of the adhesive bond between concrete specimens and CFRP overlays. *Construction and Building Materials*, *25*(2), 523-538.

Bizindavyi, L., & Neale, K. (1999). Transfer lengths and bond strengths for composites bonded to concrete. *Journal of composites for construction*, *3*(4), 153-160.

Bizindavyi, L., Neale, K., & Erki, M. (2003). Experimental investigation of bonded fiber reinforced polymer-concrete joints under cyclic loading. *Journal of composites for construction*, *7*(2), 127-134.

Brosens, K. (2001). Anchorage of externally bonded steel plates and CFRP laminates for the strengthening of concrete elements.

Carloni, C., & Subramaniam, K. V. (2010). Direct determination of cohesive stress transfer during debonding of FRP from concrete. *Composite structures*, *93*(1), 184-192.

Chajes, M. J., Finch, W. W., & Thomson, T. A. (1996). Bond and force transfer of composite-material plates bonded to concrete. *Structural Journal*, *93*(2), 209-217.

Chataigner, S., Caron, J.-F., Benzarti, K., Quiertant, M., & Aubagnac, C. (2011). Use of a single lap shear test to characterize composite-to-concrete or composite-to-steel bonded interfaces. *Construction and Building Materials*, *25*(2), 468-478.

Chen, J. F., & Pan, W. (2006). Three dimensional stress distribution in FRP-to-concrete bond test specimens. *Construction and Building Materials*, *20*(1-2), 46-58.

Chen, J. F., & Teng, J. (2001). Anchorage strength models for FRP and steel plates bonded to concrete. *Journal of Structural Engineering*, *127*(7), 784-791.

CSA-Group. (2019). Canadian Highway Bridge Design Code. In *CSA S6:19*.

Czaderski, C., Soudki, K., & Motavalli, M. (2010). Front and side view image correlation measurements on FRP to concrete pull-off bond tests. *Journal of composites for construction*, *14*(4), 451-463.

De Lorenzis, L., Miller, B., & Nanni, A. (2001). Bond of FRP laminates to concrete. *ACI materials journal*, *98*(3), 256-264.

de Waal, L., Fernando, D., Cork, R., & Foote, J. (2017). FRP strengthening of 60 year old pre-stressed concrete bridge deck units. *Engineering structures*, *143*, 346-357.

Ferracuti, B., Savoia, M., & Mazzotti, C. (2007). Interface law for FRP–concrete delamination. *Composite structures*, *80*(4), 523-531.

FIB. (2020). Fib Model Code for Concrete Structures (2020). In: International Federation of Structural Concrete.

Fowai, I., Noël, M., Esmaili, M., Martin-Perez, B., & Sanchez, L. (2025a). *Impact of test configuration and field defects on debonding mechanisms in deteriorated CFRP-concrete interface from the decommissioned Champlain Bridge* 12th International Conference on FRP composites in civil engineering, Lisbon.

Fowai, I., Noël, M., Martin-Perez, B., & Sanchez, L. (2025c). *Assessment of CFRP-concrete bond interface from the deconstructed Champlain Bridge-Comparison of single and mixed mode behaviour* 12th International Conference on FRP composites in civil engineering, Lisbon.

Fowai, I., Noël, M., Martín-Pérez, B., & Sanchez, L. (2023b). *Condition assessment of FRP-strengthened concrete bridge diaphragms using non-destructive testing* 11th International Conference on FRP composites in civil engineering, Rio de Janeiro.

Fowai, I., Noël, M., Martín-Pérez, B., & Sanchez, L. (2025d). Assessment of the CFRP–Concrete Interface Integrity of Original Champlain Bridge Diaphragms through Nondestructive and Semidestructive Testing. *Journal of composites for construction*, *29*(2), 04025004.

Fowai, I., Noël, M., Yager, J., Martín-Pérez, B., Sanchez, L., Green, M. F., & Hoult, N. A. (2025e). Strain distribution and debonding behaviour of CFRP sheets with different anchorage lengths from a decommissioned concrete bridge. *Engineering structures*.

Fowai, I., Noel, M., Martín-Pérez, B., & Sanchez, L. (2023). *Integrity Assessment of CFRP-Concrete Interface on Externally Strengthened Bridge Diaphragms Using Direct Tension Pull-off Test.* 11th International Conference on Fiber-Reinforced Polymer (FRP) Composites in Civil Engineering (CICE 2023), Rio de Janeiro, Brazil.

Fowai, I., Noel, M., Martín-Pérez, B., & Sanchez, L. (2024). Assessment of CFRP-concrete interface integrity of Original Champlain Bridge diaphragms through non-destructive and semi-destructive testing [Invited paper]. *ASCE Journal of Composites for Construction*.

Ghaleh, R. Z., & Mostofinejad, D. (2022). Behaviour of EBRIG CFRP sheet-concrete joint: Comparative assessment with EBR and EBROG methods. *Construction and Building Materials*, *346*, 128374.

Green, M. F., Bisby, L. A., Beaudoin, Y., & Labossière, P. (2000). Effect of freeze-thaw cycles on the bond durability between fibre reinforced polymer plate reinforcement and concrete. *Canadian Journal of Civil Engineering*, *27*(5), 949-959.

Hao, Z.-H., Zeng, J.-J., Chen, G.-M., Dai, J.-G., & Chen, J.-F. (2024). Durability of FRP-to-concrete bonded joints subjected to 110 months accelerated laboratory and field exposure. *Engineering structures*, *305*, 117681.

Harries, K., & Sweriduk, M. (2016). Factors affecting direct tension pull-off test results of materials bonded to concrete. *Advances in Civil Engineering Materials*, *5*(1), 353-370.

Institute, J. C. (2003). Technical report of technical committee on retrofit technology. Proc., Int. Symp. on the Latest Achievement of Technology and Research on Retrofitting Concrete Structures,

Issa Fowai, Martin Noël, Martín-Pérez, B., & Sanchez, L. (2025). Assessment of CFRP-concrete Interface Integrity of Original Champlain Bridge Diaphragms through Nondestructive and semidestructive Testing. *Journal of composites for construction*.

Kabir, M. I., Samali, B., & Shrestha, R. (2017). Pull-out strengths of GFRP-concrete bond exposed to applied environmental conditions. *International Journal of Concrete Structures and Materials*, *11*, 69-84.

Kabir, M. I., Shrestha, R., & Samali, B. (2016). Effects of applied environmental conditions on the pull-out strengths of CFRP-concrete bond. *Construction and Building Materials*, *114*, 817-830.

Kanakubo, T., Furuta, T., & Fukuyama, H. (2003). Bond strength between fiber-reinforced polymer laminates and concrete. In *Fibre-Reinforced Polymer Reinforcement for Concrete Structures: (In 2 Volumes)* (pp. 133-142). World Scientific.

Karbhari, V. M., & Ghosh, K. (2009). Comparative durability evaluation of ambient temperature cured externally bonded CFRP and GFRP composite systems for repair of bridges. *Composites part A: Applied science and manufacturing*, *40*(9), 1353-1363.

Khalifa, A., & Nanni, A. (2002). Rehabilitation of rectangular simply supported RC beams with shear deficiencies using CFRP composites. *Construction and Building Materials*, *16*(3), 135-146.

Ko, H., Matthys, S., Palmieri, A., & Sato, Y. (2014). Development of a simplified bond stress–slip model for bonded FRP–concrete interfaces. *Construction and Building Materials*, *68*, 142-157.

Leone, M., Matthys, S., & Aiello, M. A. (2009). Effect of elevated service temperature on bond between FRP EBR systems and concrete. *Composites Part B: Engineering*, *40*(1), 85-93.

Li, D., Wang, X., Zhang, J., Jin, L., & Du, X. (2024). An Experimental Study and Result Analysis on the Dynamic Effective Bond Length of a Carbon Fiber-Reinforced Polymer Sheet Attached to a Concrete Surface. *Buildings*, *14*(10), 3245.

Li, P.-D., Zhao, Y., Wu, Y.-F., & Lin, J.-P. (2023). Effect of defects in adhesive layer on the interfacial bond behaviors of externally bonded CFRP-to-concrete joints. *Engineering structures*, *278*, 115495.

Li, W., & Leung, C. K. (2016). Shear span–depth ratio effect on behavior of RC beam shear strengthened with full-wrapping FRP strip. *Journal of composites for construction*, *20*(3), 04015067.

Liu, S., Pan, Y., Li, H., & Xian, G. Durability of the bond between CFRP and concrete exposed to thermal cycles, Materials (Basel) 12 (2019). In.

Lu, X., Teng, J., Ye, L., & Jiang, J. (2005). Bond–slip models for FRP sheets/plates bonded to concrete. *Engineering structures*, *27*(6), 920-937.

Mabry, N. J., Seracino, R., & Peters, K. J. (2018). The effects of accelerated Freeze-Thaw conditioning on CFRP strengthened concrete with pre-existing bond defects. *Construction and Building Materials*, *163*, 286-295.

Mazzotti, C., Savoia, M., & Ferracuti, B. (2009). A new single-shear set-up for stable debonding of FRP–concrete joints. *Construction and Building Materials*, *23*(4), 1529-1537.

Milev, S., & Tatar, J. (2023). Durability Assessment of the First Externally Bonded FRP Repair of a Publicly Owned Bridge in the United States after 26 Years of Service. *Journal of composites for construction*, *27*(5), 04023049.

Mukhtar, F. (2024). Comprehensive FRP-concrete bond behavior: Impact of test methods and the innovative UBoT. *Composite structures*, *348*, 118475.

Nakaba, K., Kanakubo, T., Furuta, T., & Yoshizawa, H. (2001). Bond behavior between fiber-reinforced polymer laminates and concrete. *Structural Journal*, *98*(3), 359-367.

Nelson, L. A., Al-Allaf, M., & Weekes, L. (2020). Analytical modelling of bond-slip failure between epoxy bonded FRP and concrete substrate. *Composite structures*, *251*, 112596.

Nelson, L. A., Weekes, L., Milani, G., & Al-Allaf, M. (2024). Generalised analytical solutions for linear and non-linear bond–slip models for externally bonded FRP to a concrete substrate. *Engineering structures*, *298*, 117025.

Neubauer, U., & Rostasy, F. (1997). Design aspects of concrete structures strengthened with externally bonded CFRP-plates. PROCEEDINGS OF THE SEVENTH INTERNATIONAL CONFERENCE ON STRUCTURAL FAULTS AND REPAIR, 8 JULY 1997. VOLUME 2: CONCRETE AND COMPOSITES,

Neubauer, U., & Rostasy, F. (1999). Bond failure of concrete fiber reinforced polymer plates at inclined cracks—Experiments and fracture mechanics model. *Special Publication*, *188*, 369-382.

Niedermeier, R. (2000). Envelope line of tensile forces while using externally bonded reinforcement. *German.] Doctoral dissertation, Dept. of Civil Engineering, Technical University of Munich (TUM)*.

Savoia, M., Ferracuti, B., & Mazzotti, C. (2003). Non linear bond-slip law for FRP-concrete interface. In *Fibre-Reinforced Polymer Reinforcement for Concrete Structures: (In 2 Volumes)* (pp. 163-172). World Scientific.

Tatar, J., & Brenkus, N. R. (2021). Performance of FRP-strengthened reinforced concrete bridge girders after 12 years of service in coastal Florida. *Journal of composites for construction*, *25*(4), 04021028.

Tomlinson, D., & Fam, A. (2015). Performance of concrete beams reinforced with basalt FRP for flexure and shear. *Journal of composites for construction*, *19*(2), 04014036.

Ueda, T., & Dai, J. (2005). Interface bond between FRP sheets and concrete substrates: properties, numerical modeling and roles in member behaviour. *Progress in structural engineering and materials*, *7*(1), 27-43.

Ueda, T., Sato, Y., & Asano, Y. (1999). Experimental study on bond strength of continuous carbon fiber sheet. 4th International Symposium on Fiber Reinforced Polymer Reinforcement for Reinforced Concrete Structures,

Wu, Y.-F., & He, L. (2019). Width effect of interfacial bond characteristics. *Construction and Building Materials*, *220*, 712-726.

Wu, Z., Islam, S., & Said, H. (2009). A three-parameter bond strength model for frp—concrete interface. *Journal of Reinforced Plastics and Composites*, *28*(19), 2309-2323.

Yuan, H., Teng, J., Seracino, R., Wu, Z., & Yao, J. (2004). Full-range behavior of FRP-to-concrete bonded joints. *Engineering structures*, *26*(5), 553-565.

Yun, Y., & Wu, Y.-F. (2011). Durability of CFRP–concrete joints under freeze–thaw cycling. *Cold Regions Science and Technology*, *65*(3), 401-412.

Zhang, W., Lin, J., Huang, Y., Lin, B., & Kang, S. (2024a). Temperature-dependent debonding behavior of adhesively bonded CFRP-UHPC interface. *Composite structures*, *340*, 118200.

Zhang, W., Lin, J., Huang, Y., Lin, B., & Liu, X. (2024b). Experimental and numerical studies on flexural performance of composite beams under cyclic loading. Structures,

Zhou, A., Qin, R., Feo, L., Penna, R., & Lau, D. (2017). Investigation on interfacial defect criticality of FRP-bonded concrete beams. *Composites Part B: Engineering*, *113*, 80-90.

Chapter 6 Evaluating debonding behaviour through mixed mode loading[1]

6.1 Abstract

This paper presents an investigation of the debonding behaviour of bond critical carbon fibre-reinforced polymer (CFRP) retrofitted reinforced concrete beams extracted from the diaphragms of a deteriorated bridge (Original Champlain Bridge) in Canada. The diaphragms were strengthened with externally bonded CFRP sheets five years before the bridge was decommissioned as a result of extensive degradation after 57 years in service. Four 2.0 m long concrete beams strengthened with two layers of CFRP were tested in bending in multiple anchorage-critical configurations. The CFRP sheets were instrumented with distributed fibre optic sensors (DFOS) along their length, as well as discrete electrical resistance strain gauges to monitor the strain distribution during the debonding process. A range of anchorage lengths, from 250 mm to 700 mm, were used to examine failure modes, ultimate load capacity, deformation behaviour, and strain and stress distribution profiles. Effective strain limits prescribed by design codes or in the reported literature were generally not representative of the maximum measured strains in the tested specimens that were subjected to the synergistic effects of service load and harsh environmental conditions for a prolonged period. Existing models in the literature underestimated the ultimate load by 18 to 41 percent, while the FIB-14 overestimated it by 15 to 126 percent. Effective strain limits specified by the American Concrete Institute (ACI PRC-440.2-23) and Canadian Highway Bridge Design Code (CAN/CSA S6:19) were 88 percent and 34 percent higher than the maximum observed strain in the debonded beams, respectively. Bond line shear stress increased with a reduction in anchorage length. A good agreement with the strain data provided by the conventional discrete electrical strain gauges and DFOS measurements along the full length of the beam was observed.

[1] A version of this chapter has been submitted for publication as: Issa Fowai, Martin Noël, Jacob Yager, Beatriz Martín-Pérez, Leandro Sanchez, Mark F Green, Neil A. Hoult. *Strain distribution and debonding behaviour of CFRP sheets with different anchorage lengths from a decommissioned concrete bridge*.

6.2 Introduction

The need for externally bonded carbon fibre-reinforced polymer (CFRP) composite materials as a cost-effective and durable alternative to traditional retrofitting of deteriorating concrete structures, including residential buildings, parking garages and complex highway bridges, will continue to grow in the coming decades. This need arises due to the deterioration of these structures caused by heavy traffic, overuse, and severe environmental conditions resulting in extensive corrosion (Chajes et al., 1994; Fanning & Kelly, 2001; Kachlakev & McCurry, 2000; Obaidat et al., 2011). Moreover, the necessity to retrofit structures is intricately linked to the considerable financial burden associated with complete replacements, as well as the environmental benefits inherent in keeping the structures in service. The effectiveness of externally bonded CFRP strengthening depends on the proper transfer of stresses between the various interfaces dictated by the physical and mechanical properties of the concrete substrate, CFRP sheets, and adhesives.

The force transfer mechanism between the concrete and the externally bonded CFRP relies predominantly on shear stresses at the bond line between the concrete-CFRP interface via the adhesive. Analytical models have been proposed to estimate the risk of premature failure of externally bonded CFRP or steel plates due to concentration of shear and normal stress observed at the sheet/plate end or crack locations. Malek et al. (Malek et al., 1998) and Brosens et al. (Brosens & Van Gemert, 2001) developed models to predict stress distributions (shear and normal) at the CFRP sheet/plate ends under flexural loading, employing an assumption to account for the shear and normal stress individually. These models have demonstrated that, although the normal stress at the interface between CFRP and concrete usually remains minimal and diminishes alongside shear stress, as the point of application of the load moves away from the plate end or crack tip, the influence of normal stresses on concrete members strengthened with steel in flexure cannot be disregarded. Given the non-uniform nature of concrete, preparation of its surface, disparities in the adhesive and CFRP thickness, and the existence of flaws at the bond line, the validity of these models to deteriorated concrete structures retrofitted with CFRP has yet to be thoroughly investigated.

Several different failure modes are associated with externally bonded composite repairs, ranging from complete loss of composite action (bond failure) to material failure (e.g., FRP rupture or concrete crushing) with full composite action (Khalifa & Nanni, 2002; Teng & Chen, 2007; Triantafillou et al., 2001). Extensive experimental and analytical data, as well as design guidelines to understand and prevent premature loss of composite action, are available in the literature (Baggio et al., 2014; Chen & Teng, 2001; Garden & Hollaway, 1998; Garden et al., 1997; Garden et al., 1998; Li & Leung, 2016; Täljsten, 1994, 1997b; Yuan et al., 2004; Yuan et al., 2001). Present design protocols typically limit the strain in the bonded FRP material and include provisions for adequate anchorage length/effective bond length to facilitate or ensure proper stress transfer to prevent the premature loss of composite action during service associated with external retrofitting schemes.

In recent decades, research endeavours have included investigations on small to large-scale samples subjected to various loading conditions (single-mode and mixed-mode loading conditions) and materials. Most projects have focused on new materials under controlled laboratory conditions, with some foundational design models derived from previous experience with externally bonded steel plates that predate field application of CFRP (Gemert, 1980; Täljsten, 1994, 1997a). Experimental work aimed at understanding the efficiency of retrofitted deteriorated concrete members with FRP has predominantly emphasised the structural behaviour (failure modes and load capacity), neglecting the influence of existing field defects on both bond transfer mechanism and the overall structural response (Andrawes et al., 2018; Buyukozturk & Hearing, 1998; de Waal et al., 2017; Ghosh & Karbhari, 2007; Gotame et al., 2022; Hag-Elsafi et al., 2004). Beam tests are considered to provide a realistic assessment of mixed-mode stress states in common field applications and are primarily conducted using either a three- or four-point bending configuration. This is crucial since the behaviour of practical field repairs with externally bonded CFRP often involves both pure mode I (tensile opening) and mode II (sliding or in-plane shear) fracture during the progression of cracking. These fracture modes cannot be captured by any single mode test such as the

direct tension pull-off test or shear-lap tests.

Understanding the mixed-mode stress states allows for a more accurate assessment of the bond line performance and the overall structural response. This understanding enables designers and engineers to account for the varying modes of fracture and loading conditions experienced by CFRP retrofitted structures. However, one key parameter that has been investigated mainly through single and double-shear tests (i.e., single-mode loading) is the effect of anchorage length on bond stress distribution and the debonding process (Bizindavyi & Neale, 1999; Brosens & Van Gemert, 1998; Chataigner et al., 2011; Chen & Pan, 2006; Chen & Teng, 2001; Garden et al., 1997; Garden et al., 1998; Hao et al., 2024; Mazzotti et al., 2009; Täljsten, 1997a; Yuan et al., 2004). The anchorage length/effective bond length is the active length needed to transfer 97 percent of the ultimate load and in which bond failure may occur (Chen & Teng, 2001). Garden et al. (Garden & Hollaway, 1998; Garden et al., 1997; Garden et al., 1998) examined the effect of anchorage lengths on reinforced concrete beams strengthened in flexure and subjected to various loading configurations. In these slender beams, the authors reported a considerable increase in the ultimate moment with a rising shear span-to-depth ratio, while a gradual decrease in ultimate load was noticed. The study observed similar cover separation failure modes at different shear span-to-depth ratios. The magnitude of the average peak shear stresses decreased with increased shear span-to-depth ratio. However, since this shear stress calculation depends on the change in strain values between neighbouring strain gauges, a better accuracy could be achieved with closely spaced strain gauges, distributed fibre optic sensors (DFOS), or feasible full-field measurements such as digital image correlation (DIC). Finally, the authors highlighted the benefits of additional plate end anchorage in delaying debonding and their effect in increasing structural stiffness after yielding the internal steel reinforcement.

To improve design criteria, it is vital to monitor the long-term performance of externally bonded applications and understand the critical factors that influence the failure process of deteriorated structural elements subjected to service loads and fluctuating environmental conditions. DFOS have emerged as a

pivotal technology in the domain of structural health monitoring (SHM), facilitating continuous, real-time assessment of structural integrity and performance. In the field of SHM, DFOS has been effectively used for the condition monitoring of various structures including bridges, tunnels, and buildings as well as in the assessment of corrosion propagation (Fan & Bao, 2021). DFOS technologies have been used to examine a diverse array of structural responses, ranging from crack opening displacements under static conditions (Zhao et al., 2024)to dynamic response of structures subjected to cyclic loading (Broth & Hoult, 2020).

The principal objective of this research paper is to investigate and enhance the knowledge on the bond behaviour of deteriorated bridge concrete members strengthened with externally bonded FRP containing field accumulated defects. Specifically, this paper will present results on the debonding behaviour of deteriorated reinforced concrete (RC) members strengthened with multiple layers of externally bonded CFRP with a focus on strain and shear-stress distribution analysis in the tested anchorage lengths for both defective and non-defective regions of the tested beams. Effective strain limits prescribed by design codes or in the reported literature and analytical shear stress-slip predictions are compared against experimental data. DFOS strain data is utilized to discuss the strain and stress distribution in sound and defective regions along the tested anchorage length. Crack kinematics and concrete deformation analysis will be presented from full-field DIC data. The accuracy of average stress distribution estimation has been shown to depend on good strain gradient data, as depicted in Equation 6.1 (Bizindavyi & Neale, 1999), which can be obtained by closely spaced strain measurement points along the bonded length.

$$\tau = \frac{E_{frp} t_{frp} (\varepsilon_{j-} \varepsilon_i)}{x_{j-} x_i} \qquad \text{(Equation 6.1)}$$

where τ represents the average shear stress between two adjacent strain readings, E_{frp} is the elastic modulus of the FRP, t_{frp} is the total thickness of the composite layers, and ε_j denotes strain reading at a specific location (x_j).

6.3 Overview of the Champlain Bridge and Environmental Exposures

Section 1.3 offers a comprehensive summary of the Champlain Bridge and the diaphragm components from which these specimens were cut. The beams tested in this study were actually strips cut from one of the CFRP-strengthened bridge diaphragms (Diaphragm #2) reported in section 1.3 (Figure 6.1).

Figure 6.1-Extraction of beam specimens from Diaphragm #2

Figure 6.2 shows the strengthening layout of the diaphragms; each diaphragm was strengthened with six double-layer vertical CFRP strips (in a U-wrap configuration) with a width of approximately 305 mm and spaces between each strip ranging from 135 mm to 150 mm. Additionally, two double-layer horizontal strips were installed as anchorages at the bottom (a few millimetres from the soffit) and the top of the diaphragms to prevent premature debonding of the vertical U-wraps. Thickness of the strips (two layers) extracted for coupon testing ranged from 3.2 mm to 3.5 mm. The thickness of the concrete diaphragms varied from 210 to 220 mm.

The presence of defects in external CFRP strengthening layers interrupts the proper transfer of stresses between the FRP and concrete substrate, and accounting for their influence on strain and stress distribution is largely absent in the literature (Li et al., 2023). Defects may increase susceptibility to environmental degradation by potentially creating pathways for the ingress of substances and reducing bond strength and load-carrying capacity over time, which may eventually lead to premature failure. In a previous study,

various non-destructive test (NDT) methods along with direct tension pull-off tests showed that the CFRP-strengthened members in this research from the Original Champlain Bridge contained a number of defects of varying size that may compromise the CFRP-concrete bond (Fowai et al., 2023a; Issa Fowai et al., 2025).

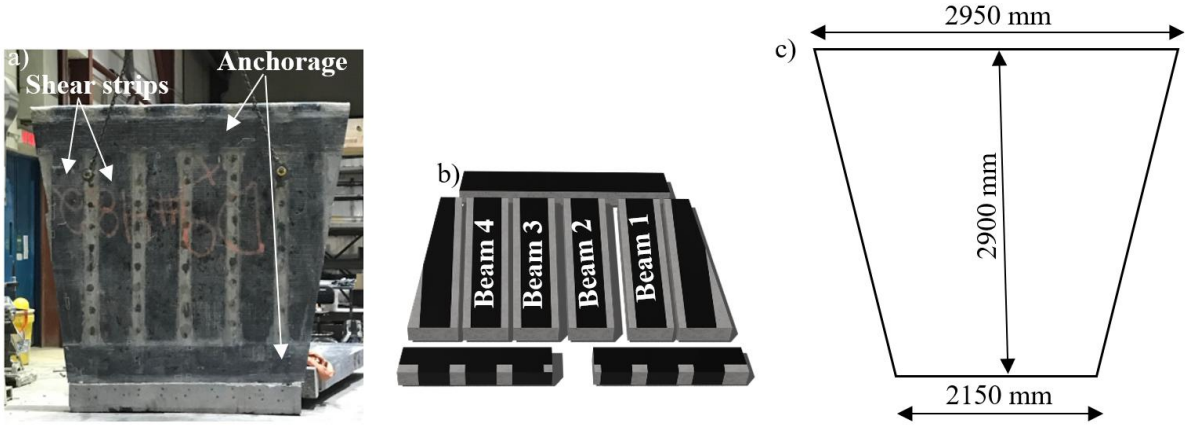

Figure 6.2-Typical bridge diaphragm CFRP strengthening scheme and dimensions: a) As-is diaphragms (orientation shown is upside down compared to in service) b) Beam sample cuts c) geometrical dimensions of original diaphragm

6.4 Material characterization and experimental methods

6.4.1 Material properties

Three concrete cores were extracted from the diaphragms and tested in compression in accordance with ASTM C39 (ASTM, 2021a). The compressive strength of the underlying concrete substrate obtained from the average of three core samples with an average diameter of 95 mm and height of 200 mm was 75.9 MPa (standard deviation of 1.30 MPa) and the estimated cracking strength of the concrete obtained from Equation 6.2 is 3.48 MPa (CSA-Group, 2019).

$$f_{cr} = 0.4\sqrt{f_c'} \qquad \text{(Equation 6.2)}$$

To evaluate the mechanical properties of the CFRP material, coupon samples were extracted from one of the diaphragms. Eighteen coupons were tested following ASTM D3039 (ASTM, 2017) to determine the tensile properties of the composite materials, four of which exhibited desirable failure modes and were used to determine the material properties. These samples were carefully extracted using an angular grinder, mallet, and concrete chisels, taking care not to damage the CFRP itself. Extracted samples were cut into

coupons of 300-mm length by approximately 25.4-mm width. Before testing, 6-mm thick aluminium tabs with bevel ends were designed, ground, and bonded to the coupons for even distribution of stress and minimizing stress concentrations over the grip region. An electrical resistance strain gauge was installed at mid height on one side of the samples (flat surface obtained after grinding of bond line) while the other surface was speckled for digital image correlation measurements. A universal testing machine operating at 2 mm/min was used to complete the coupon tests. The properties of the material from these tests are given in Table 6.1. The data from the samples that experienced grip failure were excluded from the determination of material properties presented in Table 6.1.

Table 6.1-Cured CFRP sheet properties (obtained from testing)

	Coupon 1	Coupon 2	Coupon 3	Coupon 4	Average Values	Standard Deviation
Tensile strength (MPa)	542	557	588	642	582	38.2
Elongation at break (%)	0.93	1.17	1.31	1.03	1.11	0.15
Modulus of elasticity (GPa)	56.1	49.6	50.3	50.1	51.6	2.65
Length (mm)	300	300	300	300	300	-
Width (mm)	25.4	25.4	25.4	25.4	25.4	-
Thickness (mm)	3.68	3.56	3.39	3.29	3.48	0.15

6.4.2 Test set up

One of the three extracted bridge diaphragms discussed in (Fowai, 2023; Issa Fowai et al., 2025) was cut vertically into four 2.0 m long beams (2000 mm long x 430 mm wide x 210 mm deep) and these beams were tested under three-point loading at a displacement rate of 0.2 mm per minute. The beams contained no internal reinforcement along their longitudinal axis, so that all of the tension force was resisted by the CFRP sheet after concrete cracking. Initial tests exhibited premature shear failure which necessitated some modifications to the test setup so that the remaining beams reached a bond failure. These modifications included vertical clamps to provide additional shear capacity and reducing the bonded width of the FRP sheet from 305 mm to 200 mm within the critical anchorage zone (Figure 6.3). The clamps had no contact with the FRP sheet in order to not influence the bond performance. The spacers were positioned in the concrete gaps on both sides of the beam in Figure 6.3b & c. The experimental testing of the four flexural

strengthened beams was completed in two stages, as displayed in the schematic diagrams shown in Figure 6.4: each beam was used for two different anchorage length tests, for a total of eight tests. Table 6.2 provides details of each of the tested beams including the bracing condition. For each stage of testing, a 50 mm deep notch was cut on the front and back side of the concrete beam directly below the loading point without damaging the CFRP to induce a flexural crack at this location creating a stress concentration that would eventually lead to intermediate debonding.

The tested anchorage length was controlled in one of the shear spans by cutting through the FRP layer at a specified distance from the notch, while a 500 mm overhang extended over the other support. After failure was reached at one end of the beam, the supports and loading were moved to the other end of the beam for the second stage of testing, for a total of eight tests (four beams x 2 tests per beam). A beam naming convention in the form of XY-Z has been adopted for this research, where X corresponds to the beam number, Y corresponds to the testing stage, and Z corresponds to the anchorage length. For example: B1S1-L250 refers to the first stage of testing for Beam 1, with an anchorage length of 250 mm, whereas B4S2-L300 indicates the second stage of testing for Beam 4, with a tested anchorage length of 300 mm.

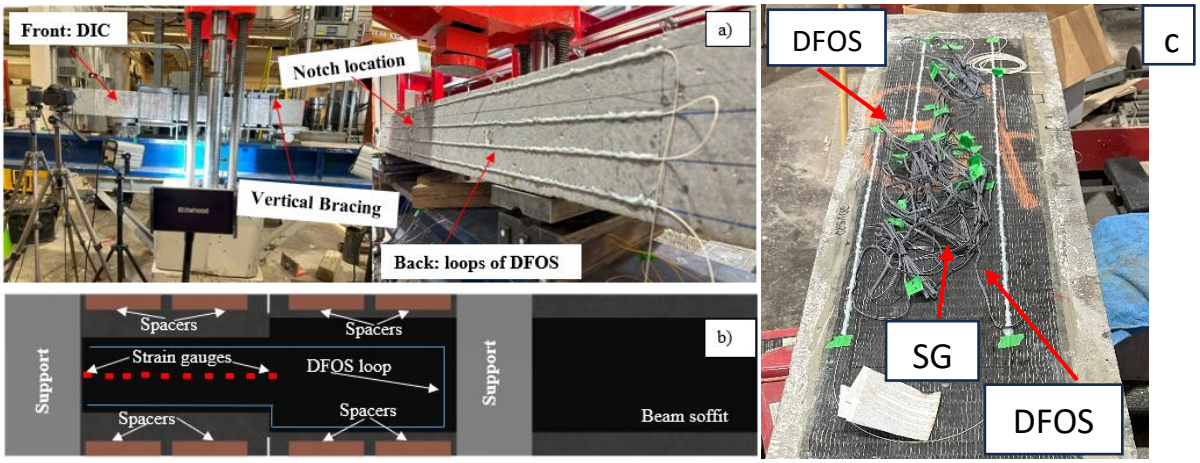

Figure 6.3-Beam sensor instrumentation layout on various sides and test set up a) Experimental setup b) Strain instrumentation layout c) Strain gauge (SG) and DFOS installation

Table 6.2-Beam details

Beam ID	Shear span (mm)	CFRP width in anchorage region (mm)	Number of SG in anchorage (spacing)	DFOS paths (loops) on CFRP	Bracing condition
B1S1-L250	350	305	8 (25 mm)	-	Unbraced
B1S2-L400	500	305	8 (25 mm)	-	Unbraced
B2S1-L500	600	305	10 (25 mm)	-	Unbraced
B2S2-L400	500	200	9 (25 mm)	-	Braced
B3S1-L500	600	200	10 (50 mm)	2	Braced
B3S2-L600	700	200	10 (50 mm)	2	Braced
B4S1-L700	800	200	10 (50 mm)	2	Braced
B4S2-L300	400	200	10 (50 mm)	3	Braced

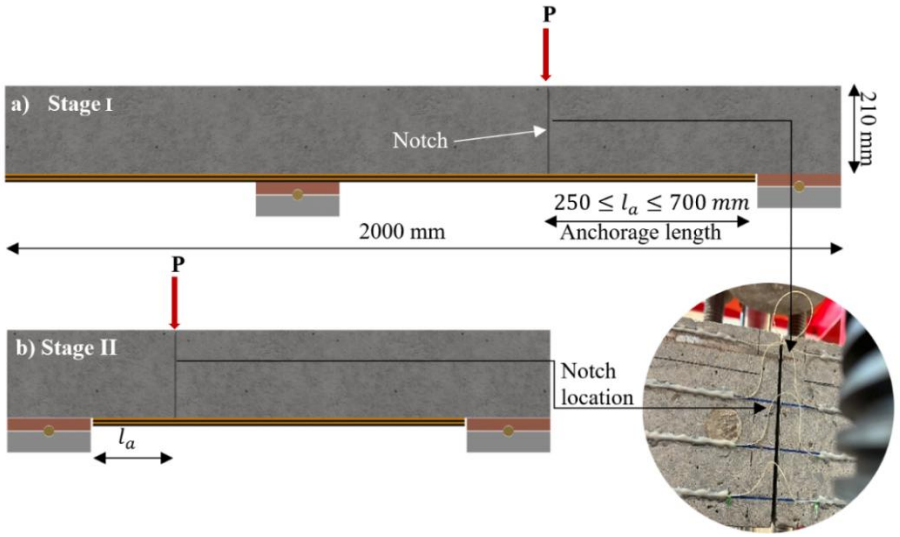

Figure 6.4-Sketch of experimental test stages with beam notch: a) Stage 1 with controlled anchorage length and overhang b) stage 2 with controlled anchorage only

6.4.3 Beam Instrumentation

The strains in the CFRP sheets were monitored with 2-3 loops of nylon coated distributed fibre optic sensors (DFOS) along the entire length as well as discrete electrical resistance strain gauges (Figure 6.3). Four out of eight tests were conducted with DFOS. To prevent damage to the DFOS cables close to the supports, a minimum unbonded distance of 35 mm was maintained between the support and the starting point of the DFOS cable. The strain gauges were closely spaced at the loading point (notched location), where failure was expected to initiate and propagate towards the sheet ends within the tested anchorage length. A minimum spacing of 25 mm was maintained for beams not instrumented with DFOS, while the beams

equipped with DFOS had electrical strain gauges at a minimum spacing of 50 mm (Table 6.2). Concrete strains along the side of the beams were measured using a two-dimensional DIC system and four loops of DFOS (Figure 6.3). Installation of the DFOS and strain gauges required proper and careful cleaning of the bonding surface with solvent and degreaser to clean the bonded area of dust or oil. Strain gauges were installed using cyanoacrylate while Loctite two-part adhesive (EA E-20HP) was used to bond the fibre optic sensors to the concrete or CFRP, as done by Brault and Hoult (Brault & Hoult, 2019). Since the DFOS on the concrete was installed on the saw-cut portions of the beams, no additional grinding was required before sensor installation since the surface was smooth.

A Luna ODiSI 6104 DFOS analyser was used to measure distributed strains. The system has a sensor spacing of 2.6 mm, a maximum sensing length of 50 m per channel, and an accuracy of ±1 microstrain at the sensor core. DIC data on the concrete and deformation data on crack kinematics around the notch was achieved using Aramis 2D DIC systems and DSLR cameras.

6.5 Results and discussion

6.5.1 Failure modes

In the eight tests conducted, two main types of failure were observed. Most commonly, debonding failure occurred (Figure 6.5), while three tests (B1S1-L250, B1S2-L400 and B22S1-L500) resulted in sheet-end shear failure (Figure 6.6). Analysing the strain up to the point of failure of the sheet-end shear failure specimens revealed that two of the three beams exhibited partial debonding around the vicinity of the notch prior to failure. Nonetheless, a complete debonding was not observed prior to the formation of shear cracks at the sheet end. As shown in Table 6.3, one of these beams (B2S1-L500) experienced the highest experimental recorded strain of any of the tested specimens, which is evidence of the imminent debonding in the tested anchorage length. The sheet-end shear failure typically involved diagonal shear cracks that initiated at the endpoint/cut-off point of the CFRP sheets and propagated rapidly towards the loading point;

this issue was addressed in subsequent tests by enhancing the remaining beams' shear capacity through external steel bracing.

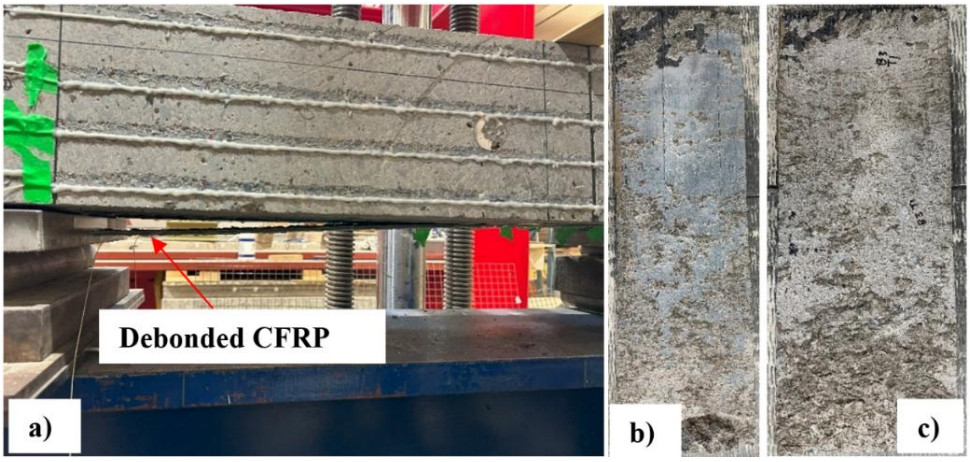

Figure 6.5-Typical failure modes: a) debonded sheet b) Interfacial debonding c) cohesive debonding

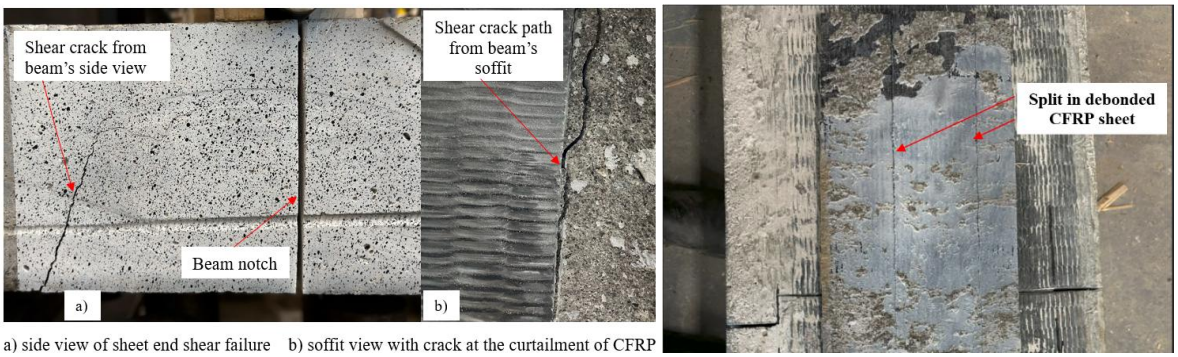

Figure 6.6-Typical CFRP failure modes a) Sheet end shear failure; b) Interfacial debonding surface from beam B4S1-L700 with split in fibre direction

The failure modes and ultimate loads of all tested specimens are summarized in Table 6.3. Both the CFRP sheet-end shear failure and CFRP debonding failure were brittle, occurring suddenly within the tested shear span. After failure, observation of the CFRP sheet revealed two distinct debonding planes, as depicted in Figure 6.5.

The first type occurred at the adhesive-concrete interface, with traces of cementitious concrete material and a large area of exposed adhesive/primer. The second type of debonding failure was cohesive, occurring within the substrate with a thin layer of concrete attached to the CFRP sheets. There was no clear trend between the type of debonding failure and the failure load or tested anchorage length. However, the

thickness of the substrate attached to the CFRP sheets was slightly higher near the point of the applied load than towards the sheets' end close to the support.

Table 6.3-Summary of ultimate load and failure modes

Beam ID[a]	Ultimate load (kN)	Max CFRP strain (με)	Max tensile stress (MPa)	Max shear stress (MPa)	Crack width at failure (mm)	Failure mode[b]
B1S1-L250	-[c]	2057	105.9		-[d]	Sheet-end shear
B1S2-L400	201.8	3581	184.4	4.2	-[d]	Sheet-end shear (imminent debonding)
B2S1-L500	184.5	4495	231.5	7.9	0.6	Sheet-end shear (imminent debonding)
B2S2-L400	94.4	3888	200.2	4.8	0.9	Debonding failure (A)
B3S1-L500	134.5	4359	224.5	6.3	0.7	Debonding failure (S)
B3S2-L600	185.7	4296	221.2	6.1	-[d]	Debonding failure (S)
B4S1-L700	111.3	4469	230.2	7.6	-[d]	Debonding failure (A)
B4S2-L300	152.8	3833	197.4	6.8	0.7	Debonding failure (S)

[a]B1S1-L250: Beam 1 stage 1 with a 250 mm tested anchorage length; B4S2-L300: Beam 4 stage 2 with a 300 mm tested anchorage length
[b]S: debonding failure in substrate; A: debonding failure at adhesive interface
[c]load data was lost due to technical glitch
[d]DIC readings not available

Given the quantity of substrate adhered to the debonded CFRP strips and surface cracks, it is reasonable to infer that a good surface preparation occurred during the field installation of the CFRP materials on the bridge. Therefore, the interfacial debonding at the concrete-adhesive interface (Figure 6.6) could be associated either with the effect of prolonged degradation of the bond line under the synergistic field conditions (combined service load and environmental distress) over the years, or inadequate curing caused by low temperatures at the time of installation.

A detailed visual inspection of this full-scale concrete bridge diaphragm as documented in separate studies (Fowai et al., 2023b; Fowai, 2023; Issa Fowai et al., 2025) revealed the random dispersion of air voids at various locations, including the CFRP-concrete interface, within cured fibres, and between layers of strips through the saw-cut edges of the diaphragms. The accumulation of these minor imperfections has the potential to give rise to larger voids within the composite material, which can in turn disrupt the transfer of stresses between the layers of CFRP strips or between the strips and the underlying concrete substrate. Additionally, instances of bond-separation issues were observed between the underlying concrete substrate

and the patch mortar that was used to repair the concrete surface prior to bonding the CFRP wraps (Fowai et al., 2023b; Fowai, 2023; Issa Fowai et al., 2025) . The patch material is a mortar or paste that was used to fill and level the deteriorated concrete surface before applying the CFRP strips. The incompatibility between these materials inhibits stress transfer and exacerbates damage progression during normal service loading and environmental changes. These separations ultimately result in a reduced load-carrying capacity, limiting the effectiveness of the CFRP strengthening, as well as increased vulnerability to degradation from moisture ingress, and chemical exposure, as further confirmed by tension pull-off testing of one of the other diaphragms following an exhaustive visual assessment. While 96% of the pull-off tests achieved the expected cohesive failure mode within the concrete substrate, most of the low-strength results exhibited mixed mode or adhesive failures. In some cases, samples even failed during the drilling process due to complete bond discontinuities between the CFRP layers and concrete (Fowai et al., 2023b; Fowai, 2023; Issa Fowai et al., 2025).

Beam B4S1-L700 uniquely experienced a split in the CFRP strip during the debonding process, which may be due to the presence of cracks in the CFRP sheets aligned parallel to the fibres (Figure 6.6). Similar parallel cracks in the CFRP sheet were also observed in one of the other diaphragms during visual inspection indicating a loss of load transfer between the fibres and the saturating matrix as detailed in (Fowai et al., 2023b; Issa Fowai et al., 2025). The strain distribution, discussed in more detail in following sections, shows the progressive debonding progress from the region of high-stress concentration (notch location/loading point) and propagation to the ends of the bonded CFRP sheet.

6.5.2 Ultimate capacity and deformation behaviour

Table 6.3 summarizes the ultimate load capacity and the observed failure modes for all tested beams. Unfortunately, due to a technical glitch during the calibration procedure for beam B1S1-L250, the load data was lost. Beams with longer anchorage lengths had increased moment capacity under the same failure modes. For instance, a 30 percent increase in moment capacity was observed between B4S2-L300 and

B3S1-L500. The notable decrease in the moment capacity of beam B4S1-L700, which was tested with the longest anchorage length of 700 mm, was attributed to the splitting of the CFRP sheet during the test shown in Figure 6.6b along with subsequent interfacial debonding during the failure process. This splitting of the CFRP sheet could be related to the presence of initial cracks in the CFRP sheets due to field conditions (loads & environmental factors) of the bridge. All the anchorage lengths tested in this study are above the minimum code provisions or those calculated from available analytical models, and hence, a significant increase in ultimate moment was not expected since the effective bond length or stress transfer length is less than the tested anchorage lengths. However, varying load capacities of different tested beams could be influenced by the level of deterioration of the concrete substrate before the CFRP field retrofitting.

6.5.3 Strain distribution in CFRP bonded length

The strain distributions as a function of distance along the CFRP sheet were measured with the DFOS. Four tests were conducted with DFOS (B3S1-L500, B3S2-L600, B4S1-700, and B4S2-L300) installed on the CFRP at the soffit of the beam. Similar strain behaviour was noticed for the two loops of DFOS cables installed in each test, therefore only selected results for beams B3S1-L500 and B3S2-L600 will be presented (Figure 6.7 to Figure 6.11). Figure 6.7a shows the measured experimental strain at different load levels along the bonded length of CFRP in Beam B3S1-L500. The horizontal axis is measured from the end of the sheets near the support. DF50 refers to the strain measurements at 50 mm from the end of the CFRP sheet, obtained from distributed fibre optic sensor (DFOS). Similarly, DF500 represents the DFOS strain data at the notch location (situated 500 mm from the end of the CFRP sheet near the support). In B3S1-L500 (see Figure 6.7a), CFRP initial debonding occurred at the loading point (notched location 500 mm from the support) around 50 kN to 75 kN, as evidenced by the plateau (i.e., low strain gradient) in the strain curve shown in Figure 6.7a at 50 kN which becomes flatter at 75 kN. This indicates a lack of stress transfer over the plateau distance (high strain regions with uniform strain) at a given load stage. The width of the plateau region increased throughout the test; with increasing load, CFRP debonding shifted the active bond stress transfer zone (effective bond length) further from the notched location, continuing until complete

debonding of the CFRP strip occurred. At any specific load level, the strains in the FRP decrease away from the loading point. The fluctuation in peak values on the curve (Figure 6.7a) represents the initiation of interfacial cracks during the debonding process. The ultimate strain reached in B3S1-L500 at the notch location was 4359 microstrain.

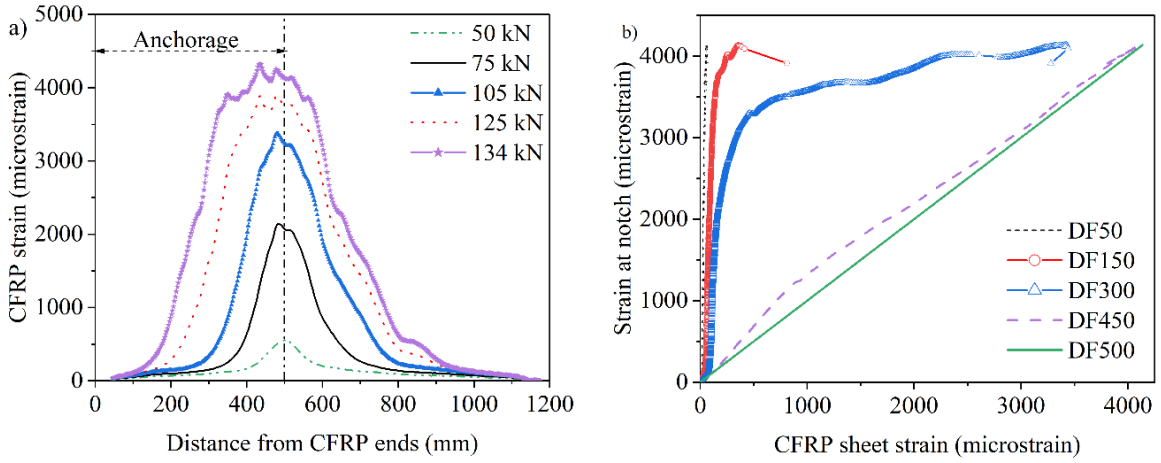

Figure 6.7-Strain behaviour of B3S1-L500: a) Strain-Distance response b) DFOS notch strain versus CFRP sheet strain response

Figure 6.7b depicts the convergence of discrete strain measurements along the length of beam (B3S1-L500) with the strain at the notch where debonding initiated. The horizontal axis represents the measured experimental strain at various points along the length of the beam. As high strain values are reached, the CFRP sheet strain measurements along the length of the beam progressively approach the maximum strain at the notch/loading point, signalling the onset of progressive debonding around the ultimate loads. The region near the end of the CFRP exhibited no significant increase in strain values until complete debonding occurred (DF50-DF150 located 50,100, and 150 mm, respectively, away from the CFRP ends). For instance, the maximum strain recorded at DF-150 (150 mm from CFRP ends) was only 19% of the maximum strain achieved in beam B3S1-L500, and as the remaining bonded length decreased, the CFRP capability to take more strain vanishes rapidly. Figure 6.8 illustrates the variation in strain gradient throughout the loading stages for B3S1-L500, displaying an initial rise in gradient, followed by a decline representing debonding. The strain gradient was calculated as the rate of change of strain with respect to position ($gradient = {}^{\Delta\varepsilon}/_{\Delta x}\ with\ \Delta x = 50\ mm$). DF175 refers to the average strain gradient over a 50 mm interval centred at

175 mm from the sheet end. Debonding initiated in proximity to the notch upon the attainment of a strain level of approximately 3600 microstrain (DF175). Strain gradients closer to the notch location (e.g., DF425) approached zero near the end of the test prior to failure, while the peak strain gradients shifted further away from the notch.

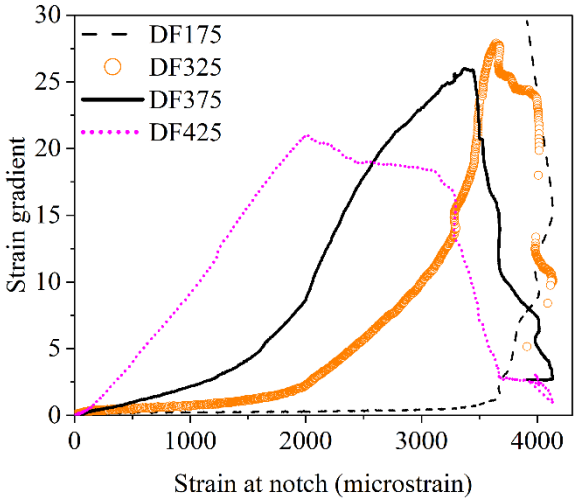

Figure 6.8-Strain gradient depicting debonding in B3S1-L500

In Figure 6.9, the strain behaviour is presented for B3S2-L600 to depict the debonding process and shift in the stress transfer zone within the tested anchorage length. In B3S2-L600 (See Figure 6.9a), initial debonding started at the loading point (notched location 600 mm from the support). A change in stiffness is noticeable around 50 kN to 75 kN for locations around the notch (see DF600 from Figure 6.9b).

In general, the strain readings captured by the strain gauges and the DFOS exhibited strong agreement particularly under low loads (up to 75 kN in the case of B3S1-L500) (Figure 6.10). However, the electrical resistance strain gauge recordings at higher load levels did not perfectly align with DFOS values (Figure 6.11). A possible reason for this could be that the DFOS was not bonded at the same location across the width of the beam (see Figure 6.3), meaning different local effects on strains may be captured by the two measurement techniques. Additionally, localized variation in the thickness of the adhesive bond line may contribute to the discrepancies observed in strain measurements. The strain distribution observed in Figure 6.7 to Figure 6.11 exemplified the typical behaviour found in all debonded beams. Nonetheless, a higher level of fluctuation was noticed in strain data collected from strain gauges due to localized effects as

opposed to the smoother curves derived from the DFOS data (Figure 6.7 to Figure 6.11). CFRP debonding strains were also generally higher in beams with longer shear spans. The maximum strain for B4S2-L300 with the shortest anchorage length was 12 percent lower than that of B3S2-L600 and 17 percent lower than B4S1-L700, respectively.

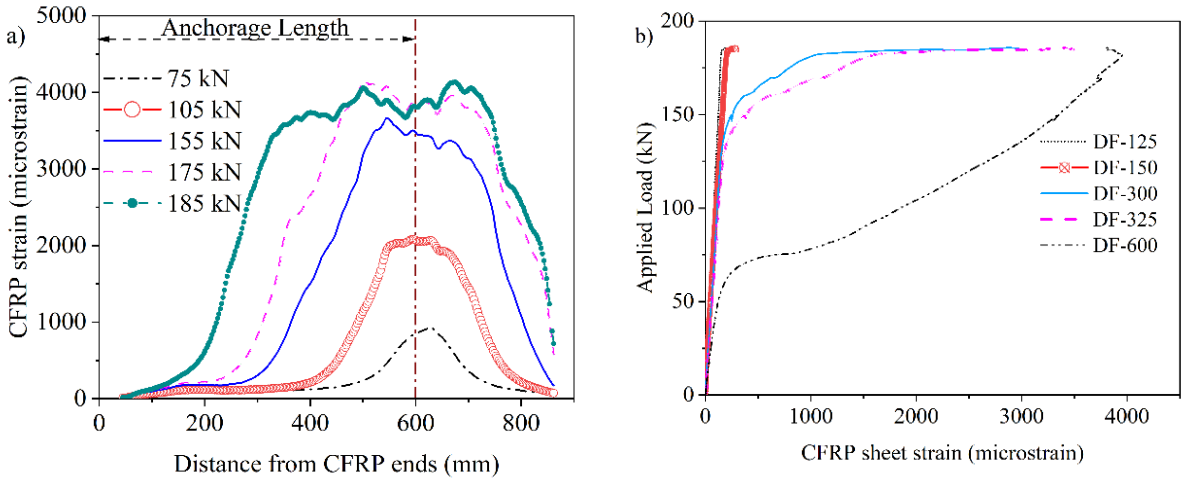

Figure 6.9-Strain behaviour of B3S2-L600: a) Strain-Distance response b) Load-Strain response

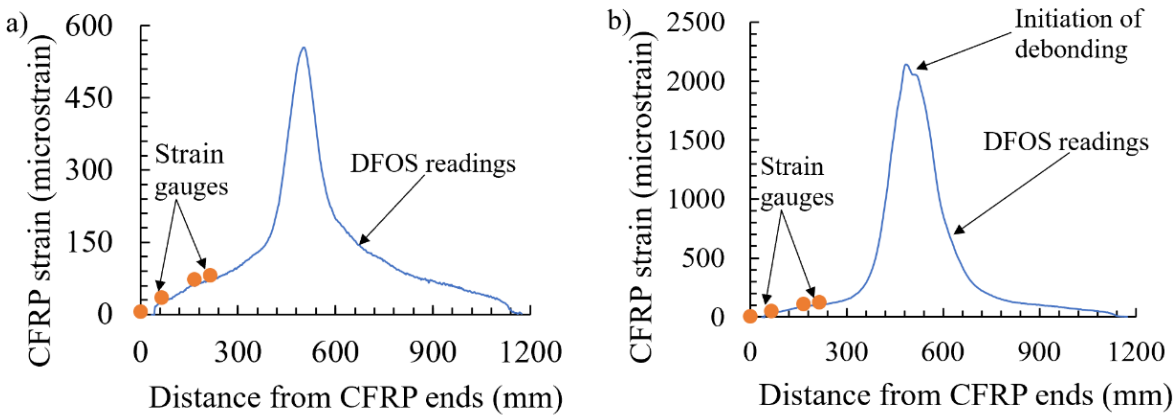

Figure 6.10-Comparison between strain measurement techniques at low load level for B3S1-L500: a) Strain gauge and DFOS data at 50 kN b) Strain gauge and DFOS values at 75 kN

Figure 6.12 illustrates a comparison of maximum experimental strain values across different anchorage lengths in relation to prescribed code limits. While an increased in the maximum was observed with increase in anchorage length, a constant maximum strain was achieved for anchorage lengths of 500 mm and beyond, irrespective of the debonding failure mode. It is also notable that the ultimate strain observed from all debonded beams (see Table 6.3) was approximately half the value calculated based on the ACI

PRC-440.2-23 provisions for debonding strain (Table 6.4). The strain limit prescribed in the Canadian code (CAN/CSA S6:19) also exceeded the maximum experimental strain observed in the beams that experienced debonding (B4S1-L700) by approximately 34 percent.

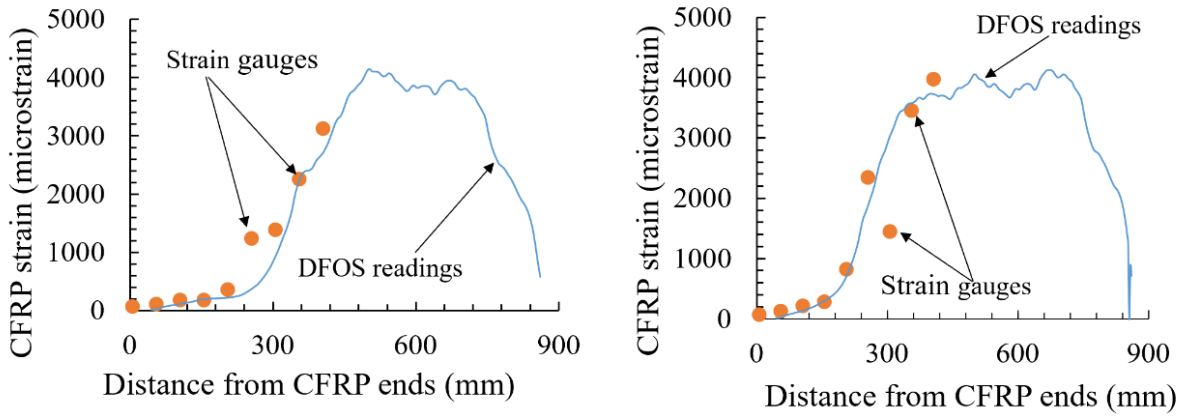

Figure 6.11-Comparison between strain measurement techniques close to ultimate for B3S2-L600: a) Strain gauge and DFOS data at 175 kN b) Strain gauge and DFOS data at 185 kN

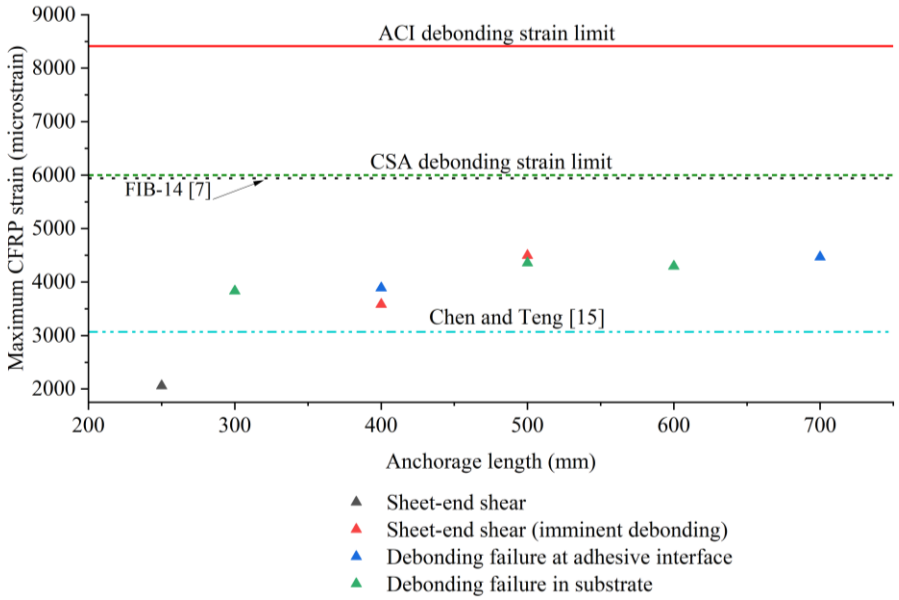

Figure 6.12-Maximum tensile strain correlation with anchorage length

It is important to note that existing models in the literature draw primarily from extensive experimental data on externally bonded applications using new materials (concrete, FRP, or adhesive) without necessarily accounting for the impact of degradation at the bond line or within the separate materials. This contrasts with the concrete substrates examined in this study, which had been constructed with high strength concrete

and in service for nearly six decades prior to its decommissioning due to extensive deterioration. Experimental work leading to the development of the existing models are typically conducted under favourable laboratory temperature conditions while the installation of CFRP on these bridge elements was completed during the winter, potentially impacting the epoxy resin's curing process due to the prevailing low temperatures.

As illustrated in Figure 6.2, beams were not extracted from the top anchorage zone, where a higher incidence of bond line defects were observed during the initial condition assessment. The concrete in this region exhibited significant damage, rendering it unsuitable for in-plane bending tests. It is expected that the strain variation depicted in Figure 6.7 and Figure 6.9 will closely resemble the strain distribution within the defect-free regions of the anchorage zones; however, the presence of field-induced defects is likely to result in lower average peak strains in the anchorage zones. The general influence of these defects on the distribution of strain and shear stress at the CFRP-concrete interface is discussed in the subsequent sections.

6.5.4 Strain distribution across defective regions in CFRP bonded length

Defects and debonded regions in concrete structures externally bonded with CFRP are known to have impacts on the durability and load bearing capacity of the retrofitted structure (Ascione, 2016; Li et al., 2023; Zhou et al., 2017). Before structural testing, thorough assessments of damage in the retrofitted bridge diaphragms were conducted using localized and global NDT methods. The evaluation involved a detailed visual inspection and a conventional coin-tapping approach, as well as infrared thermography and an automated Wichitech digital tap hammer to cross-validate the results from other methods (Fowai et al., 2023b; Issa Fowai et al., 2025). These identified defects (voids, air pockets and debonds) were then monitored via DFOS instrumentation during the structural loading to understand strain and stress transfer mechanisms over these defective regions. Three defects were located on the tension side of B3S1-L500, with one defect (50 mm x 80 mm) being within the tested anchorage length (reduced width area) as shown in Figure 6.13. One 20 mm x 130 mm defect was also found in B4S1-L700 outside the reduced width area.

The local strain distribution over and around defective regions in an externally bonded composite may be complex depending on defect type, size, and applied load. Defects can create stress concentrations and reduce the load-carrying capacity. In the case of defects at the FRP-concrete interface, the bond stress transfer is interrupted, and a lower strain gradient is expected (depending on the size of the defect relative to the sheet width). In this study, strain measurements from DFOS instrumented over defective areas of the beams showed constant strain readings until near the ultimate load when a slight gradient in strain was observed as shown in Figure 6.14a, which exhibits strains over a defect situated within the full width region of B4S1-L700. This can be contrasted with Figure 6.14c, which shows a significant strain gradient over a non-defective region at the same distance from the notch/loading point for B4S1-L700.

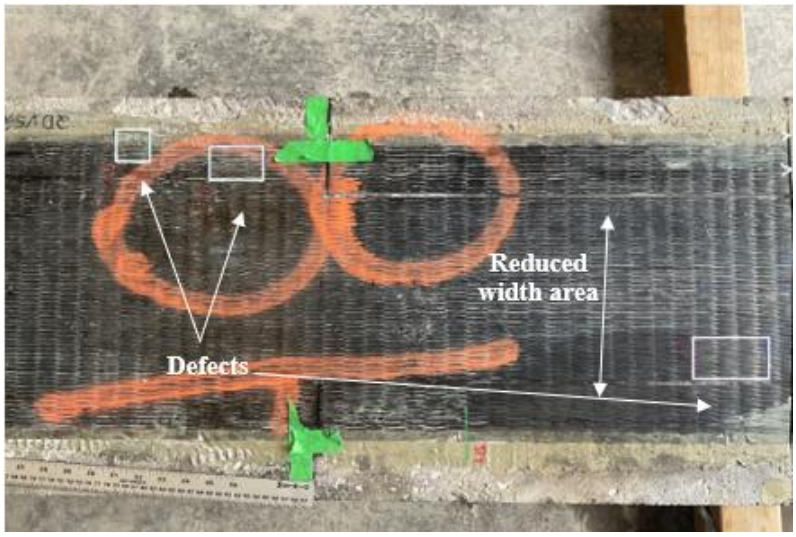

Figure 6.13-NDT identified defects in B3S1-L500

Similar behaviour is observed in Figure 6.14b, where a low strain gradient was also observed. Figure 6.14b shows strain values of a defect located 390 mm from the loading point covering one fourth of the bonded width in the reduced width area of B3S1-L500. Since the defect was located near the sheet end, the maximum strain at the ultimate load for the defect observed in B3S1-L500 was only 145 microstrain implying low bond stress transfer in these zones and no major conclusions can be drawn about the effects of the defect on effective strain limits.

6.5.5 Shear stress distribution in CFRP bonded length

The maximum shear stress at the FRP-concrete interface for each beam that experienced debonding is compared in Table 6.3. Shear stresses were calculated from the local strain gradient along the tested anchorage length and utilized to determine the average shear stress between two points using Equation 6.1. In this study, DFOS data allowed for a strain reading every 2.6 mm, providing better capture of stress distribution non-linearity compared to traditional measurements obtained from strain gauges usually spaced further apart. Similar to strain plots, stress plots are measured from the end of the CFRP in the tested anchorage length. The shear stress distribution will generally give a positive magnitude on one side of the loading point and a negative magnitude in the other, relative to the loading configuration, as shown for B3S1-L500 at the 60 KN load level in Figure 6.15. Absolute values for shear stresses within the tested anchorage length (reduced width area) are used below for subsequent comparisons.

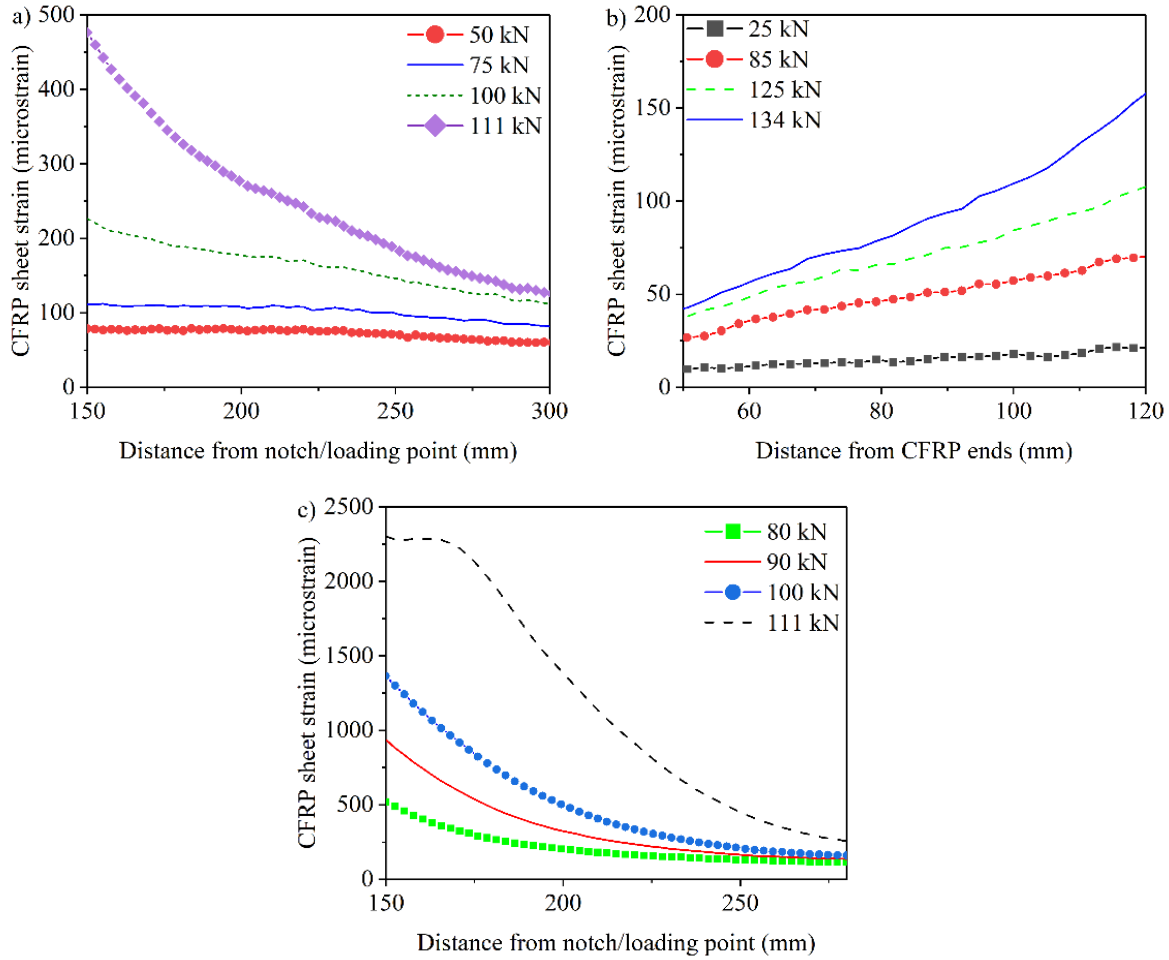

Figure 6.14-Strain distribution over debonded areas a) B4S1-L700 b) B3S1-L500 c) Strain distribution over non-defective region at same distance (B4S1-L700)

Before bond line cracking, the shear stress distribution within the anchorage length is expected to follow an exponential decay, with bond line cracks developing at the peak shear stress, creating a distinct debonded zone in the pre-peak region and uncracked bond line regions within the softening branch in the stress distribution profiles as shown in Figure 6.15. The progression of these microcracks will cause the location of the peak shear stress to shift away from the loading point until stress transfer becomes compromised with the emergence of macro cracks in the concrete (Figure 6.16). The prediction of the experimental shear stress-slip is shown in Figure 6.18 from different bond-slip models documented in the existing literature (Ko et al., 2014; Lu et al., 2005; Nakaba et al., 2001; Nelson et al., 2020; Nelson et al., 2024; Neubauer & Rostasy, 1999). In determining the experimental shear stress-slip curve, shear stress and crack opening data for B3S1-L500 under load levels of 30 kN, 75 kN, 105 kN and 125 kN was used. The experimental slip was derived from the crack opening measurement (at the notched location), assuming that the cumulative slip on each side of the notch is equivalent to the notch opening. It is worth highlighting that higher shear stresses (6-7 MPa, in proximity to the values anticipated by the analytical models) did develop at locations slightly distanced from the notch.

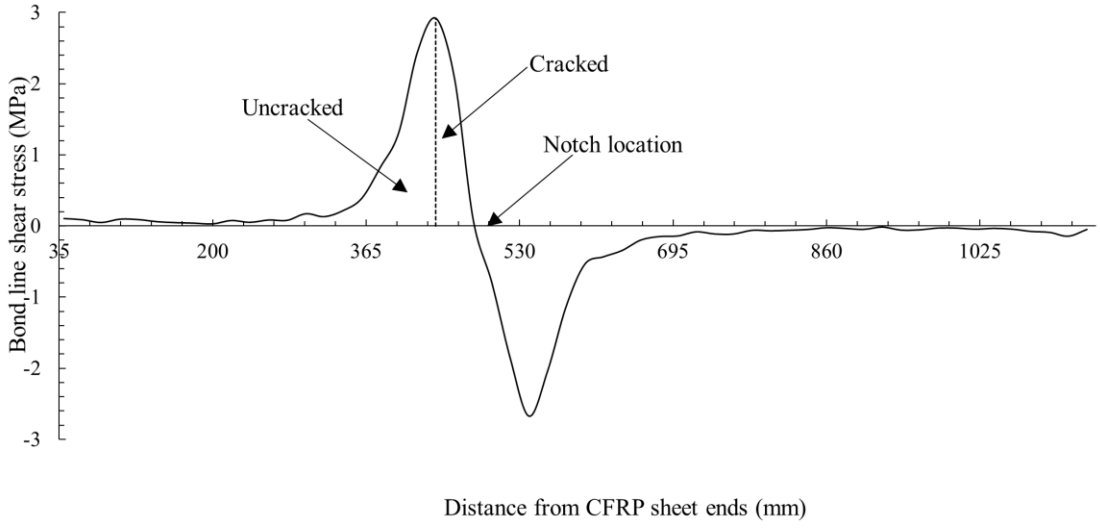

Figure 6.15-Bond line shear stress distribution for B3S1-L500 at 60 KN load

The non-linear model developed by Nakaba et al (Nakaba et al., 2001) and the simplified model proposed by Lu et al (Lu et al., 2005) demonstrated a close correspondence with the shear stress distribution pattern

observed from the experimental results. In contrast, the bilinear model formulated by Ko et al (Ko et al., 2014)overestimated the maximum experimental shear stress in Table 6.3 by more than 58 percent. This model heavily relies on the compressive strength of the concrete in defining the bond parameters, including slip and stress. Figure 6.16 shows the distribution of shear stresses along the bonded length at different load levels. The experimental shear stress distribution under low load conditions (see Figure 6.16a and Figure 6.17a) exhibited a close resemblance to the patterns documented in existing literature for exponential and power functions (Nakaba et al., 2001; Nelson et al., 2020; Nelson et al., 2024). However, under higher loads, the shear stress distribution became characterized by fluctuating peaks.

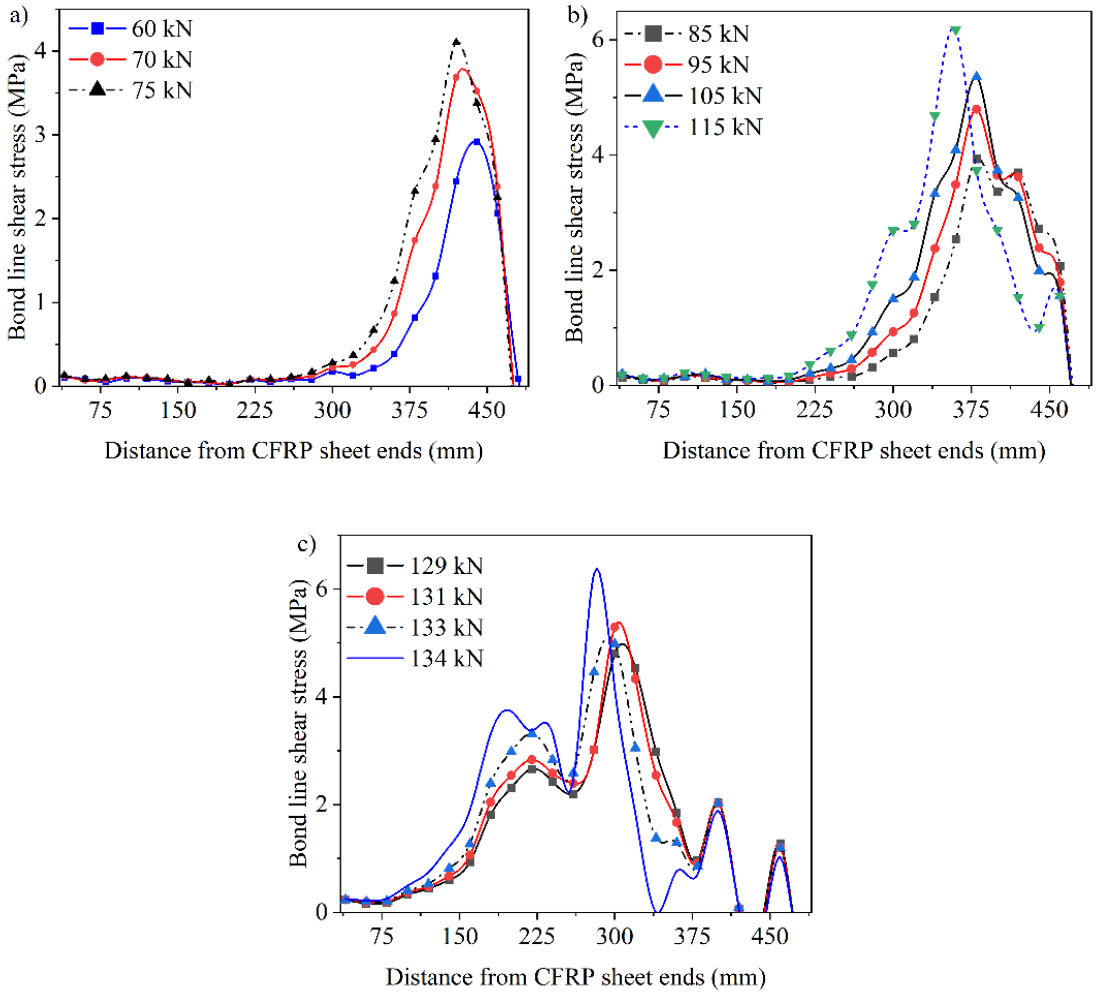

Figure 6.16-Shear stress distribution at various load levels: a) low load level b) medium load level c) around ultimate loads for B3S1-L500

This specific pattern of shear stress peaks was consistently observed across all the beams listed in Table 6.3, with singular peaks noticeable at lower loads, and multiple peaks emerging at higher load levels. The fluctuation in shear stress distribution, particularly around the ultimate load, can be attributed to the condition/roughness along the cracks during the debonding process and possibility of local defects that were undetected during the condition assessment (Yuan et al., 2004).

Current shear stress analytical models assume constant material thickness and uniform stress distribution without discontinuities. These assumptions present a challenge for existing models to accurately predict experimental results, especially when random flaws at the bond line between the CFRP and concrete or prior concrete repair work in the field application are to be considered. Beams B3S1-L500 and B3S2-L600 exhibited maximum shear stresses of 6.28 MPa and 6.11 MPa, respectively. These values were found to be 5 percent and 8 percent lower than the fib-14 predictions (Table 4).

On the other hand, B4S1-L700 had a maximum shear stress of 7.63 MPa. Across these beams, the location of maximum shear stresses shifted from the vicinity of the loading point toward the end of the CFRP sheet as the load level increased, ultimately reaching the maximum shear stress near the centre of the tested anchorage length (reduced width area). However, beam B4S2-L300, with the shortest anchorage length, exhibited a different behaviour; the maximum shear stress occurred at the sheet ends, reaching a peak value of 6.75 MPa, representing a 2 percent increase compared to the fib-14 prediction.

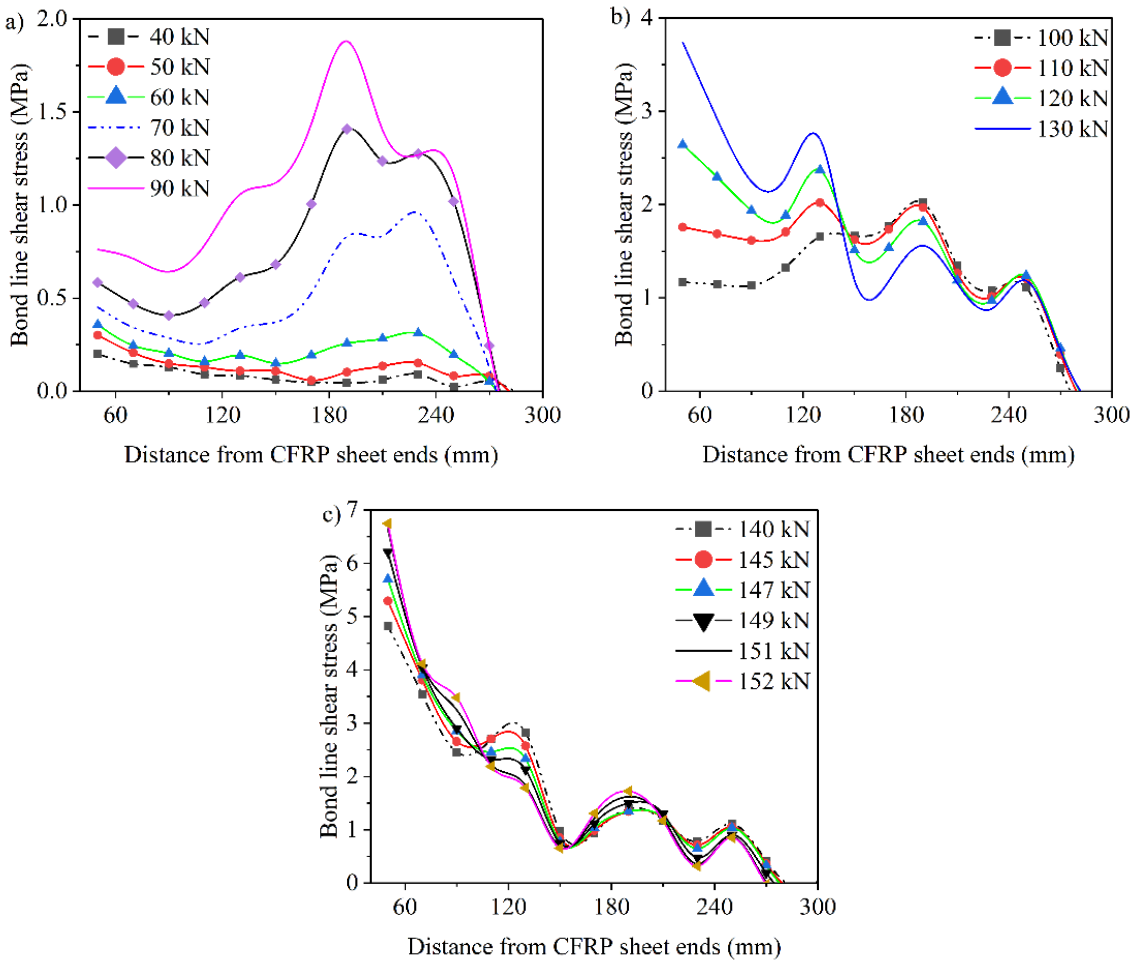

Figure 6.17-Shear stress distribution at various load level for B4S2-L300: a) Shear stress at low b) Shear stress at medium load level c) Shear stress at around ultimate loads

In this beam, the peaks of the shear stress shifted from the loading point towards the ends of the CFRP sheet at lower load levels, stabilized at higher loads around the midpoint of the tested anchorage length, and near the ultimate loads the peaks shifted towards the CFRP sheet ends (Figure 6.17). In B4S2-L300, the shear stress at the end of the CFRP, even at lower load levels, significantly exceeded those observed in beams with longer anchorage lengths. The maximum shear stress across the defect area ranged between 0.54 and 1.13 MPa. These values represented approximately 8 percent to 15 percent of the maximum peak shear stress in those beams. As depicted in Figure 6.19, the shear stress behaviour over the defective areas exhibited non-linearity even at low load levels, characterized by multiple shear stress peaks.

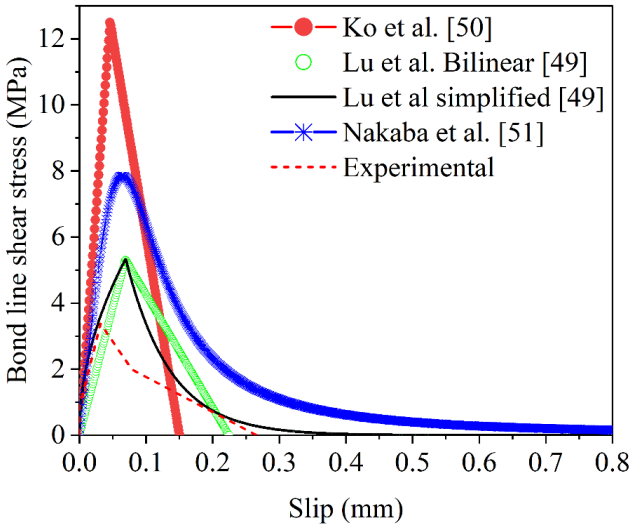

Figure 6.18-Predicted shear-slip behaviour from existing models

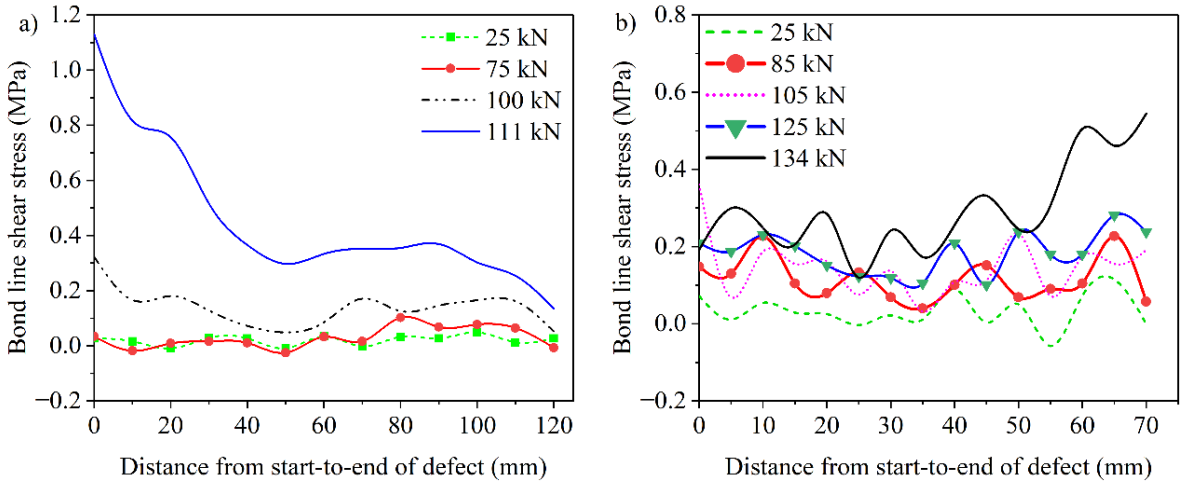

Figure 6.19-Shear stress distribution over debonded areas shown in Figure 14: a) Shear stress for defect in B4S1-L700 b) Shear stress for defect in B3S1-L500

It is important to highlight that although bond strength data specific to these bridge elements prior to deconstruction were not documented, existing studies on accelerated aging in laboratory settings have indicated a loss of mechanical properties in the adhesive. This loss has resulted in a reduction of bond strength ranging from 8% to 48 %, depending on the exposure conditions, duration, and testing protocols (Cruz et al., 2023; Hao et al., 2024; Liu et al., 2021; Tatar & Hamilton, 2016).

6.5.6 Effective bond length

Based on the strain distribution illustrated in Figure 6.7 to Figure 6.9, the load transfer mechanism can be

divided into three distinct zones: the fully debonded region, the stress transfer zone and the stress-free region. Within the fully debonded region, the maximum strain remains constant (i.e., low strain gradient), while a strain gradient is apparent in the stress transfer region. The tensile force within the concrete is transferred to the CFRP within the stress transfer region and as the load increases this active transfer region shifts away from the loading point, indicating that only a portion of the bonded length actively participates in load transfer, such that any extension beyond this length does not necessarily result in corresponding increase in load. This interfacial parameter is critical to understanding the length of the bonded CFRP necessary for anchorage. The estimated values of this effective bond length parameter as predicted from analytical models in existing literature and various codes is presented in Table 6.4.

Table 6.4-Summary for debonding limiting condition from available codes

Code/ model	$L_a, L_e, L_{b,max}$ Expressions	L_a, L_e or $L_{b,max}$ Predicted (mm)	Debonding limiting condition	Predicted value (equivalent strain)
(ACI, 2023a)	$L_a = \sqrt{\frac{n * E_{frp} * t_{frp}}{\sqrt{f_c'}}}$	144	$\varepsilon_{fd} = 0.41\sqrt{\frac{f_c'}{nE_{frp}t_{frp}}}$	$\varepsilon_{fd} = 8413\ \mu\varepsilon$
CHBDC[	$L_a = 0.5\sqrt{E_{frp*}t_{frp}}$	212	$\varepsilon_{fd} = 0.41\frac{f_c'}{\varepsilon_{frp}t_{frp}} \leq 0.006$	$\varepsilon_{fd} = 6000\ \mu\varepsilon$
Chen and Teng	$L_e = \sqrt{\frac{E_{frp} * t_{frp}}{\sqrt{f_c'}}}$	144	$P_u = 0.427\beta_p\beta_l\sqrt{f_c'}b_pL_e$	110 kN (3069 $\mu\varepsilon$)
FIB-14	$L_{b,max} = \sqrt{\frac{E_{frp} * t_{frp}}{2 * f_{ctm}}}$	161	$N_{fa,max} = \alpha c_1 k_c k_b b\sqrt{E_{frp} * t_{frp} * f_{ctm}}$	213 kN (5942 $\mu\varepsilon$)

L_a: Anchorage length; n: number of layers of FRP; E_{frp}: Elastic modulus of FRP in MPa; t_{frp}: thickness of FRP/layer (when n is included in the equation); ε_{fd}: debonding strain; $\mu\varepsilon$: microstrain; L_e: effective bond length; β_p: coefficient for ratio of bonded FRP to concrete; P_u: ultimate load; β_l: coefficient provided in Chen & Teng; b_p: width of bonded FRP; $L_{b,max}$: maximum anchorage length; f_{ctm}: tensile strength of concrete; $\alpha c_1 k_c k_b$: coefficients provided in fib; b: concrete width

The effective lengths derived from the experimental strain and shear stress distributions were found to be consistently between 205 to 230 mm. The anchorage length required for effective stress transfer prescribed in the Canadian code was within 8 percent of the maximum experimental effective length observed Table 6.4. Significant disparities were also observed in both the guidance provided by the International Federation

of Structural Concrete (fib) (Triantafillou et al., 2001) and the model developed by Chen and Teng (Chen & Teng, 2001). The Chen & Teng model underestimated the ultimate load/strain by 18 to 41 percent, while the FIB-14 overestimated it by 15 to 126 percent.

6.6 Conclusions

In this paper, the debonding behaviour of bond critical CFRP retrofitted beams extracted from a deteriorated bridge (Original Champlain Bridge) in Canada after decades of service was investigated. This research assesses the impact of varying anchorage lengths on the strain and shear stress distribution of the deteriorated concrete beams. The study also examined the influence of accumulated field defects on the debonding mechanism. The implementation of distributed fibre optic sensors (DFOS) facilitated an accurate estimate of the strain and shear stress distribution across the bonded CFRP sheet. Based on the findings presented in this investigation, several conclusions can be drawn:

- In deteriorated concrete members, the extent of bond line deterioration largely influences the debonding failure mode. Debonding may occur a few millimetres into the concrete or within the adhesive layer.
- Debonding limits outlined in design codes or available models in the literature do not necessarily correlate well for specimens that have been subjected to the synergistic effects of service load and harsh environmental conditions for a prolonged period. The Chen & Teng model underestimated the ultimate load by 18 to 41 percent, while the FIB-14 overestimated it by 15 to 126 percent. Effective strain limits in the CFRP were unconservative for both provisions from the American Concrete Institute (ACI) and Canadian Highway Bridge Design Code (CHBDC).
- The average peak value of the interfacial shear stress increases with a reduction in anchorage length. B4S2-L300 with an anchorage length of 300 mm demonstrated a maximum shear stress of 6.75 MPa, representing a 10 percent increase compared to B3S2-L600 with an anchorage length of 600 mm.

- Load transfer was limited in areas with field defects identified from various NDT methods. However, as these defects were located away from the notch/crack location, the effect of the defects on bond performance could not be fully assessed. Further research into the effects of bondline defects in externally bonded strengthening systems is recommended.
- This study found a good agreement with strain data provided by conventional discrete electrical gauges and DFOS. However, DFOS installed along the length was essential in observing the shift in shear stress peak, especially in the beam with the shortest anchorage length.

6.7 References

ACI. (2023a). Design and Construction of Externally Bonded FiberReinforced Polymer (FRP) Systems for Strengthening Concrete Structures—Guide (ACI PRC-440.2-23). In. Farmington Hills, MI, 2023: American Concrete Institute.

Andrawes, B., Shaw, I. D., & Zhao, H. (2018). *Repair & strengthening of distressed/damaged ends of prestressed beams with FRP composites*.

Ascione, F. (2016). The influence of adhesion defects on the collapse of FRP adhesive joints. *Composites Part B: Engineering*, *87*, 291-298.

ASTM. (2017). Standard Test Method Tensile Properties of Polymer Composite Materials. In *ASTM D3039*. West Conshohocken, PA: ASTM.

ASTM. (2021a). Standard Test Method for Compressive Strength of Cylindrical Concrete Specimens. In *ASTM C39*. West Conshohocken, PA.

Baggio, D., Soudki, K., & Noel, M. (2014). Strengthening of shear critical RC beams with various FRP systems. *Construction and Building Materials*, *66*, 634-644.

Bizindavyi, L., & Neale, K. (1999). Transfer lengths and bond strengths for composites bonded to concrete. *Journal of composites for construction*, *3*(4), 153-160.

Brault, A., & Hoult, N. (2019). Monitoring reinforced concrete serviceability performance using fiber-optic sensors. *ACI structural journal*, *116*(1), 57.

Brosens, K., & Van Gemert, D. (1998). Plate end shear design for external CFRP laminates. *AEDIFICATIO Publishers, Fracture Mechanics of Concrete Structures*, *3*, 1793-1804.

Brosens, K., & Van Gemert, D. (2001). Anchorage of externally bonded reinforcements subjected to combined shear/bending action. Proceedings of the international Conference on FRP composites in Civil Engineering,

Broth, Z., & Hoult, N. A. (2020). Dynamic distributed strain sensing to assess reinforced concrete behaviour. *Engineering structures*, *204*, 110036.

Buyukozturk, O., & Hearing, B. (1998). Failure behavior of precracked concrete beams retrofitted with FRP. *Journal of composites for construction*, *2*(3), 138-144.

Chajes, M. J., Thomson Jr, T. A., Januszka, T. F., & Finch Jr, W. W. (1994). Flexural strengthening of concrete beams using externally bonded composite materials. *Construction and Building Materials*, *8*(3), 191-201.

Chataigner, S., Caron, J.-F., Benzarti, K., Quiertant, M., & Aubagnac, C. (2011). Use of a single lap shear test to characterize composite-to-concrete or composite-to-steel bonded interfaces. *Construction and Building Materials*, *25*(2), 468-478.

Chen, J. F., & Pan, W. (2006). Three dimensional stress distribution in FRP-to-concrete bond test specimens. *Construction and Building Materials*, *20*(1-2), 46-58.

Chen, J. F., & Teng, J. (2001). Anchorage strength models for FRP and steel plates bonded to concrete. *Journal of Structural Engineering*, *127*(7), 784-791.

Cruz, R., Correia, L., Cabral-Fonseca, S., & Sena-Cruz, J. (2023). Durability of bond of EBR CFRP laminates to concrete under real-time field exposure and laboratory accelerated ageing. *Construction and Building Materials*, *377*, 131047.

CSA-Group. (2019). Canadian Highway Bridge Design Code. In *CSA S6:19*.

de Waal, L., Fernando, D., Cork, R., & Foote, J. (2017). FRP strengthening of 60 year old pre-stressed concrete bridge deck units. *Engineering structures*, *143*, 346-357.

Fan, L., & Bao, Y. (2021). Review of fiber optic sensors for corrosion monitoring in reinforced concrete. *Cement and Concrete Composites*, *120*, 104029.

Fanning, P. J., & Kelly, O. (2001). Ultimate response of RC beams strengthened with CFRP plates. *Journal of composites for construction*, *5*(2), 122-127.

Fowai, I., Noël, M., Martin-Perez, B., & Sanchez, L. (2023a). *Integrity assessment of CFRP-concrete interface on externally strengthened bridge diaphragms using direct tension pull-off test* 11th International Conference on FRP composites in civil engineering, Rio de Janeiro.

Fowai, I., Noël, M., Martín-Pérez, B., & Sanchez, L. (2023b). *Condition assessment of FRP-strengthened concrete bridge diaphragms using non-destructive testing* 11th International Conference on FRP composites in civil engineering, Rio de Janeiro.

Fowai, I., Noel, M., Martín-Pérez, B., & Sanchez, L. (2023). *Integrity Assessment of CFRP-Concrete Interface on Externally Strengthened Bridge Diaphragms Using Direct Tension Pull-off Test.* 11th International Conference on Fiber-Reinforced Polymer (FRP) Composites in Civil Engineering (CICE 2023), Rio de Janeiro, Brazil.

Garden, H., & Hollaway, L. (1998). An experimental study of the influence of plate end anchorage of carbon fibre composite plates used to strengthen reinforced concrete beams. *Composite structures*, *42*(2), 175-188.

Garden, H., Hollaway, L., Thorne, A., & ROBUST. (1997). A preliminary evaluation of carbon fibre reinforced polymer plates for strengthening reinforced concrete members. *Proceedings of the institution of civil engineers-structures and buildings*, *122*(2), 127-142.

Garden, H., Quantrill, R., Hollaway, L., Thorne, A., & Parke, G. (1998). An experimental study of the anchorage length of carbon fibre composite plates used to strengthen reinforced concrete beams. *Construction and Building Materials*, *12*(4), 203-219.

Gemert, D. V. (1980). Force transfer in epoxy bonded steel/concrete joints. *International Journal of Adhesion and Adhesives*, *1*(2), 67-72.

Ghosh, K. K., & Karbhari, V. M. (2007). Evaluation of strengthening through laboratory testing of FRP rehabilitated bridge decks after in-service loading. *Composite structures*, *77*(2), 206-222.

Gotame, M., Franklin, C. L., Blomfors, M., Yang, J., & Lundgren, K. (2022). Finite element analyses of FRP-strengthened concrete beams with corroded reinforcement. *Engineering structures*, *257*, 114007.

Hag-Elsafi, O., Alampalli, S., & Kunin, J. (2004). In-service evaluation of a reinforced concrete T-beam bridge FRP strengthening system. *Composite structures*, *64*(2), 179-188.

Hao, Z.-H., Zeng, J.-J., Chen, G.-M., Dai, J.-G., & Chen, J.-F. (2024). Durability of FRP-to-concrete bonded joints subjected to 110 months accelerated laboratory and field exposure. *Engineering structures*, *305*, 117681.

Issa Fowai, Martin Noël, Martín-Pérez, B., & Sanchez, L. (2025). Assessment of CFRP-concrete Interface Integrity of Original Champlain Bridge Diaphragms through Nondestructive and semidestructive Testing. *Journal of composites for construction*.

Kachlakev, D., & McCurry, D. (2000). Behavior of full-scale reinforced concrete beams retrofitted for shear and flexural with FRP laminates. *Composites Part B: Engineering*, *31*(6-7), 445-452.

Khalifa, A., & Nanni, A. (2002). Rehabilitation of rectangular simply supported RC beams with shear deficiencies using CFRP composites. *Construction and Building Materials*, *16*(3), 135-146.

Ko, H., Matthys, S., Palmieri, A., & Sato, Y. (2014). Development of a simplified bond stress–slip model for bonded FRP–concrete interfaces. *Construction and Building Materials*, *68*, 142-157.

Li, P.-D., Zhao, Y., Wu, Y.-F., & Lin, J.-P. (2023). Effect of defects in adhesive layer on the interfacial bond behaviors of externally bonded CFRP-to-concrete joints. *Engineering structures*, *278*, 115495.

Li, W., & Leung, C. K. (2016). Shear span–depth ratio effect on behavior of RC beam shear strengthened with full-wrapping FRP strip. *Journal of composites for construction*, *20*(3), 04015067.

Liu, S., Yang, Z., Zhang, J., & Zhao, J. (2021). Study on bond-slip degradation model of CFRP and concrete interface under sulfate erosion environment. *Composite structures*, *267*, 113877.

Lu, X., Teng, J., Ye, L., & Jiang, J. (2005). Bond–slip models for FRP sheets/plates bonded to concrete. *Engineering structures*, *27*(6), 920-937.

Malek, A. M., Saadatmanesh, H., & Ehsani, M. R. (1998). Prediction of failure load of R/C beams strengthened with FRP plate due to stress concentration at the plate end. *Structural Journal*, *95*(2), 142-152.

Mazzotti, C., Savoia, M., & Ferracuti, B. (2009). A new single-shear set-up for stable debonding of FRP–concrete joints. *Construction and Building Materials*, *23*(4), 1529-1537.

Nakaba, K., Kanakubo, T., Furuta, T., & Yoshizawa, H. (2001). Bond behavior between fiber-reinforced polymer laminates and concrete. *Structural Journal*, *98*(3), 359-367.

Nelson, L. A., Al-Allaf, M., & Weekes, L. (2020). Analytical modelling of bond-slip failure between epoxy bonded FRP and concrete substrate. *Composite structures*, *251*, 112596.

Nelson, L. A., Weekes, L., Milani, G., & Al-Allaf, M. (2024). Generalised analytical solutions for linear and non-linear bond–slip models for externally bonded FRP to a concrete substrate. *Engineering structures*, *298*, 117025.

Neubauer, U., & Rostasy, F. (1999). Bond failure of concrete fiber reinforced polymer plates at inclined cracks—Experiments and fracture mechanics model. *Special Publication*, *188*, 369-382.

Obaidat, Y. T., Heyden, S., Dahlblom, O., Abu-Farsakh, G., & Abdel-Jawad, Y. (2011). Retrofitting of reinforced concrete beams using composite laminates. *Construction and Building Materials*, *25*(2), 591-597.

Täljsten, B. (1994). *Plate bonding: Strengthening of existing concrete structures with epoxy bonded plates of steel or fibre reinforced plastics* Luleå tekniska universitet].

Täljsten, B. (1997a). Defining anchor lengths of steel and CFRP plates bonded to concrete. *International Journal of Adhesion and Adhesives*, *17*(4), 319-327.

Täljsten, B. (1997b). Strengthening of beams by plate bonding. *Journal of materials in Civil Engineering*, *9*(4), 206-212.

Tatar, J., & Hamilton, H. (2016). Bond durability factor for externally bonded CFRP systems in concrete structures. *Journal of composites for construction*, *20*(1), 04015027.

Taylor, B. a. (2013). *Champlain Bridge Approach Spans, Edge Girder Condition Assessment and Rehabilitation Requirement*.

Teng, J., & Chen, J. (2007). Debonding failures of RC beams strengthened with externally bonded FRP reinforcement: behaviour and modelling. Proceedings of the first Asia-Pacific conference on FRP in structures (APFIS 2007),

Triantafillou, T., Matthys, S., Audenaert, K., Balázs, G., Blaschko, M., Blontrock, H., Czaderski, C., David, E., Di Tomasso, A., & Duckett, W. (2001). Externally bonded FRP reinforcement for RC structures. In (Vol. 14): International Federation for Structural Concrete (fib).

Yuan, H., Teng, J., Seracino, R., Wu, Z., & Yao, J. (2004). Full-range behavior of FRP-to-concrete bonded joints. *Engineering structures*, *26*(5), 553-565.

Yuan, H., Wu, Z., & Yoshizawa, H. (2001). Theoretical solutions on interfacial stress transfer of externally bonded steel/composite laminates. *Doboku Gakkai Ronbunshu*, *2001*(675), 27-39.

Zhao, L., Tang, F., Li, G., Lin, Z., & Li, H.-N. (2024). Crack monitoring of tension members with distributed fiber optic sensor considering substrate strain redistribution and coating/fiber interfacial slip. *Engineering structures*, *300*, 117267.

Zhou, A., Qin, R., Feo, L., Penna, R., & Lau, D. (2017). Investigation on interfacial defect criticality of FRP-bonded concrete beams. *Composites Part B: Engineering*, *113*, 80-90.

Chapter 7 – Finite element modelling approaches of debonding in CFRP-Retrofitted Concrete[4]

7.1 Abstract

The integrity of the interface between carbon fibre-reinforced polymers (CFRP) and concrete is the most critical factor affecting the long-term performance of concrete members strengthened with CFRP. Although numerous finite element models have been developed to correlate experimental findings for concrete elements externally bonded with CFRP, most of these studies have focused on modelling the CFRP-concrete interface under pristine conditions and often assume a perfect bond between CFRP and concrete, which can lead to overestimations, even for structural components strengthened with new materials in controlled environments. This study uses an experimentally calibrated cohesive zone material law to develop three-dimensional finite element models to predict the debonding mechanisms between deteriorated concrete and CFRP under mode II and mixed mode loading conditions. The validity of the proposed modelling approaches is first evaluated by modelling four beams documented in the literature and is subsequently applied to the case of CFRP-concrete joints extracted from 57-year-old bridge elements exposed to severe subzero environmental conditions in Montreal, Canada. The proposed model is used to explore how concrete material properties and loading orientations influence the debonding behaviour and failure mechanism initiated by intermediate crack-induced debonding while critically highlighting the challenges of modelling the bond between aged concrete and CFRP. The comparison between the developed FEM models and the experimental results demonstrates that the proposed CZM models effectively capture the debonding process for both concrete members strengthened with pristine materials and concrete specimens tested from a deteriorated concrete bridge, with a maximum error of 12% in the

[4] A version of this chapter has been submitted for publication as: Issa Fowai, Martin Noël, Beatriz Martín-Pérez, Leandro Sanchez. *FEM simulation approaches of debonding in CFRP-Retrofitted Concrete: A Case Study of the 57-year-old Champlain Bridge from Montreal.*

peak strain at failure. A reduction of the maximum strain of up to 12% was observed when the peel angle increased during shear loading of the CFRP-concrete interface compared to pure mode II loading.

7.2 Introduction

Carbon fibre-reinforced polymer (CFRP) has gained significant attention in civil engineering, particularly for structural strengthening. The bond between the CFRP and concrete is critical for effectively transferring loads and enhancing structural performance. Over the past decade, extensive research has focused on the bond behaviour in FRP-strengthened concrete elements through both experimental (Bizindavyi & Neale, 1999; Ferracuti et al., 2007; Li et al., 2023; Lu et al., 2005) and numerical studies (Arruda et al., 2016; Buyle-Bodin et al., 2002; Godat et al., 2007; Gotame et al., 2022; Mostofinejad & Hosseini, 2017; Obaidat et al., 2010; Pham et al., 2006; Tedesco et al., 1999; Xu et al., 2015; Yu et al., 2017). Although laboratory experiments and numerical simulations have demonstrated the effectiveness of FRP for repairs, there is a scarcity of field performance data regarding FRP performance over time (Buyle-Bodin et al., 2002; Fowai et al., 2025e; Milev & Tatar, 2023; Tatar & Brenkus, 2021; Tedesco et al., 1999).

The field performance of FRP retrofits is essential in understanding the long-term benefits of composites for strengthening critical infrastructures, and the fact that field structures are often cracked or damaged before retrofitting highlights the importance of predicting the debonding mechanism of CFRP-strengthened members of real-structures exposed to both service load and fluctuating environmental conditions. In CFRP strengthening applications, debonding the CFRP from the concrete can compromise the safety and functionality of the repaired structure (Coronado & Lopez, 2007, 2010).

Debonding failure mechanisms are generally categorized into plate-end debonding and intermediate crack-induced debonding. Plate-end debonding is caused by high shear and normal stresses at the abrupt termination of the FRP, while intermediate crack-induced debonding initiates from the stress concentrations that occur at the tip of flexure or flexure-shear cracks (Mostofinejad & Hosseini, 2017).

Extensive experimental research has been conducted to investigate the debonding failure mechanisms in structural elements strengthened with CFRP (Au & Büyüköztürk, 2006; Fowai et al., 2025e; Mazzotti et al., 2009; Teng & Chen, 2007). These experimental studies have led to various laboratory test setups to examine the interface debonding of CFRP from concrete (Mukhtar & Faysal, 2018). However, finite element analysis has been relatively limited, particularly concerning the interfacial behaviour between the concrete and FRPs; existing finite element models primarily focus on predicting the load-deflection behaviour of strengthened members (Godat et al., 2007). Numerous FEM studies assume perfect bond conditions, which is unrealistic in the case of deteriorated concrete members retrofitted with CFRP, particularly those with preexisting cracks or bond-separation issues between concrete and the patch mortar typically used for repairs prior to CFRP application. The patch mortar is a mortar or plaster that is used to fill and level surface irregularities in the deteriorated concrete surface before the installation of the CFRP strip.

On the other hand, the numerical modelling of debonding at the CFRP-concrete interface from deteriorated concrete structures retrofitted with CFRP is a complex undertaking that requires proper calibration based on interface behaviour. A realistic and cost-effective computational approach to capture interface nonlinearities and the stress state at the CFRP-concrete interface is the modelling of zero-thickness interface elements, specialized link elements (springs) or contact elements between the FRP and concrete to account for the relative displacement between the CFRP and concrete under load. Coincident nodes are established at the CFRP-concrete interface, and a cohesive zone material law is defined for the interface elements. This methodology, referred to as the cohesive zone model, has demonstrated reliable predictive capabilities for FEM (Al-Saawani et al., 2022; Alhassan et al., 2020; Viñuela et al., 2022; Zhang et al., 2021; Zhelyazov, 2024). The CZM approach uses a set of constitutive laws that describe the traction (normal and tangential stresses) and separation (normal gap and tangential sliding) behaviour of the interface. It allows for modelling the initiation and propagation of debonding based on either the traction-separation or fracture energy of the CFRP-concrete interface. The CZM approach allows for the modelling of mode-I debonding

in the normal direction, mode II debonding for tangential separation, and mixed-mode debonding for combined normal and tangential slip based on the input CZM parameters. Accurate predictions of the strength, stiffness, and ductility behaviour of concrete members externally bonded with FRP rely on the application of interface bond models within suitable numerical tools (Ueda & Dai, 2005).

This study aims to outline modelling guidelines or practices for in-service structures by examining the stress and strain distribution along the strengthening layer. It also addresses the challenges associated with modelling deteriorated concrete components that have been strengthened with CFRP. Detailed 3D finite element models were developed using ANSYS APDL to investigate the nonlinear bond behaviour between deteriorated concrete bridge elements, aged 57 years, that were strengthened with CFRP while in service. The results generated from FEM were compared with experimental data obtained by the authors through flexural (Fowai et al., 2025e) and two different shear-lap test configurations (Fowai et al., 2025b). Various modelling approaches for the CFRP-concrete interface were examined, and the CZM model developed was first validated against results previously reported in the literature (Obaidat et al., 2010). The remainder of the paper focuses on a parametric and sensitivity analysis of the input parameters of the CZM, the properties of the concrete (accounting for material deterioration), and the mode of loading (pure shear or mixed-mode).

7.3 Overview of the Champlain Bridge and Environmental Exposure

Detailed accounts of the bridge and its deconstruction rationale are available in section 1.3, companion publications, along with findings from the thorough condition assessment of the extracted bridge diaphragms before the structural tests on the bond behaviour of the composite materials used in the repair (Fowai, 2023, 2024).

7.4 Overview of experimental studies

7.4.1 Experimental work by Obaidat (Obaidat, 2011; Obaidat et al., 2010)

The selected beams from the literature used for validation in this study were based on the experimental and numerical work conducted by (Obaidat, 2011) to investigate debonding issues associated with structural retrofitting using FRP. The original beams had rectangular cross-sections measuring 150 mm in width and 300 mm in height, with a length of 1,960 mm.

Each of the four beams was reinforced in tension with two 12-mm diameter bars and in compression with two 10-mm diameter bars. The steel reinforcement was held in place using 8-mm stirrups placed at 100 mm center-to-center spacing along the beam, as illustrated in Figure 7.1a. Three beams were strengthened with unidirectional CFRP plates, 1.2 mm thick and 50 mm wide, bonded to the soffit of the beams, shown as RB1, RB2, and RB3 in Figure 7.1.

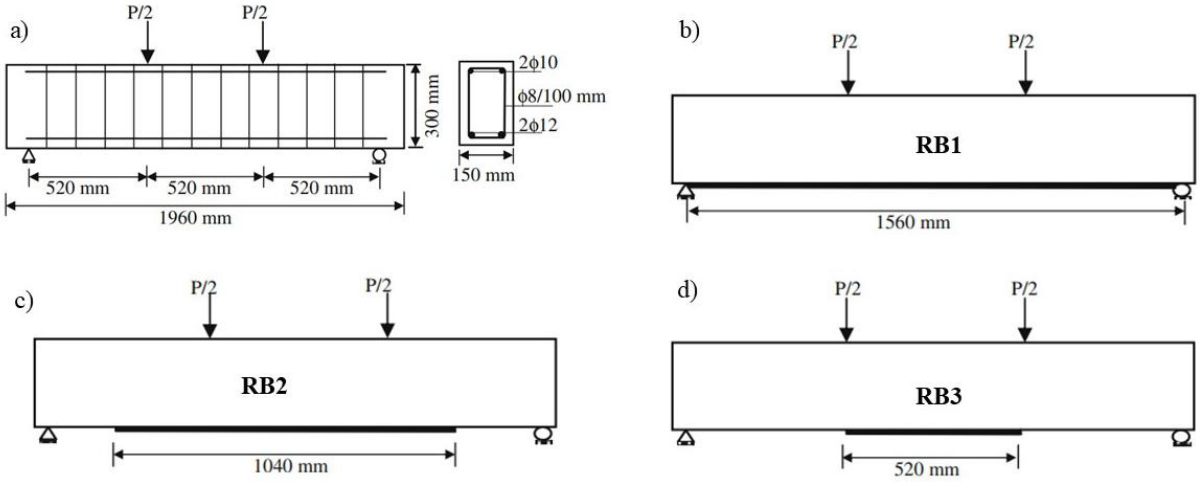

Figure 7.1-Experimental beams from Obaidat et al. (2010) a) Control beam b) RB1 b) RB2 c) RB3

7.4.2 Flexural Beams from the Champlain Bridge Specimens

One of the three diaphragms from the Champlain Bridge was vertically cut into four beams, each measuring 2,000 mm in length, 430 mm in width, and 210 mm in depth. These beams had no internal reinforcement and relied on the double-layer CFRP sheets to resist tensile forces following concrete cracking. These beams were subjected to three-point loading at a 0.2 mm/min displacement rate (Figure 7.2).

Vertical steel clamps were used to provide additional shear capacity, and the bonded width of the FRP sheet was reduced from 305 mm to 200 mm within the critical anchorage zone to control debonding. The clamps had no contact with the FRP sheet to not influence the bond performance. Comprehensive data on the experimental setup and findings are reported elsewhere (Fowai et al., 2025e). The experimental program for each beam was completed in two stages, completing eight tests across four beams. Each beam was tested with a different anchorage length. A 50-mm deep notch was created on both sides of the beams beneath the loading point to induce a flexural crack and facilitate intermediate debonding. The tested anchorage length was controlled in one of the shear spans by cutting through the FRP layer at a specified distance from the notch while a 500-mm overhang extended over the other support. A beam naming convention in the form of XY-Z was adopted, where X corresponds to the beam number, Y corresponds to the testing stage, and Z corresponds to the anchorage length. This study models beam B3S1-L500 as described in Table 7.1.

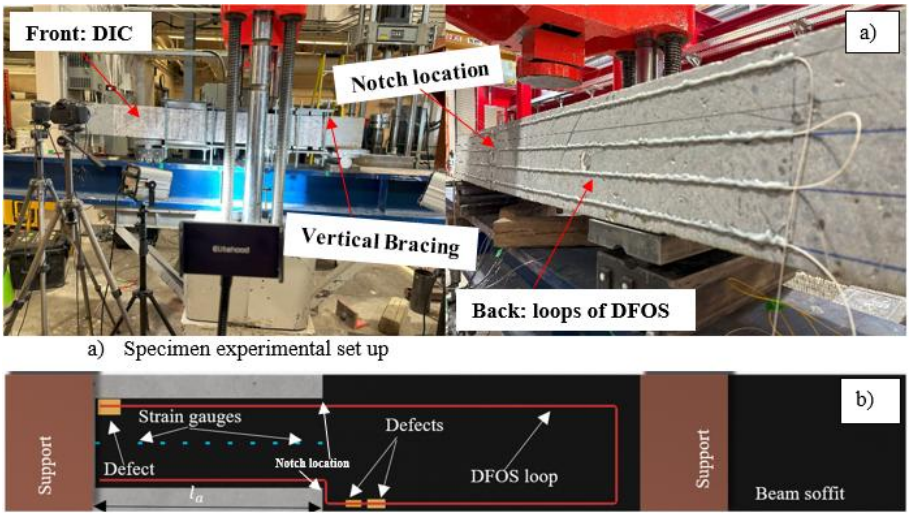

Figure 7.2-Beam setup with specimen instrumented with distributed fibre optic sensors (DFOS)

Table 7.1-Beam specimen from the author's previous work (Fowai et al., 2025e)

Beam ID	Shear span (mm)	CFRP width in anchorage region (mm)	Number of SG in anchorage (spacing)	DFOS paths (loops) on CFRP	Bracing condition
B3S1-L500	600	200	10 (50 mm)	2	Braced

During the experimental testing, the strains in the CFRP sheets were monitored with 2 loops of nylon-coated distributed fibre optic sensors (DFOS) along the entire length as well as discrete electrical resistance strain gauges (see Figure 7.2).

To prevent damage to the DFOS cables close to the supports, a minimum unbonded distance of 35 mm was maintained between the support and the starting point of the DFOS cable. A spacing of 50 mm was maintained for the strain gauges. Concrete strains along the side of the beams were measured using a two-dimensional DIC system and four loops of DFOS (Figure 7.2). Installation of the DFOS and strain gauges required proper and careful cleaning of the bonding surface with solvent and degreaser to clean the bonded area of dust or oil.

Strain gauges were installed using cyanoacrylate while Loctite two-part adhesive (EA E-20HP) was used to bond the fibre optic sensors to the concrete or CFRP, as done by Brault and Hoult (Brault & Hoult, 2019). Since the DFOS on the concrete was installed on the saw-cut portions of the beams, no additional grinding was required before sensor installation since the surface was smooth. A Luna ODiSI 6104 DFOS analyser was used to measure distributed strains. The system has a sensor spacing of 2.6 mm, a maximum sensing length of 50 m per channel, and an accuracy of ±1 microstrain at the sensor core.

7.4.3 Conventional single shear-lap and double shear-lap tests from Champlain Bridge specimens

In the experimental work undertaken by the authors (Fowai et al., 2025b) on the bond performance of the bridge specimens under mode II loading, nine concrete specimens measuring 150 mm x 250 mm x 220 mm, each with a free-end length of 150 mm that could be directly gripped by the universal testing machine, were tested in direct shear. The bonded width of the CFRP for all nine specimens was 50 mm. Eight concrete prisms were cut from the diaphragms for the double shear-lap samples, measuring 150 mm x 500 mm x

220 mm. The width of the CFRP on both the front and back of the blocks was reduced to 50 mm. A horizontal notch was provided on both sides of the bonded width to initiate a crack at the mid-height of the specimens under tensile loading. Figure 7.3 depicts the conventional single shear-lap and double shear-lap tests in progress. In the experimental testing of the conventional single shear-lap specimens, a three-dimensional digital image correlation (DIC) system was used to capture full-field strain and displacement measurements from the front of the samples. For the double shear-lap specimens, three strain gauges were installed on the back of the samples in addition to the 3D DIC system positioned at the front.

Figure 7.3- Shear-lap specimens a) Conventional single shear-lap b) Double shear-lap

7.5 Development of Finite Element Model

Three-dimensional nonlinear FE models were created for the beams and shear-lap specimens described in Section 3 using ANSYS APDL. The same element types were selected for both the Champlain Bridge beams and the research conducted by Obaidat (Obaidat, 2011; Obaidat et al., 2010) used for validation.

7.5.1 FE analysis from beam tested by Obaidat (Obaidat, 2011; Obaidat et al., 2010)

The concrete was modelled using SOLID185, which is a 3D 8-node element capable of predicting crack formation in tension and crushing in compression. The stress-strain relationship for concrete under compression and tension was defined using the Menetrey-William model in ANSYS APDL (Figure 7.4). The material parameters used to define the yielding function included compressive strength, tensile strength, and biaxial compressive strength. In Figure 7.4, the variable k_{cm} denotes the plastic strain at uniaxial

compressive strength. The symbol k_{cr} represents the ultimate effective plastic strain in compression. The variable Ω_{ci} indicates the stress at the start of nonlinear hardening during plastic deformation, while Ω_{cr} is the residual compressive relative stress. The term k_{tr} is the plastic strain limit in tension, and Ω_{tr} represents the residual tensile relative stress. f_c' and f_{cr} represent the concrete's uniaxial compressive strength and tensile strength, respectively. The measured reported compressive strength of the concrete was 30 MPa, with a tensile strength of 1.81 MPa and an elastic modulus of 25,740 MPa. The steel reinforcement was assumed to exhibit an elastic, perfectly plastic behaviour, as illustrated in Figure 7.5, with identical properties for both tension and compression, and it was modelled using the 3D truss element LINK180. The elastic modulus and yield strength were input as 209 GPa and 507 MPa, respectively, as reported by the authors. Poisson's ratios of 0.2 for concrete and 0.3 for steel reinforcement were used in the FEM analysis.

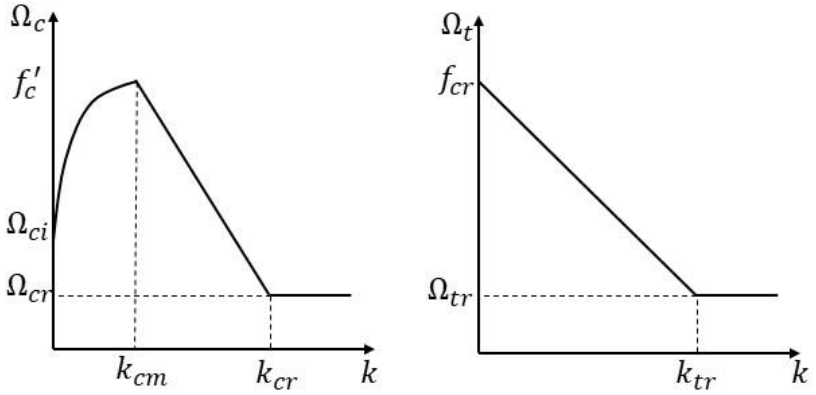

Figure 7.4-Concrete under compression and tension

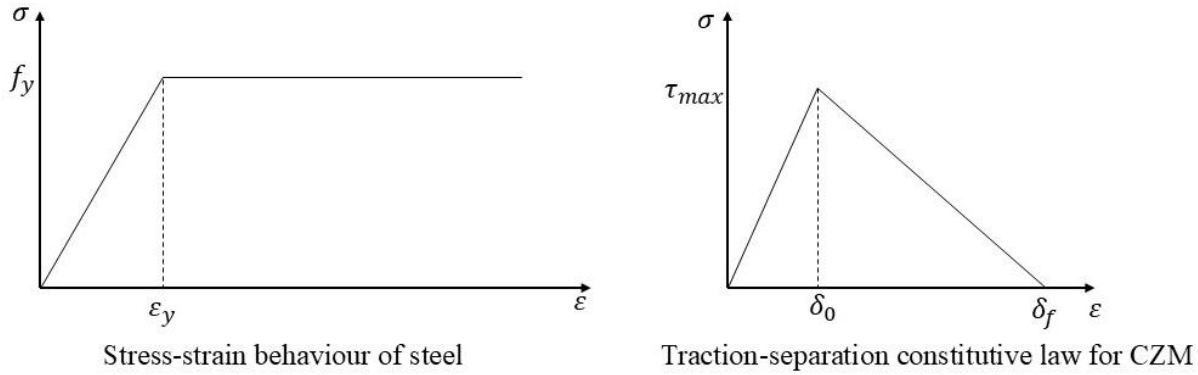

Figure 7.5-Constitutive law for steel and cohesive zone interface

The CFRP was modelled using the 4-node shell element SHELL181, assuming a linear elastic isotropic behaviour. The elastic modulus of the unidirectional CFRP material is 165 GPa, with a Poisson's ratio of 0.3. The CFRP-concrete interface was modelled using contact elements (CONTA174 and TARGE170) defined in the cohesive zone model. The CONTA174 is an 8-node, higher-order element that can be located on 3D solid surfaces or shell elements with or without mid-side nodes. Figure 7.5b shows the bilinear traction-separation constitutive law. A maximum shear stress and normal stress of 1.5 MPa and 1.81 MPa were used, as reported by the authors. The support and loading plates were modelled using SOLID185 elements with linear elastic material behaviour. The selected element types are shown below (Figure 7.6).

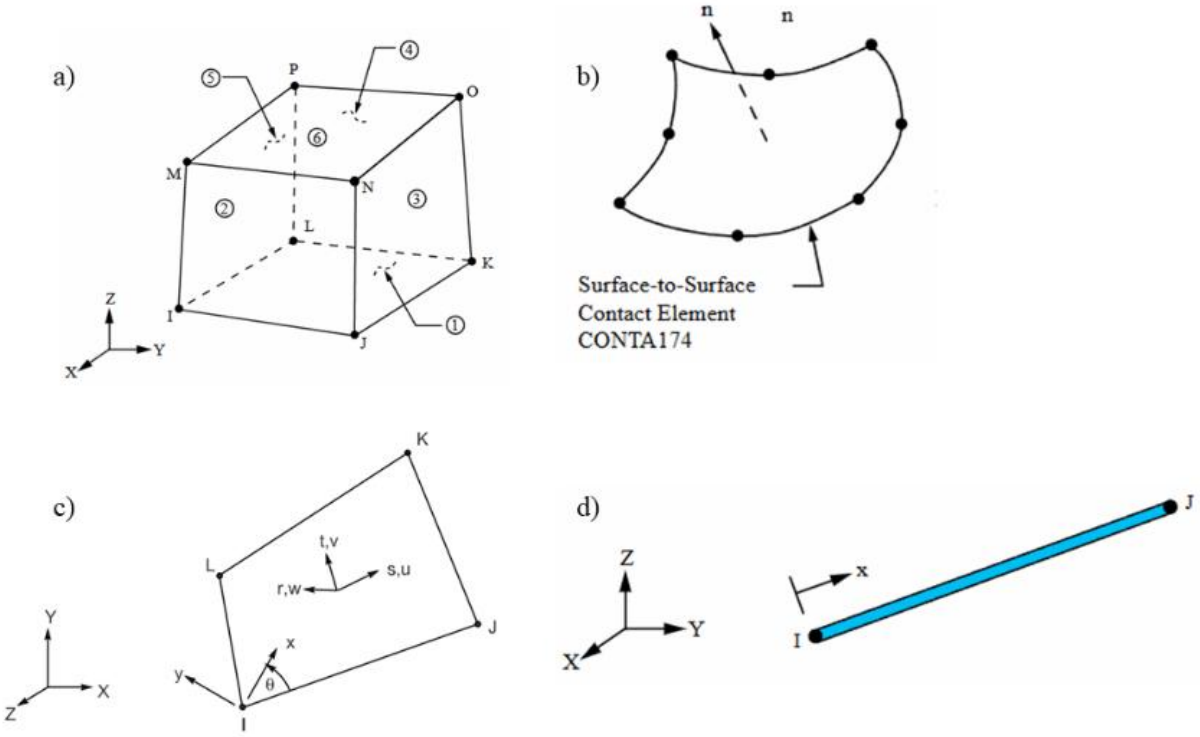

Figure 7.6-Element selection a) SOLID185 b) CONTA174 c) SHELL181 d) LINK180 (ANSYS, 2025)

To reduce computational costs, a quarter-beam model was used to validate the work reported by Obaidat (Obaidat, 2011; Obaidat et al., 2010). The symmetry boundary conditions were implemented by constraining the nodes along the two symmetry planes in perpendicular directions (Figure 7.7).

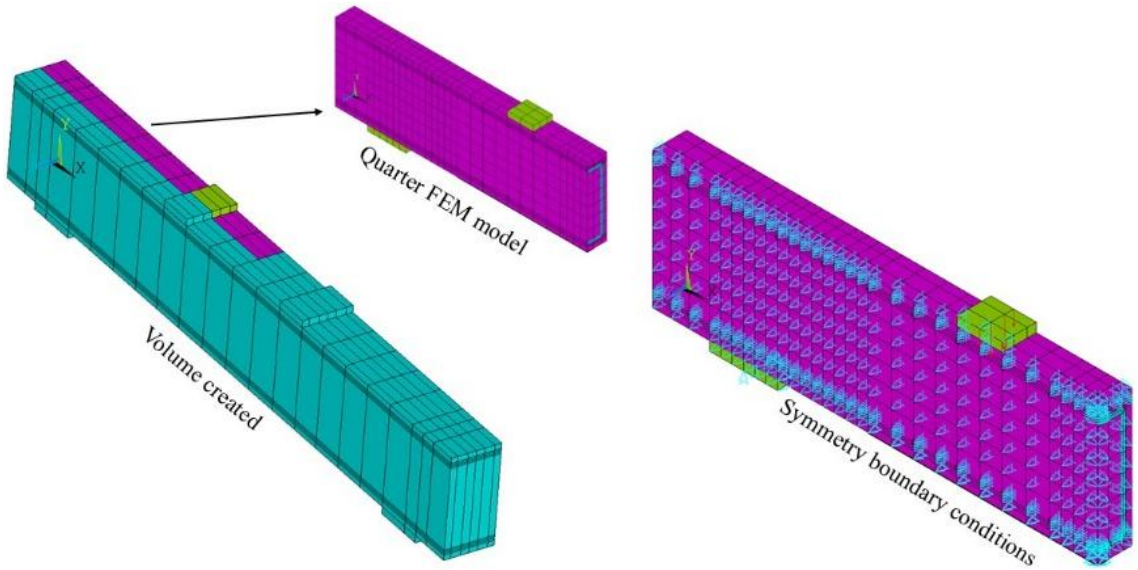

Figure 7.7-Model creation and boundary conditions

7.5.2 Finite element analysis from Champlain Bridge specimens

In developing the finite element model for the deteriorated concrete specimens, it was crucial to recognize that the direct application of mechanical properties of both the CFRP and concrete obtained experimentally is inadequate for establishing a reliable correlation between the FEM models and experimental results for a 57-year-old structure. The modeling process for these deteriorated specimens required the consideration of numerous interacting complexities and numerical assumptions inherent in the FEM model. Specific factors, such as the observed variability in bond-slip response across the specimens, the effect of repair materials installed prior to CFRP application, and the observed progression of damage (mode II or mixed mode) during testing, were all carefully evaluated through a detailed parametric and sensitivity analysis. During this parametric analysis, a minimum of seven models were developed for each input parameter of the CZM, which accounts for the debonding failure. As illustrated in Figure 7.8, a 3D nonlinear FE model was developed for the beam depicted in Figure 7.2 from the deconstructed Champlain Bridge. The mesh sensitivity analysis indicated that an element size of 25 mm is suitable for accurately modelling the beam response.

The durability of the CFRP-concrete interface under environmental exposure is influenced by the nature/combination and severity of conditions; however, this natural exposure data is absent from the current study. Environmental factors critically affect the CFRP-concrete bond, impacting both short term and long- term durability (Myers & Ekenel, 2005; Dushimimana et al., 2024). Excess humidity and water ingress can weaken the CFRP-concrete interface leading to decreased bond strength (Imani et al. 2022). In cold climates such as Canada, repeated freeze-thaw cycles induce stresses within the concrete and CFRP-concrete interface that leads to microcracking and reduced bond strength. It is also reported that elevated and low temperatures adversely affect the adhesive performance (Myers & Ekenel, 2005; Salameh et al. 2024). Although the damage in the 57-year-old concrete was not explicitly incorporated into the model, nor was environmental exposure considered in the developed models, the degradation of the bond line was represented by the smearing of the experimental bond stress-slip relationship. This approach implicitly captures the effect of localized defects on bond performance.

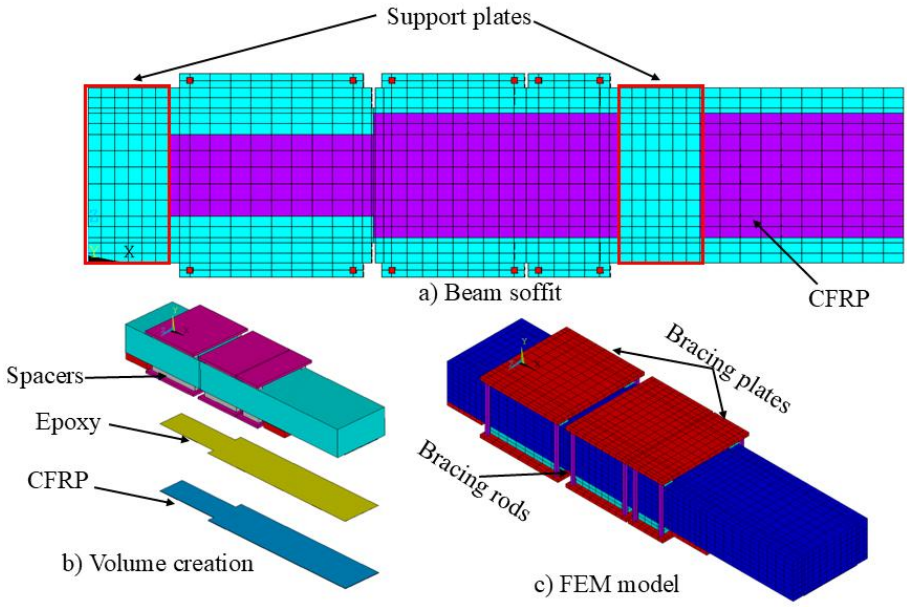

Figure 7.8-3D FEM for Champlain Bridge beams

The concrete was represented using the SOLID185 element. The behaviour of the concrete was modelled in accordance with the stress-strain curve shown in Figure 7.4. The compressive strength of the concrete substrate, derived from the average of three core samples (77.7 MPa, 75.0 MPa and 74.9 MPa) with an

average diameter of 95 mm and height of 200 mm, was 75.9 MPa (standard deviation of 1.30 MPa), and the estimated cracking strength of the concrete obtained is 3.48 MPa (CSA-Group, 2019). The elastic modulus of the concrete with a compressive strength of 76 MPa is 38,020 MPa. The steel components (support, spacers, bracing rods and clamping plates) were modelled as elastic, perfectly plastic materials, as shown in Figure 7.5.

The input parameters for the steel materials, including the elastic modulus and yield strength, are detailed in Table 7.2. All steel elements were modelled using the SOLID185 element, with the exception of the bracing rods, which were modelled using the LINK180 element.

Table 7.2- Material input for steel components used in modelling beam specimens

	Supports	Spacers	Bracing rods	Clamping plates
Elastic modulus (GPa)	200	200	200	200
Yield strength (MPa)	355	355	420	355

The double-layer CFRP sheet was modelled as linear elastic until failure. The average tensile strength of the CFRP determined from coupon tests is 582 MPa, with an elastic modulus of 52 GPa.

The CZM model used to characterize the CFRP-concrete interface's constitutive behaviour requires either five or six input parameters, depending on the debonding mode (Mode I, Mode II, or mixed mode). The adhesive was represented using a zero-thickness contact pair defined by CONTA174 and TARGE170 elements. Table 7.3 presents the material constants used to define the bilinear behaviour of the CFRP-concrete interface with traction and separation distances. For the mixed mode debonding experienced by the beams, the CZM input parameters included both normal and tangential slip, which were defined by C1, C2, C3, C4, C5, and C6.

In Table 7.3, shear stress and slip are calibrated from experimental results, whereas the normal stress was estimated based on the tensile strength of the concrete, an approach typical in existing literature, since the tensile capacity of concrete is lower than the capacity of the adhesive in tension.

Table 7.3-Material constant for bilinear material behaviour of CZM

Constant	Meaning	Property	CZM values used
C1	σ_{max}	Maximum normal contact stress	0.35-3.35 MPa
C2	δ_n^c	Contact gap at the completion of debonding	0.06-0.44 mm
C3	τ_{max}	Maximum equivalent tangential contact stress	1.50-4.50 MPa
C4	δ_t^c	Tangential slip at the completion of debonding	0.13-0.88 mm
C5	α	Ratio of slip at maximum stress to slip at failure	0.10-0.70 mm
C6	β	Non-dimensional weighting parameter	0 and 1

A refined 3D FEM model was used to simulate the debonding between the CFRP and concrete under shear loading (Figure 7.9). The same material properties and element types previously described for the concrete, CFRP and the adhesive interface for the beam specimens were also applied to the shear-lap specimens model in this study. Under the mode II dominated bilinear CZM model, as illustrated in Figure 7.5, it is assumed that the separation of the CFRP from the concrete is dominated by the displacement jump that occurs tangentially to the interface (tangential slip). For the pure mode II debonding, the CZM input parameters are activated by the data items C1, C2, C3, C4, and C5 (with C1 $=-\sigma_{max}$).

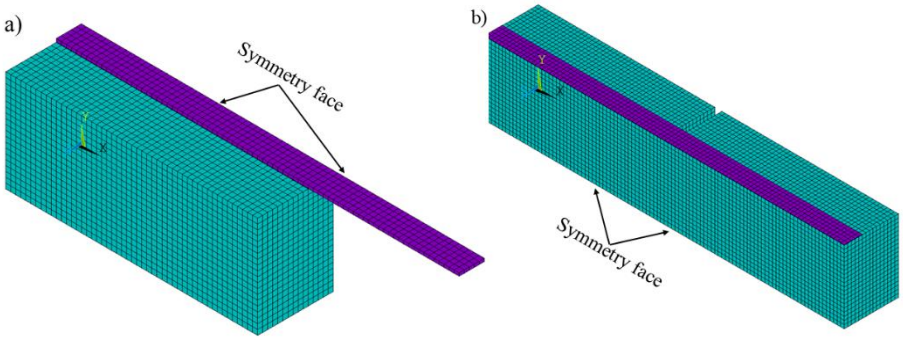

Figure 7.9- FEM half-model mesh a) Conventional single shear-lap b) Double shear-lap

7.6 Finite Element Results

7.6.1 Validation on beam tested by Obaidat (Obaidat, 2011; Obaidat et al., 2010)

7.6.1.1 Failure modes

The failure modes of all the beams are in agreement with the experimental observations reported by the author. The control beam failed in flexure after yielding of the tensile reinforcement (Figure 7.10), while all the CFRP-strengthened beams experienced debonding failure irrespective of the bonded length. Although Obaidat's original work did not include strain data, this study presents the axial strain and stress distributions along the length of the beam derived from the ANSYS APDL models.

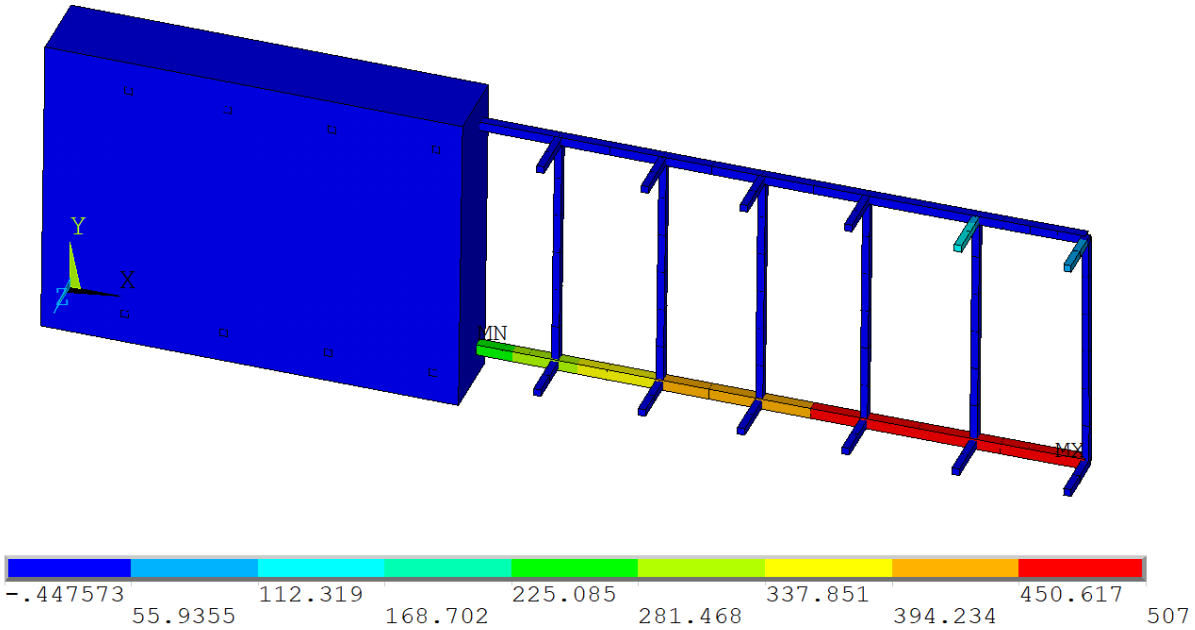

Figure 7.10-Yielded tensile reinforcement of control beams (with tensile stress in MPa)

7.6.1.2 Load-displacement behaviour

Figure 7.11 and Figure 7.12 illustrate the comparison of experimental and numerical results regarding the load-displacement relationship for different beam configurations. In Figure 7.11 and Figure 7.12, the FE models developed in this research are called the "current ANSYS model". The FE models reported in the existing literature used as benchmark for the validation are referred to as the "Obaidat's ABAQUS model", while the experimental work by Obaidat are called Experimental Control, Experimental RB1, RB2 and

Experimental RB3 respectively. The FEM models developed in this study using ANSYS APDL closely matches the numerical modelling undertaken by Obaidat (Obaidat, 2011; Obaidat et al., 2010) using ABAQUS. The prediction from ANSYS APDL also aligns well with Obaidat's experimental results. The reported ultimate experimental load values for the control beam, RB1, RB2, and RB3 are respectively 99.5%, 97.1%, 92.4%, and 96.9% of the ANSYS APDL numerical prediction of the load-carrying capacity of the beams, as shown in Figure 7.11 and Figure 7.12.

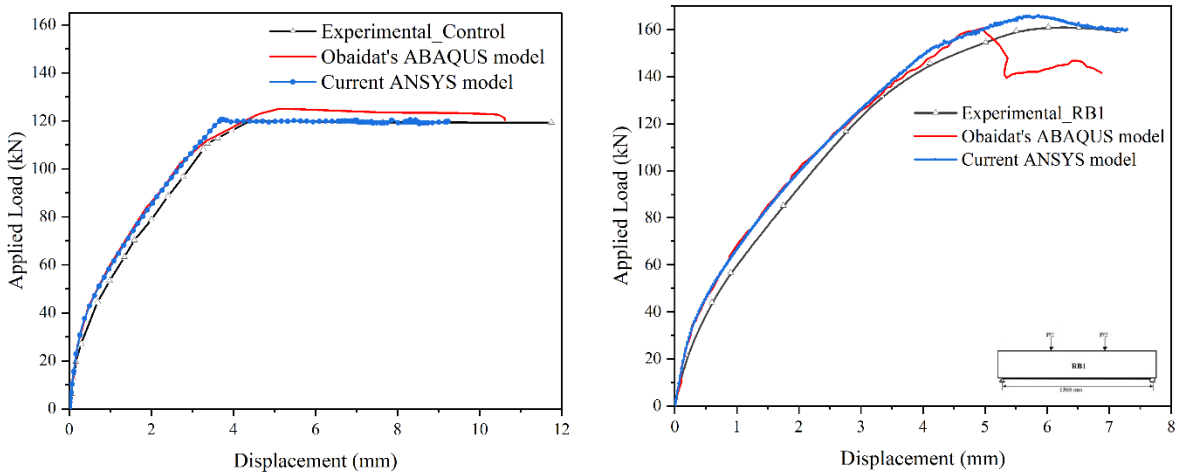

Figure 7.11-Load-displacement curves a) Control Beam b) RB1

It is important to note that although there is an almost 8% difference between the ANSYS prediction for RB2 and the experimental value, a similar discrepancy is also observed in the ABAQUS prediction conducted by Obaidat. The difference in the ultimate load obtained from the ANSYS models was between 0.1% for RB1 and 3.6% for the control beam of the original numerical validation performed by Obaidat. The relative differences between the ANSYS APDL predictions and the experimental results, as well as the FEM results reported in the literature, are minimal. This confirms the level of accuracy that can be achieved using the CZM approach in modelling CFRP debonding, regardless of the modelling tool used.

For all the beams, regardless of the bonded length, the load-displacement response in the initial loading up to 20 kN was identical. The load-displacement behaviour remained closely matched up to around the peak loads, where the stiffness of the FEM models was slightly higher than that of the experimental beams.

Several factors may have contributed to this slight discrepancy in the FEM results near the peak load. In the original experimental work, the beams were retrofitted after preloading to the point of first cracking, a condition that was not accounted for in either Obaidat's FEM models or in the current study. In addition, no existing shrinkage cracks in the experimental beams were considered. Both Obaidat's simulations and this current FEM analysis assumed a perfect bond between the concrete and steel, ignoring any slippage between the two materials under deformation. Moreover, the input parameters for the CZM constitutive laws reported by Obaidat et al. were not calibrated based on experimental results but were instead predicted using available analytical models for bond-slip behaviour.

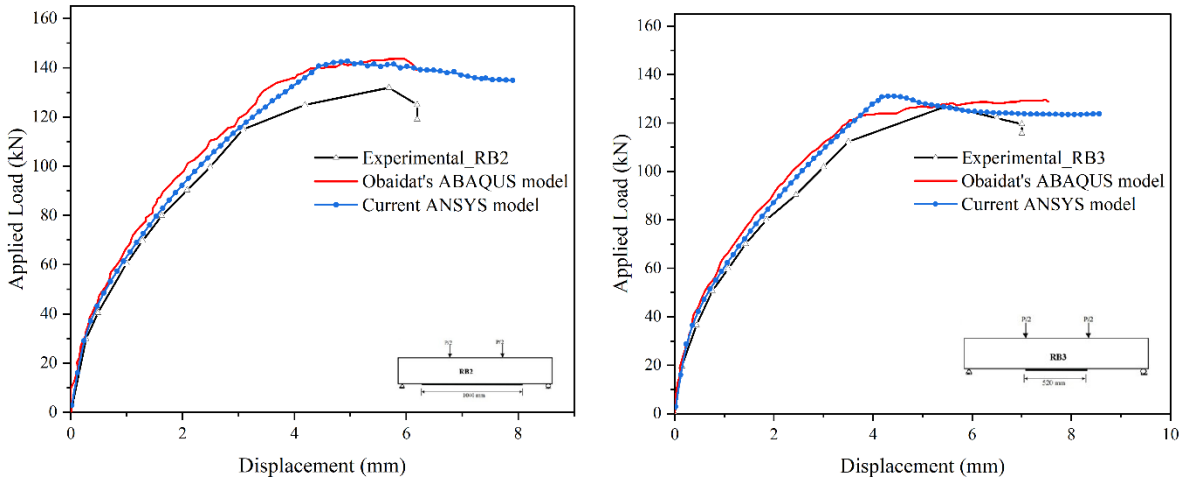

Figure 7.12-Load-displacement curves a) RB2 b) RB3

The results from the simulation also confirm that an increase in the bonded area of the CFRP is associated with an increase in the load-carrying capacity of the retrofitted beams.

7.6.1.3 Stress and Strain Distribution

Obaidat's work did not include strain data, making a direct comparison with the strain measurements obtained in this study impossible. This research presents the axial strain and stress distributions along the length of the beam, derived from ANSYS APDL models. Figure 7.13 and 16 illustrate the axial strain and stress distribution along the length of specimens RB1 and RB2 (quarter models), respectively.

The maximum strain observed at the peak load for RB1 is 3,990 microstrain (see Figure 7.13). At this point, the peak axial stress in the FRP is measured at 659 MPa, which represents only one-third of the ultimate tensile strength of the FRP as reported by the manufacturer in the original work by Obaidat (Obaidat, 2011; Obaidat et al., 2010). Debonding, initiates between 160 kN and 163 kN, indicating a slight plateau at the middle of the CFRP (705 mm from the left support) in RB1.

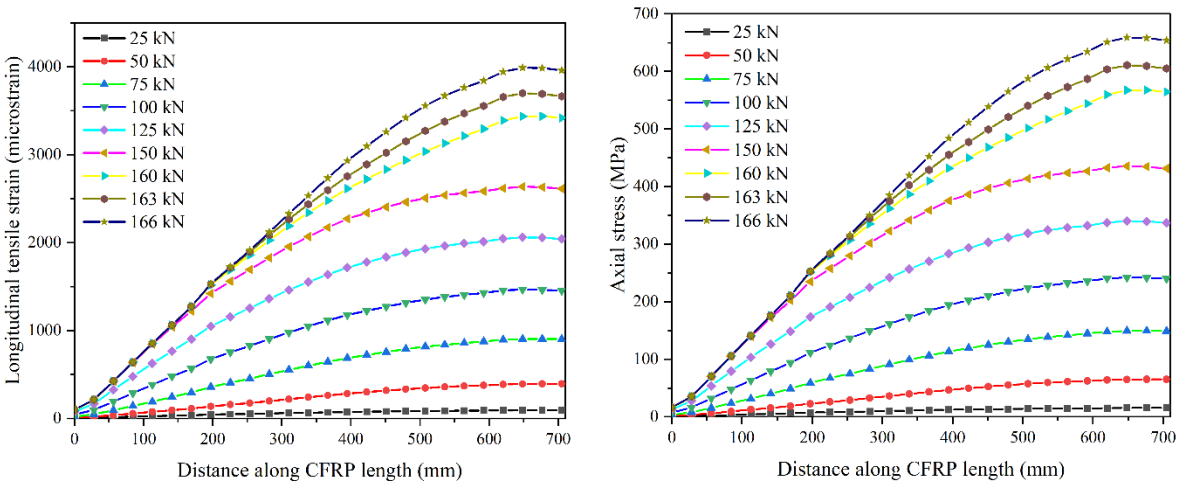

Figure 7.13-Axial strain and stress distribution along the CFRP for RB1

Figure 7.13 also suggests that the contribution of the FRP to the load-carrying capacity of the beam becomes significant in the later stages of the tests, particularly after the steel reinforcement has yielded. Up to 150 kN, the rate of increase in strain and stress at the middle of the CFRP remains constant. For instance, the stress rises by 91 MPa from 75 kN to 100 kN, by 97 MPa from 100 kN to 125 kN, and by 94 MPa from 125 kN to 150 kN.

However, a notable increase in stress of 133 MPa occurs when the load advanced from 150 kN to 160 kN. This pattern is similarly reflected in the corresponding strain behaviour. Figure 7.14 illustrates the strain and stress distribution for RB2, which has a bonded length of 520 mm in the quarter model configuration. At the peak load, RB2 showed a lower peak strain of 2,240 microstrain, approximately 56% of the peak strain observed in RB1. The corresponding peak stress for RB2 is 370 MPa.

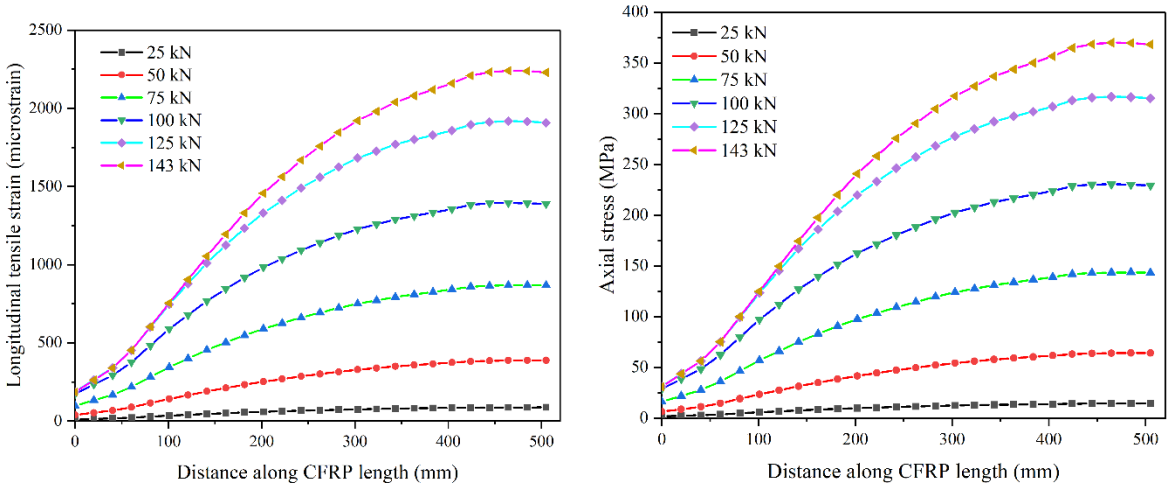

Figure 7.14-Axial strain and stress distribution along the CFRP for RB2

7.6.2 Validation on Beam tested from the Champlain Bridge

7.6.2.1 Failure modes

Similar to the experimental observation, the failure mode observed in the modelled specimen from the Champlain Bridge flexural tests (B3S1-L500) was caused by debonding of the CFRP sheet from the concrete (see Figure 7.15). The debonding started at the notch location and propagated towards the ends of the CFRP, as evident in the strain plots.

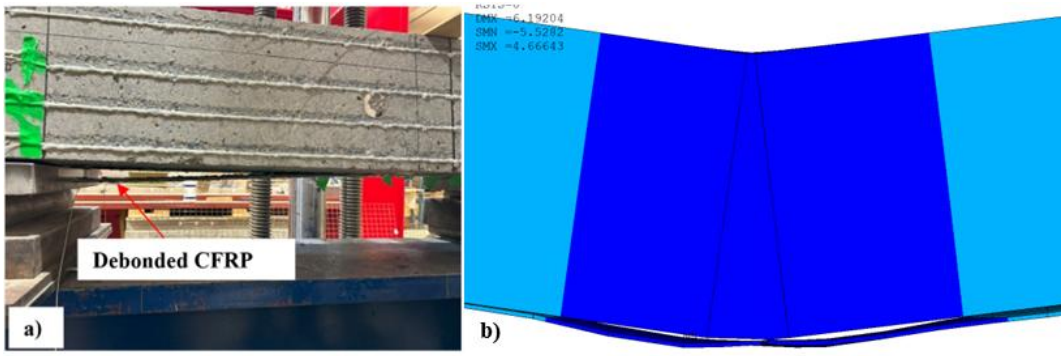

Figure 7.15-Debonded beam specimen a) experimental b) numerical model

The predicted load capacity for the FEM model of 137 kN was 1.9 % higher than the ultimate experimental load of 134.5 kN. However, the experimentally measured displacement of 4.61 mm was 18.2 % lower than the FEM prediction of 5.45 mm. The corresponding CZM input parameters were as follows: C1 was set to

0.35 MPa, C2 was 0.125 mm, C3 was set to 2 MPa, a value of 0.25 was used for C4, while 0.1 was used for C5, and C6 was set to 1.

The load-displacement curve for this beam is included in the appendix. Initial stiffness deviations suggest potential calibration issues with the displacement sensors, precluding direct load-displacement comparison. Significant discrepancies were observed between the experimental and FEM predictions under both the perfect bond assumption and the CZM model (see Appendix F.3)

7.6.2.1 Axial strain and stress analysis along CFRP length

Figure 7.16a illustrates the measured experimental strain alongside the numerically derived strain values at different load levels along the bonded length of CFRP in Beam B3S1-L500. The horizontal axis is measured from the end of the sheets near the left support. The notch was positioned 500 mm from the end of the sheet. For the 57-year-concrete specimens, the experimental strain demonstrated a good correlation with the numerical value; however, the numerical strain values were somewhat higher than the experimental values. This discrepancy may be attributed to several factors, including the variability in the CFRP-concrete bond-slip response. In the numerical models, the experimental bond-slip response is calibrated and smeared across the bonded area. In addition, factors such as variability in material thickness (e.g., epoxy, patch material) and the quality of the bond as moistened or damped concrete were noticed at the CFRP–concrete interface of the original bridge diaphragm during different bond tests undertaken by the authors, in addition to a number of defects of varying size that may compromise the CFRP-concrete bond (Fowai, 2024), all influence the difference in the FEM prediction.

It is also important to emphasize that the CFRP installation work on the evaluated bridge specimen was done during the winter period with an ambient temperature of less than 10°C, which may have affected the required curing duration for the resin used. The lack of documentation makes it challenging to discern if compensation was made in terms of the pot life or curing condition under this unfavorable installation

scenario. At any given load level, the strains in the FRP decrease away from the loading point. Consistent with experimental observation, the numerical model successfully captured the progression of CFRP debonding that occurred at the loading point. This indicates a lack of stress transfer over the plateau distance (high strain regions with uniform strain) at a given load stage. The width of the plateau region increased with increasing load, and CFRP debonding shifted the active bond stress transfer zone further from the notched location towards the left support. It is also evident that a stronger correlation of strain was noted on the right side of the notch, where the full width of CFRP was bonded. In contrast, a higher prediction in strain measurements was observed on the left side of the notch, where the width of the CFRP was reduced and debonding took place. The strain at the left support was also higher than the right support potential due to the curtailment of CFRP at the left support, which can result in higher stress levels.

The ultimate experimental strain reached in B3S1-L500 at the notch location was 4,359 microstrain, which was 12.3% lower than the numerical peak strain of 4,895 microstrain at the ultimate experimental load of 134 kN.

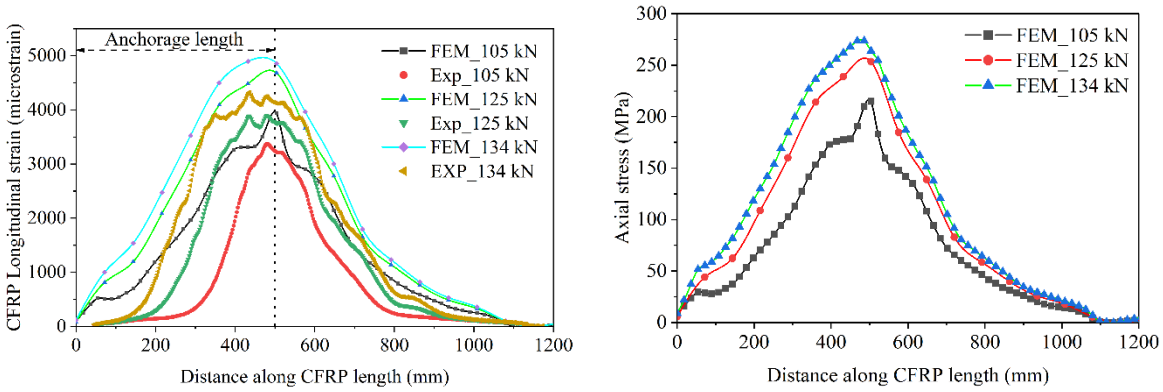

Figure 7.16-Axial strain and stress distribution for Beam B3S1-L500 a) Axial strain b) stress distribution

The peak strain observed in the experiment was approximately 52% of the value calculated based on the ACI PRC-440.2-23 provisions for debonding strain (8,400 microstrain), while the numerical peak strain was 58% of the ACI PRC-440.2-23 value. The strain limit of 6,000 microstrain prescribed in the Canadian code (CAN/CSA S6:19) also exceeded the maximum experimental strain observed in the beams that

experienced debonding (B3S1-L500) by approximately 38% and the numerical strain by approximately 23%. When addressing the discrepancy in peak strain values at the global level, it is important to note that existing models in the literature draw primarily from extensive experimental data on externally bonded applications using new materials (concrete, FRP, or adhesive) without necessarily accounting for the impact of degradation at the bond line or within the separate materials. This contrasts with the concrete substrates examined in this study, which had been constructed with high-strength concrete and in service for nearly six decades prior to its decommissioning due to extensive deterioration.

It is understandable that the ultimate tensile strength of the CFRP cannot be achieved with a deteriorated concrete that is governed by a debonding failure. It is also worth noting that the proportion of ultimate tensile strength utilized is a function of not just the CFRP and concrete material properties but also the condition of the bond. As illustrated in Figure 7.16b, the peak axial stress reached was only 47% of the ultimate tensile strength of the CFRP. Figure 7.17a and Figure 7.18 present the shear stress distribution along the bond line as a function of the distance from the ends of the CFRP across various load levels. Under low load conditions, the experimental shear stress distribution (see Figure 7.17a) exhibited a close resemblance to the patterns documented in existing literature, characterized by exponential and power functions (Nakaba et al., 2001; Nelson et al., 2020; Nelson et al., 2024). However, at higher loads, the shear stress distribution displayed distinct fluctuations marked by pronounced peaks (Figure 7.18). The fluctuation in shear stress distribution, particularly around the ultimate load, can be attributed to the condition/roughness along the cracks during the debonding process and the possibility of local defects that were undetected during the condition assessment (Fowai, 2024). As shown in Figure 7.17b, the experimental shear stress behaviour over the defective areas of the beam exhibited non-linearity during the experimental work, characterized by multiple shear stress peaks. These material imperfections and localized-effect of the strain measurement all influence the correlation of the experimental stress and strain with the prediction from FEM for a 57-year-old structure.

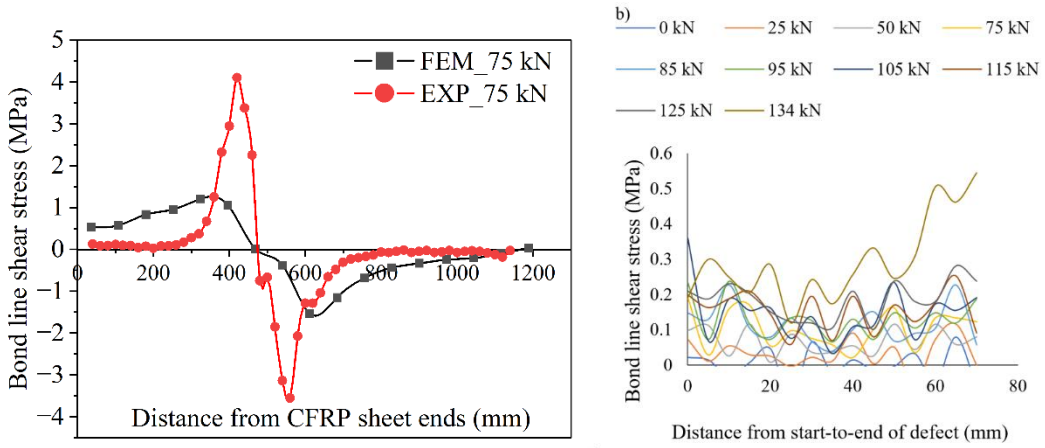

Figure 7.17-Bond-stress distribution a) Experimental against FEM at low load levels b) Experimental shear stress behaviour over the defective areas

As illustrated in Figure 7.17 and Figure 7.18, the shear stress distribution typically exhibited a positive magnitude on one side of the loading point and a negative magnitude on the other, relative to the loading configuration. Notably, the transition point of the shear stress from positive to negative was well captured in the numerical model (see Figure 7.17a).

When comparing the experimental and FEM shear stress distribution at low load levels, significant discrepancies were observed in the stress distribution. The experimental bond stress distribution showed pronounced peaks, which can be attributed to the variability in local bond quality. In contrast, the FEM results showed a more consistent trend with smaller fluctuations. It is noteworthy that the experimental shear bond strength for this beam was 6.3 MPa, while the maximum shear stress across the defect area in the beam was 0.54 MPa, representing approximately 8.6 % of the maximum bond stress. The smeared bond-stress value for the FEM model was 2 MPa. At high load levels, the experimental data exhibited multiple peaks compared to the FEM model.

However, a better correlation between the experimental and numerical model was achieved, with both the experimental and FEM showing increase and decrease of bond-stress at similar points, although differing in magnitude (with the FEM providing an average of the experimental values).

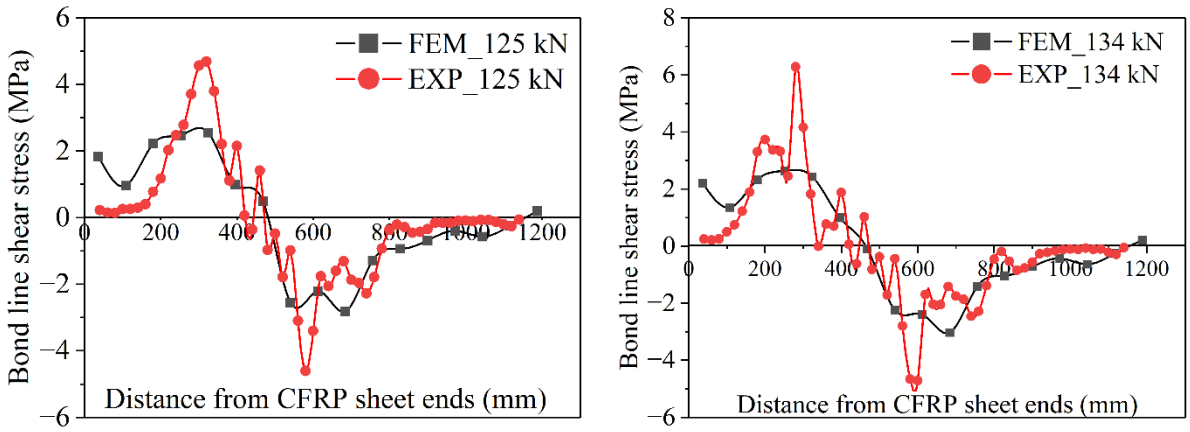

Figure 7.18- Bond stress distribution at high load levels

7.6.3 Validation on shear-lap specimens tested from the Champlain Bridge

The 3D DIC setup used for full-field strain and displacement measurements allows for the evaluation of the out-of-plane displacement in the specimens during testing. In a conventional single shear-lap setup, out-of-plane displacement primarily arises from the inherent eccentricity of the test setup, where the CFRP is only bonded to one side of the concrete prism (Figure 7.3). This configuration induces rotational movement during testing. This out-of-plane rotation-induced bending results in negative strain at the front face of the FRP, leading to reduced net strain measurements from the DIC. The experimentally recorded out-of-plane displacements were incorporated into the finite element model by applying both horizontal and vertical displacements to the griping section of the CFRP strips. These models are classified as mixed-mode models, since the CFRP-concrete interface is subjected to both tangential slip and normal peeling, whereas shear-lap models with only horizontal displacements are categorised as pure shear models. In both the pure shear and mixed-mode models of the single lap specimen, a 10-mm incremental displacement was applied to 100-mm length of the free overhanging portion of the CFRP to simulate the gripping effect shown in Figure 7.3. The CZM input values for the results presented in this section are given in Table 7.4. In the double-shear-lap specimen, the concrete prism on one side of the notch was constrained in all directions, while the concrete prism on the opposite side of the notch was subjected to a 10-mm incremental displacement.

Table 7.4-CZM input values for shear-lap specimens

Constant	Property	Single shear-lap	Double shear-lap
C1	σ_{max}	0.35 MPa	-0.35
C2	δ_n^c	0.125 mm	0.125
C3	τ_{max}	3.0 MPa	3.0 MPa
C4	δ_t^c	0.25 mm	0.25 mm
C5	α	0.10 mm	0.10 mm
C6	β	1	-

7.6.3.1 Failure modes

Both the conventional single shear-lap and double shear-lap tests demonstrated debonding, as was observed during the experimental tests. The predicted load capacity of 38 kN for the FEM model of the single shear-lap was 14.2 % lower than the ultimate experimental load of 43.4 kN. In the double shear-lap specimen, debonding initiated at the notch location and propagated towards the ends of the CFRP. For the single shear-lap specimen, debonding began at the free end of the CFRP where the load was applied. Figure 7.19 shows the debonding of conventional single shear-lap models in pure shear and in mixed mode loading conditions.

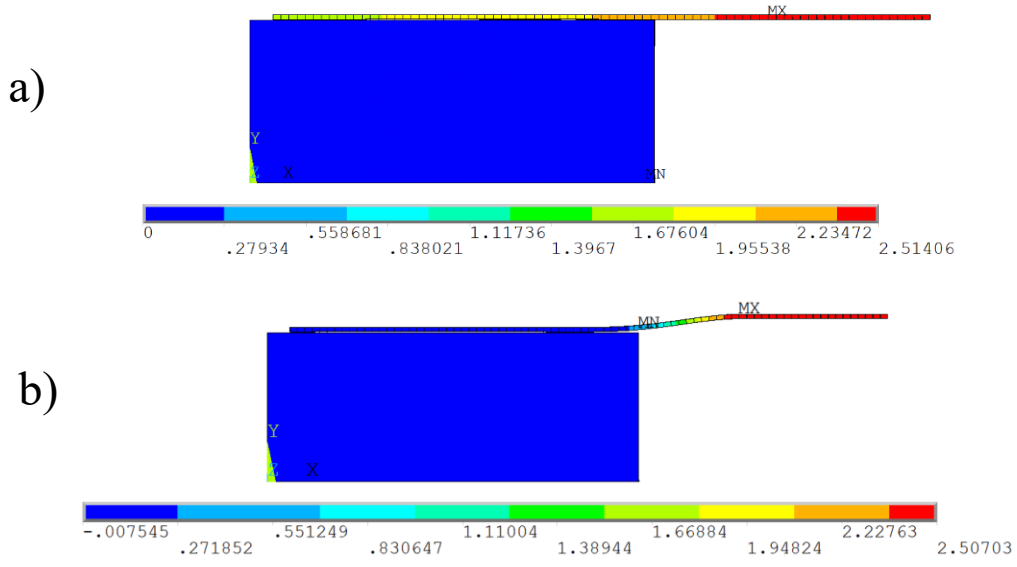

Figure 7.19-CFRP debonding after 2.5 mm displacement a) Pure shear loading b) Mixed-mode loading

7.6.3.2 Strain distribution along CFRP length

Figure 7.20 shows the axial strain profile along the CFRP bonded length of a typical shear-lap specimen for different load levels for a typical mixed-mode loading case (1-mm and 10-mm out-of-plane displacement). Generally, there is a good correlation between the experimental and numerical results along the bonded length, except the first 50 mm from the edge of the concrete block. The FEM models developed using the CZM modelling approach within ANSYS APDL successfully simulated the non-linear behaviour of the CFRP-concrete interface observed in the experimental tests. However, the pure shear mode II behaviour, as discussed in the subsequent section, failed to capture this behaviour. However, due to the sensitivity of the experimental strain measuring sensors to local phenomena such as cracks and voids, the experimental strain response exhibited irregularities at different locations along the length of the specimen. This discrepancy between the experimental and numerical strain improved with an increase in out-of-plane displacement. In the numerical models, the interface behaviour, as discussed earlier, is represented by a smeared bond stress-slip relationship calibrated from experimental data, while in the experimental tests, this stress-slip behaviour is location-dependent. Figure 7.20 also indicates localized strain variations at the ends of CFRP, where the load is applied, likely due to stress concentration in that region of the specimen. Overall, it is evident that the FEM predictions align satisfactorily with the experimental values for a 57 -year-old deteriorated concrete structure.

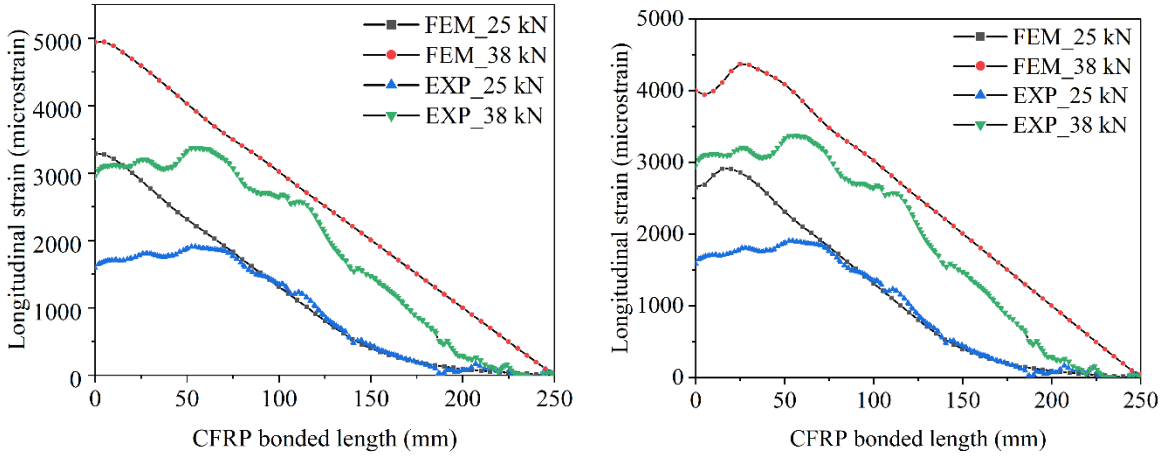

Figure 7.20-Strain distribution for single shear-lap a) 1 mm out-of-plane displacement b) 10 mm out-of-plane displacement

Figure 7.21 presents the strain distribution for the double shear-lap specimen. During the initial loading stages, the strain at the far end of the bonded length was essentially zero. As the load increased, the debonding propagated from the notch towards the end of the bonded length.

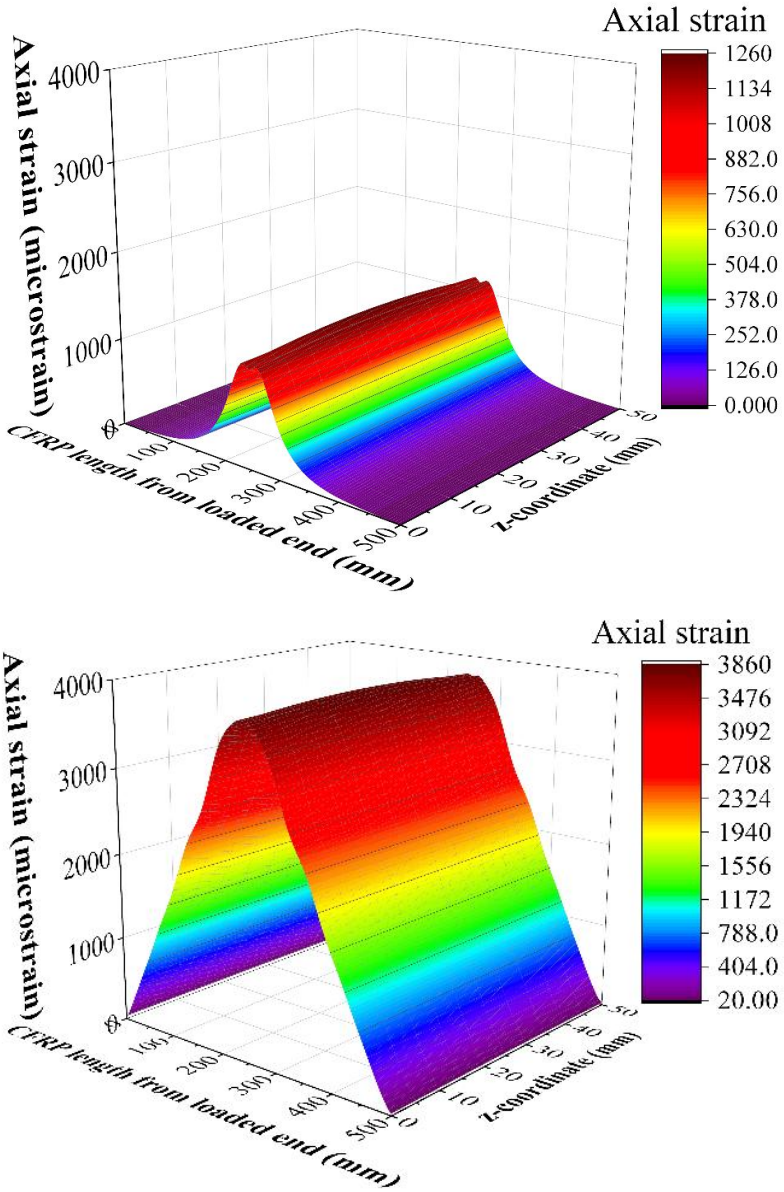

Figure 7.21-Strain distribution for double shear-lap at a) low load (29.2 kN) b) ultimate load (61.1 kN)

7.6.4 Parametric and sensitivity analysis on Champlain Bridge specimen

Several challenges arise when numerically validating experimental results of deteriorated concrete strengthened with externally bonded CFRP. One significant issue encountered was the accurate

characterization of the non-uniform degradation of concrete properties in nearly 60-year-old structural elements, including variability in material layer (mortar, adhesive etc). Various forms of deterioration, such as freeze-thaw, corrosion, and bond compatibility between old concrete and patch materials, can significantly influence the structural response of the concrete. The complex nonlinear behaviour of the CFRP-concrete interface, as derived experimentally through shear stress-slip relationships, is random in nature and can only be smeared in the numerical model. It has been observed that for aged concrete members strengthened with CFRP, bond quality can vary depending on the specific location being analyzed. In addition, experimental results may be difficult to compare with numerical models due to local variation in the heterogeneous concrete. Addressing these challenges requires a combination of experimental data with accurate constitutive models for both deteriorated concrete, CFRP and the CFRP-concrete interface. Conducting a detailed parameter sensitivity analysis is also essential to determine how the developed models are sensitive to the various input parameters. The influence of the input parameters for the concrete and the CZM, as well as the effects of loading orientation, were all investigated to evaluate their contributions to achieving a reasonable agreement between experimentally observed strain and stress in the 57-year-old deteriorated concrete and the newly developed FEM models.

7.6.4.1 CZM input parameters

The failure of the CFRP-concrete interface during the debonding process can be modelled using specialized interface or contact elements, depending on the numerical analysis tool used. The six constants (C1 to C6) defined in Table 7.3 are used to describe the constitutive behaviour of the CZM modeling ANSYS APDL . The behaviour of this interface is governed by normal and shear stresses, as well as the separation distance, including the normal gap and tangential slip. The relationships between the normal or tangential stress components of the CZM model and the corresponding normal displacement or tangential slip are defined as follows:

$$T_n = K_n \delta_n (1 - D_m)$$

$$T_t = K_t \delta_t (1 - D_m)$$

Here, T_n and T_t represent the normal and tangential traction, respectively, while K_n are K_t are respectively the normal and tangential cohesive stiffness, defined as the ratio of the maximum stress to displacement at maximum stress. δ_n and δ_t denote the normal and tangential displacement, respectively. D_m is the associated damage parameter, with a value of 0 for undamaged and of 1 for fully damaged. A sensitivity analysis performed to examine the parameters under mixed-mode loading indicated that the beam and shear-lap FEM models were particularly sensitive to the input parameter C3, which represents the tangential stress (see Figure 7.22). Other parameters had only a minor effect on the model outcomes. During this process, all other CZM parameters were kept constant while C3 was incrementally increased from 1.5 MPa to 4.5 MPa in increments of 0.5 MPa (see Table 7.5).

Table 7.5-Default value in assessing the influence of tangential shear in the CZM model

Constant	C1	C2	C3	C4	C5	C6
	0.35 MPa	0.125 mm	1.5 – 4.5 MPa	0.25	0.1	1

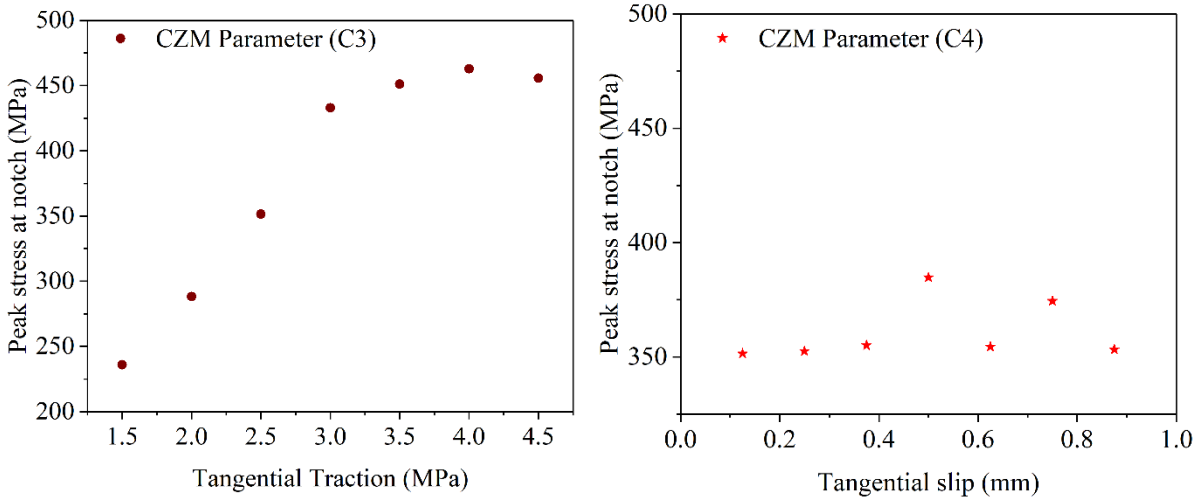

Figure 7.22- Sensitivity analysis of CZM input parameters a) C3:Tangential shear stress b) Tangential displacement at failure

During the calibration process, it was determined that a C3 value of 2 MPa for the beam or 3 MPa for the shear-lap specimens yielded a reasonable correlation between the experimental and numerical strain values for the deteriorated concrete specimens from the Champlain Bridge.

7.6.4.2 Material deterioration

No data were available to the authors for the patch mortar used to repair the deteriorated concrete prior to the installation of the CFRP. To address the reduced stiffness of the patch mortar, a compressive strength of 30 MPa was assigned to the bottom-most tensile elements in the beam (see Figure 7.23), while the remaining concrete beam retained the original compressive strength of 76 MPa. It is important to note that, despite visual inspection revealing imperfections in the bond between the patch mortar and concrete in certain areas of the concrete member, the numerical model assumed a perfect bond between the 76 MPa concrete and the patch mortar. This assumption led to the overestimation of the ultimate strain, although the strain distribution across the length of the beam exhibited a reasonable trend (see Figure 7.24). It is also worth noting that while the effects of the patch mortar are smeared uniformly along the length of the beam for simplicity in the modelling, the actual thickness of the patch mortar varied (5 mm to 10 mm) along the length of the beam (Figure 7.23). The comparison between models with mortar and those without indicates that assigning reduced strength to the bottom-most tensile elements in the beam while maintaining a perfect bond between the coincident nodes did not significantly impact the strain distribution, except for a negligible variation in peak strain at the notch where debonding began.

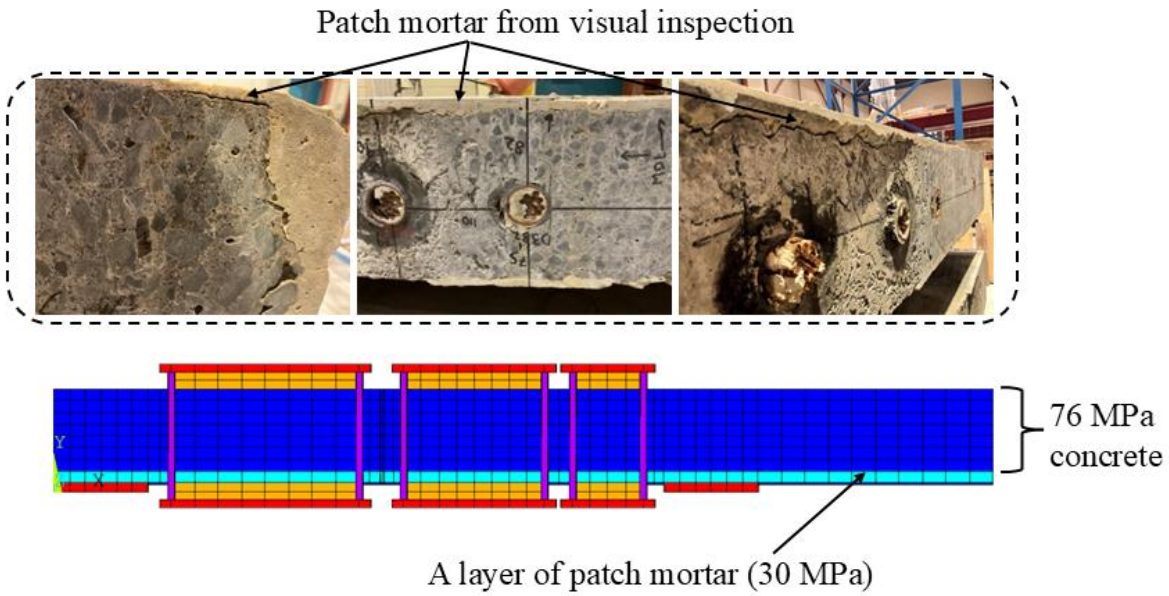

Figure 7.23-Repair mortar in structural elements and FEM model

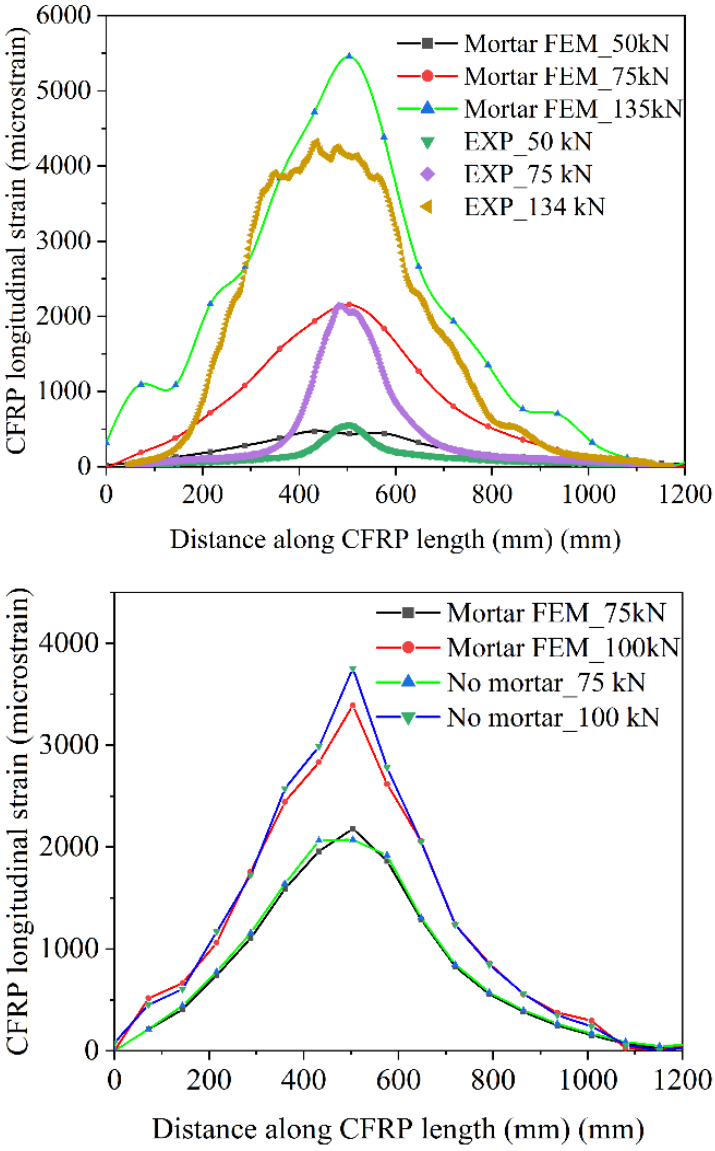

Figure 7.24-Strain profiles a) 30 MPa mortar and experimental strain b) Mortar and no mortar

7.6.4.3 Effect of peel angle

During the experimental testing of the shear-lap specimens, a certain level of out-of-plane displacement was observed (see Figure 7.25). This out-of-plane displacement is expected to affect the rate of debonding and, ultimately, the peak strain during the debonding process. To simulate this mixed-mode loading in the numerical analysis, both horizontal and small vertical displacements were applied to the free-hanging portion of the CFRP strip, as illustrated in Figure 7.26. Seven models were generated with varying amounts of out-of-plane displacement. One model was subjected only to a 10-mm horizontal displacement

(representing pure-shear loading), while the other models included vertical displacements of 0.25 mm, 0.5 mm, 1 mm, 2.5 mm, 5 mm, and 10 mm, respectively, in addition to the 10-mm horizontal displacement to subject the CFRP-concrete interface to both normal and shear stresses.

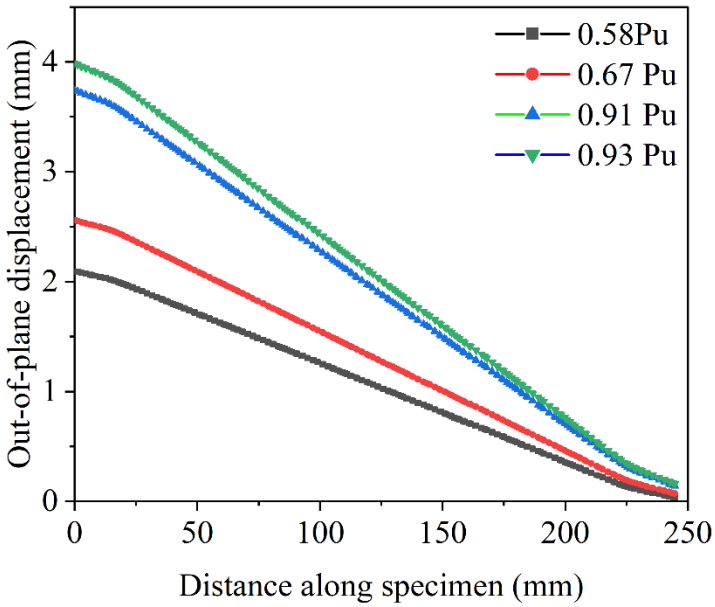

Figure 7.25-Out-of-plane deformation of single-shear specimen

Figure 7.27 and Figure 7.28 illustrate the strain distribution along the length of the CFRP under different loading conditions. The horizontal axis represents the distance from the end of the CFRP sheet near the loading point, and the strain values are extracted along the centerline of the CFRP (along the symmetric plane). Variation of the out-of-plane displacement resulted in a significant reduction in the maximum observed strains along the length of the beam when comparing extreme conditions (pure shear and 10-mm out-of-plane displacement). The strain plateau observed at maximum slip was captured in the mixed-mode models, while the pure-shear model exhibited no noticeable plateau at the loaded end of the CFRP (see Figure 7.27 and Figure 7.28). No significant difference in peak strain was observed when transitioning from the pure shear mode up to the case with a 1-mm out-of-plane displacement; the maximum strain remains constant at approximately 5,000 microstrain from the pure shear configuration to the condition with 1-mm vertical displacement. However, percentage decreases in peak strain were observed as the out-of-plane

displacement increased from 1 mm to 2.5 mm, 5 mm and 10 mm; these reductions were 3.1%, 7.2% and 11.6%, respectively (see Figure 7.27 and Figure 7.28).

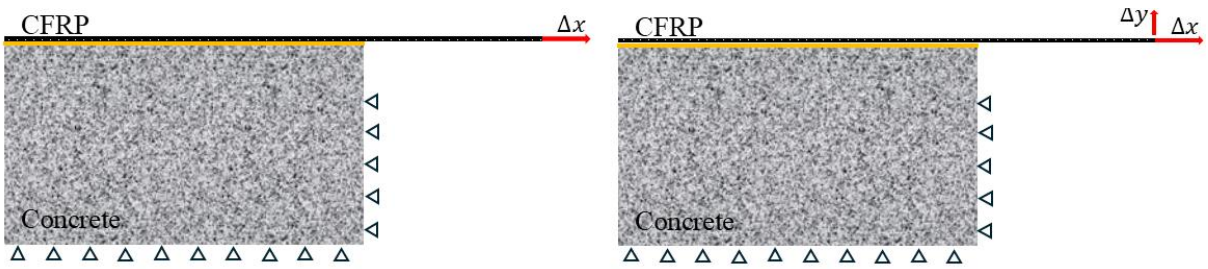

Figure 7.26-Illustration of loading conditions in pure shear and mixed mode loading

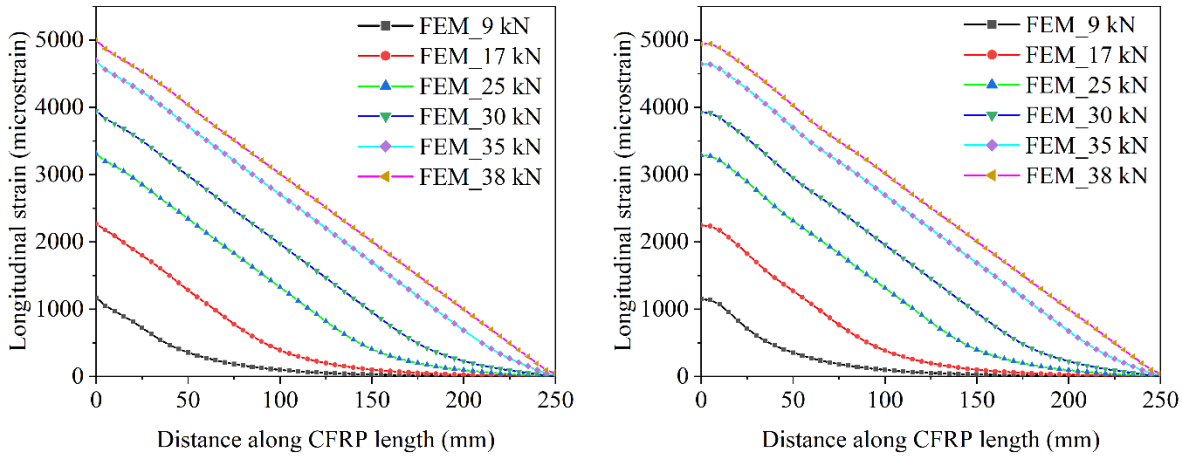

Figure 7.27-Strain distribution for conventional single shear-lap a) pure shear b) mixed-mode (1-mm vertical displacement)

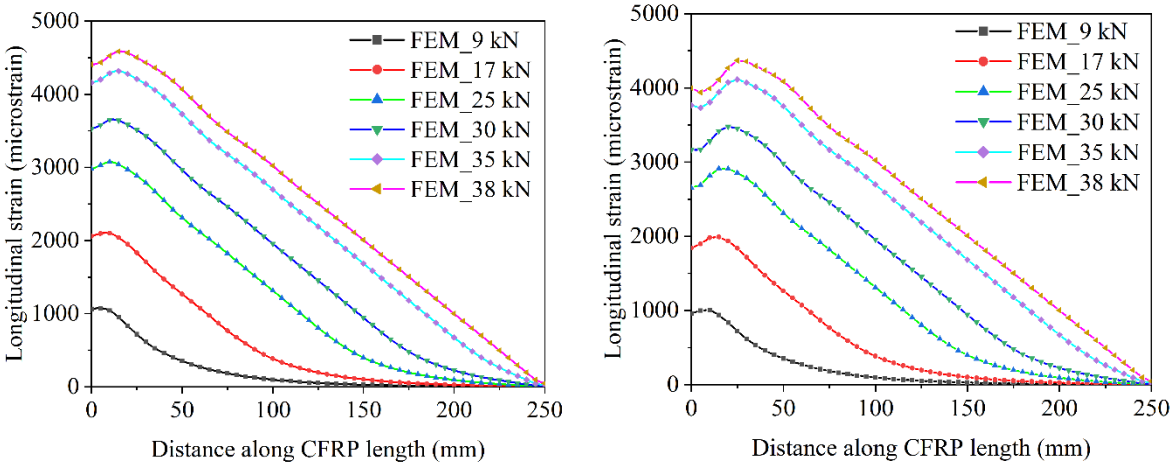

Figure 7.28-Strain distribution for conventional single shear-lap a) mixed-mode (5-mm vertical displacement) b) mixed-mode (10-mm vertical displacement)

For the deteriorated concrete shear lap tests, a good agreement in the strain distribution along the CFRP between the experimental and numerical models was observed when the ratio of the in-plane to out-of-plane displacement was closer to 1. Figure 7.29 shows a typical strain profile at ultimate load conditions when the ratio of vertical displacement to horizontal displacement is 1. Although the strain values at the loaded end vary, this discrepancy can be attributed to the stress concentration in that region of the specimen. In each of the FEM models, a negligible variation in strain was observed across the width of the specimen (see Figure 7.29).

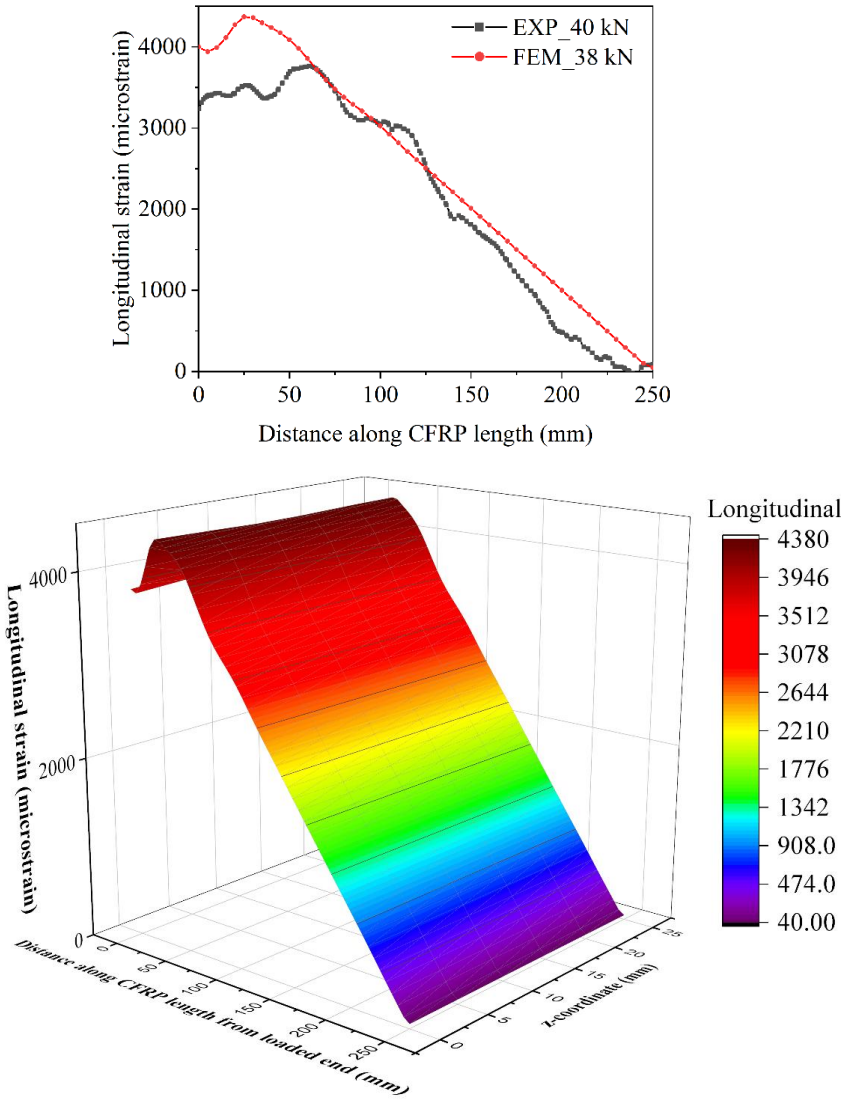

Figure 7.29-Axial strain distribution across the length and width of the specimen with a unit in-plane to out-of-plane displacement ratio

7.7 Discussion

The primary objective of this study was to develop, for the first time, a computationally efficient 3D finite element model to analyse the bond between CFRP and concrete in structural members of a 57-year-old bridge, specifically focusing on mode II and mixed-mode debonding. This research has been concerned with accurately predicting the debonding mechanism between the deteriorated concrete and CFRP in both beam and shear-lap specimens using the cohesive zone material approach. Initially, a numerical framework addressing the debonding mechanism of reinforced concrete beams strengthened with CFRP was presented by validating four beams sourced from the literature. The models, developed within a 3D FEM framework implemented in ANSYS APDL, successfully captured the debonding mechanism at pristine CFRP-concrete interface. The correlation between the results of the FEM models and the experimental results reported in the literature was excellent in terms of failure loads, displacements, and failure modes. Consequently, the CZM approach proved viable for simulating the structural response of concrete members strengthened with CFRP in ANSYS APDL.

In the subsequent part of the study, a parametric analysis was conducted to explore the behaviour of the CFRP-concrete interface in the 57-year-old concrete specimens tested in flexure as beams and in shear-lap configurations. The modeling research revealed that the correlation of experimental response and numerical predictions of the deteriorated bridge specimens is influenced by the synergistic combination of several complex factors, including: 1) local variability in the bond-slip behaviour observed experimentally but smeared within the FEM model; 2) the impact of repair materials applied prior to CFRP installation; 3) environmental conditions affecting the deteriorated concrete and curing condition of the adhesive layer; and 4) the effect of out-of-plane displacement observed during experimental tests.

During the parametric analysis, a minimum of seven models were developed for each input parameter of the CZM, which accounts for the debonding failure. The FEM models were particularly sensitive to the

input parameter C3, which represents the tangential stress. Other parameters had only a minor effect on the model outcomes.

For the 57-year-concrete beam specimens, the experimental strain demonstrated a good correlation with the numerical value; however, the numerical strain values were somewhat higher than the experimental ones. A better correlation between the experimental and numerical stress distributions was achieved at high load levels, with both the experimental and FEM showing an increase and decrease of bond stress at similar points, although differing in magnitude. In shear-lap specimens, the FEM model was unable to capture well the debonding under pure shear loading, as strain continued to increase. Nonetheless, a good correlation was observed along the length of the specimens in mixed-mode scenarios as out-of-plane displacement increased. A key feature of the developed models in this study was the flexibility in implementing contact elements to simulate the interfacial damage between the CFRP and concrete regardless of loading direction, through calibrated input parameters. As a future perspective on this work, future research could extend the proposed CZM approach to model the structural response of the full-scale diaphragms extracted from the bridge, with suggestions for investigating the effect of both mortar thickness, axial stiffness of the composite material, and the level of prestressing force in the full-scale members.

This study highlights the accuracy of strain, bond stress distribution, and axial stress behaviour in deteriorated concrete members and emphasizes the disparities between code predictions and experimental and numerical results, which enhance our understanding of the CFRP-concrete interface performance in damaged structural members. For future FEM of deteriorated concrete elements strengthened with CFRP, it would be recommended, where applicable, to consider advanced analysis tools, such as the extended finite element method (XFEM), for improved accuracy in addressing fracture mechanics and interface issues.

7.8 Conclusions

This paper examines the debonding behaviour between externally bonded CFRP and deteriorated concrete elements in various loading orientations. 3D FEM models were developed using experimentally calibrated CZM parameters to simulate the response of specimens under both mode II and mixed-mode loading conditions. The models were validated against experimental data from existing literature as well as data collected by the authors from samples taken from a 57-year-old decommissioned bridge in Canada. The following conclusions can be drawn from this research:

- Accurate modelling of the complex behaviour of the CFRP-concrete bond interface necessitates the adoption of suitable modeling techniques, such as the cohesive zone material approach. However, smeared shear bond stress-slip relationships should be calibrated correctly for deteriorated structural elements that exhibit inevitable discontinuities at the bond line.
- The developed models in this study were found to be sensitive to the shear stress at the bond line, which was calibrated from experimental data embedded in the CZM input parameter.
- Incorporating accurate CZM parameters resulted in an excellent prediction of structural response when validating studies in the existing literature. The discrepancies in peak load from validation studies in the literature were minimal, with differences of only 0.1% for RB1 and 3.6% for the control beam in the initial numerical validation conducted by Obaidat.
- The CZM approach effectively simulated the nonlinear response of the 57-year-old concrete strengthened with CFRP under both mode II and mixed-mode loadings, with only a 12% difference in peak strain between the experimentally tested beam and the numerical model, while the overall strain distribution was well correlated.
- Under mixed-mode loading conditions, a decrease in peak strain was observed as the out-of-plane displacement increased from 1 mm to 2.5 mm, 5 mm and 10 mm, with a corresponding reduction of 3.1%, 7.2% and 11.6%, respectively. The strongest correlation between

experimental and FEM numerical strain results was observed when the ratio of in-plane displacement to out-of-plane displacement was 1.

7.9 References

Al-Saawani, M. A., Al-Negheimish, A. I., El-Sayed, A. K., & Alhozaimy, A. M. (2022). Finite element modeling of debonding failures in FRP-strengthened concrete beams using cohesive zone model. *Polymers*, *14*(9), 1889.

Alhassan, M. A., Al-Rousan, R. Z., & Taha, H. M. (2020). Precise finite element modelling of the bond-slip contact behavior between CFRP composites and concrete. *Construction and Building Materials*, *240*, 117943.

ANSYS. (2025). *ANSYS 2025/R1 Theory Reference for the Mechanical APDL and Mechanical Applications*.

Arruda, M. R., Firmo, J., Correia, J., & Tiago, C. (2016). Numerical modelling of the bond between concrete and CFRP laminates at elevated temperatures. *Engineering structures*, *110*, 233-243.

Au, C., & Büyüköztürk, O. (2006). Peel and shear fracture characterization of debonding in FRP plated concrete affected by moisture. *Journal of composites for construction*, *10*(1), 35-47.

Bizindavyi, L., & Neale, K. (1999). Transfer lengths and bond strengths for composites bonded to concrete. *Journal of composites for construction*, *3*(4), 153-160.

Brault, A., & Hoult, N. (2019). Monitoring reinforced concrete serviceability performance using fiber-optic sensors. *ACI structural journal*, *116*(1), 57.

Buyle-Bodin, F., David, E., & Ragneau, E. (2002). Finite element modelling of flexural behaviour of externally bonded CFRP reinforced concrete structures. *Engineering structures*, *24*(11), 1423-1429.

Coronado, C. A., & Lopez, M. M. (2007). Damage approach for the prediction of debonding failure on concrete elements strengthened with FRP. *Journal of composites for construction*, *11*(4), 391-400.

Coronado, C. A., & Lopez, M. M. (2010). Numerical modeling of concrete-FRP debonding using a crack band approach. *Journal of composites for construction*, *14*(1), 11-21.

Dushimimana, A., Sena-Cruz, J., Correia, L., Pereira, J. M., Cabral-Fonseca, S., & Cruz, R. (2024). Effects of long-term exposure of NSM CFRP-to-concrete bond to natural and accelerated aging environments. *Composite Structures*, *340*, 118174.

Ferracuti, B., Savoia, M., & Mazzotti, C. (2007). Interface law for FRP–concrete delamination. *Composite structures*, *80*(4), 523-531.

Fowai, I., Noël, M., Esmaili, M., Martín-Pérez, B., & Sanchez, L. (2025b). Bond performance of deteriorated CFRP-concrete interface under different shear-lap configurations: A Champlain Bridge case study. *Construction and Building Materials*.

Fowai, I., Noël, M., Yager, J., Martín-Pérez, B., Sanchez, L., Green, M. F., & Hoult, N. A. (2025e). Strain distribution and debonding behaviour of CFRP sheets with different anchorage lengths from a decommissioned concrete bridge. *Engineering structures*.

Fowai, I., Noel, M., Martín-Pérez, B., & Sanchez, L. (2023). *Integrity Assessment of CFRP-Concrete Interface on Externally Strengthened Bridge Diaphragms Using Direct Tension Pull-off Test.* 11th International Conference on Fiber-Reinforced Polymer (FRP) Composites in Civil Engineering (CICE 2023), Rio de Janeiro, Brazil.

Fowai, I., Noel, M., Martín-Pérez, B., & Sanchez, L. (2024). Assessment of CFRP-concrete interface integrity of Original Champlain Bridge diaphragms through non-destructive and semi-destructive testing [Invited paper]. *ASCE Journal of Composites for Construction*.

Godat, A., Neale, K. W., & Labossière, P. (2007). Numerical modeling of FRP shear-strengthened reinforced concrete beams. *Journal of composites for construction*, *11*(6), 640-649.

Gotame, M., Franklin, C. L., Blomfors, M., Yang, J., & Lundgren, K. (2022). Finite element analyses of FRP-strengthened concrete beams with corroded reinforcement. *Engineering structures*, *257*, 114007.

Imani Jajarmi, P., Tavakkolizadeh, M., & Youssefi, A. (2022). Effect of temperature and moisture on the bond strength between fiber reinforced polymer laminates and cement-based mortar substrates. *Structural Concrete*, *23*(2), 970-992.

Li, P.-D., Zhao, Y., Wu, Y.-F., & Lin, J.-P. (2023). Effect of defects in adhesive layer on the interfacial bond behaviors of externally bonded CFRP-to-concrete joints. *Engineering structures*, *278*, 115495.

Lu, X., Teng, J., Ye, L., & Jiang, J. (2005). Bond–slip models for FRP sheets/plates bonded to concrete. *Engineering structures*, *27*(6), 920-937.

Mazzotti, C., Savoia, M., & Ferracuti, B. (2009). A new single-shear set-up for stable debonding of FRP–concrete joints. *Construction and Building Materials*, *23*(4), 1529-1537.

Milev, S., & Tatar, J. (2023). Durability Assessment of the First Externally Bonded FRP Repair of a Publicly Owned Bridge in the United States after 26 Years of Service. *Journal of composites for construction*, *27*(5), 04023049.

Mostofinejad, D., & Hosseini, S. J. (2017). Simulating FRP debonding from concrete surface in FRP strengthened RC beams: A case study. *Scientia Iranica*, *24*(2), 452-466.

Mukhtar, F. M., & Faysal, R. M. (2018). A review of test methods for studying the FRP-concrete interfacial bond behavior. *Construction and Building Materials*, *169*, 877-887.

Myers, J. J., & Ekenel, M. (2005). Effect of environmental conditions on bond strength between CFRP laminate and concrete substrate. *Special Publication*, *230*, 1571-1592.

Nakaba, K., Kanakubo, T., Furuta, T., & Yoshizawa, H. (2001). Bond behavior between fiber-reinforced polymer laminates and concrete. *Structural Journal*, *98*(3), 359-367.

Nelson, L. A., Al-Allaf, M., & Weekes, L. (2020). Analytical modelling of bond-slip failure between epoxy bonded FRP and concrete substrate. *Composite structures*, *251*, 112596.

Nelson, L. A., Weekes, L., Milani, G., & Al-Allaf, M. (2024). Generalised analytical solutions for linear and non-linear bond–slip models for externally bonded FRP to a concrete substrate. *Engineering structures*, *298*, 117025.

Obaidat, Y. (2011). Structural retrofitting of concrete beams using FRP-debonding issues.

Obaidat, Y. T., Heyden, S., & Dahlblom, O. (2010). The effect of CFRP and CFRP/concrete interface models when modelling retrofitted RC beams with FEM. *Composite structures*, *92*(6), 1391-1398.

Pham, H. B., Al-Mahaidi, R., & Saouma, V. (2006). Modelling of CFRP–concrete bond using smeared and discrete cracks. *Composite structures*, *75*(1-4), 145-150.

Salameh, A., Hawileh, R., Safieh, H., Assad, M., & Abdalla, J. (2024). Elevated Temperature Effects on FRP–Concrete Bond Behavior: A Comprehensive Review and Machine Learning-Based Bond Strength Prediction. *Infrastructures*, *9*(10), 183.

Tatar, J., & Brenkus, N. R. (2021). Performance of FRP-strengthened reinforced concrete bridge girders after 12 years of service in coastal Florida. *Journal of composites for construction*, *25*(4), 04021028.

Taylor, B. a. (2013). *Champlain Bridge Approach Spans, Edge Girder Condition Assessment and Rehabilitation Requirement*.

Tedesco, J. W., Stallings, J. M., & El-Mihilmy, M. (1999). Finite element method analysis of a concrete bridge repaired with fiber reinforced plastic laminates. *Computers & structures*, *72*(1-3), 379-407.

Teng, J., & Chen, J. (2007). Debonding failures of RC beams strengthened with externally bonded FRP reinforcement: behaviour and modelling. Proceedings of the first Asia-Pacific conference on FRP in structures (APFIS 2007),

Ueda, T., & Dai, J. (2005). Interface bond between FRP sheets and concrete substrates: properties, numerical modeling and roles in member behaviour. *Progress in structural engineering and materials*, *7*(1), 27-43.

Viñuela, J. Z., Torres, M., & Silva, R. G. (2022). Cohesive zone modeling in load–unload situations. *International Journal of Mechanical Sciences*, *222*, 107205.

Xu, T., He, Z., Tang, C. A., Zhu, W., & Ranjith, P. (2015). Finite element analysis of width effect in interface debonding of FRP plate bonded to concrete. *Finite elements in analysis and design*, *93*, 30-41.

Yu, H., Bai, Y.-L., Dai, J.-G., & Gao, W.-Y. (2017). Finite element modeling for debonding of FRP-to-concrete interfaces subjected to mixed-mode loading. *Polymers*, *9*(9), 438.

Zhang, W., Tang, Z., Yang, Y., & Wei, J. (2021). Assessment of FRP–concrete interfacial debonding with coupled mixed-mode cohesive zone model. *Journal of composites for construction*, *25*(2), 04021002.

Zhelyazov, T. (2024). Models analyzing the response of the adhesive joint between FRP and concrete: a comparative analysis. *Discover Mechanical Engineering*, *3*(1), 23.

Chapter 8 -Conclusions and recommendations

8.1 Project summary, outcomes, contributions and novelty

This comprehensive study represents the first thorough investigation into the bond performance of externally bonded on deteriorated concrete bridge elements globally. It aims to deepen our understanding of the practical differences between CFRP-concrete bond in new materials and those in ageing infrastructures strengthened with CFRP. The initial phase of this research has elucidated several fundamental issues associated with the bond between CFRP and deteriorated concrete structures, including material incompatibilities from long-term environmental exposure, construction-induced defects amplified by years of service. Phase two complements phase one by correlating observed material deterioration with the results of various structural tests. Together, these two phases have assessed whether field defects have compromised the bond integrity of the 60-year-old concrete bridge elements, as well as the influence of loading directions and test setups on the bond strength results. The study has extensively documented the implications of bond line deterioration on load transfer through stress and strain analysis, as well as the evaluation of bond strength failure loads and modes in high strength concrete. This research implemented a multiscale monitoring paradigm combining DFOS, 2D/3D digital image correlation and micro-CT to better understand damage progression and overall bond performance. These experimental findings have been integrated into FE models calibrated to capture the complex nonlinear interaction between deteriorated concrete and externally bonded CFRP materials. This research highlights the limitations of current analytical models and design codes, which were developed for new structural elements strengthened with composite materials, when applied to deteriorated concrete structures. This understanding aims to refine design codes with an emphasis on performance-based criteria.

Overall, this research identifies that, following five years of exposure to field conditions and service loads, the predominant failure mode for the CFRP-concrete interface under both single and mixed-mode loading conditions was cohesive in the concrete substrate. Quantitative analysis of 490 pull-off samples revealed

that 96% failed within the substrate, with an average pull-off strength of $0.38\sqrt{f_c'}$. This value is approximately equivalent to the cracking strength of concrete ($0.4\sqrt{f_c'}$) specified by the Canadian bridge design code. The maximum bond strength obtained varied according to testing methodology (Figure 8.1). Pull-off tests yielded a maximum bond strength of 5.54 MPa. Shear-lap tests produced comparable maximum values across configurations: single shear-lap at 7.9 MPa, double shear-lap at 7.8 MPa. Beam tests similarly resulted in a maximum bond stress of 7.9 MPa.

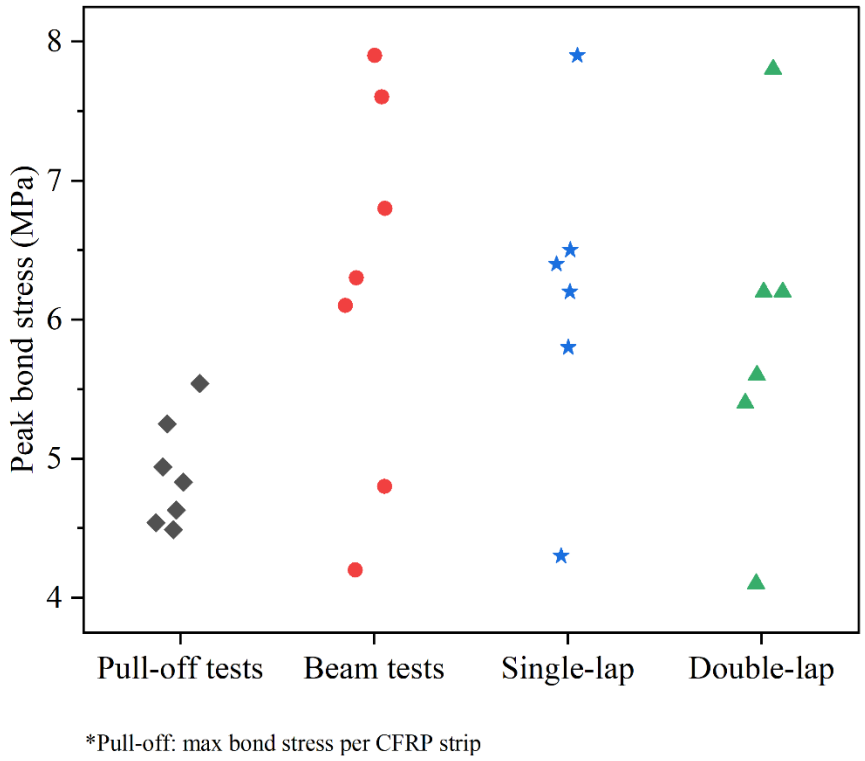

Figure 8.1-Peak bond strength correlation

It is important to note that the pull-off strength value reflects the quality of the concrete substrate and interface integrity. These measurements do not provide a quantitative value of the interface shear strength, and the minimum values prescribed in provision documents are conservative for high-strength concrete, such as that used in the diaphragms of this study. Average shear bond strength measured from the beam test ($0.72\sqrt{f_c'}$) and shear-lap tests ($0.69\sqrt{f_c'}$) respectively) were 88 and 82 percent greater than the pull-off bond strength. The pull-off bond results demonstrated high variability with a coefficient of variation

(COV) of 27%. This variability is typical in direct tension pull-off testing, arising from the heterogeneity of concrete and patch mortar, including aggregate variation, misalignment, stress concentration, and microcracks. Pull-off samples with identified defects found through non-destructive testing showed a reduced value in the bond strength and prevailing delamination of the CFRP material.

The study revealed significant differences in CFRP peak strain values across various loading configurations. Mixed loading condition (beam test) produced higher peak strain values compared to single-mode loading tests. The average peak strain from the mixed mode loading tests was 3872 microstrain, with a coefficient of variation (COV) of 21 percent. Experimental strains from the beam tests were predominately between 3500 and 4300 microstrains. Among the shear-lap test configurations, ultimate strains were, on average, higher for the conventional pull-push single shear-lap setup. The average maximum strain from the new single shear-lap tests was 2430 microstrain, with a COV of 11 percent. Conventional single shear-lap yielded an average peak strain of 3203 microstrain and a COV of 26 percent. The double shear-lap tests showed an average peak strain of 2644 microstrain, with a COV of 25 percent (Figure 8.2).

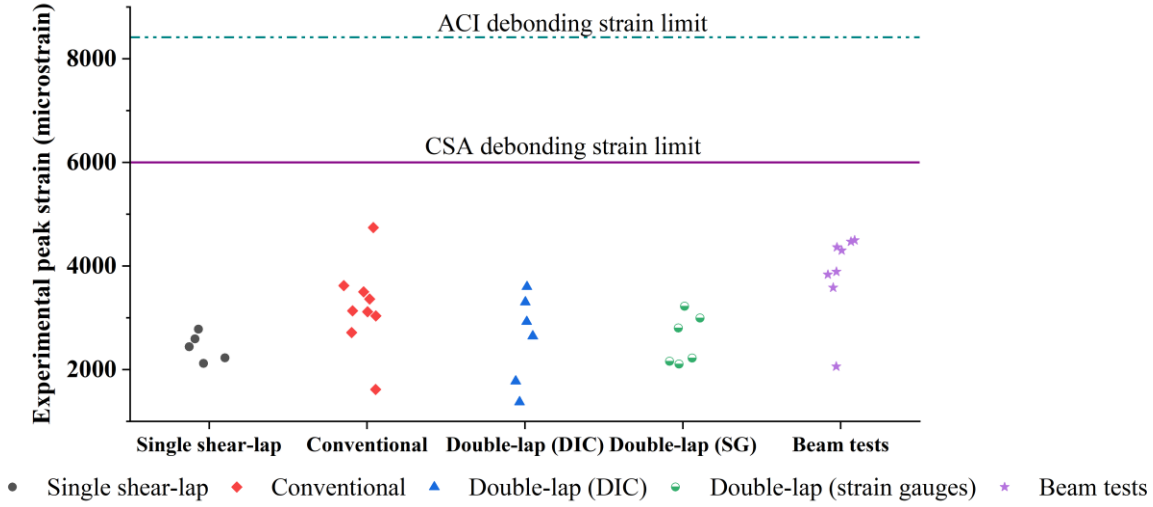

Figure 8.2-Tensile strain correlation across test setups

Experimental strains for the shear-lap tests mostly ranged from 2500 to 3400 microstrains. The ultimate strains observed in all the beams and the shear-lap tests were approximately 50 percent of the value predicted by ACI PRC-440.2-23 for debonding. Additionally, strain limits outlined in the Canadian code

(CAN/CSA S6:19) exceeded the peak experimental strain in the beams by approximately 30 to 34 percent. The unconservative peak strain estimates from code equations for the 57-year-old deteriorated concrete elements strengthened with CFRP are problematic and can arise due to several factors. The code equations typically assume sound material properties that do not account for the effects of aging, environmental exposure and microstructural degradation that occur over decades. Prior deterioration, such as cracking, chemical induced degradations directly lowers the level of strain developed experimentally during the various bond tests, as crack initiation and progression occurs at lower strains, limiting the deformation capacity. The level of deterioration in the concrete also compromises the bond between the concrete and CFRP, influencing effective strain transfer. Incorporating deterioration factors in strain prediction equations is a reliable approach to avoid unsafe design for retrofitted structures.

This dissertation and related publications present a comprehensive and holistic evaluation of long-term CFRP bond performance on deteriorated bridge infrastructure. The novelty is demonstrated through several key aspects including: the first-of-its-kind condition assessment combining visual inspection, advanced NDT, and semi-destructive testing; the establishment of an extensive field dataset on long-term CFRP bond performance, filling a significant literature gap and enabling direct comparison with other studies in the future; the creation of the largest database of pull-off test results, and the development of novel testing setups to evaluate the CFRP-concrete interface under single and mixed-mode loading. This study serves as a pioneering effort in linking/correlating CFRP-concrete bond line deterioration to actual field performance under different loading conditions. This integrated, field-based, and innovative approach sets a new benchmark for assessing CFRP-strengthened structural components. The unique contributions made by the author from this research include:

- A comprehensive literature review on methods of evaluating the CFRP-concrete bond, identifying research gaps in high-performance concrete and deteriorated concrete structures strengthened with composite materials.

- Bridging knowledge gaps from previous condition assessments studies that primarily focused on NDT or a few pull-off tests. The completion of this research has allowed the author to conduct an assessment that combines NDTs and semi-destructive field-testing methods, offering a more holistic assessment.
- Correlating results from NDT, semi-destructive and destructive, to establish a substantial database that can be used to interpret NDT findings in terms of actual bond strength. This linkage between bond imperfections identified through advanced NDT techniques to bond strength measurements will inform the revision of existing guidelines that focus solely on quality assurance through unconservative minimum pull-off test value. This knowledge will aid practitioners in evaluating CFRP strengthened systems without necessitating extensive destructive testing.
- Establishing the largest database of its kind, consisting of 490 pull-off tests, can serve as benchmarks for comparing new and existing structural elements of varying concrete grades (normal strength and ultra-high-performance concrete with high-strength concrete) in future studies.
- The completion of this research has allowed the development of two innovative bond assessment test setups proposed for future experimental research to evaluate CFRP-concrete bonds under either mode-II or realistic mixed-mode loading.
- Implementing advanced sensing techniques such as distributed fiber optic sensors, and two-dimensional and three-dimensional digital image correlation in a single multi-level study to compare accuracy against conventional sensing methods such as strain gauges. This multi-instrumented approach enables detailed characterization of damage propagation and performance monitoring throughout the experiment work.
- The development of the CZM FEM models in this research demonstrated the inadequacy of assuming a perfect bond between CFRP and deteriorated concrete, emphasizing the need to account for experimentally observed misalignment in test setups, and the complexities of bond line deterioration for achieving accurate predictions in aged specimens.

8.2 Conclusions

Externally bonded CFRP offers significant advantages over traditional repair methods, making it an attractive solution for rehabilitating the increasing number of deteriorating concrete structures worldwide. Understanding how CFRP performs in real-world conditions will remain crucial for its effective application. The primary objective of this research was to enhance understanding of the bond performance of a CFRP retrofitting intervention applied to the Champlain Bridge, a landmark structure in Canada. This study aimed to establish correlations between diverse testing and assessment methodologies. By examining how different load orientations and test setups affect bond behaviour and determining the impact of field defects on bond integrity, the research enables a direct comparison among various single and mixed-mode bond tests. An extensive database was generated on deteriorated high-strength concrete bridge elements facilitating future research comparisons.

Various non-destructive testing (NDT) techniques were employed to evaluate the CFRP-concrete bond integrity, including coin tapping, hammer tapping, and infrared thermography. Combined with five different structural tests, these techniques aid in correlating NDT findings with the actual bond performance of the CFRP-concrete interface and determine the effect of loading direction and test setup on interface bond transfer. FEM numerical modelling revealed challenges in accurately representing the CFRP-concrete bond interface for deteriorated concrete members using Cohesive Zone Material models in ANSYS APDL. Although the preparation of laboratory-cast, undamaged reference specimens for direct comparison with bond test results from the bridge elements was not performed in this study, a preliminary comparison of specimens documented in existing literature is presented in Chapter 5.

One significant finding from this study, was the discrepancy in bond strength measurements among different testing methods. Specifically, the average bond strength values derived from the beam and shear-lap tests were 82-88% higher than that from direct tension pull-off test, which are commonly used for

quality control in field structures. This suggest that the reliance solely on pull-off tests may substantially underestimate the actual bond capacity under service conditions. Given the variability in pull-off strength results, performance standards should consider factors such as concrete type and application to better reflect real-world conditions.

Comparable peak strain values were observed between single and double shear-lap tests; however, mixed-mode loading resulted in higher peak strains compared to single-mode loading, although bond strength values were similar across beam and shear-lap tests. The experimental measured strains were significantly lower than the limits specified by design codes, suggesting discrepancies between these limits and the real performance of specimens exposed to prolong environmental wear and service loads. This also highlights the need for future investigations into the interaction of high-strength concrete and externally bond CFRP materials.

The research found that bond line degradation influenced the fracture surface, with pull-off testing revealing adhesive failure between layers, mixed mode failure between concrete and CFRP, and separation during drilling. Beam tests indicated failure at the adhesive-concrete interface, with traces of cementitious concrete material and a large area of exposed adhesive/primer and typical cohesive debonding failure within the substrate with a thin layer of concrete attached to the CFRP sheets.

Comparison with existing literature indicated that laboratory-prepared specimens, with lower concrete strength and CFRP axial stiffness, attained higher strain values than the deteriorated bridge specimens in this study. In the experimental work, load transfer was notably limited in areas with field defects, identified from various NDT methods, with defective regions achieving only 8-15% of the maximum peak shear stress. These defective regions also exhibited non-linearity with multiple shear stress peaks.

The comprehensive findings from this work have been documented in scientific publications, detailing the performance of the Champlain Bridge concrete elements retrofitted with CFRP. The numerical modelling phase highlighted the complexities in modeling CFRP-strengthened deteriorated concrete. Challenges including the characterization of the non-uniform degradation of concrete properties, variability in material layers, and out-of-plane displacement observed in the experimental conventional single shear-lap tests, all of which are crucial for accurate capturing bond response in ageing infrastructure that have undergone multiple repair interventions. Based on the results gathered from the various stages of this comprehensive assessment of the bond integrity between CFRP and concrete in deteriorated concrete bridge elements, the following summarized conclusions and observations were made while the specific detailed conclusions are included in the different chapters:

- **Limitations of selected NDTs for Condition Assessment**: The inherent limitations of individual NDT techniques necessitate a multi-method approach for comprehensive structural assessment. Integrating localized methods such as coin and hammer tapping with area scanning techniques such as infrared thermography provides a more robust and reliable structural integrity evaluation.
- **Condition Assessment**: This phase of the work revealed that defects in the bridge diaphragm were primarily concentrated in areas with multiple layers of CFRP and near the diaphragm-girder joints experiencing significant force transfer. NDT assessment revealed that over 95% of the CFRP-bonded area remained intact after over half a decade of exposure to aggressive environmental conditions in Montreal. The direct tension pull-off confirmed NDT results, showing that approximately 96% of the tested CFRP pull-off samples exhibited failure in the concrete substrate, indicating good bond durability. However, it was observed that the minimum values of the direct tension pull-off test set by current design codes neglected concrete type and application to reflect real-world conditions.
- **Single Mode loading**: The customized design implemented for the new single shear-lap test setup and double shear-lap tests effectively characterized the bond between FRP and concrete under shear loading. However, the new single shear-lap configuration experienced out-of-plane rotation, which

reduced net strain measurements. In contrast, the double shear-lap configuration minimized out-of-plane displacement. Similarly, the strain observations showed that the experimental strains were significantly lower than the code values, with measurements averaging approximately 56% of the debonding strain limit set by ACI PRC-440.2-23 and 27% lower than the limits established by CAN/CSA S6:19. A non-uniform strain distribution was observed across the FRP sheet width. Comparison of the experimental strains from the shear-lap tests in this research with values from the literature of similar geometry and lower material strength showed that pristine laboratory-prepared specimens with lower material strength (concrete compressive strength and axial stiffness) showed higher peak strain values than the deteriorated bridge elements which had higher concrete strength and axial stiffness tested in this research.

- **Mixed Mode loading**: Experimental observations from beam tests revealed that bond line deterioration in degraded concrete significantly influenced debonding failure mechanisms within the concrete or the adhesive layer. The flexural beam tests also demonstrated that existing design codes and literature models inadequately predict debonding limits for deteriorated concrete members strengthened with bonded CFRP. Specifically, the Chen and Teng model underestimated the ultimate load and strain by 18 to 41 percent, while the FIB-14 model overestimated these values by 15 to 126%. The ultimate strain recorded in all debonded beams was approximately 50% of the values calculated according to ACI PRC-440.2-23 provisions for debonding strain, and the strain limit provided in the Canadian code (CAN/CSA S6:19) exceeded the maximum experimental strain by 34%. Additionally, load transfer was limited in areas with field defects identified by various NDT methods. The maximum bond stress over defective areas represented only 8-15% of the maximum peak bond stress in the beams.
- **Comparison of single and mixed-mode loading:** The average bond strength values derived from beam and shear-lap tests exceeded those from direct tension pull-off tests by 88% and 82%, respectively. The mixed mode loading in the beam tests induced higher peak strains than the single mode loading scenarios in the shear-lap tests. There is a minor discrepancy in the effective bond

length beam from the beam tests and single shear-lap configurations. The estimated stress transfer length from the beam tests ranged from 205 to 230 mm across beams, while shear-lap tests showed approximately 150-155 mm in transfer length. However, the minimum bonded width in the beam tests, set at 200 mm, was twice the bonded width of the new single shear-lap configuration and twice the total bonded width of 100 mm from the double shear-lap tests (considering both surface). The bonded width of the beams are also four times greater than that of the conventional single shear-lap specimens.

- **Advanced sensing technologies**: This research demonstrated a strong correlation between strain data from three measurements in measured peak strains: conventional discrete electrical strain gauges, distributed fibre optic sensing (DFOS), and full-field 3-dimensional digital image correlation (DIC). However, DFOS, installed longitudinally in beam tests, proved crucial for observing the nonlinear behaviour of bond stress. In shear-lap tests, strain and corresponding bond stress curves derived from DIC showed enhanced stability and reduced data scatter compared to bond stress-slip data from gauges reported in the existing literature
- **Finite Element Modelling**: Accurate modeling of the bond interface between CFRP and concrete for deteriorated interfaces requires appropriate techniques, such as the cohesive zone material approach. The incorporation of the CZM approach led to highly accurate predictions of structural response of beams originally tested by Obaidat et al. with a maximum discrepancy in peak load of 3.6%. The calibrated CZM models successfully captured the nonlinear behaviour of the 57-year-old deteriorated concrete specimens extracted from the Champlain bridge under both mode II and mixed-mode loadings, with only a 12% difference in peak strain between experimental results and numerical predictions for the flexural beams. Under shear-lap configurations, the best correlation between experimental results and FEM numerical strains occurred when an out-of-plane displacement was introduced as observed experimentally. An excellent agreement in strain distribution was captured when the ratio of in-plane displacement to out-of-plane displacement is set to 1 for the conventional single shear-lap test configuration.

This comprehensive study on the field performance of CFRP retrofits on the deconstructed Champlain Bridge diaphragms from Montreal, involving non-destructive evaluations, multiple destructive testing and numerical simulations, demonstrates that after over half a decade of exposure to the synergistic effect of the severe Canadian weather in Montreal and service loads, the CFRP composite material remained in generally good condition. Observations of critical bond degradation in some regions of the bridge elements, primarily linked to poor installation practices, were evident over this short service life of the composite repair which was exacerbated under service conditions. Despite this, the CFRP-concrete interface maintained a relatively good durability under harsh environmental exposure given the large, bonded area. The various bond testing revealed that the level of deterioration in the underlying concrete substrate significantly impact the effective strains that can be developed in the CFRP composite materials.

In conclusion, this research establishes a comprehensive methodology for assessing the long-term performance of CFRP-concrete interfaces in field structures. It simultaneously developed new tools for bond assessment in the laboratory setting and provides extensive database in the relatively under researched area of CFRP-concrete interaction in high-strength concrete. The integration of NDTs, various destructive testing techniques, along with advanced sensing and numerical modelling, this research offers a robust approach that future engineers and bridge management practitioners can follow to develop improved and better-targeted maintenance and repair protocols. Engineer do not need to implement the comprehensive approached described in this thesis but can use this finding as a resource to provide specific management recommendation for similar crumbling infrastructures. This work has practical significance in calling for optimizing the design guidelines revisions to overcome it currents limitation in predicting the stress and strain response of deteriorated strengthened concrete members.

8.3 Recommendations for Future Work

This research presents the first comprehensive assessment of the CFRP-concrete bond interface in real structural elements exposed to fluctuating weather conditions and service loads. The insights gained from this project have led to the following recommendations aimed at enhancing our understanding of the bond between CFRP and deteriorated concrete members:

- **Establishment of quality database**: A rigorous database should be established to document the bond performance of in-situ structural elements retrofitted with composite materials, prioritizing material and structural testing for CFRP-strengthened structures designated for decommissioning. Data fusion from multiple NDT sources should be emphasized for comprehensive structural integrity assessment.
- **High-strength materials**: Research on CFRP-concrete bond behaviour for high-strength concrete is less complete than for regular-strength concrete. Current design codes limit FRP application to normal-strength concrete due to a lack of understanding of CFRP bond behaviour with high-strength concrete.
- **Microanalysis**: While the current research has contributed to our understanding of the effect of bond line defects on stress distribution, further detailed research into the effects of bonding defects in externally bonded strengthening systems is recommended. Research to correlate the microstructural performance of CFRP-concrete bond interface to structural bond performance is a recommended future research path.
- **Analytical modelling**: The application of advanced FEM procedures for modelling the debonding mechanism in deteriorated concrete with externally bonded CFRP is under-explored. There is a lack of research focused on developing FEM models that incorporate time-dependent environmental exposure effects on bond deterioration. Integrating the digital twin concept into FEM models will help real-time defect mapping and progressive damage tracking and this will transform FEM tools into a life-cycle management system for CFRP-strengthened bridges. A

digital twin allows for real-time monitoring and simulation of the physical structural system, providing a comprehensive understanding of how environmental factors impact bond performance over time.

- **Realistic loading**: CFRP installation of bridges usually occurs while the structure is still subjected to a certain load level. More research is needed to investigate the impact of pre-strain or stress on initial CFRP-concrete bond strength. This current work has also considered the effect of test setup and loading direction on bond performance. Other mixed mode loading, such as the variable angle peel tests and punching peel tests, could be of research interest. Appended to this document is a viable design for testing the CFRP-concrete interface under variable peel angles.
- **Sensing techniques**: It should be paramount to utilize innovative sensing techniques (e.g., distributed fibre optic sensors, digital image correlation) to understand multidirectional performance and local failure. DFOS sensors can continuously monitor strain profiles under live loads and thermal cycles, allowing for a detailed understanding of temperature-induced strain variations, particularly in fluctuating environmental conditions. These sensors can also be used to detect early-stage delamination before visible cracking occurs, enabling predictive maintenance, especially in CFRP repair where damage is masked. By synchronizing these advanced sensing techniques, it is possible to achieve an integrated sensor fusion for multidirectional analysis. This approach can support future engineers in moving from conservative code-based design practices to performance-driven CFRP repairs for aging bridges.
- **Standardization:** Standard protocols should be established for testing CFRP-concrete bond under mode-II loading. Although mode II loading, which is characterized by in-plane shear interactions at the CFRP-concrete interface, has been extensively studied in the laboratory, no standardized protocol currently exists. Researchers often design their tests in a customized manner, which complicates direct comparisons of experimental results across different studies focusing on mode-II bond tests. A standard protocol that specifies the test setup and configuration, including

specifications for dimensions, loading apparatus, and alignment methods can help to ensure reproducibility and accuracy of results.

Appendix A: Non-destructive tests for concrete

A.1 Rebound hammer

For the sake of simplification and highlighting the randomness of the values obtained for the rebound hammer test, a plot of the obtained values is presented in the graphs below. These values were extracted from the concrete regions between the strips and the diaphragm-slab joint.

The rebound hammer test was performed in accordance with ASTM C805 using Proceq rebound hammer device. The procedure involved cleaning the area between the CFRP strips with a rub stone and compressed air and 10 spots that were evenly spaced along each concrete strip were then marked and tested. The test was conducted by vertically pushing the plunger on the device against the concrete surface downwards (ensuring that the impact hammer is perpendicular to the surface of the concrete) and readings from each spot were recorded. The rebound hammer is one of the most used NDT to assess the uniformity of the concrete. Several factors can influence the rebound number in Table 0.1 and Figure A.0.1 to Figure A.0.3, including the relative stiffness and conditions of the near-surface concrete layer, variations in concrete consolidation.

A slight variation was observed in the average values rebound values for the three diaphragms. The average rebound numbers recorded as 54.42, 50.72, and 52.50 for diaphragms 1, 2, and 3, respectively (see Table 0.1). The coefficient of variations for these values were calculated to be 4.18%, 8.76%, and 7.46%, respectively. These recorded values suggest that the underlying concrete substrate in the three diaphragms exhibited similar hardness and uniformity. Consequently, it was expected that the as-is compressive strength of the three diaphragms will be comparable, irrespective of the damage to each concrete three diaphragms. Testing confirmed that the compressive strength of the diaphragms is approximately 76 MPa, consistent with high-strength concrete.

Table 0.1-Average rebound hammer values

	Diaphragm 1		Diaphragm 2		Diaphragm 3	
	Mean	SD	Mean	SD	Mean	SD
Strip 1 (between CFRP strip 1&2)	54.1	2.05	52.4	5.30	48.9	5.36
Strip 2 (between CFRP strip 2&3)	54.3	2.00	52.7	3.97	54.4	2.17
Strip 3 (between CFRP strip 3&4)	54.2	2.74	51.6	2.63	50.5	5.10
Strip 4 (between CFRP strip 4&5)	54.2	1.66	49.1	5.62	52.3	2.36
Strip 5 (between CFRP strip 5&6)	55.4	2.72	47.9	4.58	56.4	4.35

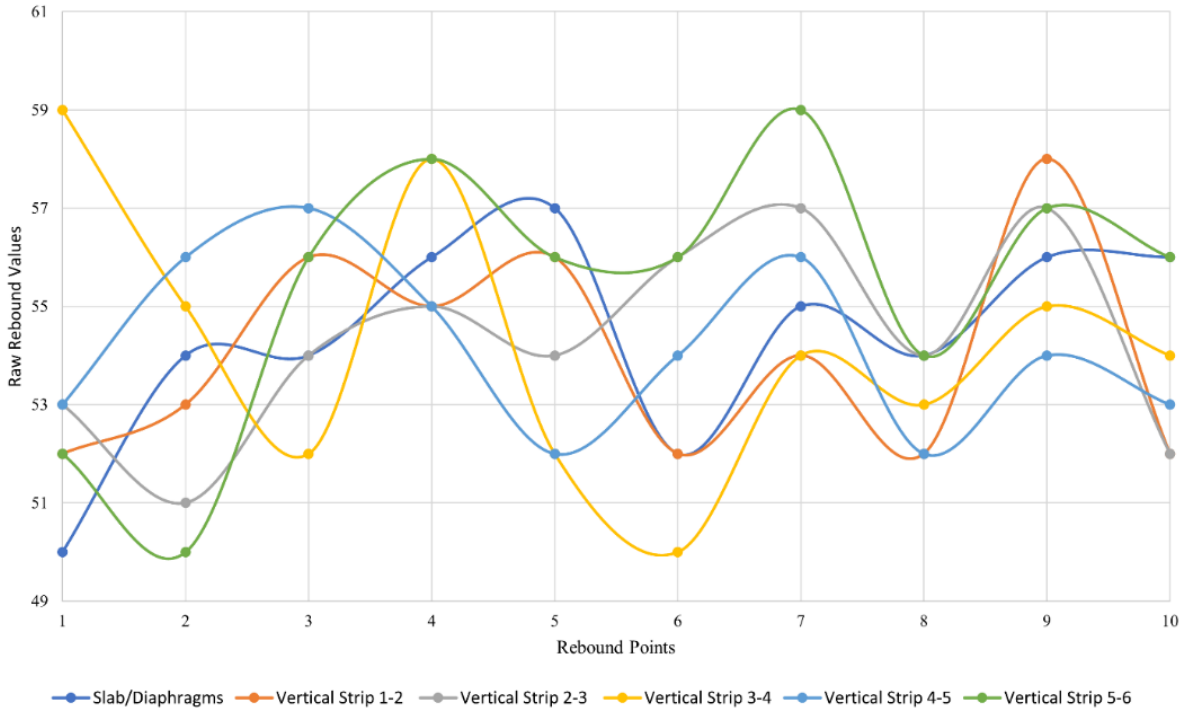

A.0.1-Rebound hammer values of diaphragm I

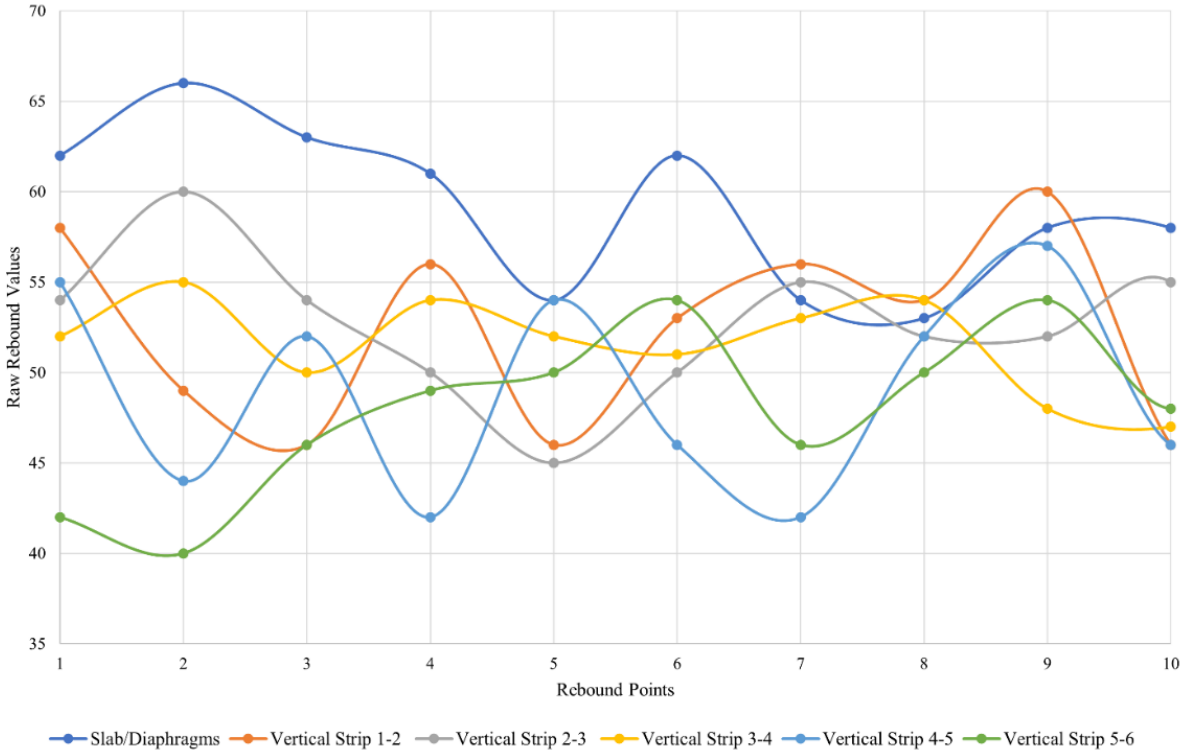

A.0.2-Rebound hammer values for diaphragm II

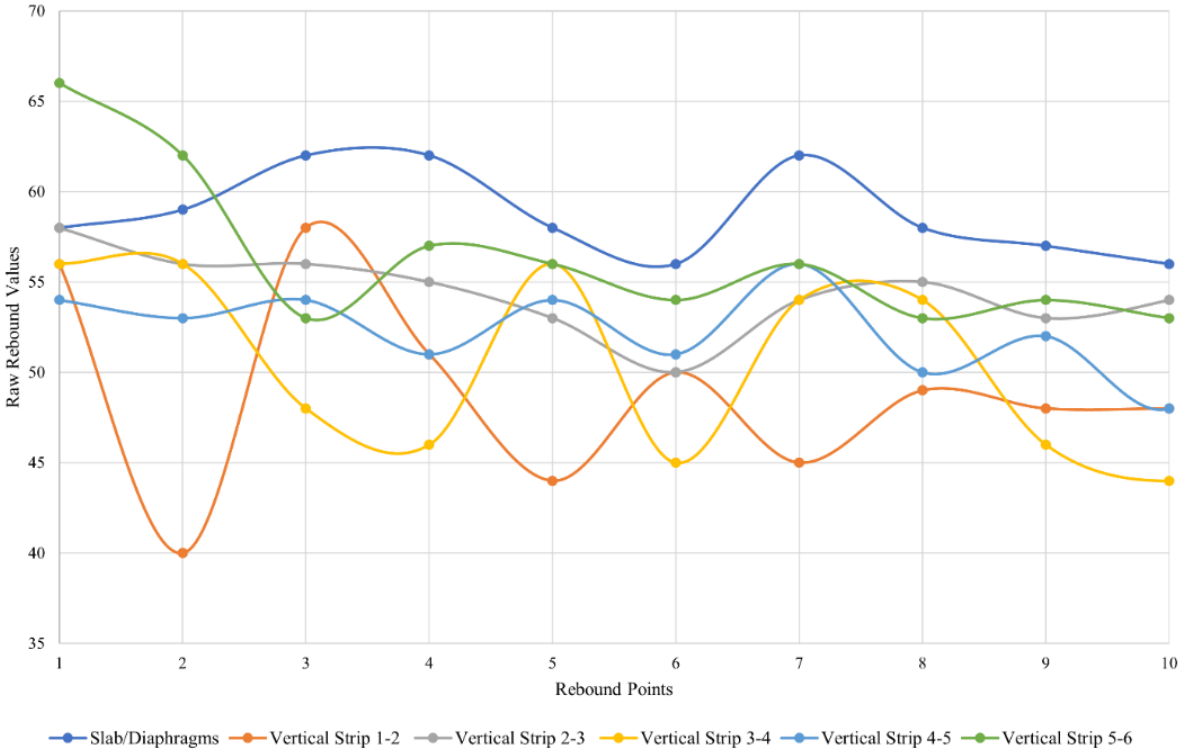

A.0.3-Rebound hammer values for diaphragm II

A.2 Ultrasonic Pulse Velocity (UPV)

Due to size of the members, access to both surfaces at the same time was impossible hence the UPV was conducted using the indirect method. In this approach the transducer and receiver are placed on the same surface. Values obtained for the diaphragms are plotted in below. The strips here refer to regions of concrete between the vertical CFRP strips. Hence strip 1 represent the concrete strip between CFRP strip 1 and 2 and strip 5 corresponds to the concrete strip between the CFRP strips 5 and 6. The visual inspection of the concrete gaps between the CFRP strips did not reveal visible cracks; however, the indirect UPV testing indicates that the concrete in the diaphragms is of poor quality. The UPV measurement for the six surfaces of the three diaphragms were analysed and presented in km/s according to the quality assessment methods described in (Saint-Pierre et al. 2016), summarized in Table 0.2. Table 0.3 presents the average UPV values per surface for the six inspected surfaces, along with the raw data for each strip in Figures A.0.4 to A.0.9. As indicated in Table 0.3, average UPV values per surface ranged from 2.43 km/s -2.58 km/s across the diaphragms indicating a poor-quality concrete.

Table 0.2- Concrete Quality Designation (Saint-Pierre et al. 2016)

UPV (km/s)	Concrete Quality
>4.5	Excellent
3.6-4.5	Good
3-3.6	Doubtful
2.1-3	Poor
<2.1	Very poor

Table 0.3-Average UPV values (km/s)

	Diaphragm 1		Diaphragm 2		Diaphragm 3	
	Side1	Side2	Side1	Side2	Side1	Side2
Strip 1 (between CFRP strip 1&2)	2.69	2.54	2.12	2.38	2.13	2.23
Strip 2 (between CFRP strip 2&3)	2.37	1.87	2.40	2.47	3.13	2.33
Strip 3 (between CFRP strip 3&4)	2.31	2.83	2.13	2.82	2.83	2.20
Strip 4 (between CFRP strip 4&5)	2.23	2.70	3.04	2.62	2.01	3.15
Strip 5 (between CFRP strip 5&6)	2.78	2.26	2.62	2.62	2.03	2.51
	2.48	2.44	2.46	2.58	2.43	2.48

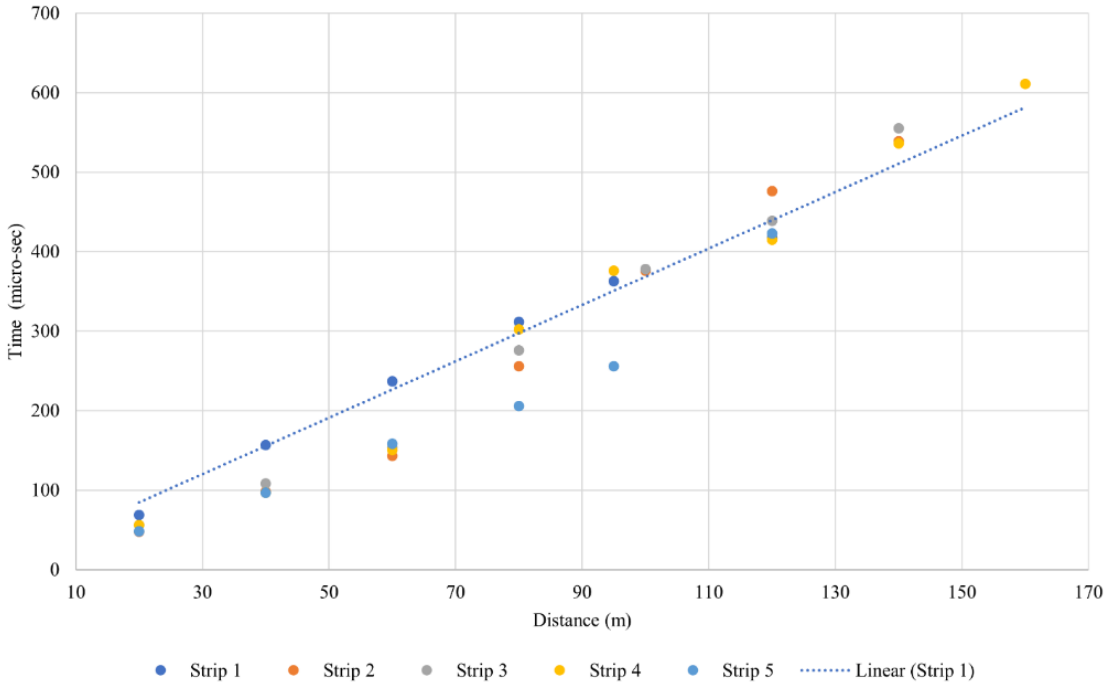

A.0.4-UPV readings for diaphragms I Surface 1

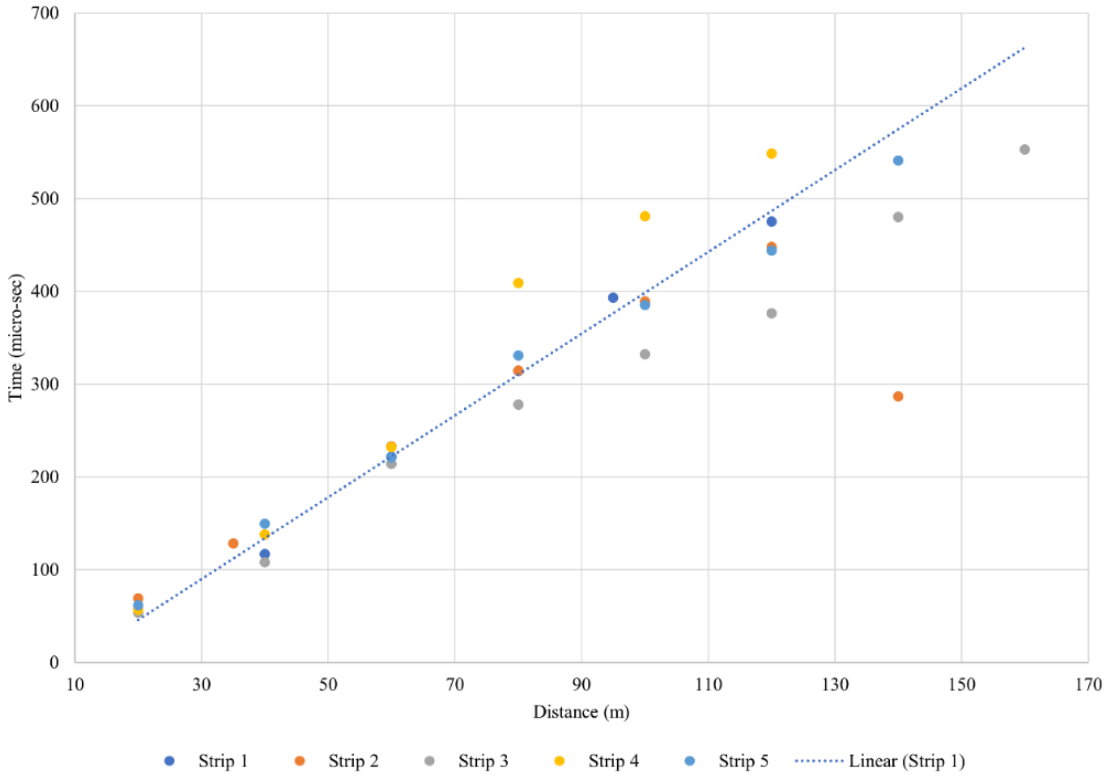

A.0.5-UPV readings for diaphragms I Surface 2

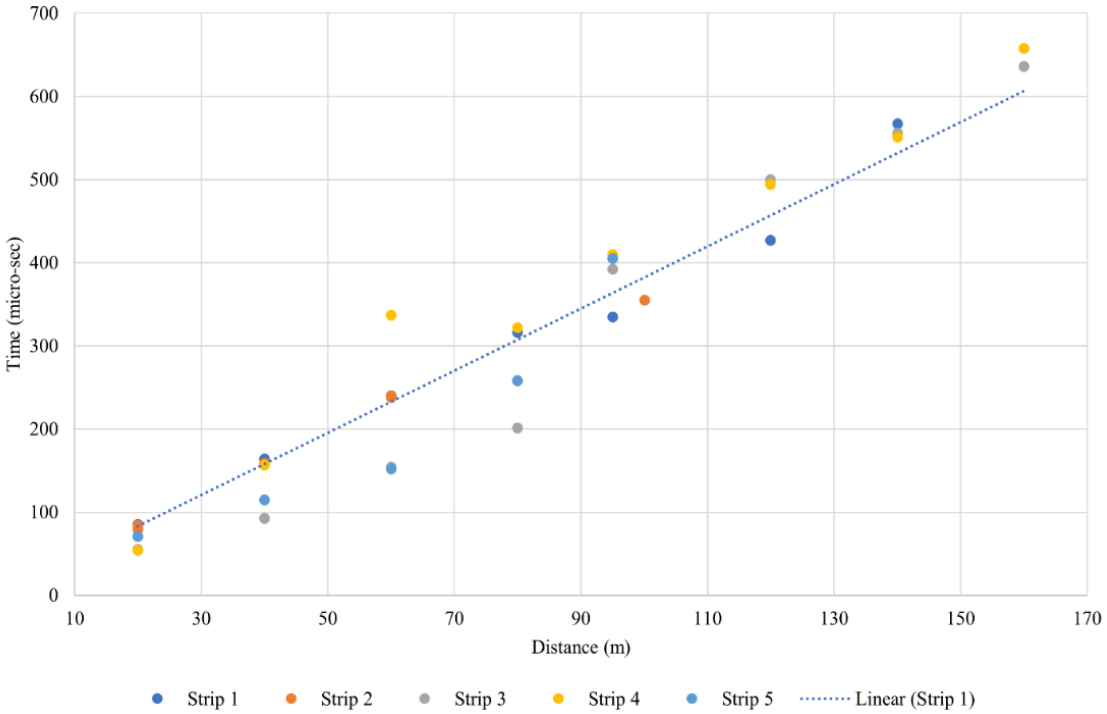

A.0.6-UPV readings for diaphragms II Surface 1

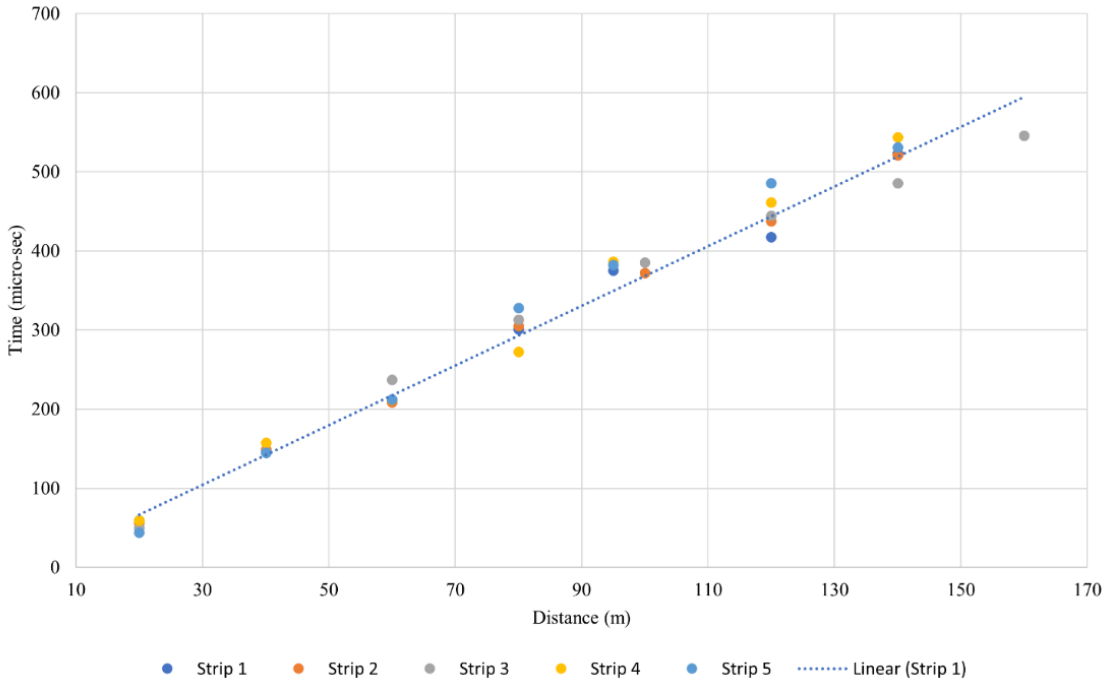

A.0.7-UPV readings for diaphragms II Surface 2

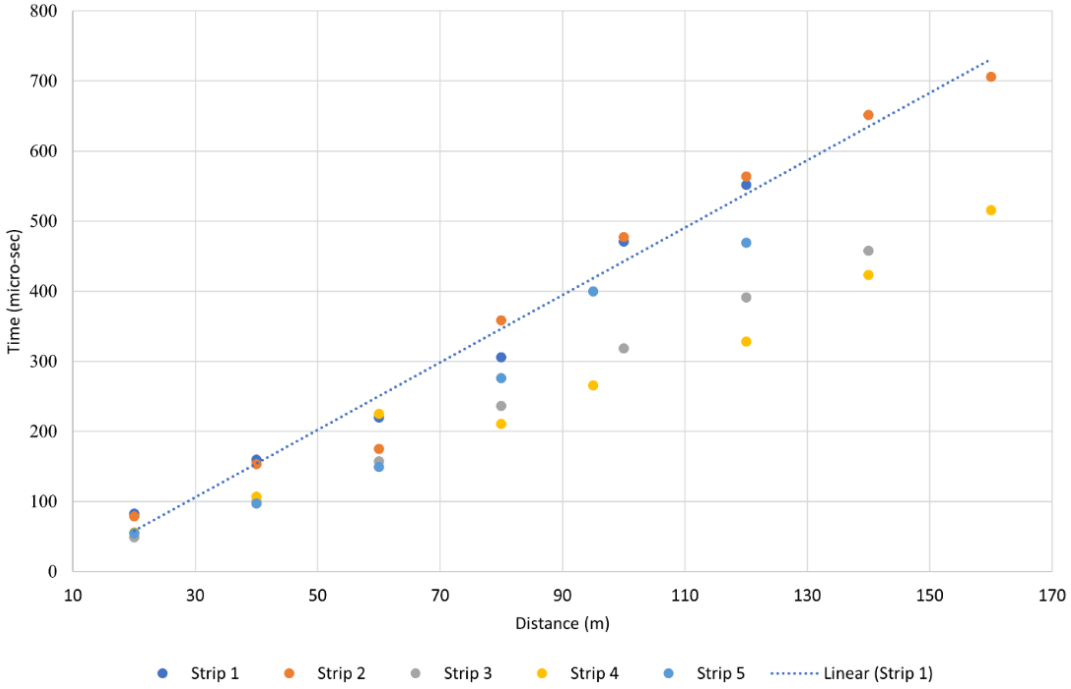

A.0.8-UPV readings for diaphragms III Surface 1

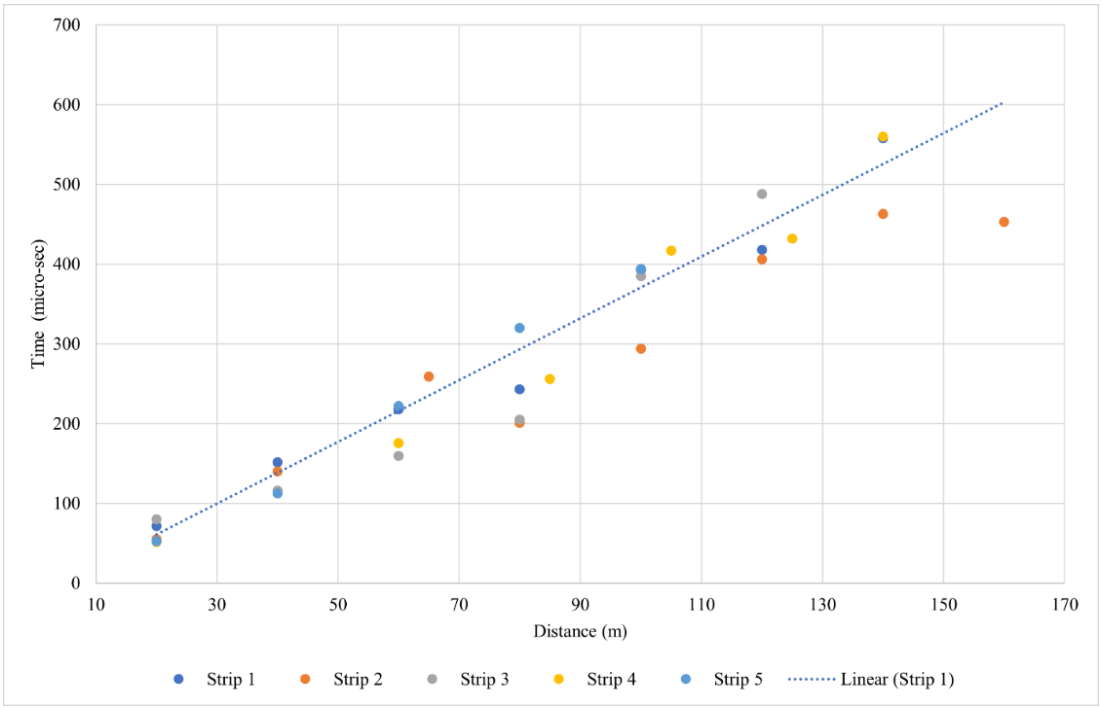

A.0.9-UPV readings for diaphragms III Surface 2

Reference

Saint-Pierre, F., Philibert, A., Giroux, B., & Rivard, P. (2016). Concrete quality designation based on ultrasonic pulse velocity. *Construction and Building Materials*, *125*, 1022-1027.

Appendix B: Defect locations

The location of all defects located on the front and back surfaces of the CFRP wraps as obtained from visual inspection and other NDT testing mentioned earlier are shown below. In these images, major defects are numbered in red while minor problems and small issues are shown in yellow and purple respectively. Benign issues such as over usage of paste are shown in blue.

B.1 Diaphragm I

B.0.1-Defects on top surfaces of Diaphragm #1 side I (on the left) and side II (on the right)

B.2 Diaphragm II

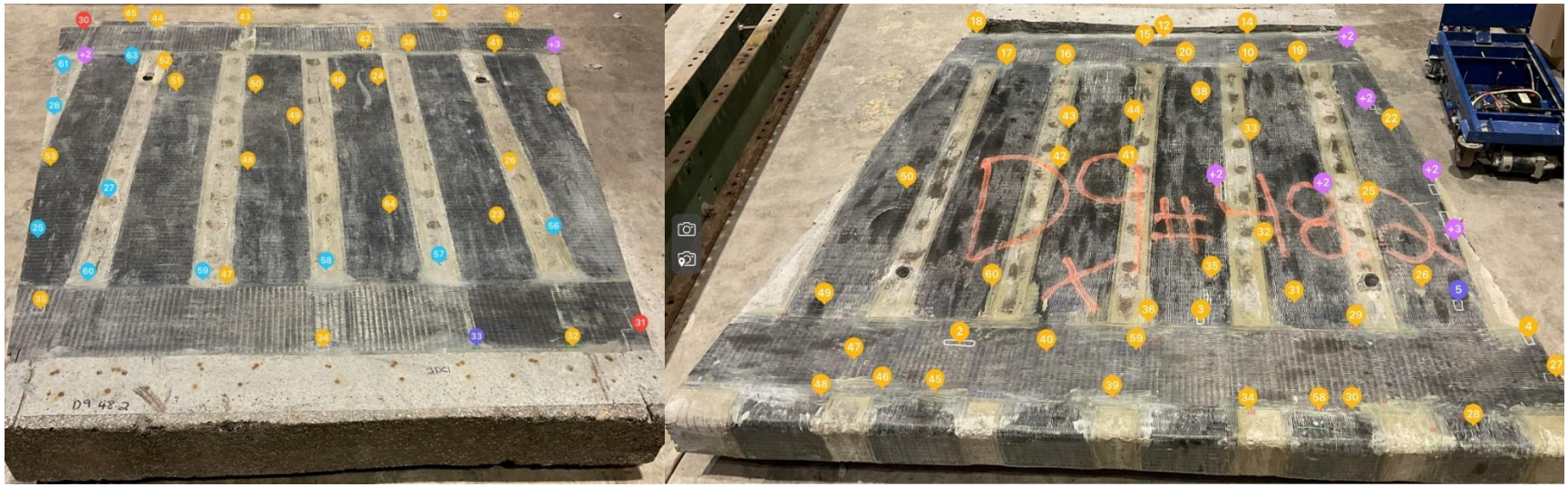

B.0.2-Defects on top surfaces of Diaphragm #2 side I (on the left) and side II (on the right)

B.3 Diaphragm III

B.0.3-Defects on top surfaces of Diaphragm #3 side I (on the top) and side II (on the bottom)

Appendix C: Recommendation for bridge safety: Best Practices for Future Maintenance and Repair of CFRP-strengthened concrete structures

This section of the appendix uses knowledge gained from the investigation into the rapid deterioration of the Champlain Bridge to emphasize proactive measures that bridge management can implement to prolong the service-life of ageing infrastructure. The information presented here builds upon and complements existing guidelines by offering practical, actionable enhancements that reflect emerging best practices and technologies advancement that are currently absent from existing guidelines. The appendix provides specific recommendations leveraging technologies to inspect hard-to-access areas of bridge structures and offers guidance on cold weather installation and material compatibility, which were significant issues neglected during the CFRP installation undertaken on the bridge elements examined in this thesis. Although some guidelines reference NDT and semi destructive methods, the integration of sensor-based monitoring represents an emerging practice that has not yet been adopted or codified in existing standards. The detailed recommendation for semi-destructive testing, such as pull-off tests, are based on extensive data collected by the author from the deteriorated Champlain Bridge. This data can serve as a benchmark for future comparisons and highlight the use of the pull-off test not only for quality control but also for correlating bond line deterioration with bond performance.

- **Documentation of Inspections:** whether conducting routine visual inspections or thorough biennial inspections, it is essential that detailed recording of identified signs of wear, corrosion or damage to the CFRP material be well kept for both primary and secondary load-carrying members. This documentation will serve as baseline data for future research, especially in the event the structure is decommissioned for study.
- **Use of Technology:** While real-time monitoring of the structural health of the retrofitted structured may not always be practical, the option to use Unmanned Aerial Vehicle for structural elements

that are difficult to access should be strongly considered. This approach could facilitate the development of rapid response protocols for significant findings during field inspections.

- **Importance of environmental exposure data:** It is no secret that rehabilitation designs should be prioritized over the construction of new structures when possible. In existing structures changes in environmental conditions and traffic loads should be well documented when planning repair interventions, particularly in regions subject to harsh environmental conditions.
- **Familiarity with Inspection Guidelines:** Inspectors and maintenance personnel must be knowledgeable about national and international guidelines for FRP inspection, including resources such as the National Cooperative Highway Research (NCHRP) Report 514. In Canada, the design and installation of FRP rehabilitation systems should adhere to the requirements specified in the national standards for bridges (CAN/CSA S6) and the CSA S806 standard for buildings applications. Industry standards such as the American Concrete Institute guideline ACI PRC-440.2-23 provide a valuable and reputable reference for best practices and technical guidance in the application of FRP materials.
- **Cold Weather Installation:** When applying FRP in cold regions, special attention should be given to ensuring that the adhesive cures properly at the appropriate temperature during cold season installations. Technology such as vacuum infusion will help minimize installation imperfections.
- **Compatibility of Material:** Special effort should be placed in understanding the compatibility of the concrete patch mortar or grout, newly installed FRP, and the existing deteriorated concrete to ensure structural integrity or composite behaviour.
- **Inspection Methods:** Both localized point inspection and area scanning methods should be prioritized in CFRP-concrete bond inspection.
- **Embedded Sensor Technology:** when possible, to better understand the performance of composite repaired structures or monitor optimal cure conditions embedded sensors such as fiber optic sensors, piezoelectric sensors and thermocouples can be used. This will allow for history on when defects

are introduced to the bond line and how performance changes throughout different seasons and over time. The collected data will also enable more informed decision-making regarding maintenance, potential repairs, or replacement, enhancing the longevity of the structure.

- **The role of semi-destructive testing for field structures:** NDT inspection should be followed by semi-destructive tests, such as the direct tension pull-off test, to correlate NDT findings with the actual bond performance. As discussed in Chapter 4 of this thesis, the current standard for pull-off testing mandates a minimum of three tests to evaluate the bond performance of composite-strengthened structures, serving as a quality control measure. In maintenance contexts, pull-off tests can be used to assess the condition of existing CFRP systems and guide decisions about additional retrofitting strategies. The work presented in Chapter 4 demonstrated that the pull-off test is critical for benchmarking the adhesive performance of repair structures. Although the Pull-off test does not replicate the realistic stress state that involves both shear and normal stresses at the CFRP-concrete interface, as evidenced by this extensive research, it remains a cost-effective method to quantify the adhesive bond strength in both defective and defect-free regions on CFRP retrofitted structural elements. This information can be used to identify and map out areas within the repair structure where stress transfer is compromised.

Appendix D: Details of the proposed new single and double shear-lap setup

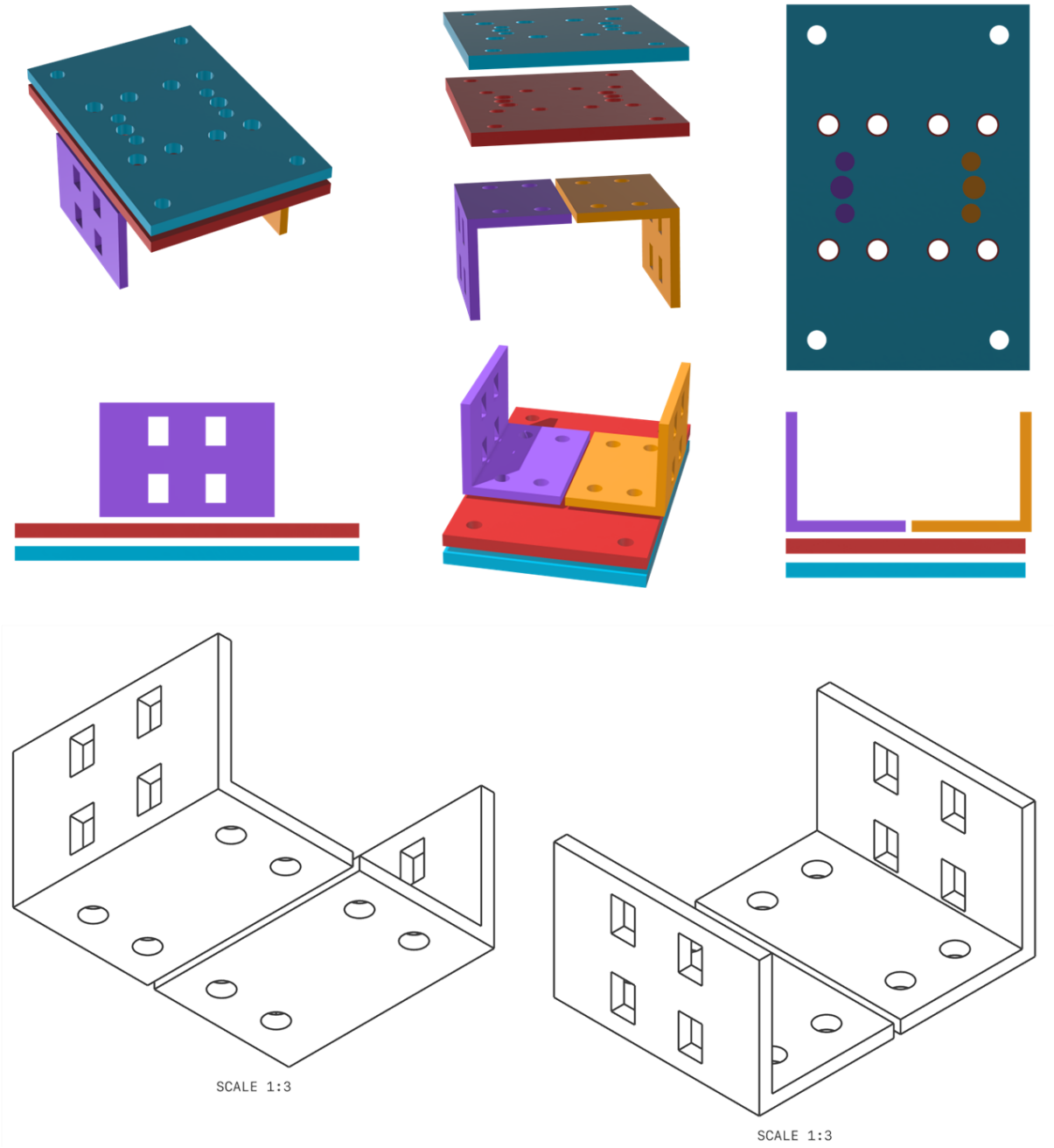

D.0.1-Isometric view of clamping system for shear-lap tests

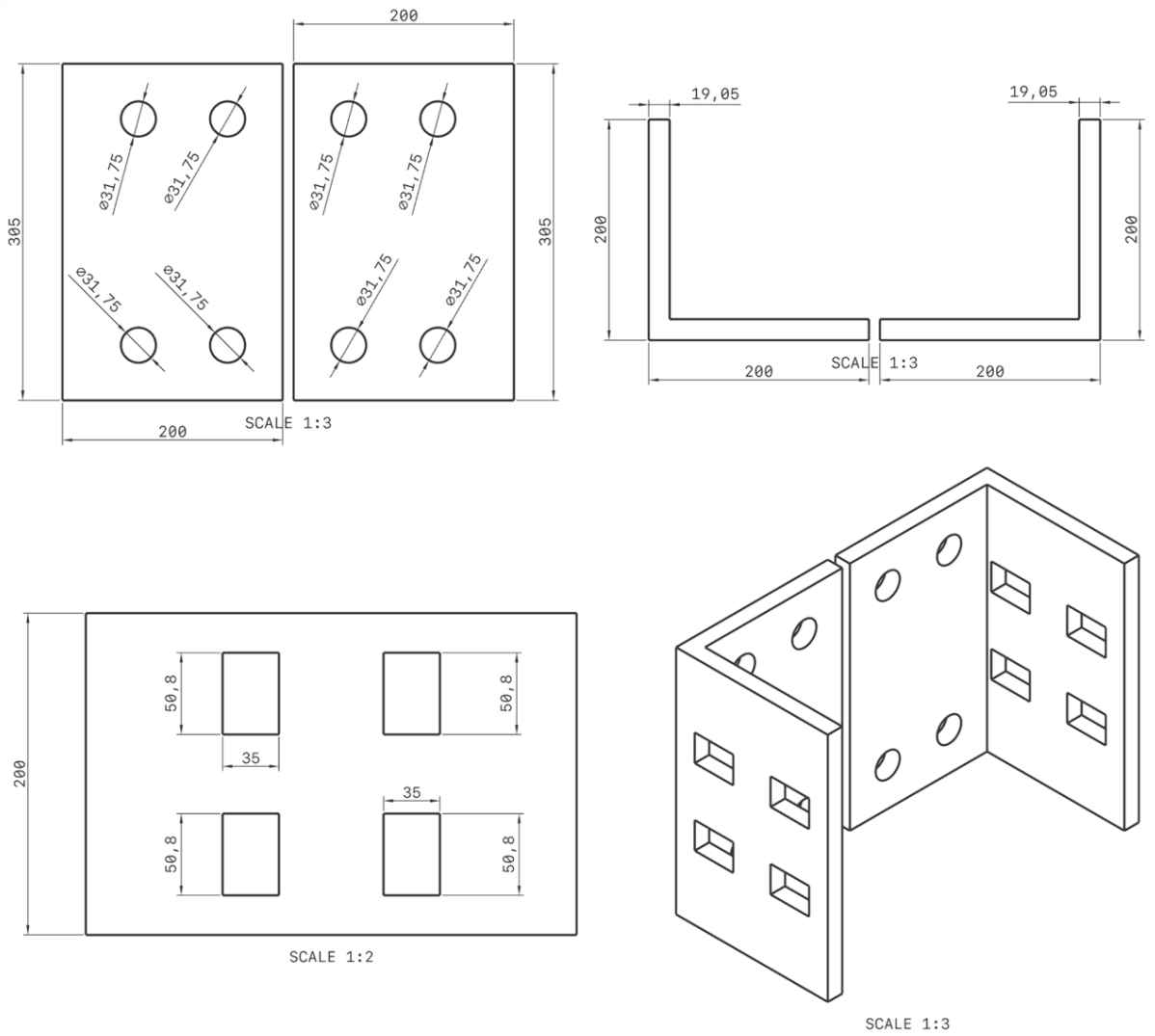

D.0.2-Dimension of angle plates

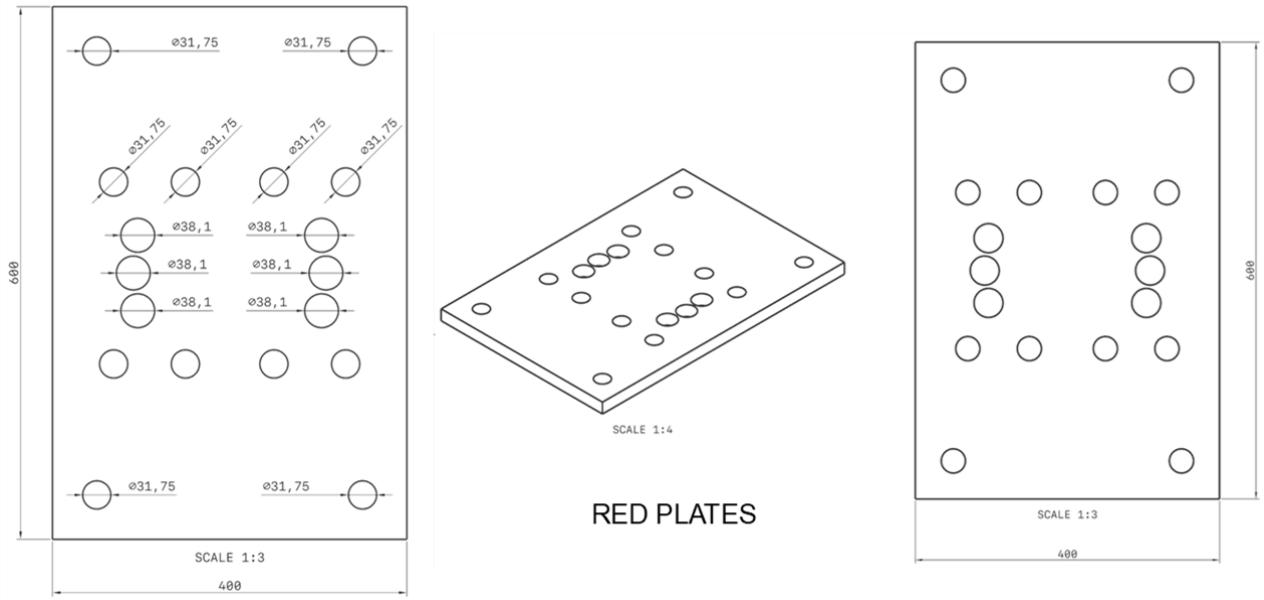

D.0.3-Red plates from D.0.1

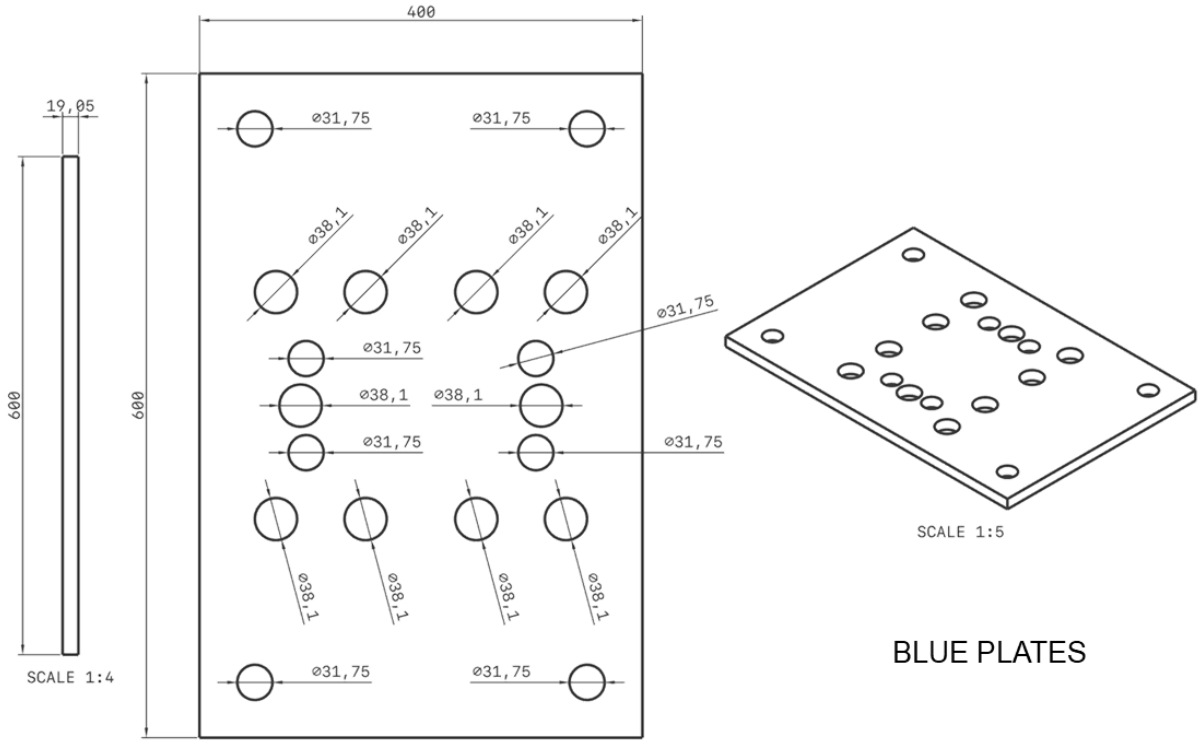

D.0.4-Blue plates from D.0.1

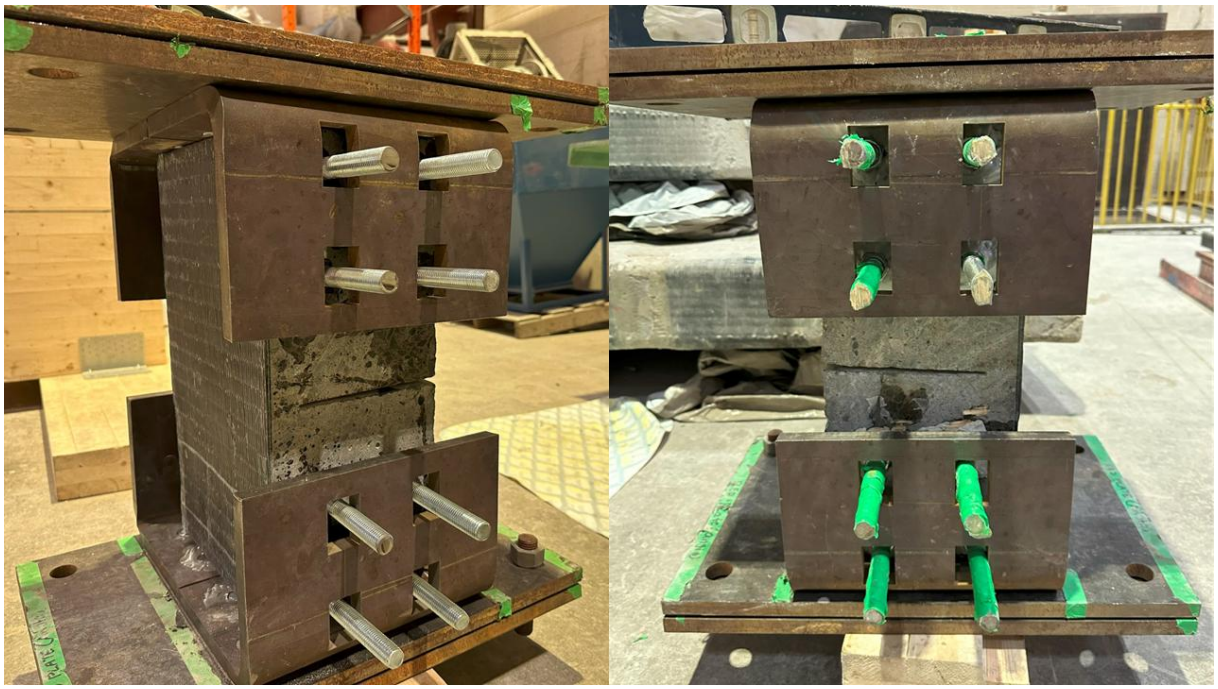

D.0.5-Final fabrication

Appendix E: Details of proposed variable angle peel setup for mixed mode loading

Results of experimental calibration can be found in (Fowai et al., 2022).

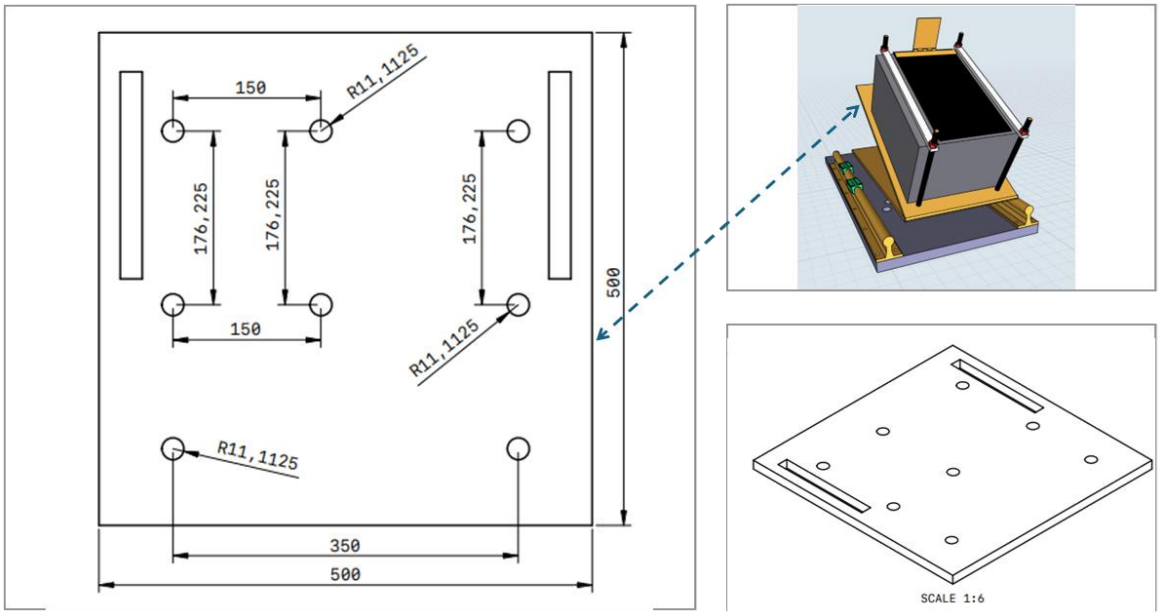

E.0.1-Dimension of sine plate

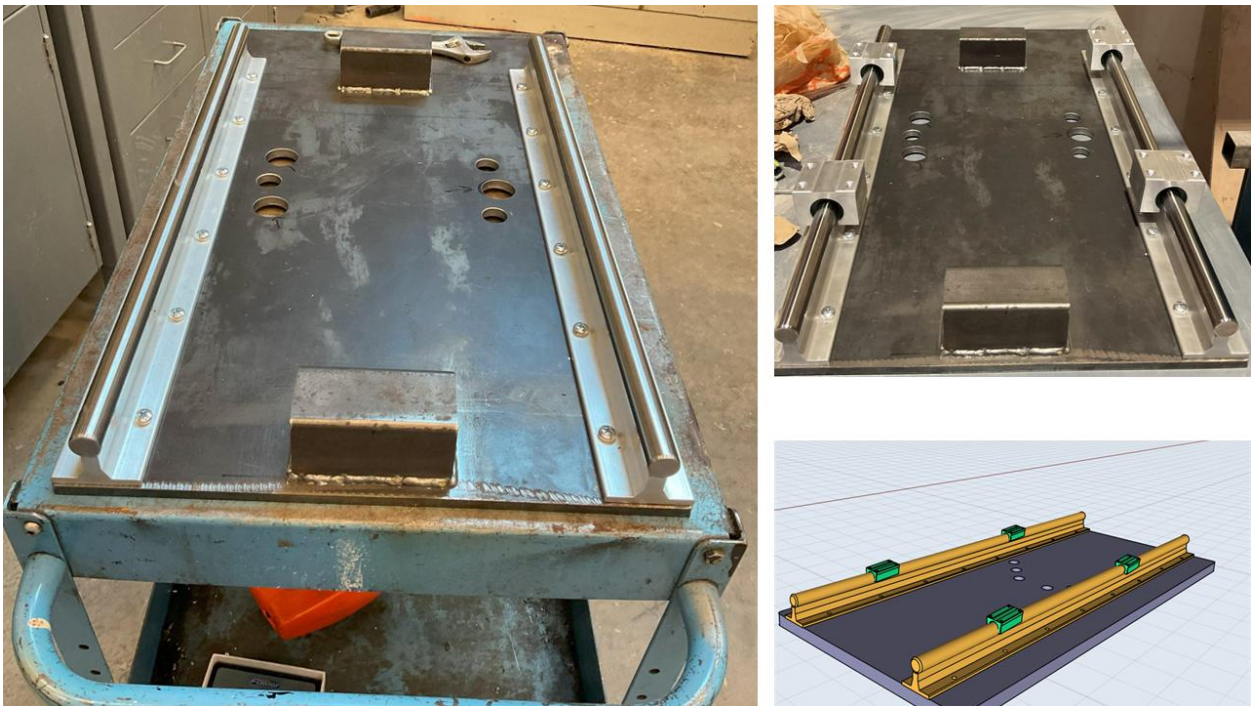

E.0.2-Fabricated base plates

E.0.3-Final fabricated sine plates

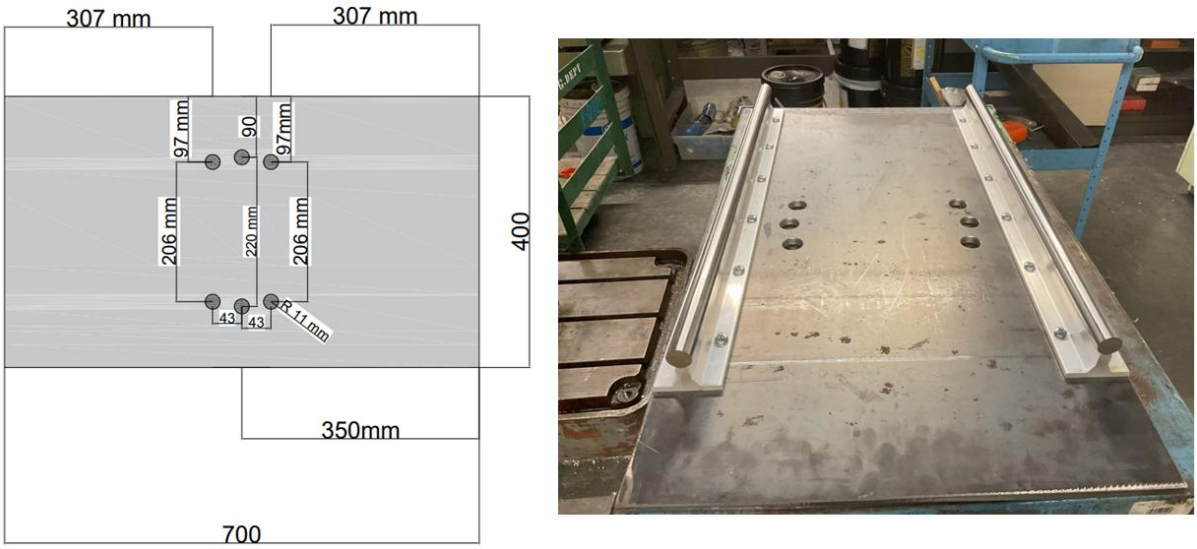

E.0.4-Dimension of base plate

Reference

Fowai, I., Noël, M., Martin-Perez, B., & Sanchez, L. (2022). Evaluation of interfacial debonding of fibre-reinforced polymer using variable angle peel test. In *Bridge safety, maintenance, management, life-cycle, resilience and sustainability* (pp. 2526-2532). CRC Press.

Appendix F: Methods, Obstacles, and Insight Gained

F.1 Reference specimens and pilot tests

Prior to conducting the bond tests detailed in Chapters 4 to 6, preliminary pilot experiments were performed using newly cast laboratory specimens. These trials aimed to calibrate and comprehend the behaviour of the various test setups before application on the unique bridge diaphragms received from the Champlain Bridge. The outcomes of these pilot studies validated the need for specific modifications, such as the addition of external shear reinforcement (bracing rods) during beam testing. They also confirmed the reliability of the condition assessment techniques, as well as established protocols for executing the direct tension pull-off tests. Although the results from the pilot trials cannot serve as direct reference specimens for the bridge elements due to variation in material properties and quality of the extracted data during the pilot tests, they provide valuable insight into the holistic approach adopted for the evaluation of the field performance of the CFRP retrofits on the Champlain bridge diaphragms. In Chapter 5, a few references of undamaged specimens from existing literature were used for direct comparison with damaged bridge specimens from the bridge diaphragm under shear-lap behaviour. Future research could focus on a comprehensive, direct comparison between undamaged specimens specifically prepared to match the material properties (CFRP, concrete and adhesive) of the extracted bridge elements.

F.0.1-Formwork and laboratory specimens for direct tension pull-off tests

F.0.2-Mock samples for direct tension pull-off testing and concrete failure mode

F.0.3- Laboratory specimen preparation for bending tests

F.0.4-Laboratory prepared specimens and beams extracted from the Champlain Bridge for bending tests

F.2 Pull-off test geometry, specimen extraction and defective samples

The 490 pull-off specimens were extracted from a single surface of one of the three diaphragms (Diaphragm #1) described in section 1.3. The scoring depth ranged between 6-12 mm into the substrate (see Figure F.0.5). The aluminium disc used had a diameter of 50 mm (see Figure F.0.5). It also worth mentioning that large diameters, 75 mm and 100 mm are also commercially available and suitable for such bond tests.

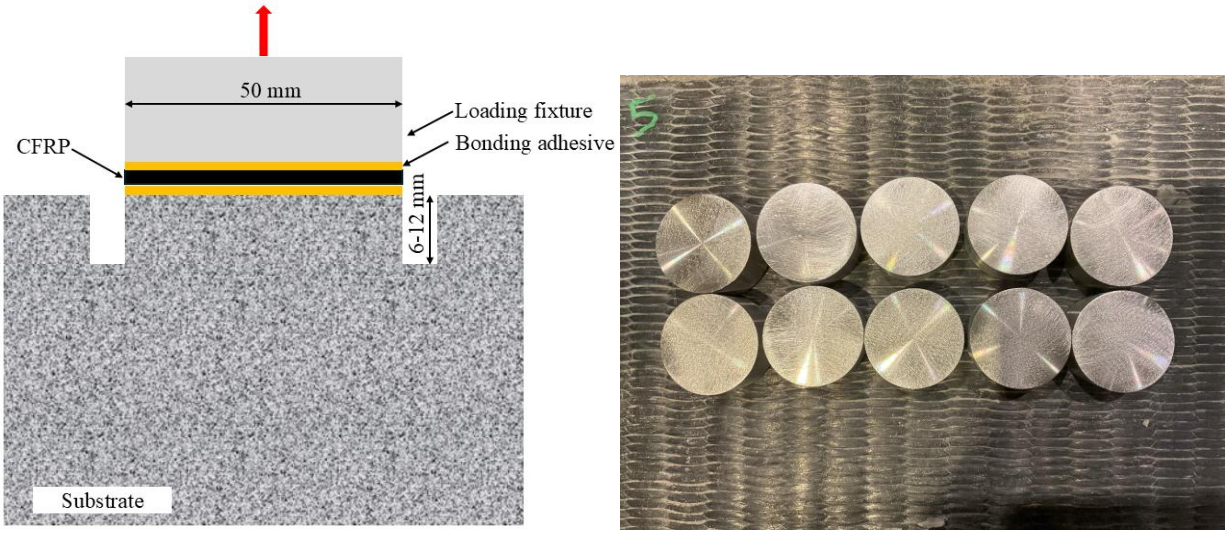

F.0.5-Specimen dimensions for direct tension pull-off testing and loading disc

Figure F.0.6 shows the scoring surface of the 490 pull-off specimens taken from Diaphragm #1.

F.0.6-Pull-off specimens extracted from surface 1 of Diaphragm #

The initial NDT condition assessment revealed defects, specifically debonds, at various layers of the strengthened diaphragm (Diaphragm #1) subjected to direct tension pull-off tests. Most of these issues were found on the anchorage strips (see Table 0.1). Some of the debonds marked by NDT experienced a total detachment of the multi-layer composite repair during the initial scoring process. In other cases, separation between different layers was noticed (see Figure F.0.7-F.0.9).

Table 0.1-Bond strength values of defective regions of Diaphragm #1 identified by NDT

Sample ID	Pull-off bond strength value	Defect location
1	0	Anchorage strip
2	0.66	Anchorage strip
3	0.84	Anchorage strip
4	0.99	Anchorage strip
5	1.22	Anchorage strip
6	2.97	Anchorage strip
7	2.19	Anchorage strip
8	0.87	Anchorage strip
9	1.62	Anchorage strip
10	2.5	Anchorage strip
11	0	Anchorage strip
12	1.49	CFRP strip 2
13	2.3	CFRP strip 3
14	3.78	CFRP strip 4
15	1.42	CFRP strip 4
16	1.5	CFRP strip 5
17	0	CFRP strip 5
18	2.53	CFRP strip 6
19	2.58	CFRP strip 6
20	0.99	CFRP strip 6
21	1.33	CFRP strip 6
22	4.63	CFRP strip 6
23	2.42	CFRP strip 6
24	3.55	CFRP strip 6
25	2.64	CFRP strip 6
26	1.23	CFRP strip 6
27	1.26	CFRP strip 6
2	0.66	Anchorage strip
3	0.84	Anchorage strip
4	0.99	Anchorage strip
5	1.22	Anchorage strip
6	2.97	Anchorage strip
7	2.19	Anchorage strip
8	0.87	Anchorage strip
9	1.62	Anchorage strip
10	2.5	Anchorage strip
11	0	Anchorage strip
12	1.49	CFRP strip 2
13	2.3	CFRP strip 3
14	3.78	CFRP strip 4
15	1.42	CFRP strip 4
16	1.5	CFRP strip 5
17	0	CFRP strip 5
18	2.53	CFRP strip 6
19	2.58	CFRP strip 6
20	0.99	CFRP strip 6
21	1.33	CFRP strip 6

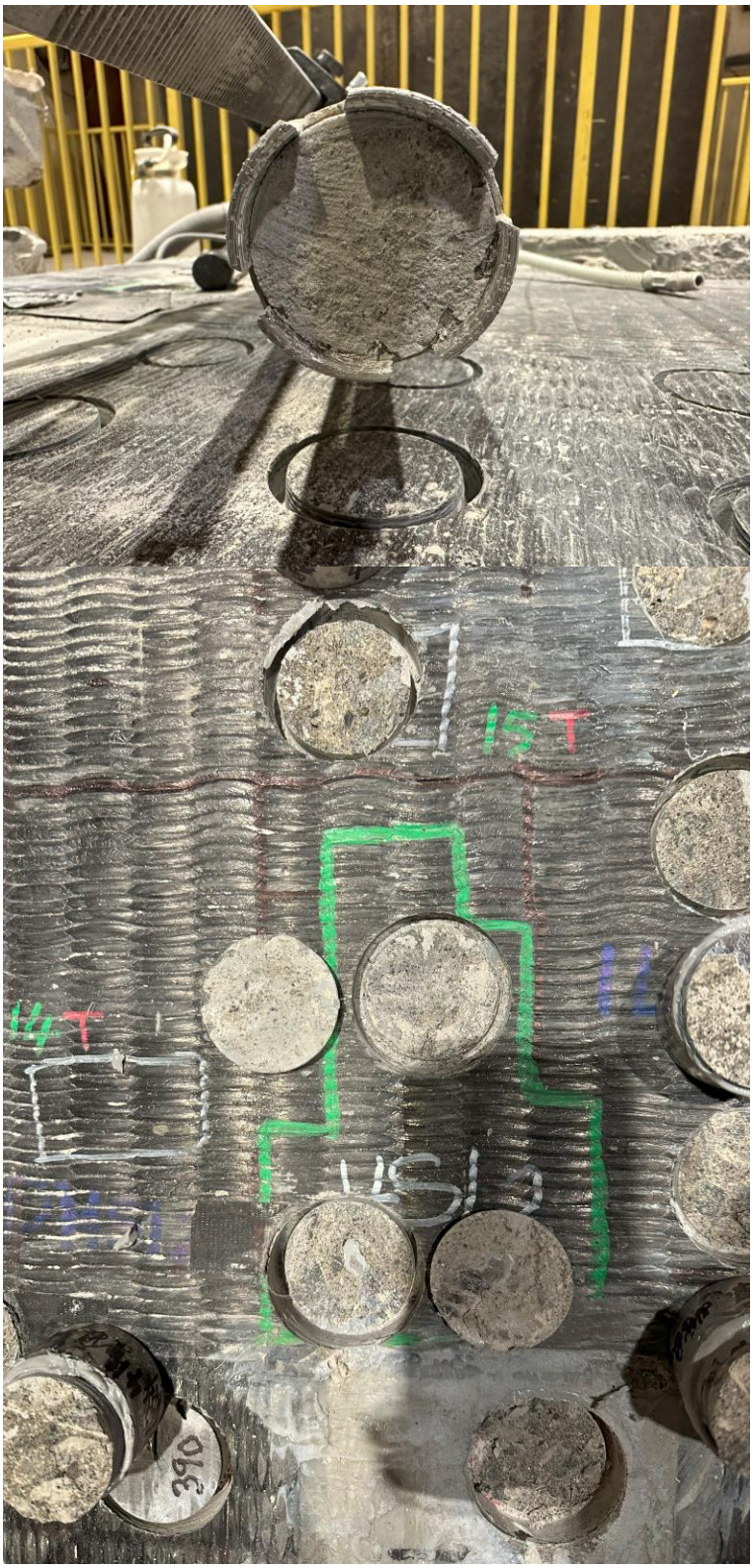

F.0.7-Detachment of defective specimens in the anchorage zone during initial scoring

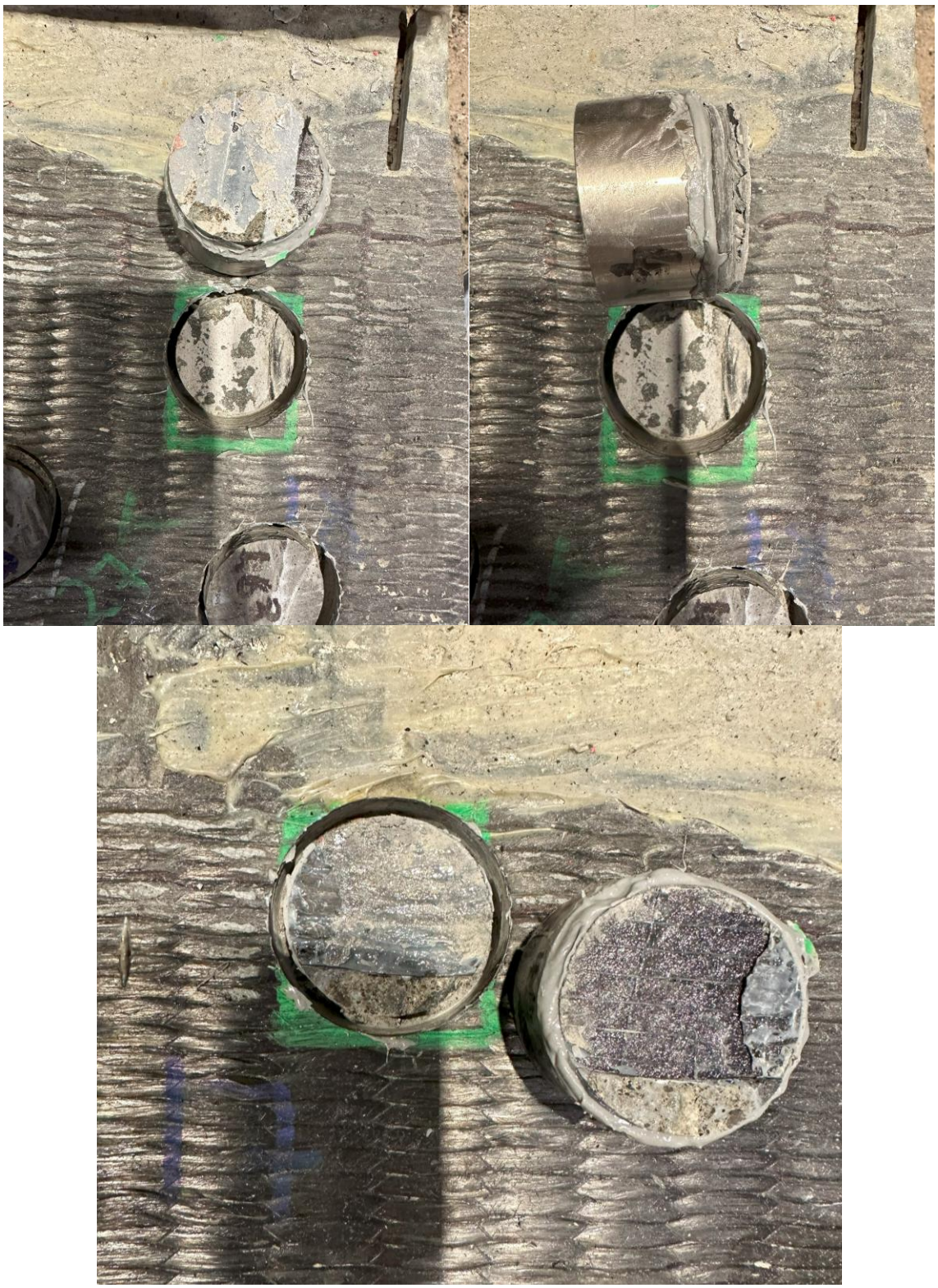

F.0.8-NDT identified defective zones and pull-off failure modes

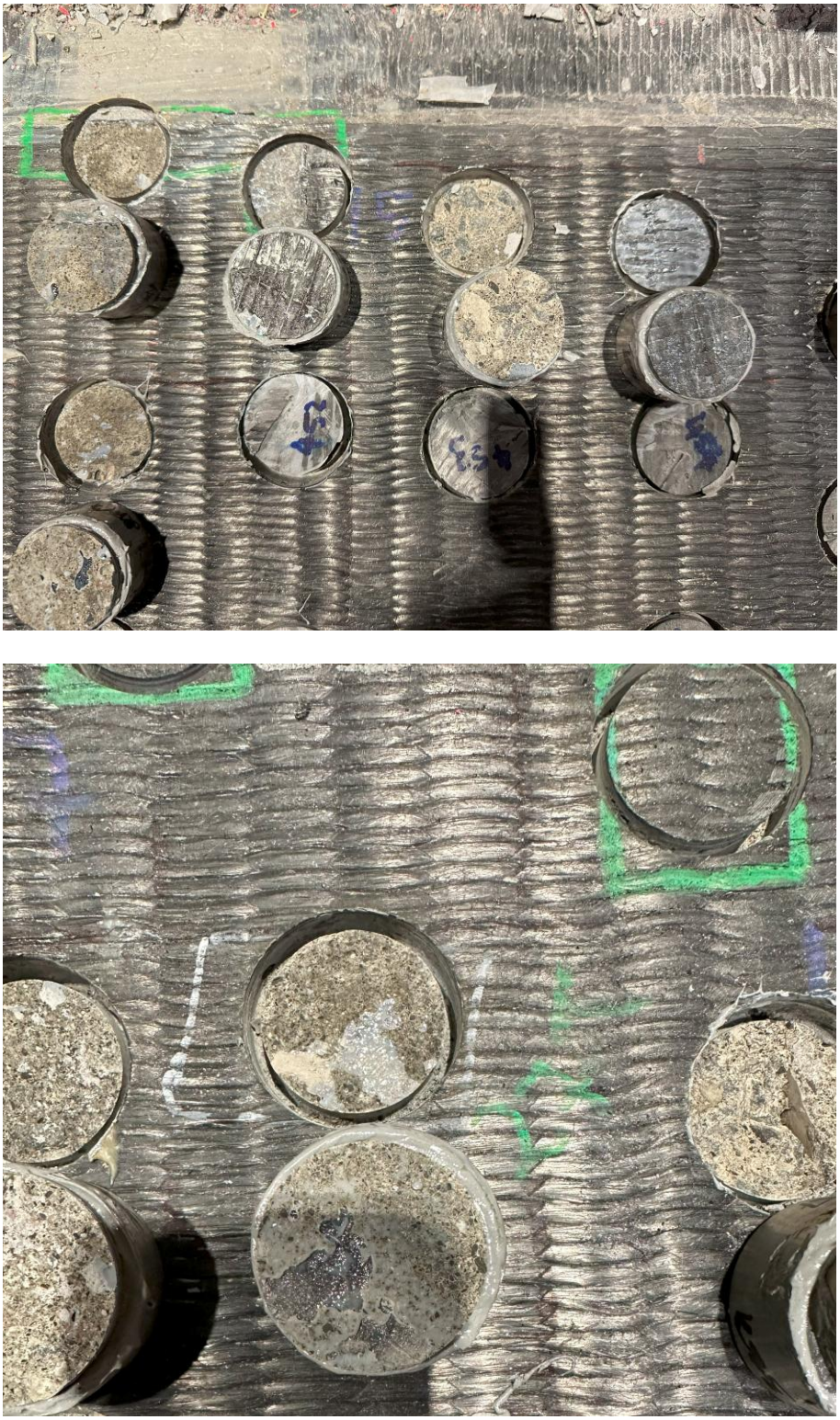

F.0.9-Bond separation between layers in defective pull-off specimens

F.3 FEM model calibration

It is important to note that the plots below are intended for reference only, as a potential calibration issue with the displacement sensor resulted in a stiffness response of the experimental beam that is not typical. The core challenge in matching the load-displacement curve under the perfect bond assumption stems from neglecting the critical nonlinear effect at the bond line, damage, and slip phenomena that fundamentally govern the actual load-displacement response. This simplification led to significant overestimation of the stiffness and ultimate load. Incorporating a substantial reduction in the elastic modulus of the concrete to represent the concrete damage and mortar patches yielded a better prediction.

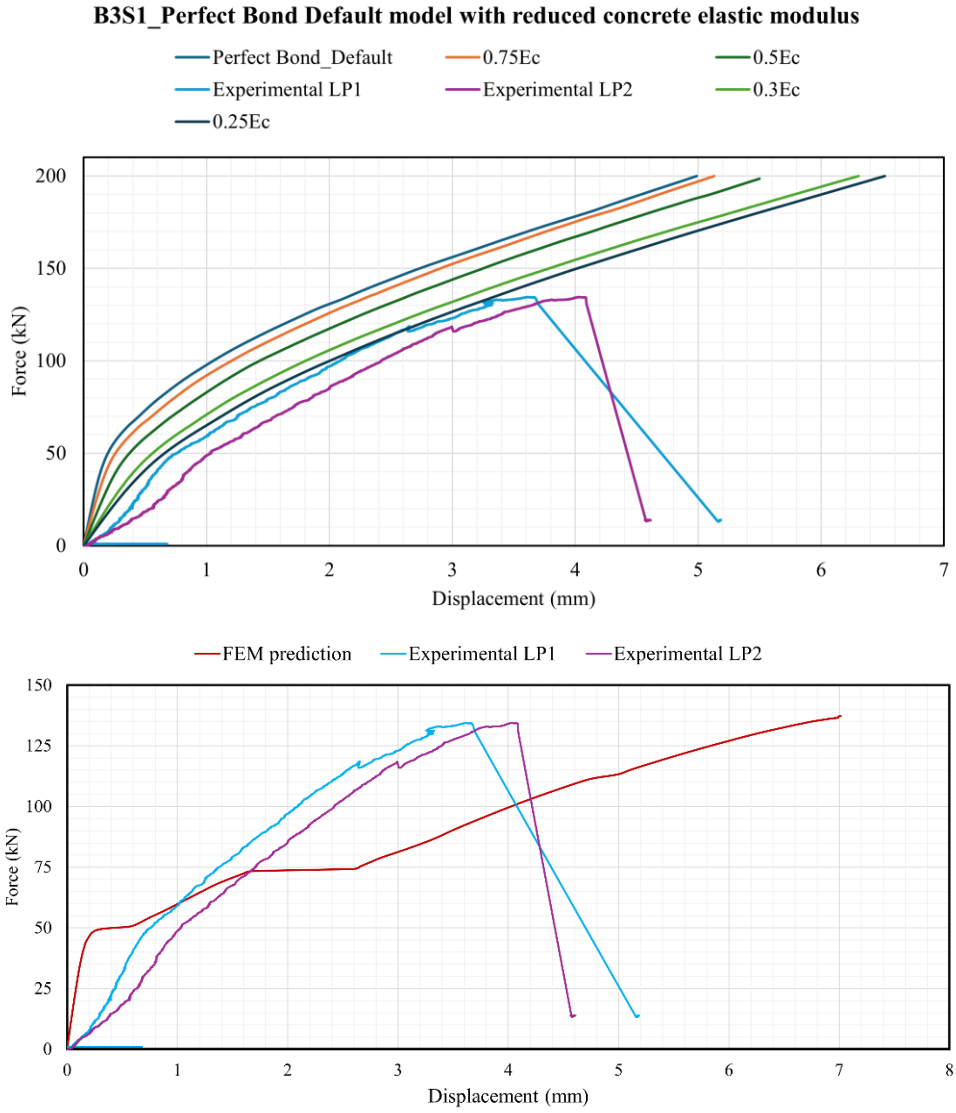

F.0.10-Load displacement Curves for B3S1-L500